MOLECULAR DESIGN AND SYNTHESIS OF NEW METAL-FREE ORGANIC CHROMOPHORES FOR DYE SENSITIZED SOLAR CELLS

Thesis

Submitted in partial fulfillment of the requirements for the degree of

DOCTOR OF PHILOSOPHY

By

PRAVEEN NAIK

DEPARTMENT OF CHEMISTRY

NATIONAL INSTITUTE OF TECHNOLOGY KARNATAKA

SURATHKAL, MANGALORE - 575 025

February, 2018

DECLARATION

By the Ph.D. Research Scholar

I hereby declare that the Research Thesis entitled "**Molecular design and synthesis of new metal-free organic chromophores for dye sensitized solar cells**" which is being submitted to the **National Institute of Technology Karnataka, Surathkal** in partial fulfillment of the requirements for the award of the Degree of **Doctor of Philosophy** in **Chemistry** is a *bonafide report of the research work carried out by me*. The material contained in this Research Thesis has not been submitted to any University or Institution for the award of any degree.

Praveen Naik

Reg. No. 138018CY13F08

Department of Chemistry

Place: NITK - Surathkal

Date:

CERTIFICATE

This is to certify that the Research Thesis entitled "**Molecular design and synthesis of new metal-free organic chromophores for dye sensitized solar cells**" submitted by **Mr. Praveen Naik** (Register Number: **138018CY13F08**) as the record of the research work carried out by him *is accepted as the Research Thesis submission* in partial fulfillment of the requirements for the award of degree of Doctor of Philosophy.

Prof. A. Vasudeva Adhikari

Research Guide

Date:

Chairman - DRPC

Date:

DEDICATED TO MY

BELOVED PARENTS

ACKNOWLEDGEMENTS

I extend my sincere thanks to all the research scholars in the Department of Chemistry for their constant help and support.

Mere words are not enough to express my gratitude to my family, father Mr. A. Annappa Naik, mother Mrs. Sharada, brothers Mr. A. Kiran Naik and Mr. A. Arun Naik for their constant support, encouragement and prayers. Finally, I thank the God almighty for strengthening me during hardships to successfully complete this endeavor.

PRAVEEN NAIK

ABSTRACT

The quest for neat and cost effective renewable energy has led to added research attention on organic photovoltaics. Over the past two decades, the dye-sensitized solar cell (DSSC), which belongs to the thin film photovoltaic technology, has emerged as an attractive and promising low-cost solar device after the inventive research work reported by Gratzel group. Among the different components of DSSCs, the dye as a photosensitizer plays a crucial role in the process of the cells, which include sunlight harvesting and electron injection from excited dye into the CB edge of TiO_2. At present, there is a considerable interest among the researchers to design and develop new *n*- type organic chromophores for DSSC application. In this context, it was planned to design, synthesize and investigate the photovoltaic performance of new organic dyes based on *N, N* dimethylaniline (**Series-1A, *n*-C$_{1-5}$**) and carbazole (**Series-1B** to **5, *n*-C$_{6-21}$**) as *n*-type sensitizers/co-sensitizers. In addition, it has been contemplated to design and investigate three new carbazole based dyes (**Series-6, *p*-C$_{1-3}$**) as potential *p*-type sensitizers for DSSC application.

Based on the detailed literature survey, twenty one new *n*-type organic sensitizers/co-sensitizers and three *p*- type organic sensitizers were designed with various design strategies. They were successfully synthesized following appropriate synthetic protocols. Further, they were well-characterized by spectral, optical and electrochemical analyses. Their optical and electrochemical parameters along with molecular geometries were optimized, and DFT has been employed to apprehend the effect of structures of organic sensitizers/co-sensitizers on their photovoltaic performances. Finally, the synthesized dyes were subjected to the photovoltaic studies. Among *n*-type organic sensitizers, the cell fabricated with ***n*-C$_{13}$** displayed the optimum *PCE* of **3.55**%. Whereas, the co-sensitization studies, indicated that, under the same conditions, the device co-sensitized using ***n*-C$_6$** dye with **NCSU-10** sensitizer showcased upheld *PCE* of **9.55**%. Finally, the new three *p*-type organic dyes were sensitized on NiO and their photovoltaic results revealed that, ***p*-C$_2$** sensitized DSSC exhibited optimum photovoltaic performances which are comparable with that of the bench mark reference **P1**. To sum up, by appropriately optimizing the molecular structures of metal-free organic dyes, it is possible to further ameliorate the photovoltaic performance of the cells.

Keywords: carbazole; co-sensitizers; DFT; DSSC; *n*-type sensitizers; *p*-type sensitizers; Photovoltaic devices

CONTENTS

LIST OF FIGURES

LIST OF TABLES

ABBREVIATIONS:

CB	: Conduction band
CE	: Counter electrode
D-π-A	: Donor-π-acceptor
DFT	: Density functional theory
DSSC	: Dye sensitized solar cells
e^-	: Electrons
Eq	: Equation
EW	: Electron withdrawing
FF	: Fill factor
Fs	: Femtosecond
FTIR	: Fourier-transform infra-red
FTO	: Fluorine-doped tin oxide
h+	: Holes
HOMO	: Highest occupied molecular orbital
HR-MS	: High resolution mass spectroscopy
ICT	: Intra-molecular charge transfer
IPCE	: Incident photon to current efficiency
J_{SC}	: Short-circuit photocurrent density
LHE	: Light harvesting efficiency
LUMO	: Lowest unoccupied molecular orbital
n- type DSSC	: *n*- Type dye sensitized solar cell
n-SC	: *n*-Type semiconductor
n-C_{1-5}	: *n*-Type chromophores carrying *N,N*-dimethylaniline as electron donor
n-C_{6-8}	: *n*-Type chromophores carrying carbazole as electron donor with D-A configuration
n-C_{9-12}	: *n*-Type chromophores carrying carbazole as electron donor with D-π-A configuration
n-C_{13-15}	: *n*-Type chromophores carrying carbazole as electron donor with D-π-A-π-A configuration
n-C_{16-18}	: *n*-Type chromophores carrying carbazole as electron donor with D-D-π-A configuration
n-C_{19-21}	: *n*-Type chromophores carrying carbazole as electron donor with A-π-D-π-A configuration

NHE	: Normal hydrogen electrode
NiO	: Nickel oxide
NMR	: Nuclear Magnetic Resonance
PCE	: Photon conversion efficiency
Ppm	: Parts per million
p-SC	: *p*-Type semiconductor
Pt	: Platinum
p-type DSSC	: *p*-Type dye sensitized solar cells
p-C$_1$	: *p*-Type chromophores carrying *N,N*-dimethyl barbituric acid as an acceptor
p-C$_2$	: *p*-Type chromophores carrying *N,N*-diethyl thiobarbituric acid as an acceptor
p-C$_3$	: *p*-Type chromophores carrying *N*-ethyl rhodanine acid as an acceptor
Ru (II)	: Ruthenium (II)
VB	: Valence band
V$_{OC}$	: Open-circuit voltage
SC	: Semiconductor
TD-DFT	: Time dependent-density functional theory
TiO$_2$	: Titanium dioxide
WE	: Working electrode

GENERAL INTRODUCTION

Abstract:

This chapter deals with a brief introduction on photovoltaics followed by an account on dye-sensitized solar cells (DSSCs). It also contains the working principles, various components and photovoltaic parameters of DSSCs. Further, it covers broad objectives of the present research work as well as the outline of thesis structure.

1.1 INTRODUCTION ON PHOTOVOLTAICS

Energy is essential to every aspect of human life, and from the beginning of the 21st century, the energy demand has gone up quickly due to an increasing global population. The energy crisis and environmental concerns intensified the need for utilization of renewable energy sources. In this regard, sunlight is an abundant natural resource of energy. The energy provided by the sun in one hour exceeds the energy consumption globally in an entire year and so, many scientists showed interest to find ways for harnessing this energy (Lewis 2007. Hasan and Sumathy 2010, Gong et al. 2012).

Photovoltaic cells are devices that are able to convert solar energy into electrical energy without exhaust of both greenhouse gases and another polluting agent. The phenomenon of conversion of photons to electricity is known as the photovoltaic effect. In 1839, French physicist Alexandre Edmond Becquerel discovered photovoltaic effect. Later, in 1941 first silicon monocrystalline solar cell was constructed. A traditional solar cell consists of two doped crystals, one doped with *n*-type impurities (*n*-type semiconductor), which injects electrons into the conduction band of the *n*-type semiconductor, and the other doped with *p*-type impurities (*p*-type semiconductor), which injects electron holes into the valence band of the *p*-type semiconductor.

The aim of solar cell research is to increase the solar energy conversion efficiency to provide a cost-effective sustainable energy source. Solar to electrical power conversion efficiency of the best silicon based devices is around 25%. Silicon based photovoltaic modules are robust and have a lifetime of about 25 years. In spite

of high efficiency, the cost is a major drawback. Due to this drawback of silicon solar cells, DSSC can be considered as a viable alternative. Actually, silicon technology is a market leader in photovoltaic technologies, however, dye sensitized solar cell (DSSC) belonging third generation thin film solar cell technology has become an important and promising technology in the field of photovoltaics.

1.2 DYE SENSITIZED SOLAR CELL (DSSC)

DSSC belongs to organic-based photovoltaic cells. It is a promising low-cost, an alternative to existing crystalline silicon and thin film photovoltaic technologies, discovered by Grätzel and O'Regan in 1991 (Grätzel et al. 2005). The DSSC or Grätzel cell is a sandwiched system wherein four different components, *viz.* the dye, the semiconductor, the electrolyte and the platinum electrode are brought together to generate electric power from light energy without undergoing any permanent chemical transformation. DSSCs have attracted considerable attention after Grätzel's report because of the following reasons:

- Efficient use of DSSC can meet our increasing energy demand
- DSSC is environmentally friendly
- Organic sensitizers own advantages of easy production and design versatility
- Highly economical

DSSC can be broadly classified into two types, based on nature of sensitizer used in it. They are:

- ➢ *n*-Type dye sensitized solar cell
- ➢ *p*-Type dye sensitized solar cell

1.2.1 *n*-Type dye sensitized solar cell (*n*-Type DSSC)

The *n*-type DSSCs usually consists of the following features:

a. An anode made up of a glass sheet with a transparent conductive layer

b. A mesoporous semiconductor oxide layer (typically, TiO_2) deposited on the anode to activate electronic conduction

c. A monolayer of the chromophore, *i.e.* the sensitizer, attached to the surface of the semiconductor

d. An electrolyte, usually an organic solvent containing a redox couple, such as iodide/triiodide for the regeneration of the dye

e. A cathode made up of a glass sheet coated with a catalyst (typically platinum) to facilitate electron collection.
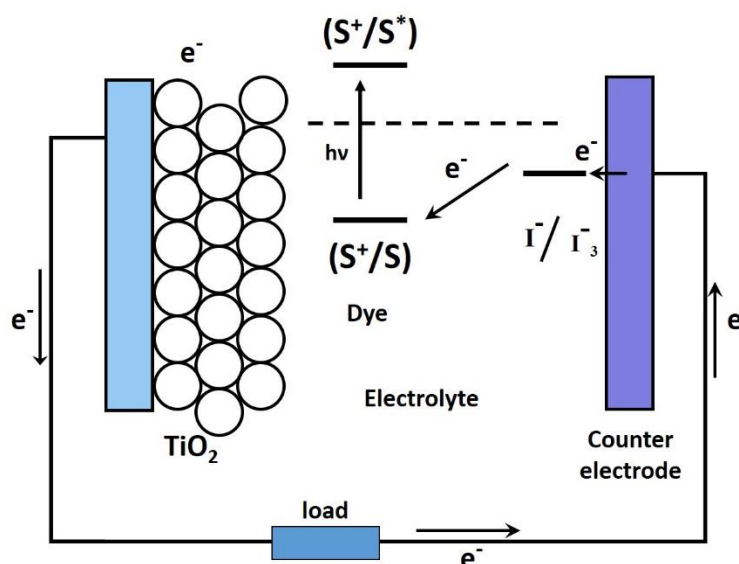
Fig 1.1: Schematic representation of *n*-type DSSC (Thomas et al. 2013)

DSSC is a mimic to the natural process of photosynthesis in plants. DSSC is a molecular machine that is one of the first of its kind devices to go beyond microelectronics into the realm of nanotechnology, wherein the use of a dye as the light harvester to produce excited electrons, TiO_2 replacing carbon dioxide as the electron acceptor, iodide/triiodide (I^-/I_3^-) replacing water and oxygen as the electron donor and oxidation product and a multilayer structure (similar to the thylakoid membrane) to enhance both the light absorption and electron collection efficiency (O'Regan and Grätzel 1991).

When exposed to sunlight (**Fig 1.1**), dye molecule gets excited from the ground state (S^0) to an excited state (S^*) from which an electron is injected into the conduction band of the mesoporous oxide film. These generated electrons diffuse to the anode and are utilized at the external load before being collected by the electrolyte at cathode surface to complete the cycle. The operating cycle can be summarized in following chemical reactions:

Anode:

$$S + h\nu \longrightarrow S^* \qquad \text{Photo excitation}$$

$$S^* + TiO_2 \longrightarrow S^+ \qquad \text{Electron injection}$$

$$2S^+ + 3I^- \longrightarrow 2S + I_3^- \qquad \text{Sensitizer regeneration}$$

Cathode:

$$I_3^- + 2e^- \longrightarrow 3I^- \qquad \text{Electron donor regeneration}$$

Cell:

$$e^- (Pt) + h\nu \longrightarrow 3I^-$$
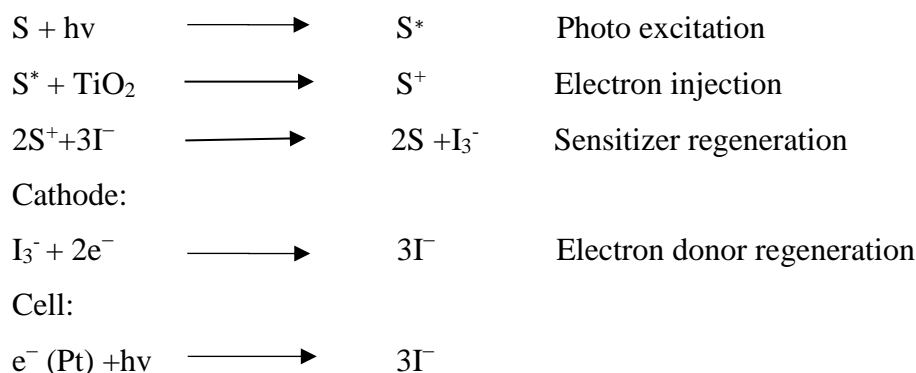
Photo injected electrons should escape from any recombination process in order to have a unit charge collection efficiency at the photoelectrode back contact. The two major unwanted processes in a DSSC are due to (i) back electron transfer, at the semiconductor-electrolyte interface, between electrons in the conduction band and the oxidized dye molecules, and (ii) reduction of I_3^- at the semiconductor surface:

$$S^* + (e^-, TiO_2) \longrightarrow S \qquad \text{Back electron transfer;}$$

$$I_3^- + 2(e^-, TiO_2) \longrightarrow 3I^- \qquad \text{Electron capture from mediator.}$$
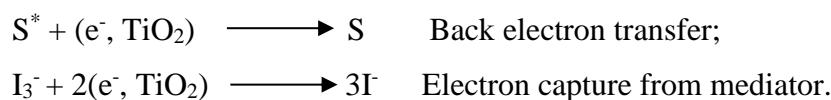
All the operations in the cell are regenerative, so none of the chemical substance undergoes any permanent chemical transformations as shown by the cell reaction.

Working principles of n-type DSSC

In DSSC's unlike conventional silicon based devices, charge separation and recombination are exclusively interfacial reactions. Further, due to the weaker van der Waals interactions between the organic molecules than those in silicon crystals and a lower dielectric constant, photo excitation of organic dyes produces a tightly bound neutral Frenkel exciton, whereas the loosely bound Wannier exciton is formed when silicon is photoexcited, which are basically considered to be free charges. DSSC cannot produce free charges directly from photo excitation, but rather requires an additional step for charge separation. Therefore, we can say that current generation DSSC is reliant on three sovereign processes, *viz.* the absorption of light by the dye molecules, the injection of electrons from the excited state of photosensitizer and its transport through the semiconducting layer. **Fig 1.2** shows the various energy levels present in a typical DSSC and also the electron flow with the solar cell. Upon illumination, the dye molecule is photo-excited in a few seconds followed by ultrafast

injection from S^* to TiO$_2$ on the sub-pico second time scale (intramolecular relaxation of the excited sensitizer might complicate the injection process), wherein they are rapidly(less than 10fs) thermalized by lattice collisions and phonon emissions. The fairly slow rate (nanosecond) of dye (S*) relaxation ensures that the injection efficiency is 100%. The ground state of the chromophore is then recuperated by the electrolyte in the microsecond domain, successfully annihilating S^* and seizing the recombination of an electron in TiO$_2$ with S^* that happens in the millisecond time range. This is followed by two processes: electron percolation through the semiconducting film and reduction of the triiodide at the counter electrode, completing the circuit.
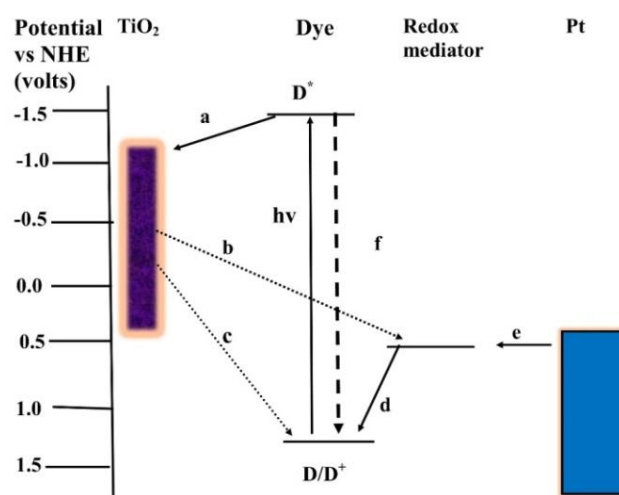
Fig 1.2: Schematic illustration of the energy levels in a typical *n*-type DSSC specifying the various competing photophysical pathways. They include (a) electron injection, (b) electron recombination with the acceptor species in the electrolyte, and (c) with dye cations, (d) regeneration of dye cations by the electrolyte, (e) reduction of the electrolyte at the counter electrode, (f) relaxation of the dye molecule from the excited state

1.2.2 *p*-Type dye sensitized solar cell (*p*-type DSSC)

The *p*-type DSSC is a sandwich structured device composed of a photoactive working electrode (cathode), a passive counter electrode (anode), and redox electrolyte. An alternative route for constructing a DSSC involves a *p*-type semiconductor (usually NiO) which serves as a photoactive cathode. **Fig 1.3** depicts the schematic representation of a *p*-type DSSC. In this case, the adsorbed dye injects holes into the

semiconductor valence band, where they diffuse to the cathode contact, while the excited electrons are transferred to the electrolyte through which they diffuse to the anode.
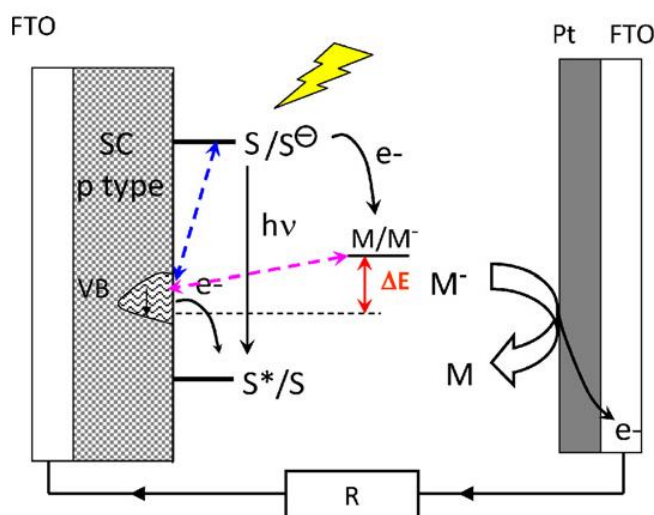
Fig 1.3: Schematic representation of a *p*-type DSSC showing electron transfer processes involved in the operation of the cell during working of the cell and the energy wasting charge recombination and interfacial interception processes. (Odobel et.al. 2012)

The basic requirements for the use of this "inverted" type of dye adsorbed on photocathodes are mainly (i) the HOMO level of the dye must be sufficiently below the valence band of the *p*-semiconductor and (ii) the LUMO level must be sufficiently higher in energy than the redox potential of the I_3^-/I^- system.

Working principle of a p-type DSSC

Fig 1.4 illustrates the key processes in a *p*-type DSSC under illumination (Qin et al. 2010). On excitation, visible light is absorbed by the dye sensitizer (S). This leads to the formation of its excited state (S*) which decays by hole injection into the valence band of the *p*-type semiconductor (*p*-SC) to form the charge separated state S^-/*p*-SC. A redox shuttle (the couple M/M^-) reacts then with the reduced sensitizer to restore the ground state of the sensitizer. Then, the holes in the semiconductor move to the back collector of the working electrode and the reduced species (I^-) in the electrolyte diffuses to the platinum electrode. This charge collection gives rise to a cathodic photocurrent in the external circuit. Various processes taking place in the cell are summarized below:

Dye | NiO + hν → Dye* | NiO   (excitation)

Dye* | NiO → Dye$^-$ | NiO + h$^+$ (NiO)   (hole injection)

Dye$^-$ NiO + h$^+$(NiO) → Dye | NiO   (geminate recombination)

Dye$^-$ | NiO + 1/2 I$_3^-$ → Dye | NiO + 3/2 I$^-$ (dye regeneration)

3/2 I$^-$ → 1/2 I$_3^-$ + e$^-$ (Pt)   (regeneration of I$_3^-$ at the counter electrode)
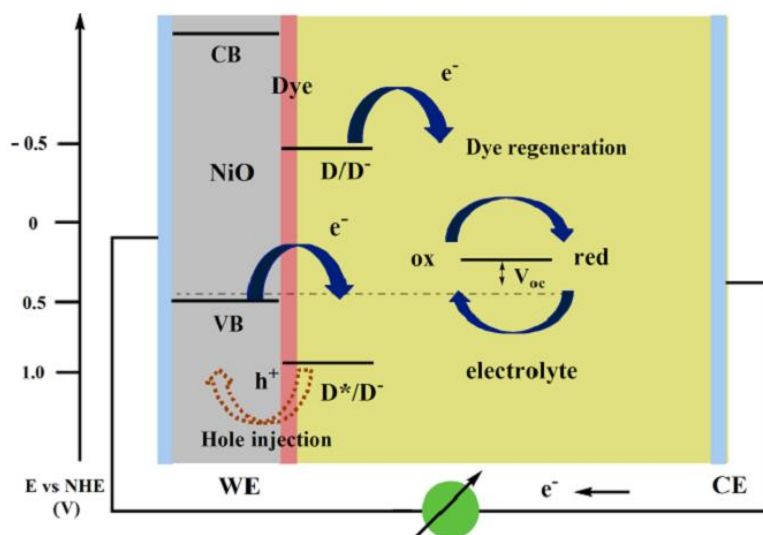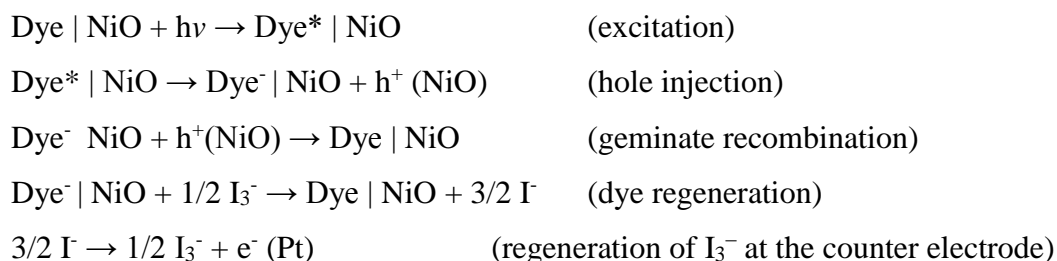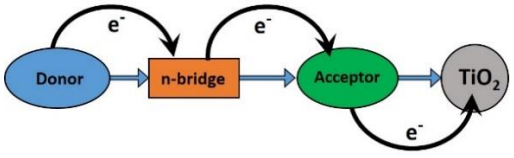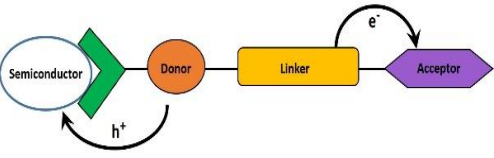
Fig 1.4: Schematic diagram illustrating the key processes in a *p*-type DSSC (Qin et al. 2010)

Comparison between n-type and p-type DSSCs

n-type DSSC	*p*-type DSSC
The *n*-type DSSC is a sandwich structured device composed of a photoactive working electrode (anode), a passive counter electrode (cathode), and a redox electrolyte	The *p*-type DSSC is a sandwich structured device composed of a photoactive working electrode (cathode), a passive counter electrode (anode), and a redox electrolyte
When the dye absorbs Sunlight, an electron is excited from the HOMO to the LUMO level of the dye, followed by injection into the conduction band of the *n*-type semiconductor (usually TiO$_2$)	When the dye absorbs, the holes are injected into the valence band of the *p*-type semiconductor (*p*-SC) (usually NiO)

Design of organic chromophores is as follows	Design of organic chromophores is as follows
The general design of *n*-type dyes consists of both electron-donor (D) and electron-acceptor (A), wherein the anchoring group is attached on the electron-acceptor	The general design of *p*-type dyes consists of anchoring group is attached on the electron-donor (D), which is far from electron-acceptor (A)
Electron Injection: On photo-excitation, the dye must inject an electron into the conduction band of the semiconductor before it eases back to the ground state.	Hole Injection: On photo excitation, the dye must inject a hole into the Valence band of the semiconductor before it eases back to the ground state.
It consists of a photoactive anode and a passive cathode. The LUMO level of the dye should be more negative than the CB edge of *n*-SC to facilitate efficient electron injection.	It involves a photoactive cathode and a passive anode. The HOMO level of the dye should be more positive than the VB position of *p*-SC to facilitate efficient hole transfer.

1.3 PHOTOVOLTAIC PARAMETERS OF DSSCs

The photovoltaic performance of DSSCs is mainly analyzed by parameters such as incident photon to current efficiency (*IPCE*), open-circuit voltage (V_{OC}), short-circuit photocurrent density (J_{SC}), fill factor (*FF*), and the overall conversion efficiency (*PCE*). Techniques used to characterize the complete solar cell device are very important since the properties of all components are dependent on the complex interplay arising in a complete device. Techniques used also provide appropriate illumination intensities close to real operation conditions of a solar cell. Sometimes, additional techniques are used for characterization of the dyes in solution and when

adsorbed on NiO / TiO$_2$ film. The combination of results obtained for the complete device as well as for the individual components is utilized to identify and understand the role of novel organic dyes in DSSCs as sensitizers/co-sensitizers. Some of the important photovoltaic parameters have been discussed in the following section.

1.3.1 Short circuit photocurrent (*J$_{SC}$*)

The *J$_{SC}$* value is the photocurrent per unit area (mA.cm^{-2}) when a DSSC under irradiation is short-circuited. The *J$_{SC}$* value can be derived by integrating the IPCE spectra to give equation (**Eq. 1.1**).

$$J_{sc} = e \int IPCE(\lambda) I_s(\lambda) d\lambda \tag{1.1}$$

In which, *I$_s$(λ)* is the photo-flux at wavelength λ under standard AM 1.5 simulated sunlight. Thus, to gain a high J_{SC} value, ideal molecular designs of organic dye sensitizers should feature the following characteristics: (i) intense and broad sunlight-harvesting capability, (ii) strong interactions between dye sensitizers and TiO$_2$ surfaces.

1.3.2 Open-circuit photovoltage (*V$_{OC}$*)

The V_{OC} value is the difference in electrical potential between two terminals of a cell under illumination when the circuit is open. The V_{OC} can be expressed by the **Eq. 1.2**.

$$V_{OC} = \frac{E_{cb}}{e} + \frac{k_B T}{e} \ln \left(\frac{n}{N_{cb}}\right) - E_{redox} \tag{1.2}$$

where *e* is the elementary charge, *n* is the number of the electrons in TiO$_2$, k_B is the Boltzmann constant, *T* is the absolute temperature, N_{cb} is the effective density of states, and E_{redox} is the redox potential of the redox couple. Thus, the maximum V_{OC} value of a DSSC corresponds to the difference between the energy level (E_{CB}) of the CB of TiO$_2$ and the redox potential of the electrolyte (I$_3^-$/I$^-$). However, the actual V_{OC} value is lower than the theoretical value due to the recombination of injected electrons with I$_3^-$ ions in the electrolyte and with dye cations.

1.3.3 Fill factor (*FF*)

The *FF* is an important parameter for a solar cell and is related to the maximum power output ($J_{mp}V_{mp}$) divided by the product of J$_{SC}$ and V_{OC} (**Eq. 1.3**).

$$FF = \frac{J_{mp} \; V_{mp}}{J_{SC} \; V_{OC}} \tag{1.3}$$

The *FF* is determined from the *J-V* curve and is an indication of how much of the area of the rectangle for $J_{SC}V_{OC}$ is filled by that described by $J_{mp}V_{mp}$ (product of maximum photocurrent density and circuit voltage). Thus, the maximum *FF* value is 1. However, such value cannot be achieved owing to the factors such as heat resistances of the substrate and counter electrode, electron transport resistance through the photoanode, ion transport resistance, and the charge-transfer resistance at the counter electrode. Therefore, careful fabrication of the cell is important for attaining high photovoltaic performance.

1.3.4 Incident photon to current conversion efficiency (*IPCE*)

The IPCE is a quantum-yield term for the overall charge-injection collection process measured using a single wavelength source. It is defined as the number of photo-electrons move through the external load divided by the number of incident photons as a function of excitation wavelength. It can be expressed as the product of light harvesting efficiency (LHE$(\lambda) = 1\text{-}10^{-A}$ where A is the absorption of the dye corresponding to λ_{abs} at wavelength λ, quantum yield of electron injection (ϕ_{inj}) from the excited sensitizer into the conduction band of the TiO_2 electrode, and the efficiency of collection of the injected electron (η_{coll}) at the FTO glass (**Eq. 1.4**).

$$IPCE \; (\lambda) = \text{LHE} \; (\lambda)\Phi_{inj} \; \eta_{coll} \tag{1.4}$$

The IPCE is therefore directly related to the amount of adsorbed dyes on the TiO_2 surface (or LHE), electron injection efficiency into the CB of the TiO_2, and electron collection efficiency in the external circuit under monochromatic illumination of the cell.

1.3.5 Photon conversion efficiency (*η*) of DSSCs

The light-to-electrical power conversion efficiency of a solar cell (*η*) is determined by V_{OC}, J_{SC}, *FF*, and I_0 (intensity of incident light, AM 1.5, 100 mW.cm^{-2}) (**Eq. 1.5**).

$$\eta \; (\%) = \frac{J_{SC} \; (mA \; cm^{-2}) \; V_{OC} \; (V)FF}{I_0 \; (mW \; cm^{-2})} \tag{1.5}$$

To attain a higher *η* value, optimization of the V_{OC}, J_{SC}, and *FF* values of the cell is

essential. To date, the *PCE* values have been improved gradually through use of properly designed organic sensitizers in DSSCs. It has been reached up to 14 % of PCE for an efficient triphenyl amine based sensitizer.

1.4 COMPONENTS OF *n-/p*-TYPE DSSC

1.4.1 Semiconductor

In *n*-type DSSCs, photo active electrode (photoanode) consists of wide band gap semiconductors such as TiO_2, ZnO, SnO_2, and chalcogenides. Due to their wide application in energy storage, they have been under extensive investigation. They facilitate light-induced redox process mainly due to the presence of the electronic structure, referred to as valence band and the conduction band. The surface area available for dye chemisorption is over a thousand fold higher than that of a flat, unstructured electrode of the same size. If a monomolecular layer of the dye is adsorbed on the surface, enough dye can be retained on a given area of the electrode to provide absorption of basically all the incident light. The necessity for DSSC to absorb far-more of the incident light was the driving force behind the development of mesoporous semiconductor material (minutely structured materials with an enormous internal surface area).

TiO_2 occurs in three crystalline forms, *viz.* rutile, anatase and brookite. Among these, anatase is perceived to be more chemically active when used in dye-sensitized solar cells. The high dielectric constant of TiO_2 (ϵ=80 for anatase) provides a good electrostatic shielding of the injected electron from the oxidized dye molecule attached to the TiO_2 (Jose et al. 2009, Lee et al. 2011), hence preventing their recombination before reduction of the dye by the redox electrolyte. High refractive index of TiO_2 (*n*=2.5 for anatase) leads to efficient diffuse scattering of light inside the porous photoelectrode, which remarkably enhances the light absorption. The band-gap of anatase is 3.2 eV at an absorption edge of 388 nm. Moreover, the conduction band edge of anatase is 0.1 eV above than that of the rutile phase; hence the maximum open circuit voltage (V_{OC}) of rutile photoanode is lower than anatase photoanode. It has also been observed that the intrinsic electrical properties of TiO_2 are profoundly affected by the crystal structure. The other major parameter which

affects the carrier concentration and mobility of electrons in transition metal oxides is the type and concentration of cation and anion defects. Among these point defects, the oxygen vacancy has been identified as the one which affects the performance of solar cells. Studies done by Meng et al. (2010), on the electron and hole dynamics show that oxygen vacancy on TiO_2 surface stabilizes the dye adsorption. Due to the strong bond between dye and the semiconductor, charge injection will be enhanced. Moreover, when the oxygen vacancy is present on the surface of TiO_2, back electron transfer becomes more predominant, as the HOMO and LUMO of the redox species are shifted to higher energy levels. In addition, the electrons that are injected from the dye molecule migrate through TiO_2 *via* hopping without the support of built-in potential.

Extensive research has been done to improve the carrier transport and dye adsorption by surface modification of TiO_2 nanoparticles. Exploratory research on doped TiO_2 and various other metal oxides have been carried out extensively to improve the surface properties and electronic structure of the photoanode. Due to its similar conduction band edge, work function and higher carrier mobility, ZnO is often considered as promising material to replace TiO_2 as photoanode. But surprisingly, the performance of ZnO is found to be consistently lower than that of TiO_2. This is attributed to the vulnerability of ZnO surface to the acidic environment, the chemical bond with the dye is easily degraded to form dye aggregates that dissipate the energy of absorbed photons.

Generally, *p*-SCs are used for fabrication of photocathodes in DSSCs. They must be resistant to photo-corrosion and easily be synthesized as nanoparticles so that they can be transformed into mesoporous films that can have large surface area. Further, the surface of the *p*-SC must exhibit high chemical affinity to an organic functional group in order to promote the chemisorption of the sensitizers on the surface. Also, the position of the valence band potential of the *p*-type SC is important because it governs the maximum V_{OC} that the cell can deliver unlike *n*-type DSSCs; there are fewer metal oxides that exhibit *p*-type semiconductivity. Nickel oxide has been widely used as *p*-type SC for the fabrication of *p*-type DSSCs because several reports are available in the literature for the preparation of porous NiO films on conducting glass for the development of electrochromic devices. NiO has also drawn

much attention due to its utilization in other applications, such as gas sensors, catalysts, magnetic materials, electrochromic devices, and fuel cells. Nickel oxide is an intrinsic non-stoichiometric material with a wide bandgap (E_g, 3.6-4.0 eV), exhibiting good thermal and chemical stability. Its valence band potential is at 0.54 V (*vs*. NHE at pH 7), which renders it a good electron donor for many photosensitizers. As a result, the reductive quenching of sensitizers is a strongly permitted process, but the low-lying valence band potential makes it difficult to obtain a large V_{OC} with such materials. Further, *p*-type metal oxides are known to be much poorer electronic conductors than *n*-type metal oxides.

Photoinduced absorption spectroscopy measurements indicate that the hole diffusion coefficient in NiO film is in the range of 10^{-8} to 10^{-7} cm^{2}s^{-1}, which is more than two orders of magnitude lower than electron diffusion coefficient in TiO$_2$. The slow diffusion of holes into NiO gives rise to a long time delay between injection of holes and their collection, thereby increasing their potential scavenging by the redox mediator. Therefore, new *p*-SCs exhibiting higher conductivity than NiO could be certainly beneficial to build efficient *p*-type DSSCs. Generally, the preparation of nanoporous NiO electrodes for DSSCs requires the synthesis of nickel dihydroxide, which is subsequently dehydrated at high temperature. However, other alternative routes were reported, such as chemical vapor deposition, electrodeposition, hydrothermal synthesis, sputtering, and sol-gel methods. Recently, Suzuki and coworkers showed that the use of poly(ethylene oxide)-poly(propylene oxide)-poly(ethylene oxide) triblock copolymers as template leads to particularly good quality NiO electrodes for *p*-type DSSCs. Later, Bach and coworkers reported that NiO films can be prepared from commercial NiO nanopowders and recently, Le Pleux and coworkers reported a simple hydrothermal method for the preparation of NiO films on FTO electrodes, which is suitable to fabricate reproducible and efficient *p*-type DSSCs.

1.4.2 Photosensitizer

Photosensitizers can be broadly classified into two major groups. They are (i) metal (Ru II) based and (ii) metal-free sensitizers. They play a vital role in generating

electron-hole pairs. An efficient photosensitizer should possess certain requirements such as:

- The photosensitizers should be capable of absorbing all incident light below the near-IR wavelength of approximately 920 nm.

- It should carry a carboxylate or phosphonate group for strong adsorption onto the semiconductor surface.

- The lowest unoccupied molecular orbital (LUMO) of the *n*-type sensitizer must be close to the edge of the conduction band of the oxide for efficient electron injection into the conduction band of the semiconductor.

- The highest occupied orbital (HOMO) of the *p*-type sensitizer must be sufficiently low too accept electron donation from an electrolyte or a hole conductive material.

- Electrons and holes in the dye must be quickly separated and injected into the respective photoactive electrodes before being recombined. This basically means that the quantum yield for charge injection must be close to 1. The dye should be stable enough and should not undergo any degradation.

1.4.2.1 Dyes for TiO₂-based *n*-type DSSCs

Over the past few decades, the metal-free organic sensitizers have grossed significant attention over the high-performing metal-based ruthenium-complex dyes due to their cost-effective, larger molar extinction coefficient, facile synthesis and flexibility in tuning the absorbing light spectrum.

In order to enhance the photovoltaic performances of the DSSCs, various design strategies are employed for designing organic dyes. Amongst the various strategies, the most commonly used D-π-A approach, wherein a rod-like structural configuration carrying electron rich (donating) and electron deficient (withdrawing) scaffolds connected through a π-spacer unit, is considered to be one of the most promising and successful architectures. **Fig 1.5** depicts the D-π-A design strategy for a metal-free organic chromophore. In such dyes, photo induced ICT phenomenon can easily be controlled and their photophysical properties can be tuned by varying donor, spacer and the acceptor moieties. As effective electron donors, several ammonia derivatives such as triphenylamine (Tian et al. 2008; Wang et al. 2013; Sivanadanam

et al. 2015), diphenylamine (Tarsang et al. 2014; Venkateswararao et al. 2013), and substituted anilines (Komatsu et al. 2013; Michinobu et al. 2014) and fused heteroaromatic systems such as carbazole (Barpuzary et al. 2014; Choi et al. 2013), indole (Li et al. 2009.; Liu et al. 2014), phenothiazine (Chen et al. 2015; Wang et al. 2015), phenoxazine (Bae et al. 2015) and coumarine (Han et al. 2015; Seo et al. 2011), have been successfully utilized. In the molecular design, the choice of anchoring functionality is usually carboxylic acid but many other fascinating units such as phosphonate, sulphonate, nitro etc. have been tried as alternative anchoring units.

Further, it has been well-established that certain interesting structural units such as cyano acrylic acid and rhodanine-3-acetic acid can act as good acceptors due to their strong electron withdrawing nature and effective binding on the surface of mesoporous TiO_2 through carboxylic acid as an anchoring functionality (Ambrosio et al. 2012; Zhang and Cole, 2015). Recently, rhodanine and barbituric acid derivatives are shown to be effective acceptor/anchoring units mainly due to their efficient electron accepting behavior as well as effective binding on the surface of TiO_2 through NH, OH or SH functionality (Matsui et al. 2012; Hosseinzadeh et al. 2015). Typically, thiophene, benzene and its derivatives have been successfully utilized as π conjugation bridges in D-π-A type molecular design of many organic dyes due to their stability, good charge transporting ability, and tunable spectroscopic and electrochemical characteristics (Wan et al. 2012). Their presence in between the electron rich donor and electron withdrawing acceptor units not only enhances π conjugation but also increases the overall stability and rigidity of resulting structures.
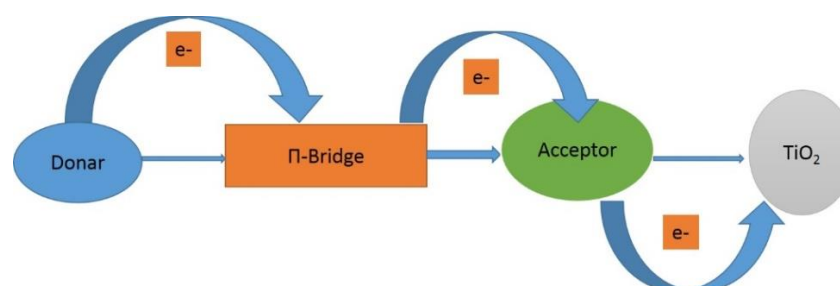
Fig 1.5: D-π-A model of a *n*-type metal-free organic chromophore

Amongst the aforementioned electron donor systems, *N,N* dimethylaniline and carbazole have been selected as electron donating moieties in the present work.

Eventually, the geometric structures of these donors play a significant role on the photovoltaic performance of the DSSCs. In effect, the dyes derived from the above said core systems are potential candidates for sensitizing DSSCs effectively, as they possess stable structure and favorable optical properties.

Chemistry of N,N-dimethyl aniline

N,N-Dimethyl aniline is a tertiary amine of aniline, consisting of a dimethyl amino group attached to a phenyl ring. The amino group attached to the phenyl ring plays an important role in the structural chemistry due to the ability of its lone pair of electron to interact with the π system of the benzene ring through *p-π* conjugation. Further, the two methyl substituents on the nitrogen atom along with its lone pair enhance the electron density on the phenyl ring of substituted aniline. Also, its electron donating capability is further enhanced due to its planar structure. The electronic structure of *N,N*-dimethylaniline is displayed in **Fig 1.6(a)**. A detailed account of literature survey pertaining to the dyes based on *N,N*-dialkylaniline core, as effective sensitizers, has been discussed in **Chapter 2**.

Chemistry of carbazole

The carbazole is a dibenzo-fused heterocyclic organic compound comprising a pyrrole ring fused between two benzene moieties. The presence of heterocyclic pyrrole ring in the system increases the electron-rich nature of carbazole. Further, carbazole is having higher thermal stability up to 240 °C. Also it can be attached to any other moiety to further enhance the ring thermal stability. In addition, the carbazole derivatives possess high charge carrying property, higher photoconductivity, and better chemical stability. The carbazole core can be easily functionalized at 3, 6 positions; also easy substitution on the nitrogen atom in the system is possible with a variety of functional groups permitting a better solubility and fine tuning of the electronic and optical properties (Thomas et al. 2015). The chemical and electronic structures of carbazole are displayed in **Figs 1.6(b)** and **(c)**. A detailed literature review reveals that a variety of carbazole based dyes have been successfully synthesized and employed in devices as efficient sensitizers, which has been elaborated in **Chapter 2**.
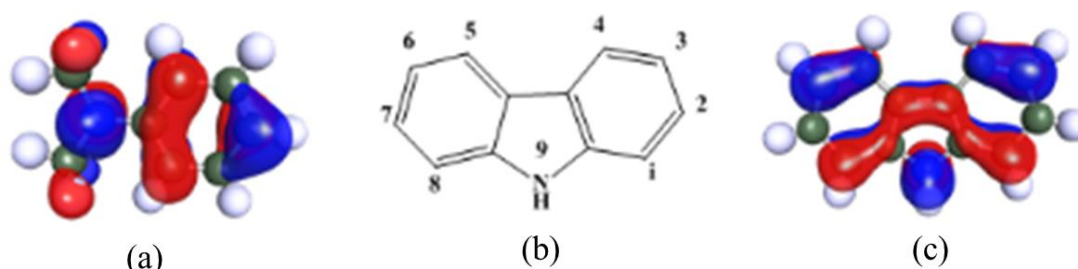
Fig 1.6: (a) Electronic structure of *N,N*-dimethylaniline, **(b)** Chemical structure of carbazole **(c)** Electronic structure of carbazole

Organic co-sensitizers for efficient DSSCs

Co-sensitization is an effective strategy generally used to enhance the photovoltaic performance of the DSSCs sensitized with efficient metal based/organic dye. Combining the organic co-sensitizer with a standard Ru (II) complex based sensitizer with broader and complementary light absorption spectra is expected to extend the light absorption ability of the cell from the UV-Vis to near-IR region of the solar spectrum (Chen et al. 2015). A brief account on the organic co-sensitizers and their performances in the DSSCs sensitized with Ru (II) complex, have been discussed in **Chapter 2**.

1.4.2.2 Dyes for NiO-based *p*-type DSSCs

Contrary to typical *n*-type DSSCs, whose operation principle is based on photo injection of excited electrons from dye to CB edge of TiO_2, in *p*-type DSSCs, the sensitizer excited-state decays by hole injection into the VB edge of the NiO. As discussed in above section, the molecular design strategy for *p*-type dyes is almost same, except the position of carboxylic acid that functions as anchoring group. Precisely, for better hole injection, the anchoring functionality should be on the donor unit. The most common design strategy for *p*-type dyes is D-π-A configuration and is shown in **Fig 1.7**. Generally, the ICT property of a D-π-A dye is strongly dependent on the electron-donating ability of the donor (D), the electron-withdrawing ability of the acceptor (A), as well as the electronic characteristics of the π-conjugated bridge. Consequently, the desired property can be tuned through chemical modification of each component. Till date, most common donor for *p*-type organic dyes is triphenylamine due to its excellent hole transporting ability. A detailed account of

literature reports on different *p*-type dyes with D-π-A configuration, along with their photovoltaic studies has been explained in **Chapter 2**.
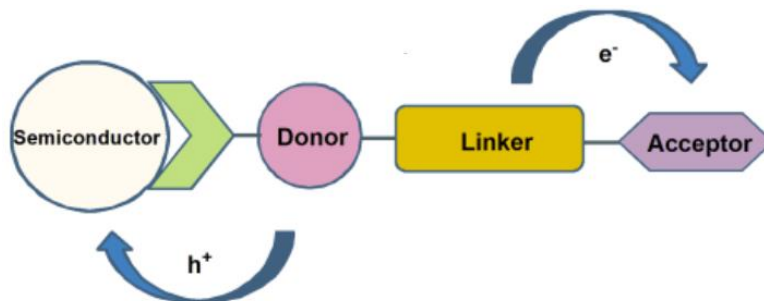
Fig 1.7: General configuration of a *p*-type DSSC (Qin et al. 2008)

1.4.3 Transparent conducting substrate

Apart from semiconductor oxide film, the transparent conducting substrates also play a vital role in deciding the DSSC performance. They function as a current collector and a support of the semiconductor layer in DSSCs.

High optical transparency allows natural sunlight to pass through to the beneath of the active material avoiding unwanted absorption of the solar spectrum. Also, it favors low electrical resistivity which reduces energy loss and facilitates electron transfer process. Although transparent conducting oxide ITO and FTO are widely used, they still appear to be increasingly problematic due to the following reasons:

- Limited availability and high cost of the rare earth element indium
- Sensitive to thermal treatment and pH environment
- Limited transparency in the near-infrared region, and mechanical brittleness

1.4.4 Electrolyte

The electrolyte is the key component of a dye sensitized solar cell. It functions effectively in transporting electrons in the cell. An efficient electrolyte works in the cell effectively with different roles:

- The photoexcited dye loses an electron before it reacts with the electrolyte.
- The oxidized dye molecule has to be reduced by the electrolyte rather than recombined with the electrons from the neighboring dye molecule.

- The reduced electrolyte reacts slowly with electrons in both TiO_2 and TCO layers.

- The reduction rate of the oxidized ion at the cathode is rapid.

The very critical constituent of the liquid electrolyte is a redox couple. The electrolyte used in DSSC mostly contains I^-/I_3^- redox ions; it functions as a charge carrier collecting electrons at the cathode and transporting electrons back to the dye molecules. The electrolyte is a neutral sink of I^- and I_3^- maintaining the redox potential in the bulk of the electrolyte *via* the fast redox reaction of the I^-/I_3^- pair.

1.4.5 Counter electrode

Low charge transfer resistance and high exchange current densities are the prerequisites of a material to be used as a counter electrode in DSSC because it is responsible for the reduction of the oxidized form of the charge mediator. Electrons arriving from the external circuit are transferred back to the redox electrolyte by the counter electrode. Since platinum (Pt) is an excellent catalyst for I_3^- reduction, it has been selected as the most suitable material for the counter electrode. But the recent studies have shown that carbon can be used as an alternative to Pt because it combines sufficient electrical conductivity and heat resistance as well as corrosion resistance and electrocatalytic activity for the I_3^- reduction.

1.5 CHARACTERIZATION OF DSSCs

A comprehensive characterization of materials, as well as fabricated device, is needed to fully understand and optimize the photovoltaic performance and their stability. One of the prominent device fabrication techniques is Blade coating, also known as doctor blading. It is a most commonly used processing method for the fabrication of large area films on rigid or flexible substances.

Normally, solar cell efficiency is determined by its current-voltage (*JV*) characteristics under standard illumination conditions. A standard solar spectrum of air mass 1.5 (AM 1.5) with an intensity of 1000 W/m^2 also referred to as 1 sun, is generally used for solar cell characterization. The illumination conditions are provided by a calibrated xenon lamp source. The current-voltage characteristics are monitored under illumination by varying an external load from zero loads (short-

circuit condition) to infinite load (open-circuit condition). From the experiments, IPCE characteristic curves are obtained in order to reveal how efficiently light of a specific wavelength is converted to current. Generally, EIS studies are performed to understand carrier transportation behavior and interfacial charge recombination processes in fabricated devices using the synthesized dyes. Currently, EIS analysis is one of the most powerful techniques used to obtain additional information, mainly interfacial reactions of photoexcited electrons in DSSCs.

The spectral techniques like FTIR, NMR, Mass spectroscopy followed by elemental analysis are largely employed to characterize the newly synthesized organic molecules. Further, the UV-Vis and fluorescence spectroscopy are generally used to investigate photophysical properties of dyes/sensitizers. Basically, for efficient light harvesting, the dye used in the device should possess good absorption as well as emission in the UV-Vis region. From these studies, absorption maxima, emission maxima, molar extinction coefficient, Stokes shift and optical band gaps can be determined. Normally, electrochemical studies, particularly CV study is to be carried out in order to evaluate electrode potentials as well as electronic distribution in its FMO energy levels of dyes/sensitizers. Eventually, the position of HOMO and LUMO energy levels of the dyes play a vital role in charge injection and dye regeneration.

1.6 THEORETICAL INVESTIGATIONS

TURBOMOLE is a quantum chemical program package, developed by Prof. Dr. Reinhart Ahlrichs at the University of Karlsruhe. It is an extremely optimized software package for large-scale quantum chemical simulations of clusters, molecules, and periodic solids (Furche et al. 2014). Turbomole utilizes Gaussian basis sets and specializes on predictive electronic structure methods with the admirable cost to performance characteristics. The methods include time-dependent density functional theory (TDDFT), explicitly correlated coupled cluster (CC) methods. The aforementioned methods are combined with ultra-efficient and numerically stable algorithms such as resolution-of-the-identity, integral-direct and Laplace transform methods.

1.7 BROAD OBJECTIVES OF PRESENT WORK

Till date, several organic chromophores have been explored as sensitizers/co-sensitizers for DSSC application. Indeed, design and synthesis of efficient dyes and the identification of parameters limiting the performance of dye sensitized solar cell are really challenging tasks. By modifying the dye structure, one can alter the optical properties as well as the energy levels, which affect largely on the light harvesting ability and different charge transfer processes in the cell. For designing sensitizers various electron donating donors such as triphenylamines, diphenylamines, substituted anilines, carbazoles, indoles, phenothiazines, phenoxazines and coumarins have been successfully utilized. Among the aforesaid donor system, *N,N*-dimethylaniline and carbazole have been selected as electron donor in the present study. A detailed account of the literature survey on organic chromophores based on *N,N*-dimethylaniline and carbazole has been discussed in **Chapter 2**. Based on the literature reports, it has been thought of designing new *n*-and *p*-type organic chromophores as effective sensitizers/co-sensitizers for DSSC application. Further, it has been planned to synthesize newly designed molecules using standard synthetic methods. Finally, it has been intended to fabricate DSSCs using newly developed chromophores, keeping semiconductor and electrolyte unchanged in the cell. It has been also contemplated to study the effect of the structure of chromophores on device parameters. It has been hoped that new sensitizers would lead to improvement in efficiency and give valuable information about structural dependence on the efficiency of DSSCs. The next chapter deals with precise objectives, derived from a detailed literature survey and design of new organic sensitizers/co-sensitizers based on *N,N*-dimethylaniline and carbazole systems.

1.8 THESIS STRUCTURE

The entire thesis has been divided into six chapters. **Chapter 1** outlines a brief introduction to photovoltaics, followed by a brief account of DSSC's. Also, it covers description on *n-/p*-type DSSCs. Further, it explains various components of DSSC's and their role in the efficient functioning of the cell. It also involves the broad objectives of the work. **Chapter 2** includes a review of literature reported on design

and synthesis of various *N,N*-dimethylaniline, carbazole and triphenylamine based sensitizers consisting of different electron donors, π-spacers and acceptor units. Further, it includes scope and objectives of the present research work, arrived at on the basis of detailed literature survey. Finally, it describes the design of seven new series comprising twenty-one *n*-type and three *p*-type organic dyes as sensitizers/co-sensitizers for DSSC application. The experimental protocols leading to the synthesis of twenty-four new organic sensitizers have been elaborated in **Chapter 3**. In addition, their structural characterization has been discussed in detail. **Chapter 4** describes a detailed account of investigation of optical and electrochemical properties of newly synthesized dyes. It also includes their theoretical investigations using DFT and TDDFT simulations. **Chapter 5** illustrates a detailed DSSC fabrication studies (both *n*- and *p*-type) using the newly synthesized dyes as sensitizers/co-sensitizers. Also, results of their photovoltaic performance have been discussed in this chapter. Further, it covers estimation of electron lifetime as well as charge transport phenomenon of fabricated devices by EIS studies. Finally, **Chapter 6** includes the summary of the entire work and important conclusions as well as the outcome of the research work.

LITERATURE REVIEW, SCOPE AND OBJECTIVES AND DESIGN OF NEW SENSITIZERS/CO-SENSITIZERS

Abstract:

Chapter 2 covers a review of the reported literature on design, synthesis and performance of both n-type and p-type organic sensitizers/co-sensitizers used in DSSCs. Further, it comprises scope and objectives of the present research work, arrived at on the basis of the literature survey. Finally, design of six new series of n-type and one series of p-type sensitizers with various structural configurations has been described.

2.1 INTRODUCTION

The quest for green and cost-effective energy generation has led to enhanced attention towards research on organic photovoltaics. In this field, dye-sensitized solar cells (DSSCs) are widely investigated due to their promising performance, eco-friendly and economically viable nature (Grätzel 2001, Hagfeldt et al. 2010). Typically, DSSCs consists of four major components, *viz.* mesoporous photo active anode (TiO$_2$), sensitizer (dye), electrolyte (I_3^-/I^-) and passive cathode (Pt electrode). Among them, the dyes play a crucial role as a photosensitizer in the process of DSSCs, which include sunlight harvesting and electron injection from the excited dye (LUMO level) into the CB edge of TiO$_2$ (Hardin et al. 2012). Several aromatic/heteroaromatic organic dyes were designed and investigated as potential *n*-type sensitizers/co-sensitizers in DSSCs with good *PCE* (Mishra et al. 2009, Ning et al. 2010). Also, the effect of their structure on device characteristics was investigated in depth.

Even though *n*-type organic chromophores possess good photophysical properties, the photovoltaic performance was found to be lower than well-established Ru (II) dyes. Eventually, the co-sensitization was developed as an effective technique. In this technique, it is possible to enhance the photovoltaic performance of DSSCs by incorporating the merits of both with Ru (II) complex dyes and metal-free organic sensitizer into the same fabricated device and thereby facilitating the cell to harvest a maximum number of photons from light.

Besides DSSCs sensitized with *n*-type chromophores, *p*-type systems comprising the photoactive cathode, *i.e.* NiO as well *p*-type organic sensitizers can also be envisioned for effective solar energy harvesting. Indeed, the development of *p*-type DSSCs can provide an access to the design and development of new sandwiched 'tandem' dye-sensitized solar cells consisting of both photoactive anode and cathode. Obviously, such tandem cells make use of *n*-type as well as *p* type organic sensitizers in a single device. It is vital that, as per the Shockley-Queisser limit, the upper theoretical limit of *PCE* for the solar cell containing only one photoactive semiconductor, while the limit for a solar cell carrying two photoactive semiconductors is 43%. Thus, the *p*-type photoactive cathode is a missing key preventing the construction of tandem dye-sensitized solar cells (Kubo et al. 2004, Cui et al. 2014)

In the following section, a brief account on literature reports on various *N,N*-dimethylaniline and carbazole based metal-free dyes employed as *n*-type sensitizers as well as triphenylamine based dyes as *p*-type sensitizers, has been discussed. Also, literature survey on interesting organic dyes derived from various aromatic systems with different design strategies, as co-sensitizers has been dealt in the following section. Some of the references on standard Ruthenium complex based chromophores have been also explained.

2.2 LITERATURE REVIEW

2.2.1 Ruthenium (II) complexe based chromophores
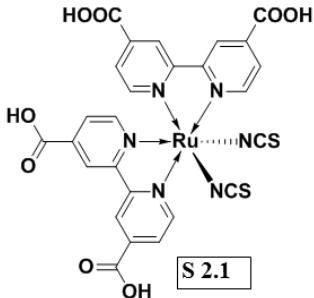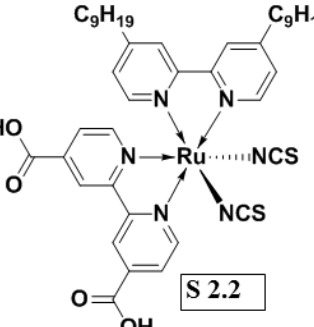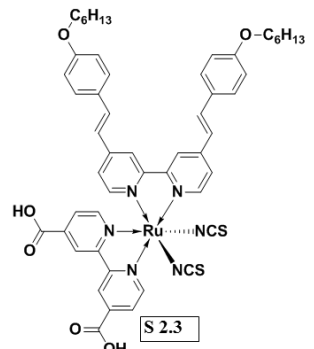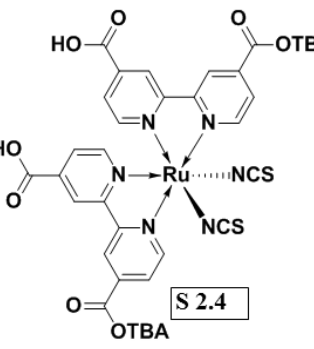
Ru (II) complexes are benchmark dyes for serving as excellent photo sensitizers and boosting overall photovoltaic efficiency due to their favorable electrochemical properties, highly stable oxidized states and wide absorption spectrum covering visible and near IR region. The Ru(II) dye can inject photoexcited electrons into the TiO_2 semiconductor layer efficiently *via* carboxylate groups which firmly attach to the surface of TiO_2 as an electron transfer channel, and link to the bipyridyl moiety to lower the energy of the ligand *p-n* orbital, Since the molecular electronic transition is a metal-to-ligand charge transfer, this structure energetically favors in the electron injection process.
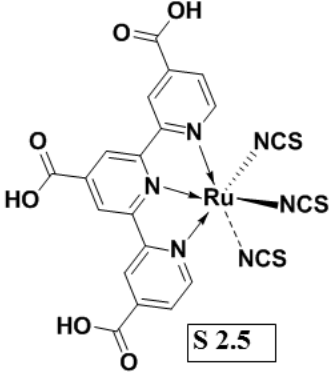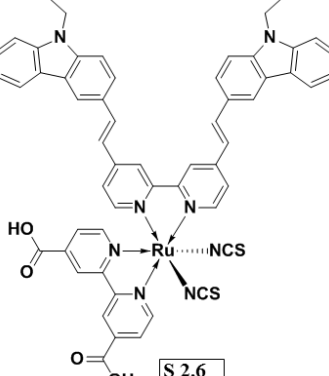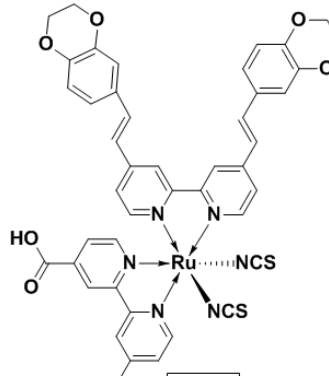
Till date, the Ru complexes are exploited as excellent photosensitizers in the construction of DSSCs due to their good optical and electrochemical properties. A wide variety of the Ruthenium (II) complexes has been reported in the literature in order to further improve the photovoltaic performance and durability of the device. At present, the DSSCs based on standard Ru(II)-polypyridyl complexes, for instance, **S2.1-S2.7** as active sensitizers, have displayed optimum overall *PCE* exceeding 10% under standard 1.5 G solar light illumination (**Table 2.1**).

The performance of dye **N3 (S2.1)** as sensitizer was almost unparalleled until the emergence of black dye (**S2.5**). Nazeeruddin et al. first reported the synthesis of a class of black dye which displayed the panchromatic sensitization character over the entire visible range extending from the near-IR region up to 920 nm. This expansion in the absorption spectrum leads to increase in maximum J_{SC} of DSSCs to be larger than 20 mA.cm^{-2}. However, the optical extinction coefficient of the Ru (II) dye is lower which requires thicker TiO_2 films to attach the sufficient quantity of the dye molecules on the surface of the photoanode. Further, for efficient charge injection, choosing an appropriate anchoring group is vital. For example, di-anchoring Ru(II) dye **N719** displayed better PCE than the protonated **N3** dye with quadri anchoring units, which is ascribed to the effect of the bound dye on the energy of TiO_2 conduction band. Furthermore, a significant advantage of these dyes lies in the metal-ligand charge transfer transition through which the photoelectric charge is injected into TiO_2 surface, which brings out superior light harvesting properties. In Ru complexes, this charge transfer takes place at a much faster rate than the back reaction, wherein the electron recombines with the oxidized dye molecule rather than flowing through the circuit. Moreover, they are chemically stable and durable.

Though ruthenium based dyes have provided a relatively high efficiency, there are several drawbacks like high cost, limited amount of noble metals availability, the complicated synthesis and purification steps and environmental pollution. To address these issues, metal-free organic dyes have been investigated and applied in DSSCs to replace ruthenium based dyes.

Table 2.1: Ruthenium (II) complex based sensitizers

Reference	Sensitizer	J_{SC} (mA.cm^{-2})	V_{OC} (V)	*FF*	*PCE* (%)
Nazeeruddin et al. (1993)		16.80	0.85	0.77	11.03
Wang et al. (2003)		14.6	0.72	0.69	7.3
Wang et al (2005)		14.61	0.71	0.67	7.0
Ito et al. (2005)		18.7	0.79	0.71	10.6

Chilba et al. (2006)		20.90	0.73	0.72	11.0
Cheema et al. (2014)		19.58	0.71	0.73	10.19
Cheema et al. (2014)		19.67	0.69	0.70	9.50

2.2.2 *n*-Type metal-free sensitizers

In recent years, the metal-free organic dyes have received massive interest due to their reasonable *PC*E compared to standard Ru (II) complexes. They possess several advantageous over the Ru (II) dyes, such as easy availability, design versatility, high molar extinction coefficients, and cost effectiveness in their synthesis. As a result, a wide variety of organic dyes were designed and developed as effective photosensitizers

in DSSCs (Mishra et al. 2009; Ooyama and Harima, 2009; Ning et al. 2010). Also, the effect of their structures on device characteristics was investigated in depth. A lot of efforts have been dedicated to the design and improvement of new metal-free organic dyes as potential photosensitizers for DSSC application.

In the literature, various strategies have been reported for dye designing. Amongst them, push-pull approach, wherein an electron rich donating and electron deficient withdrawing scaffolds connected through a π-spacer unit, is considered to be one of the most promising and successful architectures to improve the photovoltaic performance of DSSCs. In such dyes, photo-induced ICT (Intramolecular charge transfer) phenomenon can easily be controlled and their photophysical properties can be tuned by varying donor, spacer and the acceptor moieties. Several organic dyes based on electron rich triphenyl amine, diphenyl amine, aniline derivatives and fused heteroaromatic compounds such as carbazole, indole, phenothiazine, phenoxazine, perylene and cyanine systems have been reported as good sensitizers with improved photon conversion efficiency when used in DSSCs.

A survey of the pertinent literature reveals that the design strategies such as D-A, D-π-A, D-π-A-π-A, D-D-π-A and A-π-D-π-A configurations are being widely used for developing new *n*-type metal-free sensitizers with improved efficiency. These types of architecture attracted much attention mainly due to an efficient charge separation and easy movement of electron from donor to the acceptor moieties in the sensitizer. Moreover, such molecules exhibit an interesting optical properties owing to intramolecular charge transfer (ICT). Among the aforesaid organic electron donor systems, *N, N*-dimethyl aniline and carbazole systems are considered to be excellent sensitizers, as reported in the literature. Consequently, a brief account of literature review pertaining to these donor systems is described below.

2.2.2.1 *N,N*-Dialkylaniline based sensitizers

N,N-Dialkyl aniline is a tertiary amine substituted derivative of aniline, consisting of a dialkylamino group attached to a phenyl ring. In DSSCs, *N,N*-dialkyl aniline based dyes act as good donors because of their favorable electronic structure. In their structure, the amino group attached to the phenyl ring plays an important role in the structural chemistry due to the ability of its lone pair of electron to interact with the

π system of the benzene ring through *p-π* conjugation. Moreover, its electron donating capability is further enhanced due to its planar structure. Numerous novel π-conjugated systems based on *N,N*-dialkyl aniline moiety have been designed and synthesized as efficient sensitizers in DSSCs.

Hara et al. (2003) reported three novel photosensitizers (**S 2.8** to **S 2.10**) based on simple *N,N*-dimethyl aniline donor unit connected to a strong electron acceptor/anchoring cyanoacetic acid forming a D-π-A architecture. **S 2.10** showcased overall efficiency of 6.8 % than other two dyes. Later in 2005, they introduced a thiophene moiety to **S 2.8** as a π-spacer, as shown in **S 2.11**, which displayed an optimum *PCE* of 5.9 %.
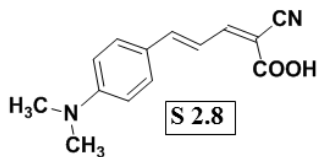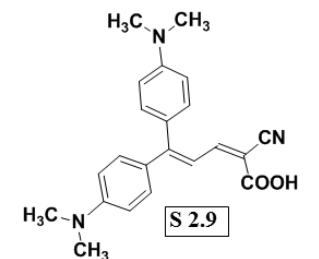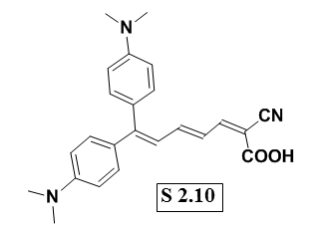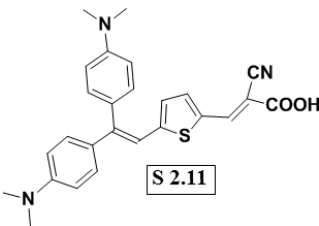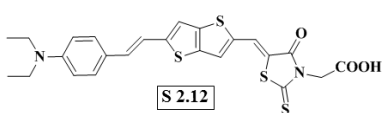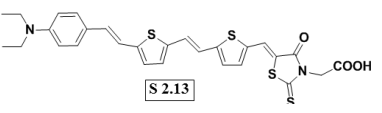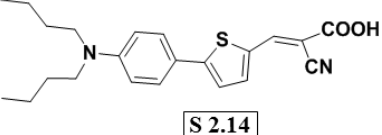
Similarly, Li and his co-workers in 2006 reported the two new organic sensitizers, *i.e.* **S 2.12** and **S 2.13**, with D-π-A architecture carrying diethylaniline as a donor moiety and rhodanine-3-acetic acid as an acceptor as well as anchoring group. The new molecules displayed optimum *PCE* of 6.2% and 3.9%, respectively.
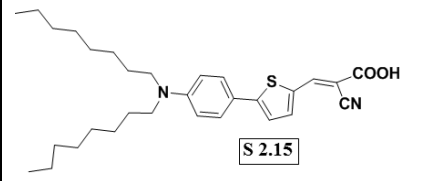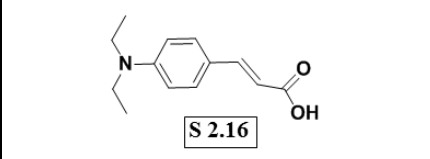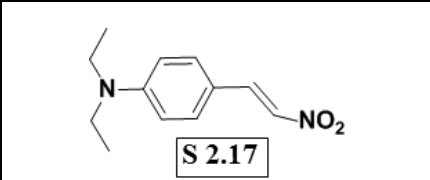
In an attempt to understand the influence of alkyl groups on the efficiency of the *N,N*-disubstituted aniline based photosensitizer, Zhang et al. (2013) synthesized two D-π-A configured organic dyes carrying *N,N*-dihexylaniline (**S 2.14**) and *N,N*-dioctylaniline (**S 2.15**) as electron donors attached to cyanoacetic acid moiety through thiophene π-spacer. The **S 2.15** exhibited higher *PCE* of 5.3 % than **S 2.14**, mainly due to reduction in unfavorable dye-aggregation.

Subbaiah and his coworkers (2013) reported that an organic chromophore, **S 2.16** with D-A architecture carrying *N,N*-diethyl aniline as a donor unit linked to strong electron anchoring carboxylic acid without any additional electron accepting unit, displayed an overall *PCE* of 1.4 %. Later in 2016, they introduced nitro group (**S 2.17**) as anchoring unit in **S 2.16** by replacing carboxylic acid group and but they found that **S 2.17** showed poor photovoltaic performance.

Further, it has been observed that, the photovoltaic performance of *N,N*-dialkylaniline based dyes as sensitizers greatly depends on their molecular geometry. A brief account of literature reports on *N,N*-dialkylaniline based donors connected to varied electron acceptor/anchoring units has been summarized in **Table 2.2**.

Table 2.2: Organic sensitizers based on *N,N*-dialkyl aniline for *n*-type DSSCs

Reference	Sensitizer	J_{SC} (mA.cm^{-2})	V_{OC} (V)	*FF*	η (%)
Hara et al. 2003	S 2.8	10.4	0.71	0.74	5.5
Hara et al. 2003	S 2.9	9.9	0.74	0.74	5.4
Hara et al. 2003	S 2.10	12.9	0.71	0..74	6.8
Hara et al. 2005	S 2.11	12.5	0.68	0.69	5.9
Li et al. 2006	S 2.12	15.23	0.56	0.73	6.23
Li et al. 2006	S 2.13	10.64	0.52	0.70	3.87
Zhang et al. 2013	S 2.14	11.14	0.62	0.72	5.0

Zhang et al. 2013	S 2.15	11.40	0.62	0.75	5.3
Subbaiah et al. (2013)	S 2.16	2.83	0.67	0.62	1.4
Subbaiah et al. (2016)	S 2.17	1.1	0.52	0.51	0.6

2.2.2.2 Carbazole based photosensitizers

The carbazole is a tricyclic heteroaromatic compound comprising a pyrrole ring fused in between two benzene moieties. The presence of heterocyclic pyrrole ring in the system increases the electron rich nature of carbazole. They are known for good thermal and photochemical stability with attractive optical properties. The carbazole unit has been widely accepted as an electron donor mainly due to its excellent hole transporting property with wide energy gap and facile functionalization at different positions (Venkateswararao et al. 2013; Wang et al. 2011). Several new metal-free carbazole based sensitizers have been designed and synthesized till date. Some of the literature reports on carbazole based organic chromophores including their photovoltaic parameters, are summarized in **Table 2.3**,

Koumura et al. (2006) reported a new D-π-A configured carbazole based dye (**S 2.18**), wherein carbazole ring acts as a donor, cyanoacetic acid functions as an acceptor unit and regio-regular hexyl substituted thiophene bridges serve as a π-linker. It displayed a better photovoltaic performance with an optimum *PCE* of 7.7%.

Tang et al. (2010) designed and synthesized a new D-D-π-A configured carbazole based organic dye (**S 2.19**). It comprises triphenylamine as donor scaffold, two units of carbazole as auxiliary donors and cyanoacetic acid as an electron acceptor/anchoring unit. In addition, they investigated the role of co-absorbent CDCA

on the photovoltaic performance of DSSCs. They obtained an enhanced photovoltaic performance in the presence of co-absorbent CDCA.

Ramkumar et al. (2012) successfully synthesized a D-$(\pi$-A$)_2$ organic dye (**S 2.20**) based on electron rich carbazole as donor linked to cyanoacetic acid as electron acceptor/anchoring unit *via* cyanovinyl biphenyl unit as a π-linker. The dye exhibited an overall *PCE* of 2.37 %. Later in 2013, they introduced cyanovinyl thiophene unit in **S 2.20** as π-spacer (**S 2.21**) which displayed increased photovoltaic performance.

Gupta and his coworkers (2014) reported a new organic chromophore (**S 2.22**) with A-π-D-π-A architecture, wherein carbazole is connected to two cyanoacetic acid units through π-spacer thiophene ring. The dye showed *PCE* of 3.8 % with J_{SC} of 8.90 mA.cm^{-2}, and V_{OC} of 0.58V.

In an effort to decrease the dye aggregation on the surface of TiO$_2$, Lin and his coworkers (2014) synthesized Y-shaped organic chromophore (**S 2.23**) with D-π-(A)$_2$ architecture and investigated its photovoltaic properties. In their research work, they introduced two units of cyanoacetic acid as acceptor/anchoring functionality, which resulted in better J_{SC} value than the dye reported by Koumura et al in 2006. Further, the experimental results revealed that, the dye **S 2.23** possess a suitable HOMO-LUMO energy level, which is required for efficient charge injection into the CB edge of TiO$_2$ as well as dye regenration from eletrolyte system.

Soni et.al. (2015) reported two novel dyes with D-π-A architecture carrying carbazole as an electron donor, vinylene-phenylene as π-bridge with rhodanine-3-acetic acid (**S 2.24**) and cyanoacetic acid (**S 2.25**) as electron withdrawing/anchoring groups. A higher *PCE* of 9.0 % has been achieved using cyanoacetic acid as an acceptor (**S 2.25**) with a cobalt based redox shuttle, while a PCE of 7.1% has been obtained with triiodide electrolyte when employed it as a photosensitizer in DSSCs.
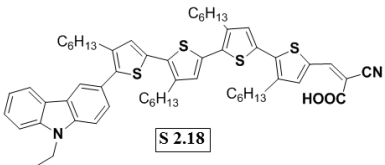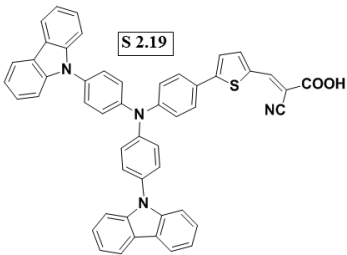
Salimi Beni et al. in 2015 reported three new D-A type carbazole based organic (**S 2.26- S2.28**) dyes carrying barbituric acid, thiobarbituric acid and thiazolidine-2,4-dione as electron anchoring groups to study the effect of anchoring groups on photovoltaic performance. The dye **S 2.28** anchored with thiazolidine-2,4-dione showed the maximum efficiency of 2.16%.
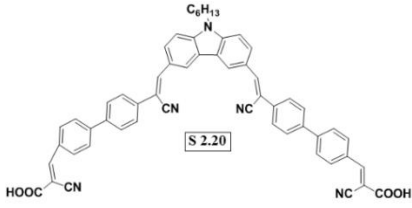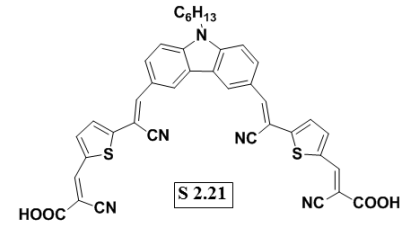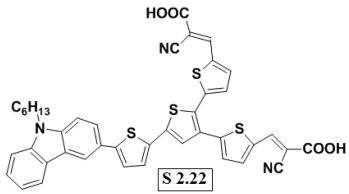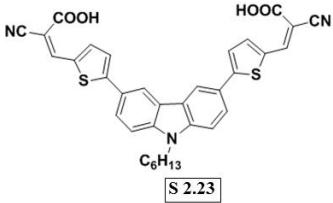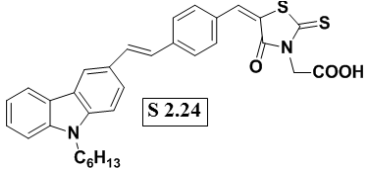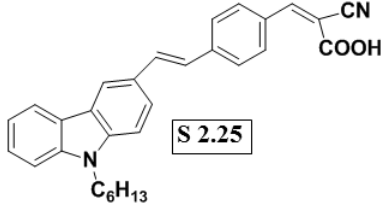
Later, in 2016 Wang and his co-workers designed and synthesized a simple D-π-A configured organic chromophore (**S 2.29**), which contains a carbazole as a donor and cyanoacetic acid as an acceptor/anchoring unit, separated by an indole ring as π-linker. The cell fabricated with **S 2.29** displayed an exceptional thermal and photochemical stability.
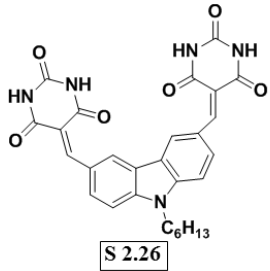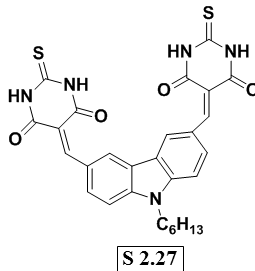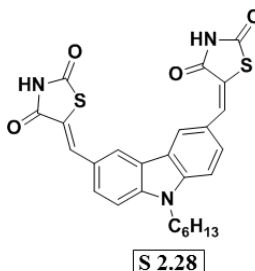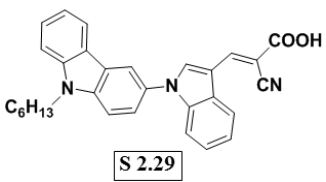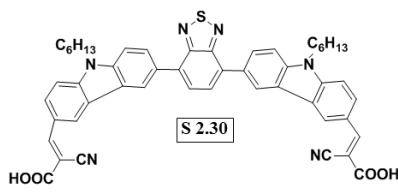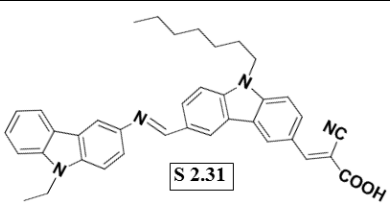
To avert dye aggregation and to reduce charge recombination process, Murali and his coworker in 2016 designed a bent shaped organic sensitizer (**S 2.30**) with A-D-π-D-A architecture. In the design, carbazole moiety acts as an electron donor, cyanoacetic acid functions as an electron acceptor/anchoring unit and 2,1,3-benzothiadiazole behaves as a π-spacer. The dye displayed an overall *PCE* of 4.35 %.
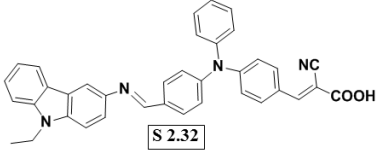
Saritha et al. (2017) reported two new D-D-π-A type carbazole-based dyes (**S 2.31-2.32**). In the design strategy, *N*-hexyl carbazole and triphenylamine were introduced as donors as well as a π-spacer units, *N*-ethyl carbazole as an auxiliary donor and cyanoacetic acid as an anchoring group. These dyes displayed optimum efficiency of 3.12 % and 2.12 %, respectively.

Table 2.3: Organic sensitizers based on carbazole for *n*-type DSSCs

Reference	Sensitizer	J_{SC} (mA.cm^{-2})	V_{OC} (V)	*FF*	η (%)
Koumura et al. (2006)		14.0	0.74	0.74	7.7
Tang et al. 2010		8.45	0.75	0.70	4.44

Ramkumar et al. (2012)		5.18	0.76	0.51	2.37
Ramkumar and anandan (2013)		7.64	0.66	0.68	4.04
Lin et al. 2014)		16.98	0.63	0.68	7.28
Gupta et al. (2014)		8.90	0.58	0.74	3.8
Soni et al. (2015)		8.4	0.59	0.48	2.4
Soni et al. (2015)		18.3	0.72	0.67	9.0

Salimi Beni et al. 2015	S 2.26	2.45	0.50	0.65	0.80
Salimi Beni et al. 2015	S 2.27	0.92	0.49	0.67	0.31
Salimi Beni et al. 2015	S 2.28	5.80	0.56	0.66	2.16
Wang et al. 2016	S 2.29	4.18	0.67	0.74	2.09
Murali et al. (2016)	S 2.30	7.51	0.76	0.76	4.35
Saritha et al. (2017)	S 2.31	8.09	0.656	0.50	3.12

Saritha et al. (2017)		7.76	0.58	0.50	2.63

2.2.2.3 Co-sensitizers for Ru (II) based DSSCs

Despite the high absorptivity of metal-free organic dyes, their PCE values are rather modest when compared to those of Ru (II) complexes, mainly due to their relatively narrow absorption profile in the visible region. In order to achieve enhanced photovoltaic performance, the dye should possess broad and intense absorption characteristic profile in the region of UV-Visible and near IR. The co-sensitization technique is one of the effective strategies generally used to obtain a broad absorption that extends throughout the UV-visible and near IR region. This technique makes use of a combination of dyes which complement each other in their absorption properties and do not interfere with the sensitization properties of the other dye.

The metal-free dyes, to be used as co-sensitizers in DSSCs, should possess some key requirements such as (i) the organic dyes should not adsorb completely with the main sensitizer in order to suppress the dye aggregation on the surface of mesoporous TiO_2, (ii) the co-sensitizer should possess large molar extinction coefficient below λ_{abs} of 450 nm or near IR region. (iii) the co-sensitizer should be able to form a compact monolayer on the surface of TiO_2 and thereby reducing the electron recombination at the TiO_2/dye/electrolyte interface (Han et al. 2012. Singh et al. 2013).

In the literature, a wide range of design strategies have been reported for the development of effective organic co-sensitizers which include D-A, D-π-A, D-D-π-A, etc. Among them, D-π-A strategy is gaining much interest now. It involves an extension of the π-electron delocalization in the dye molecule to improve its molar absorptivity coefficient. Accordingly, incorporation of conjugated heteroaromatic systems such as carbazole, indole, phenothiazine, and phenoxazine in the organic entities has proven to be an effective design strategy for extending the π-conjugation in the molecules and thereby enhancing their molar absorptivity (Mishra et al. 2010,

Hagfelt et al. 2010, Wu and Zhu 2013). Some of the important literatures pertaining to organic co-sensitizers are summarized in **Table 2.4**.

Table 2.4: Reported metal-free co-sensitizers with improved efficiency

Reference	Co-sensitizer	Sensitizer	J_{SC} (mA.cm^{-2})	V_{OC} (V)	*FF*	*PCE* (%)
Zhang et al. (2013)	**S 2.14**	Black dye	19.53	0.65	0.70	8.9
Zhang et al. (2013)	**S 2.15**	Black dye	22.36	0.71	0.73	11.6
Luo et al. (2016)	**S 2.33**	N719	17.673	0.736	0.66	8.60
Luo et al. (2016)	**S 2.34**	N719	17.628	0.758	0.67	8.95
Saritha et al. (2017)	**S 2.31**	N719	19.33	0.74	0.47	8.01

Zhang et al. in 2013 designed and synthesized two new organic dyes (**S 2.14 - 2.15**) as effective co-sensitizers in DSSCs sensitized with high performing black dye. The device co-sensitized with the dye (**S 2.15**) displayed better *PCE* of 11.6% with improved photovoltaic parameters than black dye alone. This improved photovoltaic performance of the device can be attributed to the fact that, the co-sensitizer (**S 2.15**) in the device sufficiently suppressed the dye aggregations.

Luo and his coworkers reported two new simple D-π-A configured organic dyes as effective co-sensitizers for **N719**-based DSSCs. In their design, the hexyloxy-substituted phenyl ring as an electron donor, cyanoacetic acid as an electron acceptor/anchoring unit with thiophene (**S 2.33**) or furan (**S 2.34**) as the π-spacers were used. **Fig 2.1** shows the chemical structures of **S 2.33** and **S 2.34**. In their studies, both co-sensitizers showcased higher photovoltaic performance than the cell fabricated with **N719** dye alone.
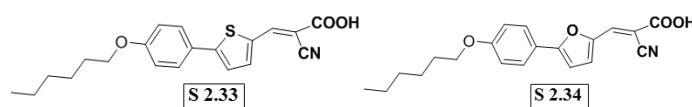
Fig 2.1: Structures of **S 2.33** and **S 2.34**.

Saritha et al. in 2017 reported two new D-D-π-A configured carbazole-based dyes **S 2.31-2.32**) as effective co-sensitizers for **N719**-based DSSCs. The dye (**S 2.31**) displayed improved PCE of 8.01% with higher J_{SC} value of 19.33 mA.cm^{-2} than that of **N-719** alone. The results indicated that, the co-sensitizer carrying *N*-hexyl carbazole showed better photovoltaic performance than the dye with triphenylamine as a donor system. Here, the improved efficiency is mainly due to its better dye matching with Ru chromophore.

2.2.3 Metal-free *p*-type sensitizers

Till date, as discussed above, the majority of the investigations in the area of DSSCs on their experimental as well theoretical studies are centered upon the sensitization by *n*-type organic semiconductors for DSSCs consisting of an active photoanode, *i.e.* TiO$_2$ and a passive cathode made of a platinum film. In fact, regular DSSCs are based on dyes sensitized upon *n*-type semiconductor such as TiO$_2$. However, the parent *p*-type systems comprising a photoactive cathode, *i.e.* sensitized NiO film can also be envisioned for effective solar energy harvesting (Odobel et al., 2010, 2012, 2013). Indeed, the development of *p*-type DSSCs can provide an access to the design and development of new sandwiched 'tandem' dye-sensitized solar cells consisting of both photoactive anode and cathode (He et al. 1999, 2000; Nakasa et al. 2005; Gibson et al. 2009; Nattestad et al. 2010; Farré et al. 2017). Manifestly, such tandem cells make use of *n*-type as well as *p* type organic sensitizers in a single device. It is vital that, as per the Shockley-Queisser limit, the upper theoretical limit of *PCE* for the solar cell containing only one photoactive semiconductor under irradiation of AM 1.5G sunlight is 30%, while the limit for a solar cell carrying two photoactive semiconductors is 43%. Thus, the efficient *p*-type DSSC is a missing key element preventing the construction of tandem dye-sensitized solar cells. From a chemist point of view, the exploration of such systems is quite essential to investigate the parameters governing the photovoltaic performance, which is equally important for the rational design of highly efficient tandem type solar cells as a future demand. A thorough literature survey reveals that there are few reports on metal-free *p*-type sensitizers, but till date, the reported efficiencies for *p*-type DSSCs are much lower than those of *n*-type DSSCs (Mishra et al., 2009; Yen et al., 2010).

In recent years, most of the reported work has been focused on D-π-A configured design for developing *p*-type sensitizers owing to their effective photoinduced intramolecular charge transfer phenomenon (Morandeira et al., 2005; Borgström et al., 2005; Mori et al., 2008; Zhu et al., 2014). From the last two decades, several different dyes derived from coumarin, thiophene, perylene imides, porphyrins and erythrosine based chromophore have been reported as *p*-type sensitizers for generation of cathodic photocurrent in NiO based DSSCs (Odobel et al., 2010, 2012, 2013). Some of the selected references have been summarized in **Table 2.5**.

Qin et al. (2008) for the first time demonstrated a successful model for the design of efficient dyes for *p*-type DSSCs. It's theoretical investigation by DFT calculations showed the LUMO is localized more on the electron difficient substituents located at the extremity of the dye. The *p*-type DSSC sensitized with dye **S 2.35** shows the efficiency of 0.08% when fabricated with NiO as a photocathode. Later, Li et al. (2010) achieved the overall efficiency of 0.15% with the same dye and photocathode.

Qin et al. (2009), in their pioneer work, introduced phenylene group to triphenylamine based D-π-A dye (**S 2.35**) as π-spacer to obtain a new dye (**S 2.36**), which on sensitized with NiO photocathode obtained an efficiency of 0.09%. Later, in 2010, they reported two new D-π-A architecture organic chromophores derived from **S 2.35** dye as effective sensitizers for *p*-type DSSC. The design strategy involves triarylamine core carrying a carboxylic group as hole donating donor, and various electron accepting groups such as tri-cyanovinylene (**S 2.37**) and 1, 3-diethyl-2-thiobarbituric acid (**S 2.38**) as the electron acceptor moieties. Further, they investigated the effect of electron withdrawing groups on the photophysical and electrochemical properties, as well as the photovoltaic performance of the dyes.

Yen et al. (2011) reported the synthesis and fabrication studies of new D-π-A arylamine-based sensitizers (**S 2.39**) for *p*-type DSSC. According to the authors, the best conversion efficiency reached 0.1%, while sensitizers with two anchoring carboxylic acids resulted in improved photovoltaic performance.

Ji and his coworkers (2011) reported the design and the synthesis of a D-π-A structured metal-free sensitizer(**S 2.40**); the dye design involves triarylamine core
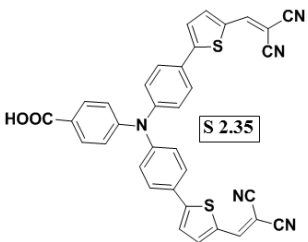
carrying two carboxylic groups as a hole donating donor, and ethoxythiophene as π-linker. The dye displayed an optimum efficiency of 0.060%.
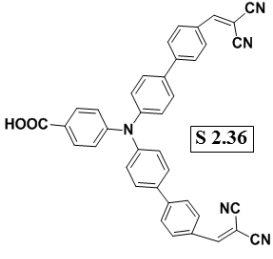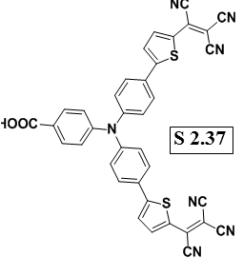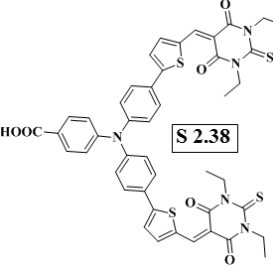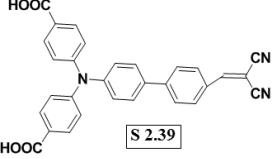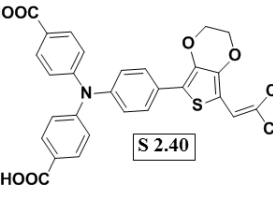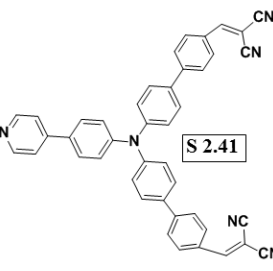
Two new organic chromophores, **S 2.41** and **S 2.42** obtained by modifying the **S 2.36** dye have been shown to be better sensitizers than **S 2.35** (Cui et al. 2013). The new D-π-A configured dyes contain pyridine and 4-phenylpyridine as anchoring groups linked to triphenylamine donor as shown in the structure. The detailed investigation demonstrates that carboxylic acid groups in **S 2.35** may have an effect on the negative shift of the valence band edge of NiO induced by surface protonation, which lowers the hole-injection process and the device photovoltage, while the 4-phenylpyridine ring works effectively without this problem to give an overall efficiency of 0.16%.
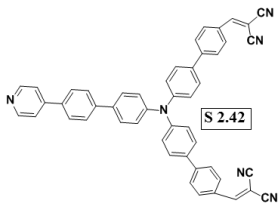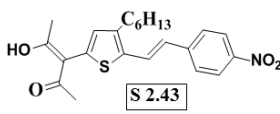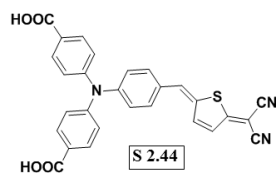
Warnan et al. (2014) reported the synthesis and the device fabrication studies of a thiophene based *p*-type DSSC (**S 2.43**). In the new design, they introduced hexyl-thiophene as a donor, nitrophenyl as an acceptor and acetylacetone as an anchoring group. It has given an efficiency of 0.03%.

Zhang and his co-workers in 2015 reported high performing *p*-type organic sensitizer (**S 2.44**). The followed design strategy includes triphenylamine as a donor, quinoid thiophene as a π-spacer and malononitrile as an electron acceptor. The dye displayed high *PCE* of 0.33 with superior J_{SC} value of 8.2 mA.cm^{-2} under standard light illumination.

Table 2.5: Reported *p*-type organic sensitizers

Reference	Sensitizer	J_{SC} (mA.cm^{-2})	V_{OC} (V)	*FF*	η (%)
Qin et al. (2009)		2.51	0.11	0.29	0.08

Qin et al. (2009)		2.48	0.10	0.36	0.09
Qin et al. (2010)		1.36	0.055	0.34	0.03
Qin et al. (2010)		3.37	0.063	0.31	0.07
Yen et al. (2011)		2.25	0.012	0.33	0.093
Ji et al. (2011)		1.74	0.090	0.38	0.060
Cui et al. (2014)		2.66	0.098	0.35	0.093

Cui et al. (2014)	S 2.42	4.05	0.12	0.34	0.16
Warnan et al. (2014)	S 2.43	1.29	0.075	0.31	0.030
Zhang et al. (2015)	S 2.44	8.2	0.12	0.34	0.33

2.3 SALIENT FEATURES OF THE LITERATURE REVIEW

Based on the detailed literature review the following observations can be made on the present state-of-art of DSSCs.

➢ The push-pull (D-A) system is widely used strategy in designing organic chromophores.

➢ A dye should have broad absorption band and a high molar extinction coefficient for efficient light harvesting.

➢ There must be at least one anchoring group for adsorption of the organic chromophores on the semiconductor surface.

➢ The HOMO-LUMO energy levels of organic chromophores should match with the respective semiconductor.

➢ There is a good scope for variation of donor moiety, π-spacer and electron acceptor/anchoring group in organic-chromophore based sensitizer with D-π-A configuration.

2.4 SCOPE AND OBJECTIVES

Even though significant advances have been made in the field of DSSCs by making use of metal-free sensitizers, still there is a scope for improving solar energy harvesting of DSSCs. In this regard, search for an efficient sensitizer is gaining much interest nowadays. The growing interest in the field is quite evident from the review reports by

Mishra et al. (2009), Odobel et al. (2009 and 2012) and Gong et al. (2017). But still, lots of work need to be carried out on development of effective sensitizers for improving the overall efficiency of solar cell. Obviously, aspects such as efficient light harvesting ability throughout the entire solar spectrum, tuning of the band gap, charge generation and separation, molecular interactions, and influence of different functional groups of sensitizers on photovoltaic parameters are to be addressed.

From the literature review, it is quite clear that there are a number of factors influencing the efficiency of DSSCs. It is fair to say that their overall performance depends on a number of parameters, such as electrodes, the semiconductor, the counter electrode, etc., but from a synthetic chemist's point of view, the geometry and electronic structure of the dye play a pivotal role. Therefore, it is an immediate challenge and requirement to design and synthesize appropriate and efficient dyes for DSSC sensitization/co-sensitization applications. Also, there is a need to study the effect of structures of sensitizers on their photovoltaic performances.

Based on the above facts and the detailed literature survey, the following main objectives have been intended in the present research work.

1) To design new push-pull configured

    (i) *n*-type metal-free organic sensitizers/co-sensitizers based on *N,N* dimethyl-4-vinylaniline and carbazole moieties with various design strategies such as D-A (**Series-1A** and **1B**), D-π-A (**Series-2**), D-π-A-π-A (**Series-3**), D-D-π-A (**Series-4**), and A-π-D-π-A (**Series-5**) architectures

    (ii) *p*-type metal-free organic sensitizers based on carbazole donor system with D-A strategy (**Series-6**)

2) To synthesize newly designed *n*-type and *p*-type organic chromophores using standard synthetic routes and optimize the reaction parameters

3) To characterize the newly synthesized intermediates and target dyes by FTIR, ^{1}H-NMR, ^{13}C-NMR and Mass spectral techniques followed by elemental analysis

4) To evaluate their optical behavior and optical band-gaps by means of UV-visible absorption and fluorescence emission spectroscopy

5) To determine their electrochemical properties and charge carrying properties using cyclic voltammetry (CV)

6) To study electronic distribution in HOMO-LUMO using Turbomole V7.1 software package

7) To fabricate DSSC devices and quantify the performance of the newly synthesized sensitizers/co-sensitizers with respect to parameters such as incident photon to current efficiency (*IPCE*), short-circuit photocurrent (*J_{SC}*), open circuit photovoltage (*V_{OC}*), fill factor (*FF*) and the Photon conversion efficiency (*PCE*)

8) To correlate chemical structures with device performance parameters of the new sensitizers

2.5 MOLECULAR DESIGN OF NEW *n*- AND *p*- TYPE SENSITIZERS

A survey of the pertinent literature reveals that organic dyes with various design strategies such as D-A, D-π-A, D-π-A-π-A, D-D-π-A and A-π-D-π-A are being used for developing new metal-free sensitizers/co-sensitizers for improved efficiency in DSSCs. Several organic chromophores have been designed and synthesized using aforementioned strategies. Most of the reported organic dyes are derived from simple organic compounds such as triphenylamine, *N*, *N*-substituted aniline, carbazole, indole, phenothiazine etc., which act as powerful electron donoating systems. Among aforementioned donors, *N*, *N*-dimethylaniline and carbazole possess good thermal, electrochemical and photochemical stabilities. Accordingly, the present research work has been aimed at design of new organic photosensitizers/co-sensitizers carrying *N, N* dimethylaniline (**Series-1A**) and carbazole (**Series-1B** to **Series-6**) as donor systems and different electron withdrawing moieties as acceptor/anchoring systems.

2.5.1 Design of Series-1A (n-C_{1-5})

In **Series-1A**, five new D-A type organic sensitizers, ***n*-C_{1-5}** consisting of *N,N*-dimethylaniline as an electron donor while barbituric acid, *N,N*-dimethyl barbituric acid, thiobarbituric acid, *N,N*-diethyl thiobarbituric acid and 4-aminobenzoic acid as electron acceptor/anchoring units, were designed. **Fig 2.2** depicts the design strategy involved in **Series-1A** chromophores, *i.e.* ***n*-C_{1-5}**.
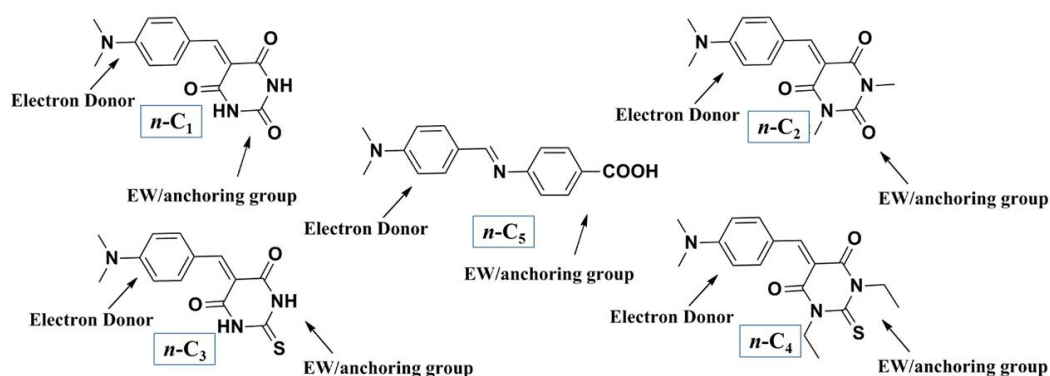
Fig 2.2: Molecular design of **Series-1A** dyes, *n*-C$_{1-5}$

2.5.2 Design of Series-1B (*n*-C$_{6-8}$)

In **Series-1B**, three new D-A configured organic sensitizers/co-sensitizers (***n*-C$_{6-8}$**) carrying carbazole ring as an electron donor, linked directly to effective electron withdrawing (EW)/anchoring units, *viz.* 4-aminobenzoic acid, sulfanilic acid and barbituric acid, were designed. **Fig 2.3** summarizes the design of **Series-1B** dyes, *i.e.* ***n*-C$_{6-8}$**.
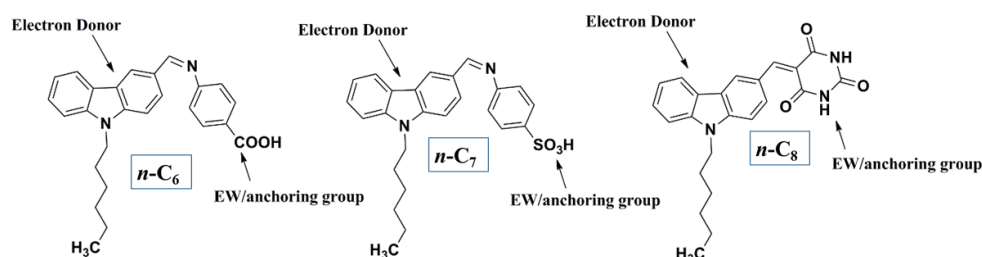
Fig 2.3: Molecular design of **Series-1B** dyes, *n*-C$_{6-8}$

2.5.3 Design of Series-2 (*n*-C$_{9-12}$)

Four new D-π-A configured sensitizers/co-sensitizers (***n*-C$_{9-12}$**) consisting of carbazole core as an effective donor, attached to a phenylene ring that functions as a π-spacer, which is further linked to different acceptor/anchoring units, *viz.* cyanoacetic acid, rhodanine-3-acetic acid, barbituric acid and thiobarbituric acid, were designed. The design strategy has been shown in **Fig 2.4** for **Series-2** dyes, *i.e.* ***n*-C$_{9-12}$**.
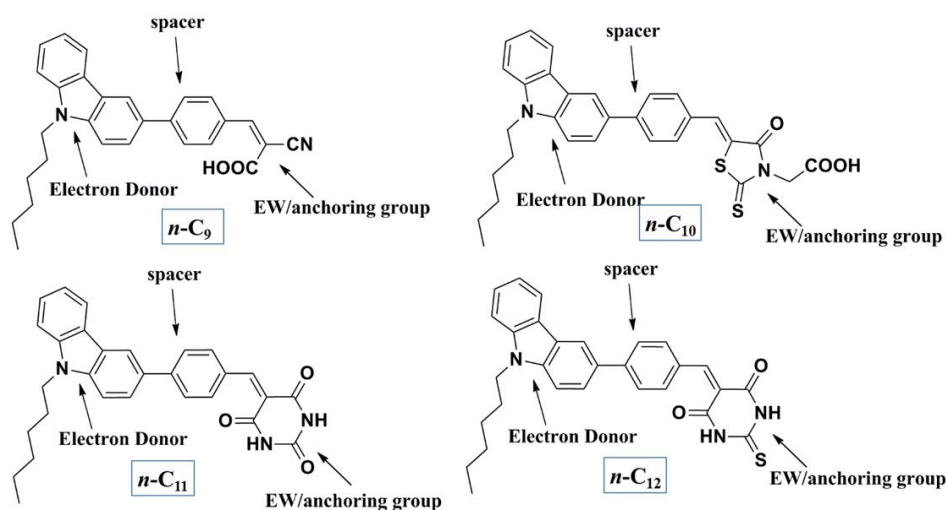
Fig 2.4: Design of **Series-2** molecules, *n-*C₉₋₁₂

2.5.4 Design of Series-3 (*n-*C₁₃₋₁₅)

Fig 2.5 displays the design approach used for three new D-π-A-π-A configured organic sensitizers/co-sensitizers of **Series-3** chromophores, *i.e. n-*C₁₃₋₁₅. The newly designed dyes comprise carbazole ring as an electron donor, cyano vinylene and thiophene groups as π-spacers, while cyanoacetic acid, rodanine-3-acetic acid and barbituric acid as electron acceptor/anchoring units.
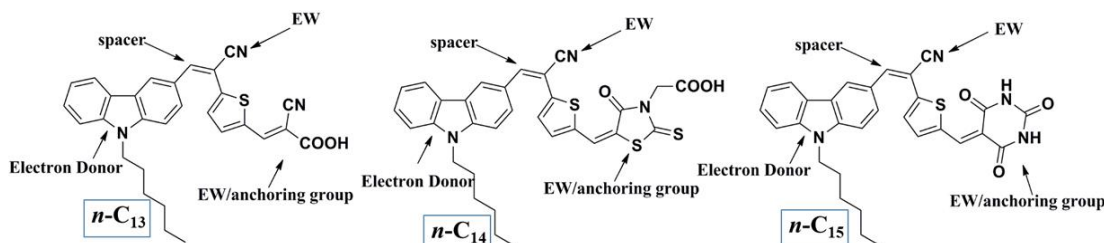
Fig 2.5: Molecular design of **Series-3** chromophores, *n-*C₁₃₋₁₅

2.5.5 Design of Series-4 (*n-*C₁₆₋₁₈)

In **Series-4**, three new organic sensitizers/co-sensitizers, *i.e. n-*C₁₆₋₁₈ with the D-D-π-A architecture, were designed as depicted in **Fig 2.6**. In the new design, carbazole acts as donor scaffold, 4-methoxyphenyl group functions as an auxiliary donor and three different units, *viz.* cyanoacetic acid, 2, 4 thiazolidinedione and barbituric acid serve as acceptor/anchoring groups.
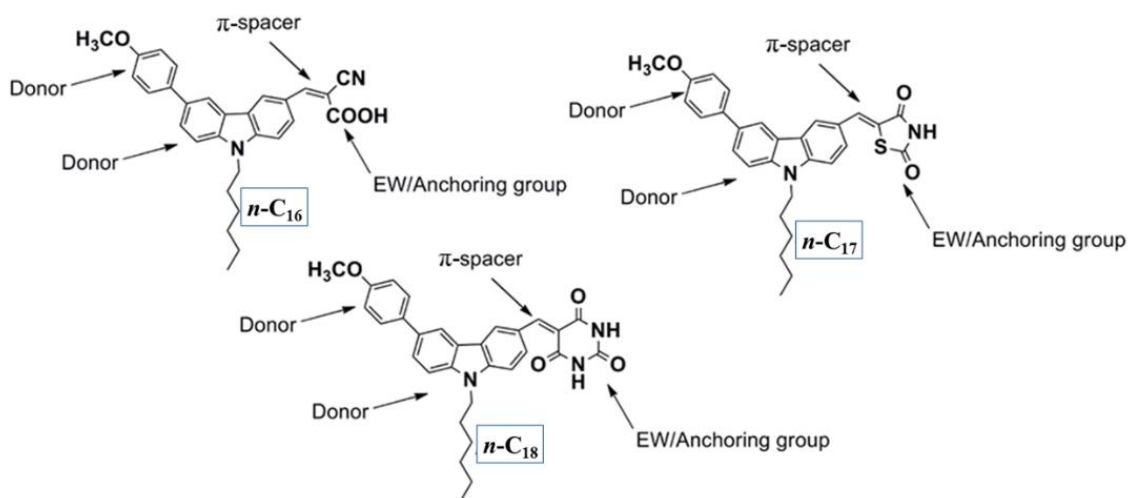
Fig 2.6: Molecular design of **Series-4** dyes, *n*-C₁₆₋₁₈

2.5.6 Design of Series-5 (*n*-C₁₉₋₂₁)

Three new unsymmetrical and bi-anchored organic sensitizers/co-sensitizers, *i.e.* *n*-C₁₉₋₂₁ with A-π-D-π-A configuration were designed in **Series-5 (Fig 2.7)**. The new design consists of carbazole moiety as an electron rich donor, vinylene and phenylene groups as π-spacers, while cyanoacetic acid, 2,4-thiazolidinedione and barbituric acid as electron acceptor/anchoring units.
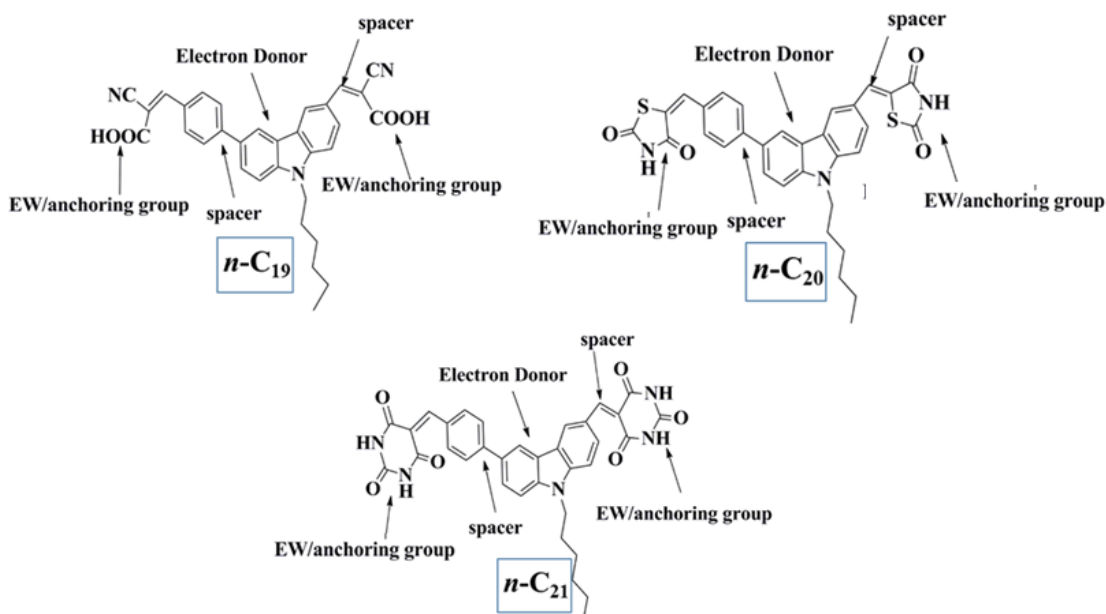
Fig 2.7: Design of **Series-5** molecules, *n*-C₁₉₋₂₁

2.5.7 Design of Series-6 (*p*-C₁₋₃)

The structural design of three new **D-A** configured *p*-type chromophores, *i.e.* *p*-C₁₋₃ is shown in **Fig 7**. In the new design, carbazole core functions as a donor, carboxylic acid serves as an anchoring group, while electron withdrawing *N,N*-dimethyl barbituric acid, *N,N*-diethyl thiobarbituric acid and *N*-diethyl rhodanine work as electron acceptor units.
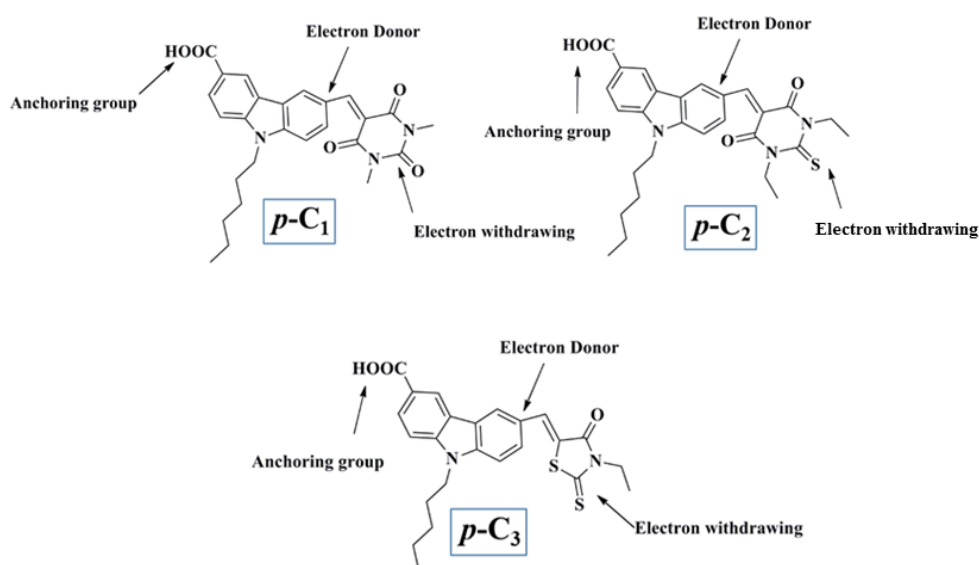
Fig 2.8: Molecular design of **Series-6** dyes, *p*-C₁₋₃

Conclusively, based on the detailed literature survey, seven new series of metal-free organic dyes, *n*-C₁₋₂₁ and *p*-C₁₋₃ have been designed as sensitizers/co-sensitizers for DSSC applications. The newly designed dyes of seven series were synthesized by adopting suitable synthetic strategies as outlined in **Schemes 3.1 to 3.7,** respectively. They have been synthesized from simple starting materials and the reaction conditions have been optimized to get the highest yield. Their purification methods have been developed and the purified compounds have been characterized by various spectral techniques such as FTIR, NMR and mass spectroscopy followed by elemental analysis. The structures of selected final compounds have been confirmed by SC-XRD studies. The synthetic strategies, procedures and structural characterization data of newly synthesized dyes have been discussed in **Chapter 3**.

SYNTHESIS AND STRUCTURAL CHARACTERIZATION

Abstract:

This chapter describes a detailed synthetic protocols used for newly designed dyes n-C_{1-21} and p-C_{1-3}. Also, it covers purification techniques adopted for new molecules. Further, it includes structural characterization of newly synthesized target dyes as well as their intermediates, using FTIR, ^1H NMR, ^{13}C NMR, Mass spectral studies and elemental analysis. Also, it deals with SCXRD study of selected dyes. It involves in depth discussion on structural elucidation of new dyes.

3.1 INTRODUCTION

In the previous chapter, design of seven new series based on *N, N*-dimethyl aniline (**Series-1A**) and carbazole core (**Series-1B-6**) with various push pull configurations (D-A, D-π-A, D-D-π-A, D-π-A-π-A and A-π-D-π-A) has been discussed in detail. Normally, the synthesis of organic molecules may be achieved by various synthetic protocols. In the present work, the newly designed dyes were synthesized by using the appropriate standard synthetic pathways for each series (**Schemes 1-7**) and the reaction conditions were optimized to acquire optimum yield. They were purified using recrystallization or column chromatography techniques, for which solvent system was identified. The pure compounds were characterized with the help of various spectral techniques and elemental analysis. In the following sections, a detailed description of experimental protocols followed for the synthesis of newly designed dyes and structural elucidation of the newly synthesized dyes and their intermediates are discussed.

3.2 EXPERIMENTAL

The materials used as well as appropriate synthetic methods followed for the synthesis of designed dyes are given under this section. Further, their structural characterization data are also included.

3.2.1 Materials and methods

The chemical and reagents such as carbazole, *N,N*-dimethylaniline, 3-bromo carbazole, 1-bromohexane, thiophene acetonitrile, 4-formyphenylboronic acid, 4-methoxyphenylboronic acid, cyanoacetic acid, 2, 4 thiazolidinedione, barbituric acid, thiobarbituric acid, *N,N*-dimethyl barbituric acid, *N,N*-diethyl thiobarbituric acid, *N*-ethyl rhodamine, sodium hydride, silver oxide, Pd(PPh$_3$)$_4$, Cs$_2$CO$_3$ and LiOH.H$_2$O were procured from Sigma Aldrich, Alfa Aesar and Spectrochem companies. All the solvents and reagents used in the reactions were synthetic grade (Merck, Loba Chemie and Spectrochem companies) and used without further purification unless stated otherwise. All the reactions were performed under inert atmosphere and the progress of the reactions was monitored using thin layer chromatography (TLC) technique. The synthesized compounds were purified using recrystallization or column chromatography methods. ^{1}H NMR and ^{13}C NMR spectra of the dyes were recorded in CDCl$_3$/DMSO-d$_6$ solvent on a Bruker Avance 400/500 MHz spectrophotometer. The chemical shift (δ) was expressed in ppm with tetramethylsilane (TMS) as an internal standard and coupling constant (J) wasexpressed in Hz. FTIR spectra were run using Bruker Alpha FTIR spectrometer. Mass and elemental analysis of the synthesized dyes were measured using LC-MS6410Q (Agilent Technologies), Waters HPLC-TOF mass analyzer and Flash EA1112 CHNS elemental analyzer (Thermo Scientific), respectively.

3.2.2 Synthesis

3.2.2.1 Synthesis of Series-1A (*n*-C$_{1-5}$)

The synthesis strategy employed for the preparation of dyes *n*-C$_{1-5}$ starting from simple 4-(*N, N*-dimethylamino)benzaldehyde (S$_1$) is summarized in **Scheme 3.1**.

3.2.2.1.1 Chemistry

In this series, the five dyes *n*-C$_{1-5}$ were synthesized by condensing 4-(*N,N*-dimethylamino)benzaldehyde with five n-based compounds, *viz*. barbituric acid, *N,N*-dimethyl barbituric acid, thiobarbituric acid, *N,N*-diethylthiobarbituric acid and 4-aminobenzoic acid through Knoevenagel/Schiff condensation. The synthetic route for *n*-C$_{1-5}$ dyes is depicted in **Scheme 3.1.**
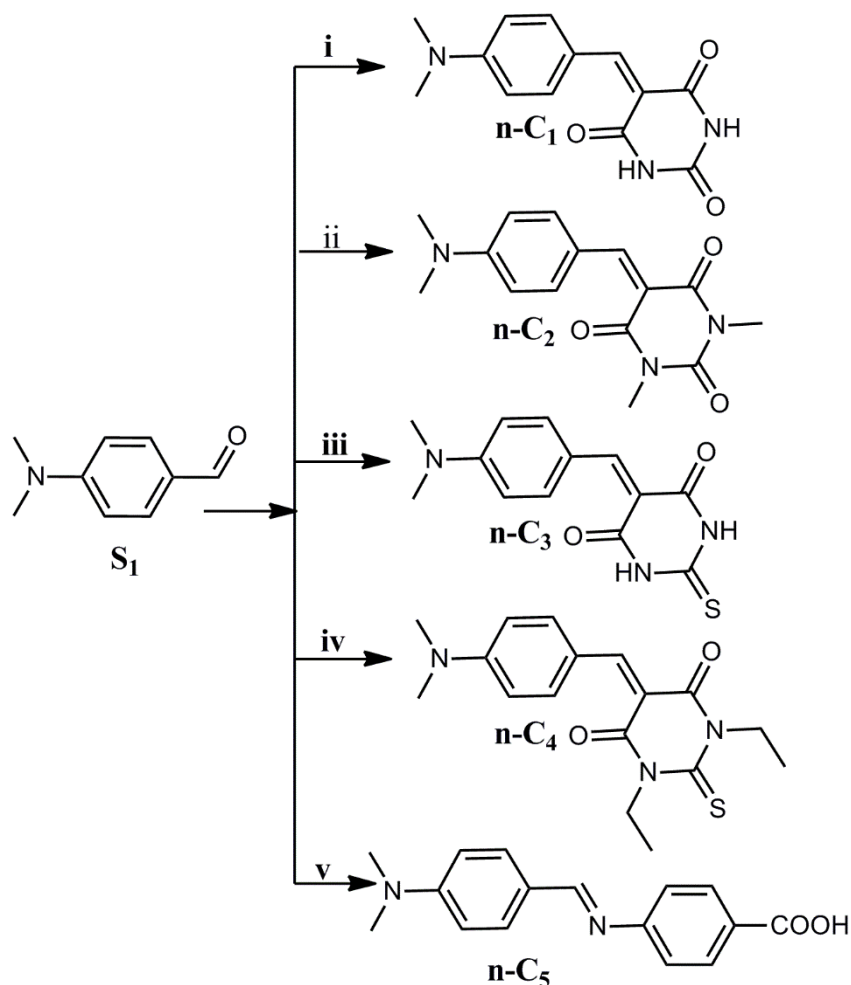
Scheme 3.1: Synthetic route of the chromophores *n-*C$_{1-5}$: (i) Barbituric acid, ethanol, 70 °C (ii) *N,N*-dimethyl barbituric acid, ethanol, 70 °C (iii) Thiobarbituric acid, ethanol, 70 °C (iv) *N,N*-diethyl thiobarbituric acid, ethanol, 70 °C (v) 4-amino benzoic acid, methanol, 60 °C.

3.2.2.1.2 Synthesis and characterization

*General method of synthesis for chromophores **n-**C$_{1-4}$*

The dyes were synthesized as per the procedures reported by Hu et al. 2011 with small modifications. In this method, 4-(*N, N*-dimethylamino)benzaldehyde (**S$_1$**, 0.5 g, 3.355 mmol) was dissolved in 15 mL of absolute ethanol and to this an appropriate amount of four different compounds, *viz*. barbituric acid, thiobarbituric acid, *N,N*-dimethyl barbituric acid and *N,N* diethyl thiobarbituric acid dissolved in 10 mL of absolute alcohol was added while stirring. The precipitated solid was filtered and

washed with absolute ethanol. The dyes **n-C$_{1-4}$** were crystallized from appropriate solvents. Their characterization data are as follows:

*5-(4-N,N-Dimethylaminobenzylidene)pyrimidine-2,4,6(1H,3H,5H)-trione (**n-C$_1$**)*

Orange colored solid, yield 91%, m.p. 186-188 ºC ^{1}H NMR (400 MHz DMSO-d$_6$, ppm): 11.06 (s, 1H), 10.93 (s, 1H) 8.44 (d, 2H), 8.15 (s, 1H), 6.81 (d, 2H), 3.13 (s, 6H). ^{13}C NMR (400 MHz DMSO-d$_6$, ppm): 165.16, 163.19, 155.93, 154.63, 150.77, 139.52, 120.45, 111.67, 110.03. Anal calculated for C$_{13}$H$_{13}$N$_3$O$_3$: C, 60.23; H, 5.02; N, 16.16; O, 18.53 found C, 60.19; H, 5.08; N, 16.21; O, 18.51; FTIR (ATR cm^{-1}): 3396 (>N-H stretching), 2926 (Ar C-H stretching). TOF MS ES+ Calculated for C$_{13}$H$_{13}$N$_3$O$_3$: 259.26. Found: 260.11 [M+H]$^+$. The obtained spectral data match with reported values (Haldar et al. 2008).

*5-(4-N,N-Dimethylaminobenzylidene)-1,3-dimethyl-pyrimidine-2,4,6-trione(**n-C$_2$**)*

High-quality orange colored single crystal of **n-C$_2$** was obtained by slow evaporation of its solution with 1:1 pet ether (60-80 ºC)/ethyl acetate solvent mixture. The single crystal was subjected to SC-XRD analysis and obtained crystal data are presented in **Table 3.1**.

Orange colored solid, yield 90%. m.p. 196-198 ºC ^{1}H NMR (400 MHz DMSO-d$_6$, ppm): 8.44 (d, 2H), 8.24 (s, 1H), 6.83 (d, 2H), 3.22 (s, 6H). 3.14 (s, 6H), ^{13}C NMR (400 MHz DMSO-d$_6$, ppm): 163.72, 161.66, 156.80, 154.73, 151.73, 139.58, 120.49, 111.68, 109.79, 28.98, 28.36, Anal calculated for C$_{15}$H$_{17}$N$_3$O$_3$: C, 62.68; H, 5.92; N,14.63; O, 16.72 found C, 62.71; H, 5.96; N, 14.63; O, 16.71; FTIR (ATR cm^{-1}): 3040 (Ar C-H stretching). TOF MS ES+ Calculated for C$_{15}$H$_{17}$N$_3$O$_3$: 287.13. Found: 288.14 [M+H]$^+$. The spectral data match with reported values (Rezende et al. 2001).

*5-(4-N,N-Dimethylaminobenzylidene)-2-thioxo-dihydro-pyrimidine-4,6(1H,5H)-dione (**n-C$_3$**)*

Red colored solid, yield 85%. m.p. 222-224 ºC. ^{1}H NMR (400 MHz DMSO-d$_6$, ppm): 12.16 (s, 1H), 12.06 (s, 1H) 8.48 (d, 2H), 8.16 (s, 1H), 6.84 (d, 2H), 3.16 (s, 6H). ^{13}C NMR (400 MHz DMSO-d$_6$, ppm): 177.98, 163.19, 155.93, 154.63, 150.77, 139.52, 120.45, 111.67, 110.03. Anal calculated for C$_{13}$H$_{13}$N$_3$O$_2$S: C, 56.66; H, 4.72; N, 15.25; O, 11.62; S, 11.62 found C, 56.71; H, 4.76; N, 15.26; O, 11.62; S, 11.65. FTIR (ATR

cm^{-1}): 3049 (Ar C-H stretching). TOF MS ES+ Calculated for $C_{15}H_{17}N_3O_3$: 275.33 Found: 276.03 [M+H]$^+$. The spectral data match with reported values (Haldar et al. 2008).

5-(4-N,N-Dimethylaminobenzylidene)-1,3-diethyl-2-thioxo-dihydro-pyrimidine-4,6-dione (n-C₄)

Superior-quality shining red colored single crystal of dye *n*-**C₄** was obtained by very slow evaporation of its solution with 1:1 pet ether (60-80 ^{o}C)/ethyl acetate solvent mixture. SC-XRD analysis was carried out for it and obtained crystal data are tabulated in **Table 3.1**.

Red colored solid, yield 85%. m.p. 236-238 ℃. ^{1}HNMR (400 MHz DMSO-d$_6$, ppm): 8.48 (d, 2H), 8.27 (s, 1H), 6.87 (d, 2H), 4.45 (s, 4H), 3.18 (s, 6H), 1.21 (s, 6H), ^{13}CNMR (400 MHz DMSO-d$_6$, ppm): 190.41, 159.30, 158.55, 155.54, 140.49, 112.08, 111.54, 109.27, 43.23, 12.77, Anal calculated for $C_{17}H_{21}N_3O_2S$: C, 61.55; H, 6.34; N, 12.67; O, 9.65; S, 9.65 found C, 61.61; H, 6.39; N, 12.68; O, 9.65; S, 9.67. FTIR (ATR cm^{-1}): 3442 (>N-H stretching), 3051 (Ar C-H stretching). TOF MS ES+ Calculated for $C_{17}H_{21}N_3O_2S$: 331.43. Found: 332.14 [M+H]$^+$. The spectral data match with reported values (Zheng et al. 2000).

Synthesis of 4-[(4-dimethylamino-benzylidene)-amino]-benzoic acid (n-C₅)

4-(*N*,*N*-Dimethylamino)benzaldehyde (**S₁**, 0.5 g, 3.355 mmol) was dissolved in 15 mL of absolute methanol and 4-aminobenzoic acid (0.5g, 4mmol) dissolved in 10mL of absolute alcohol was added while stirring. The reaction mixture was further stirred at 60 ℃ for 10 h. The precipitated solid was filtered, washed with ice-cold alcohol and recrystallized from absolute ethanol. Yellow colored solid, yield 68%, m.p. 145 ℃. ^{1}H NMR (400 MHz DMSO-d$_6$, ppm): 12.77 (s, 1H), 8.43 (s, 1H), 7.95 (d, 2H), 7.77 (d, 2H), 7.25 (d, 2H), 6.80 (d, 2H), 3.02 (s, 6H), ^{13}C NMR (400 MHz DMSO-d$_6$, ppm): 190.31, 167.94, 167.59, 161.84, 156.85, 154.70, 153.61, 153.17, 132.00, 131.67, 131.14, 131.03, 127.35, 125.02, 123.92, 121.38, 117.38, 113.03, 111.92, 111.55 Anal Calcd. For $C_{17}H_{21}N_3O_2S$: C, 71.57; H, 6.05; N, 10.47; O, 11.90; found; C, 71.62; H, s6.01; N, 10.44; O, 11.93. FTIR (cm^{-1}): (O-H stretching), 2918 (Ar C-H stretching),

1752 (>C=O stretching). TOF MS ES+ Calculated for $C_{17}H_{21}N_3O_2S$: 268.31 Found: 269.12 $[M+H]^+$.

3.2.2.2 Synthesis of Series-1B (*n*-C$_{6-8}$)

The multistep synthesis pathways of dyes ***n*-C$_{6-8}$** starting from simple *9H*-carbazole (**S$_2$**) are summarized in **Scheme 3.2.**
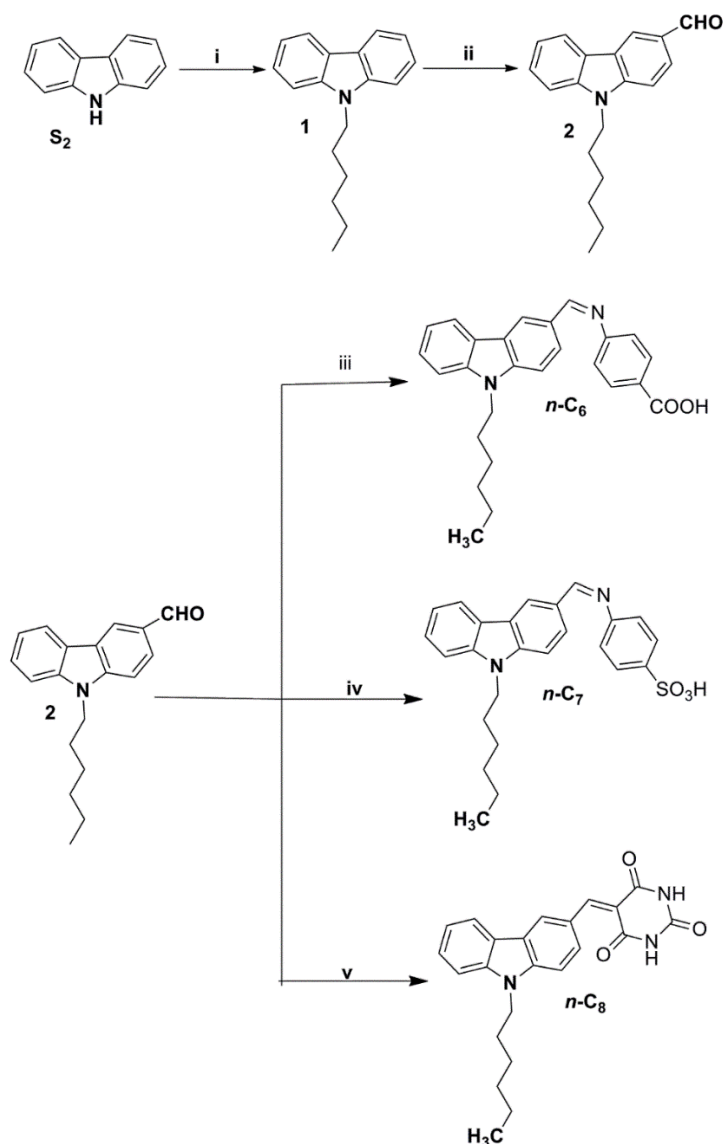
Scheme 3.2: Synthetic routes for the chromophores ***n*-C$_{6-8}$**: (i) 1-Bromohexane, NaH, DMF, RT (ii) POCl$_3$, DMF, RT (iii) 4-aminobenzoic acid, absolute methanol, 60 ºC (iv) Sulfanilic acid, absolute methanol, 60 ºC (v) Barbituric acid, absolute methanol, 60 ºC

3.2.2.2.1 Chemistry

The synthetic pathways of three new organic sensitizers/co-sensitizers ***n*-C₆₋₈** are depicted in **Scheme 3.2**. In the first step, the intermediate *N*-hexyl carbazole (**1**) was synthesized from *9H*-carbazole (**S₂**). Then, compound **1** was formylated using Vilsmeier-Hack reaction protocol to yield 9-hexyl-*9H*-carbazole-3-carbaldehyde (**2**). In the final step, the target molecules ***n*-C₆₋₈** were obtained in good yield by following Schiff/Knoevenagel condensation of 9-hexyl-*9H*-carbazole-3-carbaldehyde (**2**) with 4-amino benzoic acid, sulfanilic acid and barbituric acid, respectively. The target organic dyes and their intermediates were purified using recrystallization and column chromatography techniques. The structures of newly synthesized dyes and their intermediates were confirmed by various spectroscopic techniques including elemental analysis.

3.2.2.2.2 Synthesis and characterization

*Synthesis of 9-hexyl-9H-carbazole (**1**)*

A solution of carbazole (**S₂**, 1 g, 5.9 mmol) and sodium hydride (0.43 g, 17.92 mmol) dissolved in 10 mL of DMF was stirred at room temperature for 0.5 h under inert atm. Then 1-bromohexane (1.17 g, 7 mmol) was added to the above reaction mixture and stirring was continued for 36 h. The reaction was monitored using TLC. After completion of the reaction, the mixture was quenched into 100 mL of ice water and neutralization was done using a supersaturated solution of ammonium chloride. The precipitated yellow solid was filtered and dried. The solid was purified by column chromatography on 60 - 120 mesh silica using hexane as an eluent to give intermediate **1** as pale yellow solid. Yield 86 %. ^{1}H NMR (400 MHz, CDCl₃, δ ppm): 8.18 (d, 2H), 7.56 (m, 2H), 7.50-7.45 (m, 2H), 7.30 (t, 2H), 4.40 (t, 2H) 1.8-1.75 (m, 2H), 1.58-1.38 (m, 6H), 0.94 (t, 3H). ^{13}C NMR (100 MHz, DMSO d₆): 140.80, 139.18, 128.41, 126.95, 124.42, 123.29, 121.50, 121.29, 119.56, 111.76, 111.22, 110.00, 42.81, 31.40, 28.86, 26.53, 22.45, 14.28. The spectral data match with reported values (Park et al. 2007).

*Synthesis of 9-hexyl-9H-carbazole-3-carbaldehyde (**2**)*

A 50 mL two neck RB flask was charged with the 1.5 mL of freshly distilled DMF under an argon atm. followed by dropwise addition of 1.8 mL of POCl₃ at 0 ℃

with constant stirring till white colored Vilsmeier salt completely precipitates. Then a solution of **1** (1 g of 9-hexyl-*9H*-carbazole dissolved in 10 mL of ethylene dichloride) was added to it dropwise while stirring. Further, the reaction mixture was stirred for 24 h. After completion of the reaction, the content was quenched into 150 mL of ice-cold water and the pH was adjusted to alkaline by adding 5M sodium hydroxide solution. The precipitated solid was filtered, dried and purified using column chromatography on 200-400 mesh silica using 7:3 pet ether/ethyl acetate mixture as the mobile phase.

Yellow color solid, Yield 65%, ^{1}H NMR (400 MHz, DMSO-d_6, δ ppm) 10.06 (s, 1H), 8.76 (d, 1H), 8.31-8.29 (d, 1H), 8.01-7.99 (d, 1H), 7.80 - 7.78 (d, 1H), 7.71-7.69 (d, 1H), 7.57-7.53 (t, 1H), 7.33-7.29 (t, 1H), 4.47-4.45 (t, 2H) 1.82-1.75 (m, 2H), 1.28 - 1.18 (m, 6H), 0.81 - 0.78 (t, 3H), ^{13}C NMR (400 MHz, DMSO-d_6, δ ppm) 192.43, 144.04, 141.29, 128.69, 127.28, 127.06, 124.52, 122.70, 122.66, 121.28, 120.61, 110.56, 110.30, 49.07, 43.05, 40.52, 40.31, 40.10, 39.89, 39.68, 39.47, 39.26, 28.88, 26.48, 22.43, 14.26 Anal. Calculated $C_{19}H_{21}NO$: C, 81.68; H, 7.58; N, 5.01 found: C, 81.77; H, 7.61: N, 4.91. The spectral data match with reported values (Liu et al. 2015).

*General method for synthesis of **n-C$_{6-8}$***

In a dry 50 mL RB flask, 9-hexyl-*9H*-carbazole-3-carbaldehyde (**3**, 0.5 g, 3.355 mmol) was dissolved in 15 mL of absolute methanol. To this 3.355 mmol of respective organic acid, *viz.* 4-aminobenzoic acid, sulfanilic acid and barbituric acid was added under argon atmosphere. The reaction mixture was further stirred at 60ºC for 10 h. The reaction progress was monitored using TLC technique. After the completion, the content was cooled and precipitated solid was filtered, washed and recrystallized from absolute methanol. Their characterization data are as follows:

*((Z)-4-(((9-Hexyl-9H-carbazol-3-yl)methylene)amino)benzoic acid (**n-C$_6$**)*

Yellow solid, Yield 75%; m.p. 154-156 ºC. ^{1}H NMR (400 MHz, DMSO-d_6, δ ppm):11.50 (s, 1H), 8.69 (s, 1H), 8.52-8.49 (d, J=12 Hz, 1H), 8.40 (s, 1H), 8.29-8.18 (m, 1H), 8.08-8.06 (d, J=8 Hz, 1H) , 7.95-7.93 (d, J=8 Hz, 1H), 7.82-7.61 (m, 3H), 7.53-7.48 (d, 2H), 7.28-7.24 (m,1H), 4.44-4.43 (t, 2H), 1.80 (m, 2H), 1.30-1.25 (m, 6H), 0.84-0.82 (t, 3H). ^{13}C NMR (400 MHz, DMSO-d_6, δ ppm) 164.63, 158.97, 143.59,

140.32, 133.59, 133.10, 128.33, 128.03, 126.58, 126.11, 123.14, 122.82, 118.52, 117.79, 114.91, 111.12, 110.95, 98.89, 55.66, 43.22, 31.39, 29.00, 26.50, 22.46, 14.31. Anal. Calculated $C_{26}H_{26}N_2O_2$: C, 78.39; H, 6.53; N, 7.03 found: C, 78.36; H, 6.58: N, 7.03. FTIR (cm^{-1}): 3530 (O-H stretching), 2983 (Ar C-H stretching), 1672 (>C=O stretching). Mass: ESI-MS (+Ve mode) 398.60 (M$^+$].

*(Z)-4-(((9-Hexyl-9H-carbazol-3-yl)methylene)amino)benzenesulfonic acid (**n-C$_7$**)*

Yellow solid, Yield 56%; m.p. 206-208 °C. ^{1}H NMR (400 MHz, CDCl$_3$, δ ppm) 8.70 (s, 1H), 8.31-8.28 (d, J=8 Hz, 2H), 8.17-8.15 (d, J=8 Hz, 2H), 7.86-7.84 (d, J=8 Hz, 1H), 7.53 -7.46 (m, 3H), 7.32-7.26 (t, 1H), 4.35-4.31 (t, 2H) 1.90 (m, 2H), 1.55-1.30 (m, 6H), 0.89-0.86 (t, 3H), ^{13}C NMR (400 MHz, CDCl$_3$, δ ppm) 160.93, 144.56, 144.34, 133.61, 113.17, 106.15, 45.88, 39.64, 30.27, 28.40, 22.76, 13.79 Anal. Calculated $C_{25}H_{26}N_2O_3S$: C, 69.12; H, 5.99; N, 6.45 found: C, 69.10; H, 6.03: N, 6.45. FTIR (cm^{-1}): 3033 (Ar C-H stretching), 1572 (>C=O stretching). Mass: ESI-MS (+Ve mode) 432.30 (M$^+$].

*5-((9-Hexyl-9H-carbazol-3-yl)methylene)pyrimidine-2,4,6(1H,3H,5H)-trione (**n-C$_8$**)*

Yellow color solid, Yield 78%; m.p. 222-224 °C. ^{1}H NMR (400 MHz, DMSO-d$_6$, ppm): 11.30 (s, 1H), 11.19 (s, 1H), 9.31 (s, 1H), 8.65-8.63 (d, J=8.8 Hz, 1H), 8.55 (s, 1H), 8.20 – 8.19 (d, J=8 Hz, 1H), 7.74-7.70 (t, 2H), 7.57-7.53 (t, 1H) 7.35-7.31 (t, 1H), 4.48-4.45 (t, 2H), 1.82-1.78 (m, 2H), 1.29-1.21 (m, 6H), 0.83-0.79 (t, 3H) ^{13}C NMR (400 MHz, DMSO-d$_6$, ppm): 164.71, 162.90, 157.35, 150.77, 143.60, 141.22, 133.77, 130.01, 131.57, 127.19, 123.92, 122.87, 122.65, 120.99, 114.54, 110.71, 109.73, 43.09, 31.39, 28.95, 26.51, 22.46, 14. Anal. Calculated for $C_{23}H_{23}N_3O_3$: C, 70.95; H, 5.90; N, 10.80 found: C, 70.93; H, 5.95; N, 10.79. FTIR (ATR cm^{-1}): 3450 (>N-H stretching), 3068 (Ar C-H stretching), 1685 (>C=O stretching). Mass: TOF ESI-MS 390.18 (M+1].

3.2.2.3 Synthesis of Series-2 molecules (*n*-C$_{9-12}$)

Synthesis of carbazole based organic dyes (***n*-C$_{9-12}$**) with D-π-A configuration carrying four varied electron acceptor/anchoring units, was carried out as per **Scheme 3.3**.
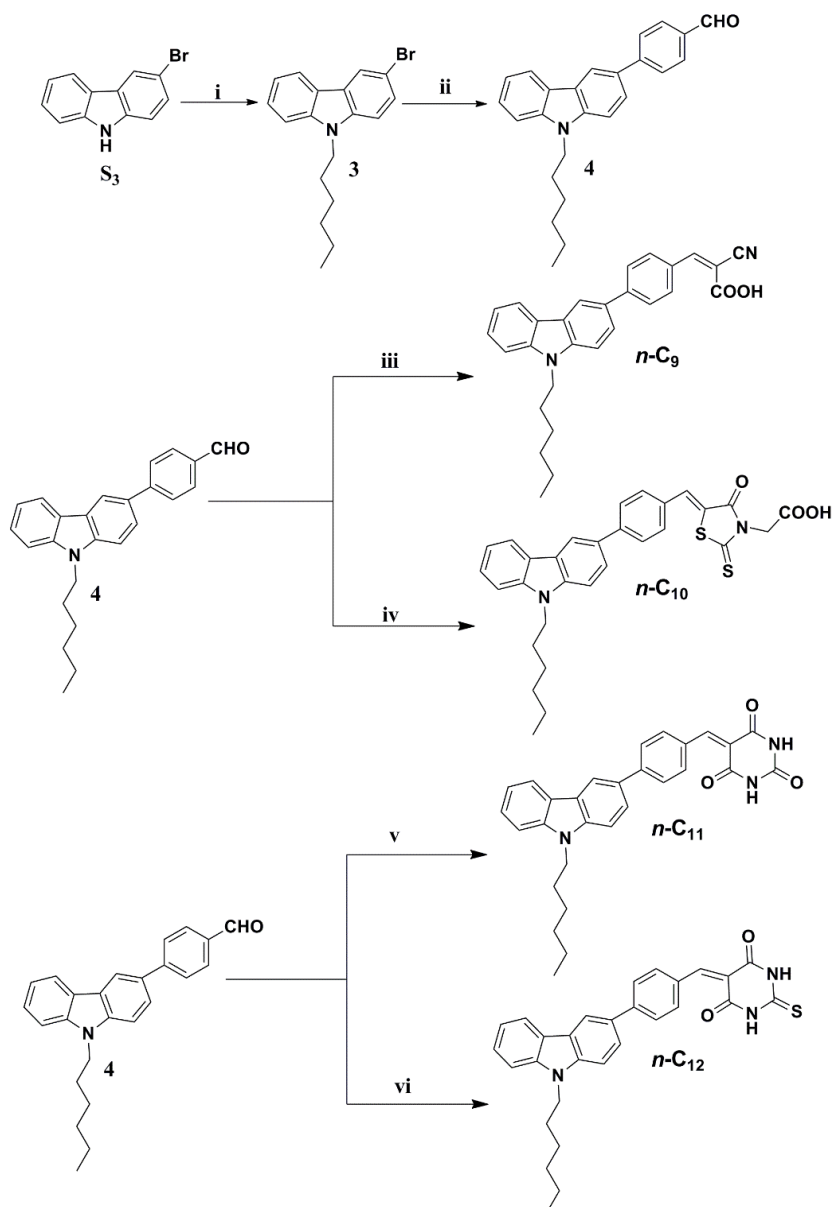
Scheme 3.3: Synthetic routes for the chromophores ***n*-C9-12**: (i) 1-Bromohexane, NaH, DMF, RT (ii) 4-formylphenylboronic acid, Cs₂CO₃, toluene, 80° C (iii) Cyanoacetic acid, ammonium acetate, glacial CH₃COOH, 110 ℃ (iv) Rhodanine-3-acetic acid, ammonium acetate, glacial CH₃COOH, 110 ℃ (v) Barbituric acid, absolute methanol, 60 ℃ (vi) Thio-barbituric acid, absolute methanol, 60 ℃

3.2.2.3.1 Chemistry

The synthetic pathways of four new metal-free heteroaromatic dyes ***n*-C9-12** are depicted in **Scheme 3.3**. The required intermediate 3-bromo-9-hexyl-*9H*-carbazole (**3**) was synthesized from 3-bromo-9H-carbazole (**S₃**) by reacting it with *n*-bromohexane

in presence of sodium hydride. The precursor 4-(9-hexyl-*9H*-carbazol-3-yl)benzaldehyde (**4**) was obtained in good yield through C-C Suzuki cross coupling of 3-bromo-9-hexyl-*9H*-carbazole (**3**) with 4-formylphenylboronic acid in presence of cesium carbonate under anhydrous condition. In the final step, the target molecules ***n*-C9-12** were obtained by following Knoevenagel condensation protocol, wherein the precursor **3** was condensed with active methylene compound, *viz.* cyanoacetic acid, rhodanine-3-acetic acid, barbituric acid and thiobarbituric acid. All the new compounds were purified using recrystallization or column chromatography technique. The structures of newly synthesized dyes and their intermediates were confirmed by various spectral techniques.

3.2.2.3.2 Synthesis and characterization

Synthesis of 3-bromo-9-hexyl-9H-carbazole (3)

A mixture of 3-bromo carbazole (**S3**, 1 g, 4.06 mmol) and sodium hydride (0.36 g, 16.24 mmol) dissolved in 10 mL of DMF was stirred for 0.5 h under an argon atmosphere at room temperature. Then 1-bromohexane (0.80 g, 4.87 mmol) was added to the above reaction mixture and stirring was continued for 10 h. The progress of reaction was monitored using TLC. After completion of the reaction, the product was poured into 100 mL of ice water and neutralization was done using supersaturated ammonium chloride solution. The precipitated yellow solid was filtered, washed with water and finally dried. The solid was purified by column chromatography on 60-120 mesh silica using hexane as an eluent to yield 3-bromo-9-hexyl-*9H*-carbazole (**3**) as a pale yellow solid. Yield 90 %. m.p. 146 °C ^{1}H NMR (400 MHz, DMSO-d$_6$, δ ppm): 8.41 (s, 1H), 8.23-8.21 (d, J=7.6 Hz, 1H), 7.63-7.58 (m, 3H), 7.51-7.47 (t, 1H), 7.24-7.20 (t, 1H), 4.41-4.37 (t, 2H), 1.74 (t, 2H), 1.24 (m, 6H), 0.82-0.79 (t, 3H). ^{13}C NMR (100 MHz, DMSO-d$_6$, δ ppm): 140.80, 139.18, 128.41, 126.95, 124.42, 123.29, 121.50, 121.29, 119.56, 111.76, 111.22, 110.00, 42.81, 31.40, 28.86, 26.53, 22.45, 14.28. Anal. Calculated for C$_{18}$H$_{20}$BrN: C, 65.45; H, 6.06; N, 4.23; found: C, 65.46; H, 6.10; N, 4.24.

Synthesis of 4-(9-hexyl-9H-carbazol-3-yl) benzaldehyde (4)

A mixture of 3-bromo-9-hexyl-*9H*-carbazole (**3**, 1 g, 3.0 mmol), 4-formyl-4-phenyl boronic acid (0.45 g, 3.0 mmol), cesium carbonate (2.96 g, 9.1 mmol), Pd(PPh$_3$)$_4$

(0.35 g, 0.3 mmol) and toluene (20 mL) was placed in 50 mL dry two neck RB flask under argon atmosphere and refluxed for 2 h. The reaction was monitored using TLC. After completion of the reaction, toluene was removed under vacuum, then 20 mL water was added to the mixture and extracted with CH_2Cl_2 (30 mL x 3). The organic phase was dried over anhydrous Na_2SO_4 and solvent was removed under vacuum. The residue was purified using column chromatography on 200-400 mesh silica using 7:3 pet ether / ethyl acetate mixture as the mobile phase. Yellow solid, Yield 56 %, m.p. 156 ºC. ^{1}H NMR (400 MHz, DMSO-d$_6$, δ ppm):10.06 (s, 1H), 8.65 (d, 1H), 8.29 (d, J=8 Hz, 1H), 8.07-8.00 (q, J=10.4 Hz, 4H), 7.91 (d, J=8.8 Hz, 1H), 7.74 (d, J=8.8Hz, 1H), 7.64 (d, J=8.4 Hz, 1H), 7.51-7.47 (t, 1H), 7.24-7.20 (t, 1H), 4.41-4.37 (t, 2H), 1.74 (t, 2H), 1.24 (m, 6H), 0.82-0.79 (t, 3H). ^{13}C NMR (100 MHz, DMSO-d$_6$, δ ppm): 193.11, 147.41, 141.04, 140.71, 134.70, 130.69, 129.83, 127.50, 126.61, 125.41, 123.30, 122.70, 121.15, 119.61, 119.57, 110.37, 110.02, 42.85, 40.56, 40.35, 10.14, 39.93, 39.72, 39.51, 39.31, 31.43, 28.96, 26.58, 22.46, 14.30. Anal. Calculated for $C_{25}H_{25}NO$: C, 83.51; H, 7.14; N, 3.94; found: C, 84.47; H, 7.09; N, 3.94.

*Synthesis of (Z)-2-cyano-3-(4-(9-hexyl-9H-carbazol-3-yl) phenyl) acrylic acid (**n-C₉**)*

A mixture of 4-(9-hexyl-*9H*-carbazol-3-yl) benzaldehyde (**4**, 0.100 g, 0.282 mmol), cyanoacetic acid (0.029 g, 0.338 mmol), and ammonium acetate (0.233 g, 3.03 mmol) and glacial acetic acid (10 mL) was taken in a 100 mL RB flask and refluxed for 12 h under argon atmosphere. The completion of reaction was checked by TLC. When the reaction completes, the thoroughly cooled reaction mixture was poured into 100 mL of ice cold water. The obtained solid was filtered and dried. The crude red colored product was purified by column chromatography using 200-400 mesh silica gel as stationary phase and $CHCl_3$: CH_3OH (10:1) as mobile phase to get red colored solid. Yield 58%; m.p. 232 -234 ºC. ^{1}H NMR (400 MHz, DMSO-d$_6$, δ ppm):11.49 (s, 1H), 8.69 (s, 1H), 8.30-8.25 (t, 1H), 8.20-8.18 (d, J = 7.6 Hz, 1H), 8.08-8.06 (d, J=8 Hz, 1H), 7.95-7.93 (d, J=8 Hz, 1H), 7.83-7.80 (m, 1H), 7.74-7.72 (m, 1H), 7.70-7.69 (m, 1H), 7.65-7.61 (m, 1H), 7.53-7.48 (m, 2H), 7.28-7.24 (m,1H), 4.44-4.43 (t, 2H), 1.80 (t, 2H), 1.30-1.25 (m, 6H), 0.84-0.82 (t, 3H). ^{13}C NMR (100 MHz, DMSO-d$_6$, δ ppm): 164.63, 158.97, 143.59, 140.32, 133.59,133.10, 128.33, 128.03, 126.58, 126.11, 123.14, 122.82, 118.52, 117.79, 114.91, 110.92, 98.99, 55.66, 43.22, 31.39, 29.00, 26.50, 22.46,

14. Anal. Calculated for $C_{28}H_{26}N_2O_2$: C, 79.62; H, 6.16; N, 6.64; found: C, 79.59; H, 6.02; N, 6.63. FTIR (ATR cm^{-1}): 3525 (-O-H stretching), 2945 (Ar C-H stretching), 2215 (-C≡N stretching). Mass: ESI-MS (+Ve mode) 422.52 (M$^+$].

*Synthesis of (Z)-2-(5-(4-(9-hexyl-9H-carbazol-3-yl)benzylidene)-4-oxo-2-thioxothiazolidin-3-yl) acetic acid (**n-C₁₀**)*

A mixture of 4-(9-hexyl-*9H*-carbazol-3-yl)benzaldehyde (**4**, 0.100 g, 0.282 mmol), rhodanine-3-acetic acid (0.065 g, 0.338 mmol), and NH₄OAc (0.233 g, 3.03 mmol) dissolved in 20 mL of glacial acetic acid was taken in a dry 100 mL RB flask. The mixture was refluxed for 12 h under argon atmosphere. The progress of the reaction was monitored by TLC technique. After completion of the reaction, the content was cooled to room temperature, then it was poured into 100 g of crushed ice and obtained red solid was filtered and dried. The product was purified by column chromatography using silica gel (200-400 mesh) and CHCl₃: CH₃OH (10:1) as mobile phase. Red colored solid, Yield 52%; m.p. 228 -230 ° C. ¹H NMR (400 MHz, DMSO-d₆, δ ppm): 8.64 (s, 1H), 8.29 (d, J=7.6 Hz, 1H), 8.05 (d, J=8 Hz, 2H), 7.96 (s, 1H), 7.91 (d, J=8 Hz, 1H), 7.80-7.77 (t, 2H), 7.73 (d, J=8.4 Hz, 1H), 7.64-7.62 (d, J=8 Hz, 2H), 7.51-7.47 (m, 1H), 7.26-7.22 (t,1H), 4.76 (s, 2H), 4.45-4.41 (t, 2H), 1.81-1.78 (t, 2H), 1.29-1.24 (m, 6H), 0.83-0.80 (t, 3H). ¹³C NMR (100 MHz, DMSO-d₆, δ ppm) 193.56, 167.79, 166.91, 144.17, 141.04, 140.65, 134.29, 132.11, 131.25, 129.77, 127.85, 126.59, 125.23, 123.32, 122.72, 121.19, 119.56. 119.39, 110.40, 110.04, 45.62, 42.86, 40.62, 40.42, 40.21, 40.00, 39.79, 39.58, 39.37, 31.45, 28.99, 26.60, 22.49. 14.33. Anal. Calculated for $C_{30}H_{28}N_2O_3S_2$: C, 68.18; H, 5.30; N, 5.30; found: C, 68.15; H, 5.34; N, 5.30. FTIR (ATR cm^{-1}): 3442 (-O-H stretching), 2956 (Ar C-H stretching). Mass: ESI-MS (+Ve mode) 529.49 [M+1].

*General method for synthesis of dyes **n-C₁₁** and **n-C₁₂***

4-(9-Hexyl-*9H*-carbazol-3-yl)benzaldehyde (**4**, 0.100 g, 0.282 mmol) was dissolved in 15 mL of absolute methanol and to this 0.282 mmol of respective active methylene compound, *viz.* barbiituric acid, thio barbituric acid, was added under argon atmosphere. The reaction mixture was further stirred at 60ºC for 10 h. After the completion, the content was cooled and precipitated solid was filtered, washed and recrystallized from absolute methanol.

5-(4-(9-Hexyl-9H-carbazol-3-yl)benzylidene)pyrimidine-2,4,6(1H,3H,5H)-trione (***n-C₁₁***)

Red colored solid, Yield 85%; m.p. 210-212 °C; ^{1}H NMR (400 MHz, DMSO-d₆, δ ppm): 11.38 (s, 1H), 11.26 (s, 1H), 8.69 (s, 1H), 8.36-8.34 (t, 3H), 8.30 (d, J=7.6 Hz,1H), 7.98-7.92 (m, 3H), 7.73 (d, J=8.4 Hz, 1H), 7.64 (d, J=8.4 Hz, 1H), 7.51-7.47 (t, 1H), 7.26-7.23 (t, 1H), 4.45-4.42 (t, 2H), 1.81-1.78 (t, 2H), 1.31-1.21 (m, 6H), 0.83-0.79 (t, 3H). ^{13}C NMR (100 MHz, DMSO-d₆, δ ppm) 164.14, 162.41, 155.03, 150.69, 145.61, 141.04, 140.74, 135.37, 131.04, 129.86, 126.59, 126.40, 125.28, 123.32, 122.75, 121.17, 119.57, 119.49, 118.30, 110.38, 110.04, 42.87, 40.63, 40.42, 40.21, 40.00, 39.79, 39.58, 39.37, 31.45, 28.99, 26.60, 22.49. 14.32. Anal. Calculated for $C_{29}H_{27}N_3O_3$: C, 74.84; H, 5.81; N, 9.03; found: C, 74.82; H,5.85; N, 9.03. FTIR (ATR cm^{-1}): 3410 (>N-H stretching), 3058 (Ar C-H stretching). Mass: ESI-MS (+Ve mode) 467.10 (m/z].

*5-(4-(9-Hexyl-9H-carbazol-3-yl)benzylidene)-2-thioxodihydropyrimidine-4,6(1H,5H)-dione (**n-C₁₂**)*

Red colored solid, Yield 85%; m.p. 206-208 °C. ^{1}H NMR (400 MHz, DMSO-d₆, δ ppm): 12.46 (s, 1H), 12.36 (s, 1H), 8.70 (s, 1H), 8.41-8.39 (d, J=8.4 Hz, 2H), 8.36 (s, 1H), 8.30-8.28 (d, J=7.6 Hz, 1H), 8.00-7.94 (m, 3H), 7.74 (d, J=7.6 Hz, 1H), 7.65 (d, J=8.4 Hz,1H), 7.51-7.47 (t, 1H), 7.26-7.22 (t,1H), 4.45-4.42 (t, 2H), 1.81-1.78 (t, 2H), 1.30-1.20 (m, 6H), 0.83-0.79 (t, 3H). ^{13}C NMR (100 MHz, DMSO-d₆, δ ppm) 177.98, 160.23, 156.00, 141.05, 135.77, 129.76, 126.63, 126.46, 122.75, 119.62, 118.30, 110.42, 40.59, 40.38, 40.17, 39.97, 39.76, 39.55, 39.34, 31.44, 28.98, 26.59, 22.48. 14.32. Anal. Calculated for $C_{29}H_{27}N_3O_2S$: C, 72.35; H, 5.61; N, 8.73 found: C, 73.32; H, 5.65; N, 8.72. FTIR (ATR cm^{-1}): 3410 (>N-H stretching), 3058 (Ar C-H stretching). Mass: ESI-MS (+Ve mode) 479.10 (m/z).

3.2.2.4 Synthesis of Series-3 dyes (***n-C₁₃₋₁₅***)

Scheme 3.4 illustrates the synthetic routes for the preparation of carbazole based organic dyes (***n-C₁₃₋₁₅***) with D-π-A-π-A configuration, carrying four varied electron acceptor/anchoring units.
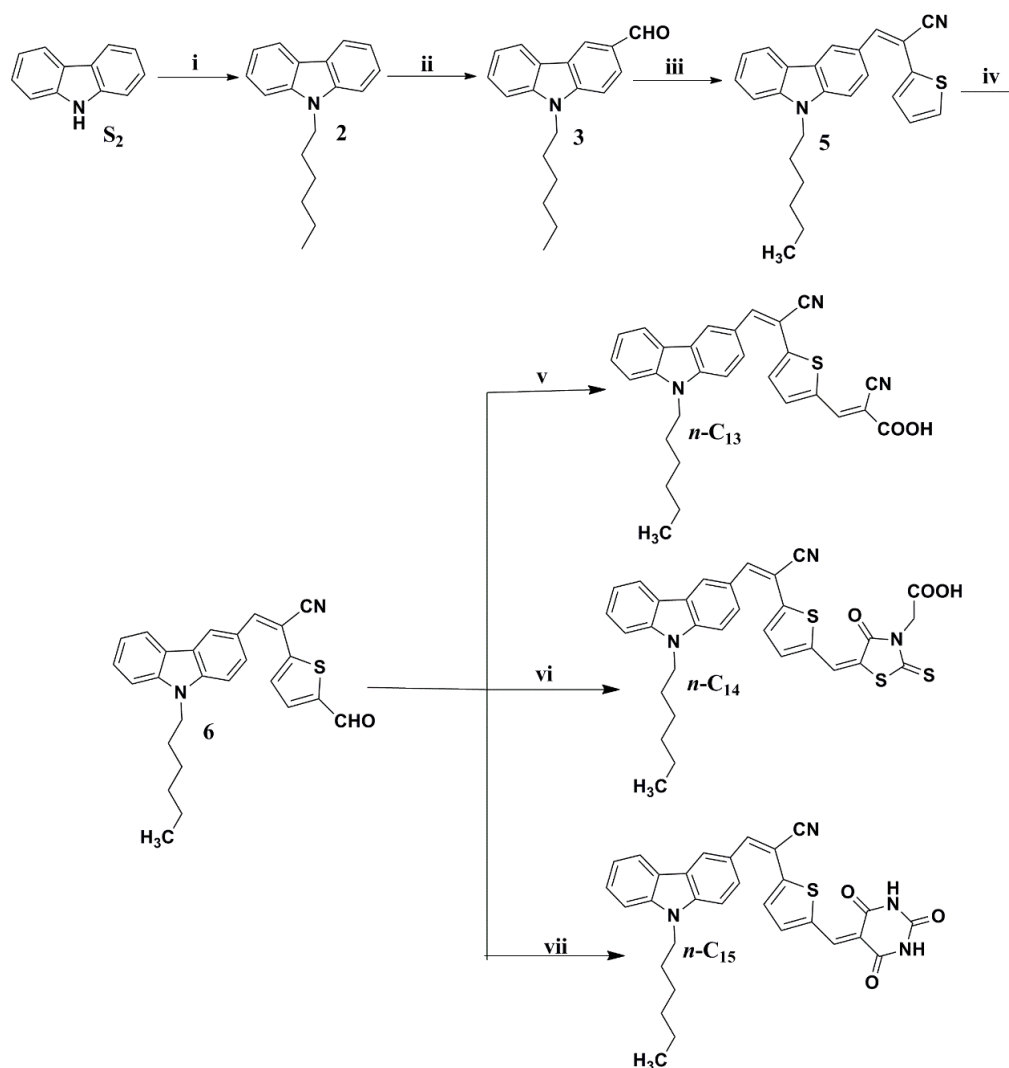
Scheme 3.4: Synthetic routes for the chromophores *n*-**C**13-15: (i) 1-Bromohexane, NaH, DMF, RT (ii) POCl₃, DMF, RT (iii) 2-(Thiophen-2-yl)-acetonitrile, NaOMe, CH₃OH, RT (iv) POCl₃, DMF, RT. (v) Cyanoacetic acid, ammonium acetate, glacial CH₃COOH, 110 °C (vi) Rhodanine-3-acetic acid, ammonium acetate, glacial CH₃COOH, 110 °C (vii) Barbituric acid, ethanol, 60 °C

3.2.2.4.1 Chemistry

The synthetic pathways of three new organic dyes *n*-**C**13-15 are depicted in **Scheme 1**. The intermediates **1** and **2** were synthesised as per the procedure described in section **3.2.2.2**. Further, the 9-hexyl-*9H*-carbazole-3-carbaldehyde (**2**) was condensed with thiophene-2-acetonitrile by Knoevenagel condensation to obtain intermediate **5**. Furthermore, intermediate **5** was subjected to Vilsmeier-Hack reaction to form the precursor **6**. In the final step, the target molecules *n*-**C**16-18 were obtained in

good yield by following Knoevenagel condensation of precursor **6** with cyanoacetic acid, rhodanine-3-acetic acid and barbituric acid, respectively. The target organic dyes and their intermediates were purified using recrystallization and column chromatography techniques. The structures of newly synthesized dyes and their intermediates were confirmed by various spectroscopic techniques.

3.2.2.4.2 Synthesis and characterization

*Synthesis of (Z)-3-(9-hexyl-9H-carbazol-3-yl)-2-(thiophen-2-yl) acrylonitrile (**5**)*

9-Hexyl-*9H*-carbazole-3-carbaldehyde (**2**, 0.6 g, 2.15 mmol) and thiophene-2-acetonitrile (0.344 g, 2.79 mmol) were slowly added separately to the 100 mL single neck RB flask containing freshly prepared sodium methoxide solution (0.085 g of sodium metal in 10 mL of methanol). The reaction mass was stirred at room temperature for 8 h. The precipitated yellow solid was filtered, washed with cold methanol and finally recrystallized from chloroform to give yellow solid, yield 72 %, m.p. 140-142 ºC. ^{1}H NMR (400 MHz, CDCl$_3$, δ ppm) 8.58 (s, 1H), 8.01 (m, 2H), 7.58 (s, 1H), 7.51 (t, 1H), 7.44 (t, 2H), 7.37 (d, 1H), 7.28 (m, 2H), 7.08 (d, 1H), 4.32 (t, 2H), 1.88 (m, 2H), 1.31 (m, 6H), 0.87 (t, 3H). Anal. Calculated C$_{25}$H$_{24}$N$_2$S: C, 78.09; H, 6.29; N, 7.28; found: C, 78.01; H, 6.25; N, 7.28.

*Synthesis of (Z)-2-(5-formylthiophen-2-yl)-3-(9-hexyl-9H-carbazol-3-yl) acrylonitrile (**6**)*

(*Z*)-3-(9-Hexyl-*9H*-carbazol-3-yl)-2-(thiophen-2-yl) acrylonitrile (**5**, 0.5 g, 1.49 mmol) dissolved in dichloroethane (5 mL) was added to the white colored Vilsmeier salt (prepared as above) while stirring and stirring was continued at room temperature for 12 h. The reaction mass was then poured into 150 mL of ice cold water and subsequently basified by using 5 M NaOH solution. The precipitated solid was collected by filtration and the crude product was purified by column chromatography on silica gel using ethyl acetate/hexane (1:5) as mobile phase to give orange colored solid. Yield: 55%, m.p. 166-168 ºC. ^{1}H NMR (400 MHz, CDCl$_3$ δ ppm) 9.88 (s, 1H), 8.64 (d, 1H), 8.14 (t, 2H), 7.73 (s, 1H), 7.56-7.26 (m, 5H), 7.07 (s, 1H), 7.36-7.26 (m, 4H), 4.31 (t, 2H), 1.88-1.35 (bs, 8H), 0.86 (t, 3H). ^{13}C NMR (400 MHz, CDCl$_3$ δ ppm): 182.46, 149.63, 142.33, 142.11, 141.61, 141.23, 141.08, 128.02, 127.56, 126.82,

126.44, 126.30, 125.98, 125.14, 124.39, 123.66, 12.48, 123.26, 122.26, 122.76, 122.44, 120.73, 120.24, 119.83, 109.39, 109.18, 43.42, 31.52, 28.95, 26.93, 22.53, 14.01. Anal. Calcd. for $C_{26}H_{24}N_2OS$: C, 75.70; H, 5.86; N, 6.83 found: C, 75.65; H, 5.93; N, 6.85. TOF MS ESI m/z calculated for $C_{26}H_{24}N_2OS$ is 412.16 found 413.17 [M+H]$^+$.

*Synthesis of (E)-2-cyano-3-(5-((Z)-1-cyano-2-(9-hexyl-9H-carbazol-3-yl)vinyl)thiophen-2-yl)acrylic acid (**n**-C13)*

A dried 100 mL RB flask was charged with a mixture of (Z)-2-(5-formylthiophen-2-yl)-3-(9-hexyl-9H-carbazol-3-yl) acrylonitrile (**5**, 0.100 g, 0.275 mmol), cyanoacetic acid (0.028 g, 0.331 mmol), and ammonium acetate (0.233 g, 3.03 mmol) dissolved in 20 mL of glacial acetic acid. The reaction mixture was refluxed for 12 h under inert atmosphere. After completion of the reaction, the mass was cooled to room temperature and was poured into 150 mL of ice cold water. The obtained solid was filtered and dried. The crude product was purified by column chromatography using 200-400 mesh silica gel as stationary phase and $CHCl_3$: CH_3OH (10:1) as mobile phase to get red colored solid. Yield 58%, m.p. 165 °C. ^{1}H NMR (400MHz DMSO-d$_6$, ppm): 8.80 (s, 1H), 8.52 (s, 1H), 8.26 (d, 1H), 8.19 (d, 2H), 8.03 (s, 1H), 7.83 (d, 1H), 7.71 (d, 1H), 7.64 (s, 1H), 7.31 (s, 1H), 7.56 (t, 4H), 1.79 (s, 2H), 1.27 (s, 6H), 0.81 (s, 2H) ^{13}C NMR (125MHz CDCl$_3$, ppm):167.03, 163.90, 162.95, 154.21, 140.79, 135.61, 135.34, 132.86, 131.57, 118.61, 115.41, 110.28, 104.85, 102.05, 58.42, 51.71, 19.21, 2.64. FTIR (ATR cm^{-1}): 3525 (-O-H stretching), 2945 (Ar C-H stretching), 2215 (-C≡N stretching), Anal calcd for $C_{29}H_{25}N_3O_2S$: C, 72.63; H, 5.25; N, 8.76 found C, 72.32; H, 5.29: N, 8.75 ESI-MS (+ve mode) m/z calculated for $C_{29}H_{25}N_3O_2S$ is 479.17 found 479.10 [m/z].

*Synthesis of 2-((E)-5-((5-((Z)-1-cyano-2-(9-hexyl-9H-carbazol-3-yl)vinyl)thiophen-2-yl)methylene)-4-oxo-2-thioxothiazolidin-3-yl)acetic acid (**n**-C14)*

A mixture of (Z)-2-(5-formylthiophen-2-yl)-3-(9-hexyl-*9H*-carbazol-3-yl)acrylonitrile (**5**, 0.100 g, 0.275 mmol), rhodanine-3-acetic acid (0.063 g, 0.331 mmol), and NH$_4$OAc (0.233 g, 3.03 mmol) was taken in a dry 100 mL RB flask. The mixture was dissolved in 20 mL of glacial acetic acid and then refluxed for 12 h under argon atmosphere. The reaction completion was monitored by TLC technique. After completion of the reaction, the content was allowed to attain room temperature, then it

was poured into 100 g of crushed ice and obtained red solid was filtered and dried. The product was purified by column chromatography using silica gel (200-400 mesh) and CHCl$_3$: CH$_3$OH (10:1) as mobile phase. Red colored solid, Yield 52%, m.p. 186 ºC. ^{1}H NMR (400MHz DMSO-d$_6$, ppm): 8.79 (s, 1H), 8.24 (d, 4H), 7.82 (s, 1H), 7.70 (s, 1H), 7.61 (d, 2H), 7.31 (s, 1H), 4.52-4.43 (d, 4H), 1.79 (s, 2H), 1.27 (s, 6H), 0.81 (s, 2H), ^{13}C NMR (400MHz DMSO-d$_6$, ppm):193.59, 167.55, 166.59, 141.70, 141.20, 134.43, 128.84, 127.24, 124.53, 124.47, 123.43, 122.37, 121.35, 120.41, 119.15, 111.02, 110.48, 48.73, 43.03, 40.65, 40.44, 40.23, 40.02, 39.81, 39.40, 31.39, 28.94, 26.53, 22.46 ,14.30 FTIR (ATR cm^{-1}): 3442 (-O-H stretching), 2956 (Ar C-H stretching), 2219 (-C≡N stretching), Anal. Calcd. for C$_{31}$H$_{27}$N$_3$O$_3$S$_3$: C, 63.56; H, 4.65; N, 7.17; found: C, 63.46; H, 4.69; N, 7.13   ESI-MS (+ve mode) m/z calculated for C$_{29}$H$_{25}$N$_3$O$_2$S is 585.12 found 585.76 [m/z]

*Synthesis of (Z)-3-(9-hexyl-9H-carbazol-3-yl)-2-(5-((2,4,6-trioxotetrahydropyrimidin-5(2H)-ylidene)methyl)thiophen-2-yl)acrylonitrile (**n-C$_{15}$**)*

A mixture of (Z)-2-(5-formylthiophen-2-yl)-3-(9-hexyl-*9H*-carbazol-3-yl) acrylonitrile (**5**, 0.100 g, 0.275 mmol), barbituric acid (0.063 g, 0.331 mmol), was taken in a dry 100 mL RB flask. The mixture was dissolved in 20 mL of absolute methanol and then refluxed for 12 h under argon atmosphere. The reaction completion was monitored by TLC technique. When the reaction completes, the content was allowed to attain room temperature, the separated solid was collected by filtration and dried. The product was recrystallized from methanol. Yield 72%, m.p. 198-200 ºC. ^{1}H NMR (400MHz DMSO-d$_6$, ppm): 11.32 (s, 2H), 8.80 (s, 1H), 8.47 (s, 1H), 8.26-8.24 (t, 3H), 8.17-8.15 (t, 2H), 7.80 (d, 1H), 7.68-7.63 (m, 2H), 7.55-7.51 (t, 1H), 7.32-7.28 (t, 1H), 4.45-4.42 (t, 3H) 1.80-1.77 (t, 3H), 1.27 (s, 6H), 0.81 (s, 2H), ^{13}C NMR (400MHz DMSO-d$_6$, ppm): 163.81, 163.67, 153.49, 150.76, 147.17, 145.63, 145.44, 142.36, 141.17, 136.17, 127.28, 126.00, 124.53, 124.31, 123.00, 122.46, 120.96, 120.61, 117.94, 111.78, 110.61, 43.06, 40.62, 39.99, 39.57, 31.38, 28.96, 26.52, 22.46, 14.29 FTIR (ATR cm^{-1}): 3410 (>N-H stretching), 3058 (Ar C-H stretching), 2191 (--C≡N stretching), Anal. Calcd. for C$_{31}$H$_{27}$N$_3$O$_3$S$_3$: C, 63.56; H, 4.65; N, 7.17; found: C, 63.46; H, 4.69; N, 7.13 ESI-MS (+ve mode) m/z calculated for C$_{29}$H$_{25}$N$_3$O$_2$S is 522.17 found 522.10 [m/z].

3.2.2.5 Synthesis of Series-4 molecules (*n*-C₁₆₋₁₈)

Scheme 3.5 illustrates the synthetic routes for the preparation of carbazole based organic dyes (*n*-C₁₆₋₁₈) with D-D-π-A architecture, carrying three varied electron acceptor/anchoring units in their structures.
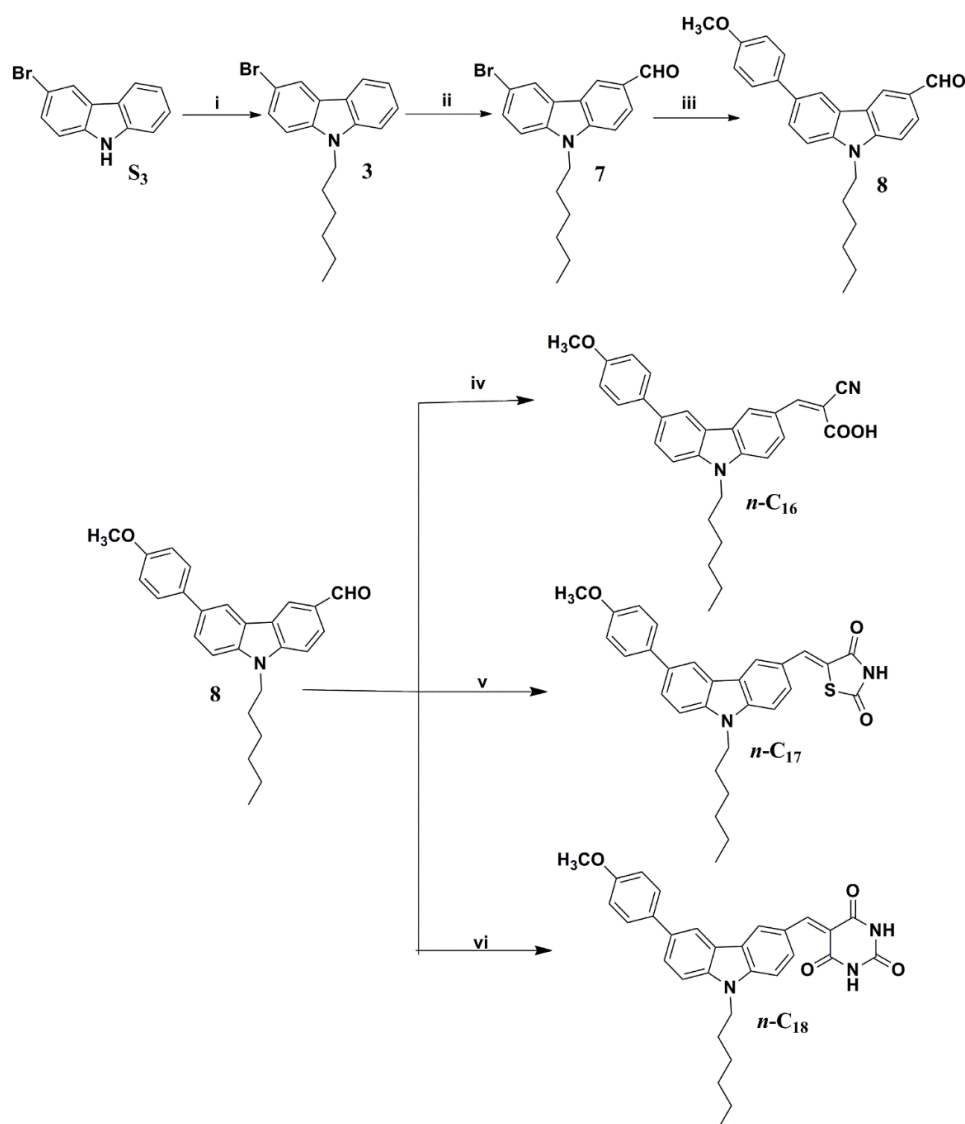
Scheme 3.5: Synthetic pathways for the synthesizing *n*-C₁₆₋₁₈: (i) 1-Bromohexane, NaH, DMF, RT (ii) POCl₃, DMF, 0 °C - RT (iii) (ii) 4-methoxyphenylboronic acid, Cs₂CO₃, toluene, 80 °C (iv) Cyanoacetic acid, ammonium acetate, glacial CH₃COOH, 110 °C (v) 2, 4 thiazolidinedione, ammonium acetate, glacial CH₃COOH, 110 °C (vi) Barbituric acid, absolute methanol, 60 °C

3.2.2.5.1 Chemistry

The synthetic pathways of the three new organic sensitizers/co-sensitizers *n*-**C16-18** are outlined in **Scheme 3.5**. The required intermediate 3-bromo-9-hexyl-*9H*-carbazole (**3**) was obtained from 3-bromo carbazole (**S3**) in presence of a base. Then, intermediate 6-bromo-9-hexyl-*9H*-carbazole-3-carbaldehyde (**7**) from **3** was obtained in moderate yield using Vilsmeier-Hack reaction protocol. The precursor 9-hexyl-6-(4-methoxyphenyl)-*9H*-carbazole-3-carbaldehyde (**8**) was obtained in good yield through Suzuki cross coupling reaction of **7** with 4-methoxyphenylboronic acid. In the final step, the obtained precursor **8** was subjected to Knoevenagel condensations with varied active methylene compound, *viz.* cyanoacetic acid, 2, 4 thiazolidinedione and barbituric acid to afford *n*-**C16-18**. The synthesized dyes *n*-**C16-18** were purified using recrystallization/column chromatography methods.

3.2.2.5.2 Synthesis and characterization

Synthesis of 6-bromo-9-hexyl-9H-carbazole-3-carbaldehyde (7)

A 1.5 mL of freshly distilled $POCl_3$ was added dropwise to the 1.8 mL of a stirred solution of anhydrous DMF at 0° C under argon atmosphere till white colored Vilsmeier salt completely precipitates. Then, a solution of **3** (1 g of 3-bromo-9-hexyl-*9H*-carbazole dissolved in 10 mL of EDC solvent) was added to the reaction mixture dropwise while stirring and stirring was continued for 36 h at room temperature. After completion of the reaction, the reaction mass was quenched into 100 mL of ice-cold water and the pH was adjusted to alkaline by adding 5N sodium hydroxide solution. The precipitated yellow solid was filtered, dried and purified using column chromatography on 200-400 mesh silica using 10:3 pet ether (60-80° C) / ethyl acetate mixture as an eluent, to get required yellow colored solid.

Pale yellow solid, Yield 80 %; m.p. 156-158 ℃. ^{1}H NMR (400 MHz, DMSO-d_6, δ ppm):10.05 (s, 1H), 8.84 (s, 1H), 8.57 (s, 1H), 8.03-8.01 (d, J=8.4 Hz, 1H), 7.83 -7.81 (d, J= 8.4 Hz, 1H) , 7.72-7.66 (m, 2H), 4.48-4.45 (t, 2H), 1.78-1.74 (t, 2H), 1.24-1.19 (m, 6H), 0.81-0.77 (t, 3H). ^{13}C NMR (400 MHz, DMSO-d_6, δ ppm) 192.23, 144.26, 140.07, 129.56, 129.06, 127.64, 125.23, 124.67, 123.98, 121.68, 112.77, 112.65,

110.66, 43.21, 31.36, 28.86, 26.45, 22.44, 14.28. Anal. Calculated $C_{19}H_{20}BrNO$: C, 63.86; H, 5.60; N, 3.92 found: C, 63.70; H, 5.63: N, 3.91

Synthesis of 9-hexyl-6-(4-methoxyphenyl)-9H-carbazole-3-carbaldehyde (8)

A mixture of 6-bromo-9-hexyl-*9H*-carbazole-3-carbaldehyde (**7**, 1 g, 2.8 mmol), 4-methoxyphenylboronic acid (0.43 g, 2.8 mmol), anhydrous caesium carbonate (2.74 g, 8.4 mmol), $Pd(PPh_3)_4$ (0.15 g, 0.1 mmol) and toluene (20 mL) was placed in 50 mL dry two neck RB flask under argon atmosphere and stirred at 80 °C for 18 h. After the completion of the reaction, the reaction mass was cooled down to room temperature, excess toluene was removed by rotary evaporator. To the content, 20 mL of water was added and extracted with CH_2Cl_2 (30 mL x 3). The organic phase was dried over anhydrous Na_2SO_4 and solvent was removed under vacuum. The residue was purified using column chromatography on 200-400 mesh silica using 10:3 pet ether (60-80 °C) / ethyl acetate mixture as the mobile phase. Pale yellow solid, m.p. 172-174 °C. ^1H NMR (400MHz, DMSO-d_6, ppm): 10.07 (s, 1H), 8.86 (s, 1H), 8.60 (s, 1H), 8.01-7.99 (d, J=8.4 Hz, 1H), 7.81-7.72 (m, 5H), 7.08-7.05 (d, J=8.5 Hz, 2H), 4.49-4.45 (t, 3H), 3.82 (s, 3H), 1.81-1.77 (s, 2H), 1.28-1.20 (m, 6H), 0.82-0.78 (t, 3H) ^{13}C NMR (400MHz DMSO-d_6, ppm):192.26, 158.92, 144.45, 140.40, 133.61, 132.78, 128.73, 128.27, 127.24, 125.81, 124.75, 123.42, 122.92, 118.82, 114.84, 110.87, 110.36, 55.64, 43.15, 40.62, 40.41, 40.20, 39.99, 39.78, 39.58, 39.37, 31.40, 28.97, 26.52, 22.46, 14.28. Anal. Calculated for $C_{26}H_{27}NO_2$: C, 81.03; H, 7.01; N, 3.64 found C, 81.01; H, 7.06: N, 3.63. TOF HRMS m/z calculated for $C_{26}H_{27}NO_2$ is 385.2042 found 386.2127 [M+1].

*Synthesis of (Z)-2-cyano-3-(9-hexyl-6-(4-methoxyphenyl)-9H-carbazol-3-yl)acrylic acid (**n-C16**)*

A dry 100 mL RB flask was charged with a mixture of 9-hexyl-6-(4-methoxyphenyl)-*9H*-carbazole-3-carbaldehyde (**8**, 0.100 g, 0.259 mmol), cyanoacetic acid (0.026 g, 0.312 mmol), and ammonium acetate (0.220 g, 2.85 mmol) dissolved in 20 mL of glacial acetic acid. The reaction mixture was stirred at 110 °C for 12 h under inert atmosphere. After completion of the reaction, the mass was cooled to room temperature and was poured into 150 mL of ice cold water. The obtained solid was filtered and dried. The crude product was purified by column chromatography using

200-400 mesh silica gel as stationary phase and $CHCl_3$: CH_3OH (10:1) as mobile phase to get red colored solid. Yield 58%, m.p. 162-164 ℃. ^{1}H NMR (400MHz, DMSO-d_6, ppm): 13.69 (s, 1H), 8.91 (s, 1H), 8.44 (s, 1H), 8.40 (s, 1H), 8.33-8.31 (d, J=8.8 Hz, 1H), 7.87-7.76 (m, 3H), 7.72-7.70 (d, J=8.4 Hz, 2H), 7.09-7.07 (d, J=8.4 Hz, 1H), 4.51-4.48 (t, 3H), 3.82 (s, 3H), 1.79 (s, 2H), 1.29-1.15 (m, 6H), 0.83-0.79 (t, 3H) ^{13}C NMR (400MHz, DMSO-d_6, ppm):164.63, 158.97, 143.59, 140.32, 133.59, 133.10, 128.33, 128.03, 126.58, 126.11, 123.14, 122.82, 118.52, 117.79, 114.91, 111.12, 110.95, 98.89, 55.66, 43.22, 31.39, 29.00, 26.50, 22.46, 14. Anal calcd for $C_{29}H_{28}N_2O_3$: C, 76.99; H, 6.19; N, 6.19 found C, 76.97; H, 6.24: N, 6.19. FTIR (ATR cm^{-1}): 3525 (-O-H stretching), 3045 (Ar C-H stretching), 2226 (-C≡N stretching), ESI-MS (+ve mode) m/z calculated for $C_{29}H_{28}N_2O_3$ is 452.21 found 453.60 [m/z].

*Synthesis of (Z)-5-((9-hexyl-6-(4-methoxyphenyl)-9H-carbazol-3-yl) methylene) thiazolidine-2, 4-dione (**n-C₁₇**)*

A mixture of 9-hexyl-6-(4-methoxyphenyl)-*9H*-carbazole-3-carbaldehyde (**8**, 0.100 g, 0.259 mmol), 2, 4 thiazolidinedione (0.036 g, 0.312 mmol), and NH_4OAc (0.220 g, 3.03 mmol) was taken in a dry 100 mL RB flask. The mixture was dissolved in 20 mL of glacial acetic acid and then` stirred at 110 ℃ for 12 h under argon atmosphere. The reaction completion was monitored by TLC technique. After completion of the reaction, the content was allowed to attain room temperature, then it was poured into 100 g of crushed ice and obtained red solid was filtered and dried. The product was purified by column chromatography using silica gel (200-400 mesh) and $CHCl_3$: CH_3OH (10:1) as mobile phase. Red colored solid, Yield 52%, m.p. 204-206 ℃. ^{1}H NMR (400MHz, DMSO-d_6, ppm): 10.06 (s, 1H), 8.86 (s, 1H), 8.59 (d, 1H), 8.52 8.48 (d, J=13.2 Hz, 2H), 7.97 (s, 1H), 7.79-7.69 (m, 5H), 7.08-7.06 (d, J=8.8Hz, 2H), 4.48-4.4.45 (t, 3H), 3.82 (s, 3H), 1.79-1.77 (d, 2H), 1.28-1.20 (m, 6H), 0.82-0.79 (t, 2H), ^{13}C NMR (400MHz, DMSO-d_6, ppm): 168.83, 158.88, 141.88, 140.26, 133.83, 133.69, 132.53, 128.55, 128.34, 125.83, 124.24, 123.85, 123.43, 122.98, 119.80, 118.74, 114.82, 110.89, 110.75, 55.65, 43.08. 40.61, 40.40, 40.19, 39.98, 39.77, 39.56, 39.35, 31.41, 28.99, 26.54, 22.47, 14.32. FTIR (ATR cm^{-1}): 3346 (>N-H stretching), 3042 (Ar C-H stretching). Anal. Calculated for $C_{29}H_{28}N_2O_3S$: C, 71.90; H, 5.78; N,

5.78; found: C, 71.87; H, 5.82; N, 5.78 ESI-MS (+ve mode) m/z calculated for $C_{29}H_{28}N_2O_3S$ is 484.18 found 485.30 [m/z].

*Synthesis   of   5-((9-hexyl-6-(4-methoxyphenyl)-9H-carbazol-3-yl)methylene)pyrimidine-2,4,6(1H,3H,5H)-trione (**n-C18**)*

A mixture of 9-hexyl-6-(4-methoxyphenyl)-*9H*-carbazole-3-carbaldehyde (**8**, 0.100 g, 0.259 mmol), barbituric acid (0.040 g, 0.312 mmol), was taken in a dry 100 mL RB flask. The mixture was dissolved in 20 mL of absolute methanol and then stirred at 110 ºC for 12 h under argon atmosphere. The reaction completion was monitored by TLC technique. When the reaction completes, the content was allowed to attain room temperature, the separated solid was collected by filtration and dried. The product was recrystallized from methanol. Yield 72%, m.p. 202-204 ºC. ^{1}H NMR (400MHz, DMSO-d$_6$, ppm): 11.32 (s, 1H), 11.20 (s, 1H), 9.33 (s, 1H), 8.72-8.70 (d, J=8.8 Hz, 1H), 8.54 (s, 1H), 8.44 (s, 1H), 7.82-7.72 (m, 5H), 7.09-7.07 (d, J=8.8 Hz, 2H), 4.51-4.47 (t, 3H), 3.82 (s, 3H), 1.81-1.80 (t, 2H), 1.29-1.21 (m, 6H), 0.83-0.79 (t, 3H) ^{13}C NMR (400MHz, DMSO-d$_6$, ppm): 168.23, 164.71, 162.90, 158.97, 152.13, 150.78, 140.00, 140.33, 133.58, 128.28, 125.83, 123.98, 123.54, 122.85, 118.49, 114.91, 114.53, 109.90, 55.66, 31.41, 29.03, 22.47, 14.32. FTIR (ATR cm^{-1}): 3456 (>N-H stretching), 2989 (Ar C-H stretching). Anal. Calcd. for $C_{30}H_{29}N_3O_4$: C, 72.72; H, 5.86; N, 8.48; found: C, 72.71; H, 5.90; N, 8.48. ESI-MS (+ve mode) m/z calculated for $C_{30}H_{29}N_3O_4$ is 495.22 found 495.40 [m/z].

3.2.2.6 Synthesis of Series-5 molecules (*n*-C$_{19-21}$)

Scheme 3.6 illustrates the synthetic routes for the preparation of carbazole based organic dyes (*n*-C$_{19-21}$) with A-π-D-π-A configuration, carrying three varied electron acceptor/anchoring units in their structure.

3.2.2.6.1 Chemistry

The synthetic routes of the three new organic sensitizers/co-sensitizers *n*-C$_{19-21}$ are showed in **Scheme 3.6.** The first intermediates 3-bromo-9-hexyl-*9H*-carbazole (**3**) and 6-bromo-9-hexyl-*9H*-carbazole-3-carbaldehyde (**7**) were prepared as per the procedure described in section **3.2.2.5.2**. The key precursor, 6-(4-formylphenyl)-9-hexyl-*9H*-carbazole-3-carbaldehyde (**9**) was obtained from **7** in good yield through

Suzuki cross coupling reaction under anhydrous condition. In the final step, the highly pure dyes *n*-**C**19-21 were obtained by following Knoevenagel condensations, wherein the precursor **9** was condensed with different active methylene compounds, *viz.* cyanoacetic acid, 2, 4 thiazolidinedione and barbituric acid. All the new compounds were purified using either recrystallization or column chromatographic technique using a suitable solvent/solvent mixture. The structures of newly synthesized dyes and their intermediates were confirmed by various spectral techniques including elemental analysis.
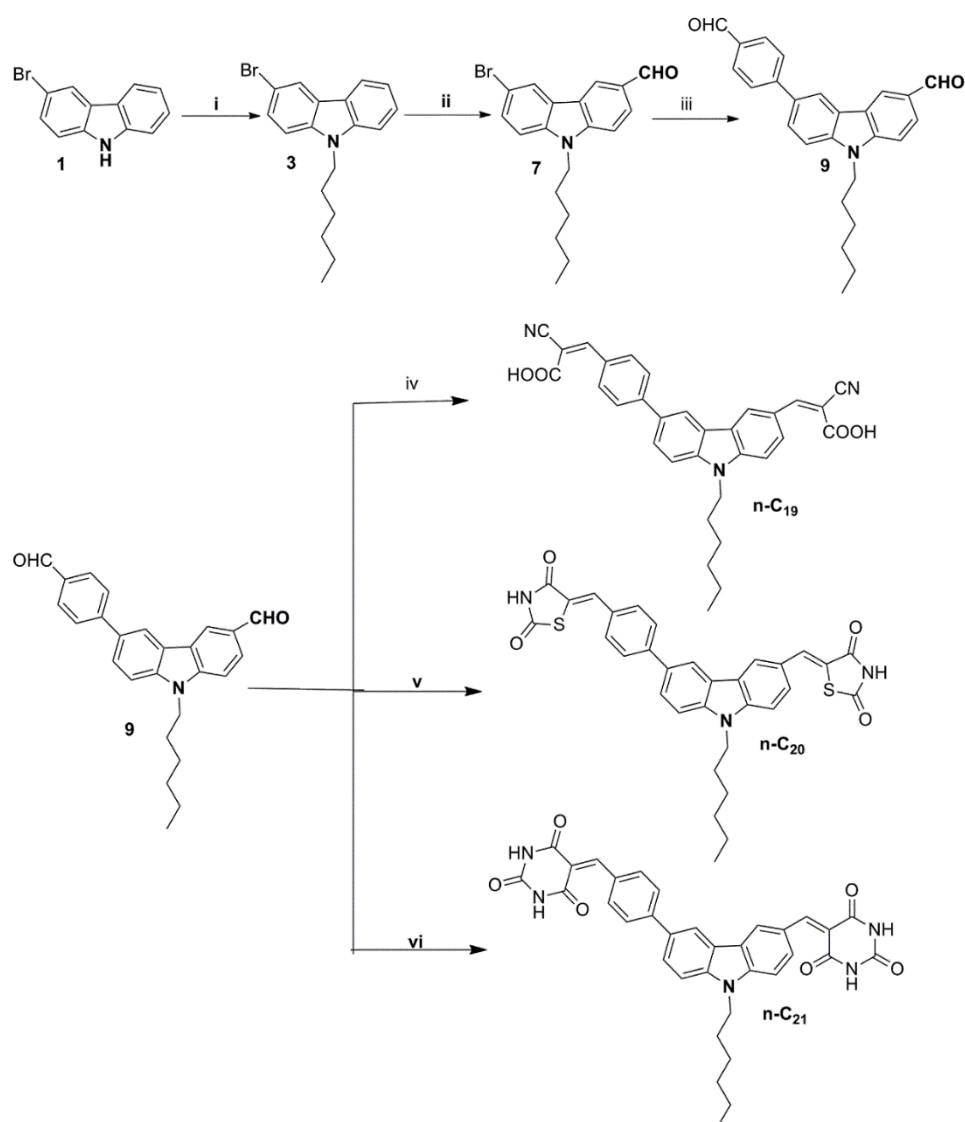
Scheme 3.6: Synthetic pathways for the synthesizing *n*-**C**19-21: (i) 1-Bromohexane, NaH, DMF, RT (ii) POCl3, DMF, 0 ℃ - RT (iii) (ii) 4-formylphenylboronic acid, Cs2CO3, toluene, 80 ℃ (iv) Cyanoacetic acid, ammonium acetate, glacial CH3COOH,

110 ℃ (v) 2, 4 thiazolidinedione, ammonium acetate, glacial CH₃COOH, 110 ℃ (vi) Barbituric acid, absolute methanol, 60 ℃

3.2.2.6.2 Synthesis and characterization

Synthesis of 6-(4-formylphenyl)-9-hexyl-9H-carbazole-3-carbaldehyde (9)

A mixture of 6-bromo-9-hexyl-*9H*-carbazole-3-carbaldehyde (**7**, 1 g, 3.0 mmol), 4-formylphenylboronic acid (0.45 g, 3.0 mmol), anhydrous cesium carbonate (2.96 g, 9.0 mmol), Pd(PPh₃)₄ (0.15 g, 0.1 mmol) and toluene (20 mL) was placed in 50 mL dry two neck RB flask under argon atmosphere and stirred at 80 ℃ for 18 h. After the completion of the reaction, the reaction mass was cooled down to room temperature, excess toluene was removed by rotary evaporator under vacuum. To the content, 20 mL of water was added and the organic layer was extracted with CH_2Cl_2 (30 mL x 3). The combined organic phase was dried over anhydrous Na_2SO_4 and solvent was removed under vacuum. The residue was purified using column chromatography on 200-400 mesh silica using 10:3 pet ether (60-80° C) / ethyl acetate mixture as the mobile phase. Pale yellow solid, Yield 52 %. m.p. 178-180 ℃. ^{1}H NMR (400MHz, DMSO-d₆, ppm): 10.08 (s, 1H), 8.91 (s, 1H), 8.85 (s, 1H), 8.11-8.09 (d, J=8.4 Hz, 2H), 8.06-7.98 (m, 5H), 7.85-7.83 (d, J=8.4 Hz, 1H), 4.54-4.50 (t, 3H), 1.83-1.80 (t, 2H), 1.34-1.15 (m, 6H), 0.83-0.79 (t, 3H). ^{13}C NMR (400MHz DMSO-d₆, ppm):193.32, 193.17, 146.96, 141.53, 130.71, 130.68, 129.03, 128.40, 127.67, 124.74, 123.55, 122.94, 120.27, 111.25, 110.62, 43.25, 31.39, 28.97, 26.50, 22.46, 14.30. Anal. Calculated for $C_{26}H_{25}NO_2$: C, 81.03; H, 7.01; N, 3.64 found C, 81.43; H, 6.57: N, 3.65. TOF HRMS m/z calculated for $C_{26}H_{25}NO_2$ is 383.1885 found 384.2127 [M+1].

2.2.3 Synthesis of (Z)-3-(4-(6-((Z)-2-carboxy-2-cyanovinyl)-9-hexyl-*9H*-carbazol-3-yl)phenyl) 2-cyanoacrylic acid (*n*-C₁₉)

A dry 100 mL RB flask was charged with a mixture of 6-(4-formylphenyl)-9-hexyl-*9H*-carbazole-3-carbaldehyde (**4**, 0.100 g, 0.275 mmol), cyanoacetic acid (0.028 g, 0.331 mmol), and ammonium acetate (0.233 g, 3.03 mmol) dissolved in 20 mL of glacial acetic acid. The reaction mixture was stirred at 110 ℃ for 12 h under inert atmosphere. After completion of the reaction, the mass was cooled to room temperature and was poured into 150 mL of ice cold water. The obtained solid was filtered and

dried. The crude product was purified by column chromatography using 200-400 mesh silica gel as stationary phase and CHCl$_3$: CH$_3$OH (10:1) as mobile phase to get red colored solid. Yield 58%; m.p. 174-178 ºC. ^{1}H NMR (400MHz DMSO-d$_6$, ppm): 13.69 (s, 1H), 8.91 (s, 1H), 8.44 (s, 1H), 8.40 (s, 1H), 8.33-8.31 (d, J=8.8 Hz, 1H), 7.87-7.76 (m, 3H), 7.72-7.70 (d, J=8.4 Hz, 2H), 7.09-7.07 (d, J=8.4 Hz, 1H), 4.51-4.48 (t, 3H), 3.82 (s, 3H), 1.79 (s, 2H), 1.29-1.15 (m, 6H), 0.83-0.79 (t, 3H). ^{13}C NMR (400MHz DMSO-d$_6$, ppm):163.57, 158.97, 143.59, 142.65, 141.35, 131.77, 131.56, 128.03, 127.66, 123.27, 122.82, 118.52, 117.79, 114.91, 111.12, 110.95, 98.89, 31.38, 29.00, 26.49, 22.46, 14.31. FTIR (ATR cm^{-1}): 3455 (-O-H stretching), 3056 (Ar C-H stretching), 2186 (-C≡N stretching). Anal. Calculated for C$_{32}$H$_{27}$N$_3$O$_4$: C, 74.27; H, 5.22; N, 8.12 found C, 74.26; H, 5.26: N, 8.12. ESI-MS (+ve mode) m/z calculated for C$_{32}$H$_{27}$N$_3$O$_4$ is 517.20 found 518.26 [m/z].

2.2.4 Synthesis of (Z)-5-((9-hexyl-6-(4-methoxyphenyl)-9H-carbazol-3-yl) methylene) thiazolidine-2, 4-dione (n-C$_{20}$)

A mixture of 6-(4-formylphenyl)-9-hexyl-*9H*-carbazole-3-carbaldehyde (**4**, 0.100 g, 0.275 mmol), 2, 4 thiazolidinedione (0.063 g, 0.331 mmol), and NH$_4$OAc (0.233 g, 3.03 mmol) was taken in a dry 100 mL RB flask. The mixture was dissolved in 20 mL of glacial acetic acid and then` stirred at 110 ºC for 12 h under argon atmosphere. The reaction completion was monitored by TLC technique. After completion of the reaction, the content was allowed to attain room temperature, then it was poured into 100 g of crushed ice and obtained red solid was filtered and dried. The product was purified by column chromatography using silica gel (200-400 mesh) and CHCl$_3$: CH$_3$OH (10:1) as mobile phase. Red colored solid. Yield 52%; m.p. 218-220 ºC. ^{1}H NMR (400MHz DMSO-d$_6$, ppm): 12.61 (s, 2H), 8.91-8.89 (d, J=7.6Hz, H), 8.80-8.77 (d, J=12.0Hz, 1H), 8.73 (s, 1H), 8.04-7.92 (m, 3H), 7.87-7.70(m, 5H), 4.50-4.47 (t, 3H), 1.80 (s, 2H), 1.28-1.21 (m, 6H), 0.82-0.79 (t, 2H). ^{13}C NMR (400MHz DMSO-d$_6$, ppm): 168.05, 158.88, 141.88, 140.26, 133.83, 133.69, 132.53, 128.55, 128.34, 125.83, 124.24, 123.85, 123.43, 122.98, 119.80, 118.74, 114.82, 110.89, 110.75, 31.41, 28.98, 26.52, 22.47, 14.31. FTIR (ATR cm^{-1}): 3406 (>N-H stretching), 3186 (Ar C-H stretching). Anal. Calculated for C$_{32}$H$_{27}$N$_3$O$_4$S$_2$: C, 66.09; H, 4.65; N, 7.23; found: C,

66.07; H, 4.68; N, 7.22 ESI-MS (+ve mode) m/z calculated for $C_{32}H_{27}N_3O_4S_2$ is 484.18 found 485.30 [m/z].

2.2.5 Synthesis of 5-((9-hexyl-6-(4-methoxyphenyl)-*9H*-carbazol-3-yl)methylene)pyrimidine-2,4,6(1H,3H,5H)-trione (*n*-C$_{21}$)

A mixture of 6-(4-formylphenyl)-9-hexyl-*9H*-carbazole-3-carbaldehyde (**4**, 0.100 g, 0.275 mmol), barbituric acid (0.063 g, 0.331 mmol), was taken in a dry 100 mL RB flask. The mixture was dissolved in 20 mL of absolute methanol and then stirred at 60 ºC for 12 h under argon atmosphere. The reaction completion was monitored by TLC technique. When the reaction completes, the content was allowed to attain room temperature, the separated solid was collected by filtration and dried. The product was recrystallized from methanol. Yield 72%; m.p. 222-224 ºC. ^{1}H NMR (400MHz DMSO-d$_6$, ppm): 11.40 (s, 1H), 11.32-11.27 (d, J=8.8 Hz, 2H), 11.20 (s, 1H), 9.36 (s, 1H), 9.30 (s, 1H), 8.75-8.69 (m, 2H), 8.35 (s, 2H), 8.04-7.95 (m, 3H), 7.84-7.74 (m, 2H), 4.51-4.49 (t, 3H), 1.81 (s, 2H), 1.29-1.25 (m, 6H), 0.83-0.80 (t, 3H) ^{13}C NMR (400MHz DMSO-d$_6$, ppm): 164.65, 164.08, 162.84, 162.35, 157.19, 154.94, 150.78, 150.69, 145.02, 144.05, 141.38, 135.27, 134.63, 133.61, 131.64, 131.40, 130.63, 127.64, 126.85, 126.51, 126.22, 124.29, 123.66, 122.82, 119.65, 118.55, 114.82, 111.35, 110.03, 43.28, 31.39, 29.02, 26.50, 22.46, 14.31. FTIR (ATR cm^{-1}): 3422 (>N-H stretching), 2995 (Ar C-H stretching). Anal. Calculated for $C_{34}H_{29}N_5O_6$: C, 67.66; H, 4.81; N, 11.61; found: C, 67.65; H, 4.84; N, 11.60. ESI-MS (+ve mode) m/z calculated for $C_{34}H_{29}N_5O_6$ is 603.21 found 603.64 [m/z].

3.2.2.7 Synthesis of Series-6 molecules (*p*-C$_{1-3}$)

Scheme 3.7 summarizes the synthetic routes for the preparation of carbazole based organic dyes (*p*-C$_{1-3}$) with D-A configuration, carrying three varied electron acceptor/anchoring units in their structures.
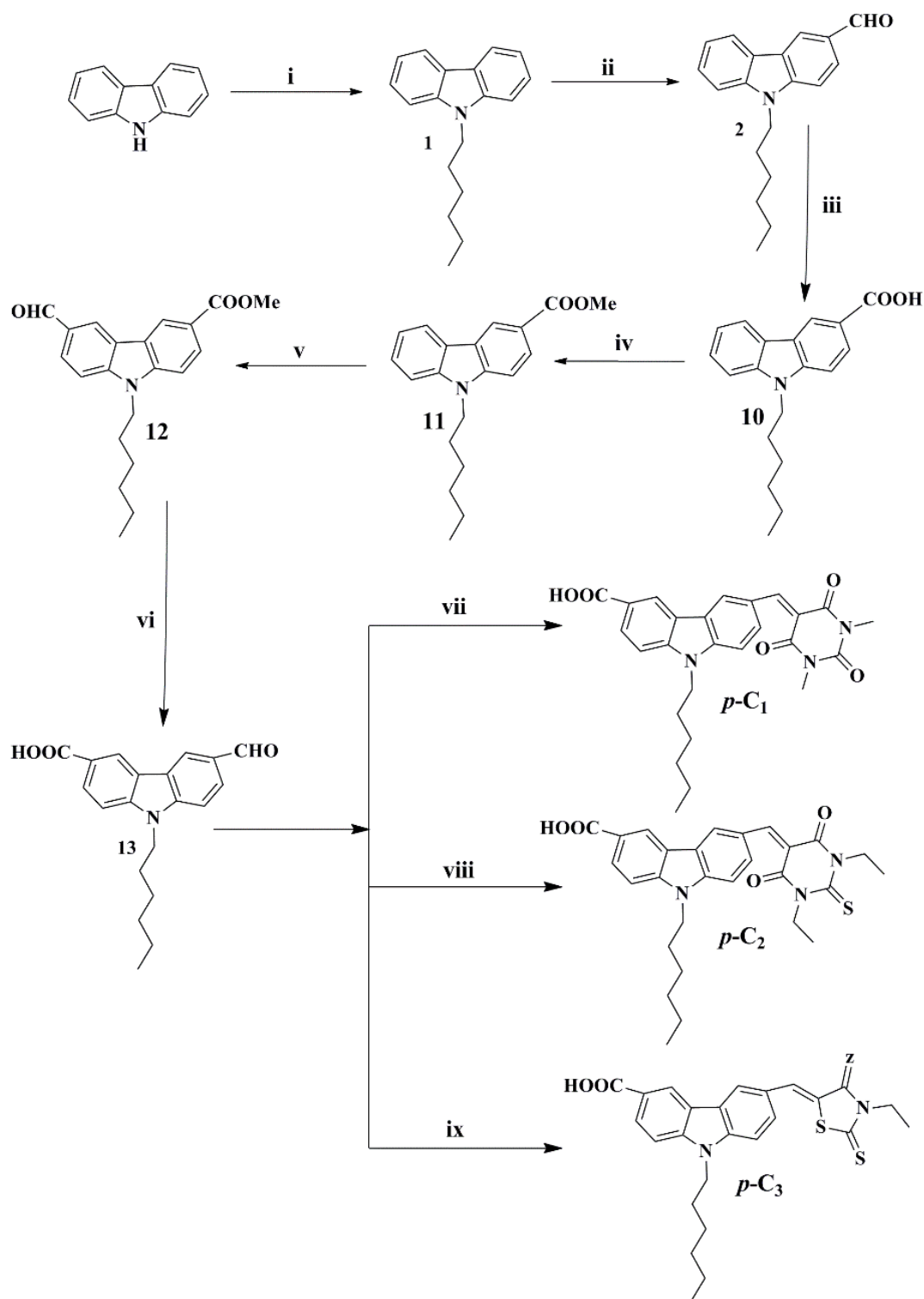
Scheme 3.7 Synthetic route for the chromophores *p*-**C₁₋₃.** (i) 1-Bromohexane, NaH, DMF, RT (ii) POCl₃, DMF, RT (iii) Ag₂O, NaOH, EtOH, RT (iv) MeOH, H₂SO₄, reflux (v) DMF, POCl₃, 90 ℃ (vi) LiOH.H₂O, 80 ℃ (vii) *N,N*-Dimethyl barbituric acid, methanol, 65 ℃, (viii) *N,N*-Diethyl thiobarbituric acid, methanol, 65 ℃, (ix) *N*-ethyl rhodanine, glacial acetic acid, 110 ℃.

3.2.2.7.1 Chemistry

The synthetic pathways of three new organic sensitizers (**p-C₁₋₃**) are depicted in **Scheme 3.7**. The intermediates **1** and **2** were synthesized according to the procedure discussed in section **3.2.2.2.2**. The intermediate **2** was oxidized to get 9-hexyl-9*H*-carbazole-3-carboxylic acid (**10**) with the help of Ag₂O using the standard procedure, reported by Qin et al. (2010). Then, carboxylic group of compound **10** was protected by esterifying (Fisher ester synthesis) to give the methyl 9-hexyl-*9H*-carbazole-3-carboxylate (**11**). Further, the ester **11** was formylated using Vilsmeier-Hack reaction protocol and the crude formylated product was hydrolyzed with lithium hydroxide to get the intermediate **13**. In the final step, the target molecules **p-C₁₋₃** were obtained in good yield by following Knoevenagel condensation of 6-formyl-9-hexyl-9*H*-carbazole-3-carboxylic acid (**6**) with *N,N*-dimethyl barbituric acid, *N,N*-diethyl thiobarbituric acid and *N*-ethyl rhodanine, respectively. The structures of newly synthesized dyes and their intermediates were confirmed by various spectroscopic techniques including elemental analysis.

3.2.2.7.2 Synthesis and characterization

*Synthesis of 9-hexyl-9H-carbazole-3-carboxylic acid (**10**)*

Sodium hydroxide (7.2 g, 179.0 mmol) was dissolved in 100 mL of ethanol. The silver oxide (4g, 17.9 mmol) was suspended in this solution and to this 9-hexyl-*9H*-carbazole-3-carbaldehyde (**2**, 1 g, 3.58 mmol) dissolved in 10 mL of toluene solution was added slowly with stirring at room temperature. The stirring was continued for 18 h under argon atmosphere. The reaction mass was filtered through celite bed. The solvent of the filtrate was removed under vacuum and the obtained residue was washed with distilled water. The product was extracted with ethyl acetate (3 × 100 mL) and the organic phase was washed with 10% sodium bicarbonate solution. Pre-cooled 10 % HCl was added to the collected aqueous layer and pH of the solution was brought to slightly acidic. The precipitated solid was filtered and dried. The residue was purified using column chromatography on 200-400 mess silica using 2:1 hexane/ethyl acetate mixture as the mobile phase. Pale yellow solid, 75%, m.p. 138-140 ℃. ¹H NMR (400 MHz, DMSO-d₆, ppm): 12.80 (s, 1H), 8.86-8.84 (d, J=8.8 Hz, 1H), 8.32 (s, 1H), 8.11 (s, 1H), 7.72 (s, 1H), 7.59-7.56 (d, J=12.4 Hz, 2H), 7.322 (s, 1H), 4.47-4.39 (t, 2H,),

1.79 (m, 2H), 1.27 (m, 6H), 0.86 (t, 3H). Anal. Calculated for $C_{19}H_{21}NO_2$: C, 77.30; H, 7.15; N, 4.72; found; C, 77.26; H, 7.17; N, 4.74.

Synthesis of methyl 9-hexyl-9H-carbazole-3-carboxylate (11)

In a 50 mL dry RB flask, 9-hexyl-*9H*-carbazole-3-carboxylic acid (**10**, 1 g, 3.39 mmol) was dissolved in 15 mL of dry methanol and 2 drops of conc. H_2SO_4 was added. The reaction mixture was refluxed for 3 h. After the completion of reaction, the product was cooled to room temperature and methanol was removed under vacuum. The residue was extracted with ethyl acetate (3 × 30 mL) and organic layer was washed with 10% sodium carbonate solution, followed by water. Then, it was dried using sodium sulfate and solvent was removed in vacuum to get yellow liquid. ^{1}H NMR (400 MHz CDCl$_3$, ppm): 8.81 (s, 1H), 8.16-8.11 (t, J=7.2 Hz, 2H), 7.50-7.23 (m, 4H), 4.26-4.23 (t, J=8 Hz, 2H), 3.96 (s, 3H), 1.86-1.79 (m, 2H), 1.35-1.23 (m, 6H), 0.86-0.83 (t, 3H). ^{13}C NMR (400 MHz CDCl$_3$, ppm): 167.97, 143.13, 141.03, 127.26, 126.33, 123.02, 122.90, 122.60, 120.66, 120.62, 119.83, 109.14, 108.19, 51.93, 43.30, 31.55, 28.90, 26.94, 22.55, 14.23, 14.18, 14.02. Anal. Calculated for $C_{20}H_{23}NO_2$: C, 77.66; H, 7.44; N, 4.53; found; C, 77.64; H, 7.49; N, 4.53.

Synthesis of 6-formyl-9-hexyl-9H-carbazole-3-carboxylic acid (13)

To 5.5 mL of freshly distilled DMF, 7.2 mL of POCl$_3$ was added slowly with constant stirring maintained at 0 ℃ under argon atmosphere. Then, a solution of methyl 9-hexyl-*9H*-carbazole-3-carboxylate (**11**, 0.5 g, 1.62 mmol) dissolved in 10 mL of ethylene dichloride was added to it while stirring. The reaction flask was allowed to attain room temperature and then heated at 90 ℃ for 12 h. The product was cooled and was poured into 150 mL of cold water. Its pH was adjusted to 1.0 with 5 M sodium hydroxide solution. The solution was extracted with ethyl acetate (3 x 30 mL) and dried over anhydrous sodium sulfate. The solvent was removed under vacuum. The obtained product was dissolved in 10 mL of methanol. To this solution, 0.25 g of LiOH.H$_2$O dissolved in 10 mL of water was added and stirred at 80 ℃ for 8 h. Then, the methanol was removed and the solution was diluted with 100 mL of water. The pH of the solution was made to just acidic by adding pre-cooled 10 % HCl. The precipitated solid was filtered and purified using column chromatography on 200-400 mess silica using 2:1 hexane/ethyl acetate mixture. Brown color solid, yield 42%. m.p. 196-198 ℃. ^{1}H NMR

(400 MHz CDCl$_3$, ppm): 10.31 (s, 1H), 8.98 (s, 1H), 8.68 (s, 1H), 8.33-8.31 (d, J=7.6 Hz, 1H), 8.10-8.08 (d, J=8.8Hz, 1H) 7.54-7.30 (m, 2H), 4.40-4.36 (t, 2H), 1.93-1.88 (m, 2H), 1.41-1.26 (m, 6H), 0.89-0.85 (t, 3H). ^{13}C NMR (400 MHz, DMSO-d$_6$, ppm): 193.52, 167.24, 164.71, 157.35, 143.01, 141.14, 135.69, 127.49, 119.70, 118.12, 110.22, 109.45, 40.60, 40.40, 40.29, 40.14, 39.79, 39.51, 39.31, 31.40, 28.92, 26.59, 22.40, 14.39. Anal. Calculated for C$_{20}$H$_{21}$NO$_3$: C, 74.30; H, 6.50; N, 4.33; found; C, 74.28; H, 6.55; N, 4.33.

*General synthetic procedure for dyes **p-C$_{1-2}$***

A clear solution of 6-formyl-9-hexyl-*9H*-carbazole-3-carboxylic acid (**13**, 0.5 g, 3.355 mmol) in 15 mL of absolute ethanol was stirred at room temperature for 0.5 h. Then, respective clear solution of *N,N*-dimethyl barbituric acid (4 mmol) or *N,N*-diethyl thiobarbituric acid (4 mmol) dissolved in 10 mL of absolute ethanol was added to it slowly with stirring. Further, the reaction mass was stirred at 65 °C for 10 h. The precipitated solid was filtered and washed with pre-cooled ethanol. The obtained dyes were purified by column chromatography with 2:1 hexane: ethyl acetate solvent system.

*6-((1,3-Dimethyl-2,4,6-trioxotetrahydropyrimidin-5(2H)-ylidene)methyl)-9-hexyl-9H-carbazole-3-carboxylic acid (**p-C$_1$**)*

Orange solid, yield 85%. m.p. 222-224 °C. ^{1}H NMR (400 MHz DMSO-d$_6$, ppm): 12.85 (s, 1H), 9.41 (s, 1H), 8.82 (s, 1H), 8.61-8.55 (m, 2H), 8.15-8.13 (d, J=8.4 Hz, 1H), 7.82-7.80 (d, J=7.6 Hz, 2H), 4.52 (s, 2H), 3.29 (s, 6H), 1.82-1.80 (m, 2H), 1.30-1.22 (m, 6H), 0.83 (t, 3H). ^{13}C NMR (400 MHz DMSO-d$_6$, ppm): 168.16, 163.21, 161.41, 157.76, 151.62, 144.16, 143.83, 134.21, 128.54, 128.35, 124.77, 123.19, 122.93, 122.64, 115.19, 110.49, 110.15, 43.37, 40.63, 40.42, 40.21, 40.00, 39.80, 39.59, 39.38, 31.36, 29.15, 28.94, 28.60, 26.47, 22.45. FTIR (ATR cm^{-1}): 3422 (-O-H stretching), 3046 (Ar C-H stretching). Anal. Calculated for C$_{26}$H$_{27}$N$_3$O$_5$: C, 67.67; H, 5.85; N, 9.11; found C, 67.66; H, 5.90; N, 9.10; m/z: calcd for C$_{26}$H$_{27}$N$_3$O$_5$: 461.20, found: 462.20 [M$^+$].

*6-((1,3-Diethyl-4,6-dioxo-2-thioxotetrahydropyrimidin-5(2H)-ylidene)methyl)-9-hexyl-9H-carbazole-3-carboxylic acid (**p-C$_2$**)*

Red solid, yield 88%. m.p. 232-236 °C. ^{1}HNMR (400 MHz DMSO-d$_6$, ppm): 12.91 (s, 1H), 9.44 (s, 1H), 8.82 (s, 1H), 8.62-8.55 (m, 2H), 8.13-8.10 (d, J=12.4 Hz, 1H), 7.82-7.80 (d, J=7.6 Hz, 2H), 4.50 (s, 2H), 4.39-4.36 (t, 2H), 1.82-1.80 (m, 2H), 1.29-1.24 (m, 12H), 0.80 (t, 3H). ^{13}C NMR (400 MHz DMSO-d$_6$, ppm): 177.18, 160.44, 156.08, 141.15, 135.67, 129.86, 126.68, 126.56, 122.83, 119.67, 118.33, 110.40, 40.45, 40.31, 40.10, 39.89, 39.57, 39.35, 31.36, 28.86, 26.52, 22.41, 14.26. FTIR (ATR cm^{-1}): 3486 (-O-H stretching), 3145 (Ar C-H stretching). Anal. Calculated for $C_{28}H_{31}N_3O_4S$: C, 61.53; H, 6.14; N, 8.31; found C, 61.51; H, 6.18; N, 8.31. m/z: calcd for $C_{28}H_{31}N_3O_4S$: 505.20. Found: 506.21 [M$^+$].

*Synthesis of (Z)-6-((3-ethyl-4-oxo-2-thioxothiazolidin-5-ylidene)methyl)-9-hexyl-9H-carbazole-3-carboxylic acid (**p-C$_3$**)*

A mixture of 6-formyl-9-hexyl-*9H*-carbazole-3-carboxylic acid (**13**, 0.5g, 3.355 mmol), *N*-ethylrhodanine (0.063 g, 4 mmol), and NH$_4$OAc (0.233 g, 3.03 mmol) was taken in a dry 100 mL RB flask. The mixture was dissolved in 20 mL of glacial acetic acid and then stirred at 110 °C for 12 h under argon atmosphere. The reaction completion was monitored by TLC technique. After completion of the reaction, the content was cooled to room temperature and then it was poured into 100 g of crushed ice. The obtained red solid was filtered and dried. The product was purified by column chromatography using silica gel (200-400 mesh) and CHCl$_3$: CH$_3$OH (10:1) as the mobile phase. Orange solid, yield 85%. m.p. 186-188 °C. ^{1}HNMR (400 MHz DMSO-d$_6$, ppm), 8.68 (s, 1H), 8.35 (s, 1H), 8.10 (s, 1H), 7.83-7.74 (m, 2H), 7.67 (s, 1H), 7.53-7.51 (d, J=6.4 Hz, 2H), 4.45 (s, 2H), 4.33 (s, 2H), 1.82-1.77 (m, 2H), 1.30-1.27 (m, 9H), 0.80 (s, 3H). ^{13}C NMR (400 MHz DMSO-d$_6$, ppm): 192.86, 167.75, 166.96, 144.14, 141.08, 140.68, 134.26, 132.16, 131.22, 129.71, 127.62, 126.57, 125.21, 123.36, 122.76, 121.14, 119.52, 119.32, 110.09, 45.68, 42.81, 40.68, 40.48, 40.27, 40.06, 39.74, 39.52, 39.32, 31.41, 28.94, 26.64, 22.47, 14.38. FTIR (ATR cm^{-1}): 3410 (-O-H stretching), 3012 (Ar C-H stretching). Anal. Calculated for $C_{25}H_{26}N_2O_3S_2$: C, 64.37; H, 5.58; N, 6.01; found C, 64.35; H, 5.62; N, 6.00; m/z: calcd for $C_{25}H_{26}N_2O_3S_2$: 466.14. Found: 467.14 [M$^+$].

3.2.3 Results and discussion

All the designed dyes were synthesized following standard synthetic protocols. The chemical structures of newly synthesized organic chromophores and their intermediates were confirmed by various spectral techniques including elemental analysis. In the following section, spectral characterization of few selected representative dyes has been discussed.

3.2.3.1 *n*-C$_{1-5}$ (Series-1A)

The ^{1}H NMR spectrum of *n*-C$_2$ is displayed in **Fig 3.1**. The spectrum showed the appearance of two unique peaks for protons of N-CH$_3$ at δ 3.23 ppm and 3.51 ppm. The aromatic protons of phenylene ring were observed in the region of δ 8.44-6.81 ppm. The ^{13}C NMR spectrum of dye *n*-C$_2$ (**Fig 3.2**) showed the characteristic signals obtained at a higher frequency (downfield region). The carbonyl carbon of *n*-C$_2$ was resonated at δ 163.72 and 161.66 ppm, whereas the remaining signals appearing in the region of δ 156.80-109.79 ppm are due to other aromatic carbons. Further, the aliphatic carbons appeared around 28.98 ppm. Furthermore, its FTIR spectrum (**Fig 3.3**), showed a sharp peak at 1652 cm^{-1} indicating the presence of carbonyl group. Its mass spectrum (**Fig 3.4**) displayed the [M+H]$^+$ peak at 288.14, which is in agreement with the calculated molecular weight for the formula of C$_{15}$H$_{17}$N$_3$O$_3$. Finally, the 3D structures of *n*-C$_2$ and *n*-C$_4$ have been confirmed from SC-XRD analysis and their crystal data are presented in **Table 2.1**. The SC-XRD studies revealed that, both the dyes *n*-C$_2$ and *n*-C$_4$ crystallize in triclinic space group *P*-1. Their cell parameters and the ORTEP diagram of the solved structures are summarized in **Fig 3.5.**
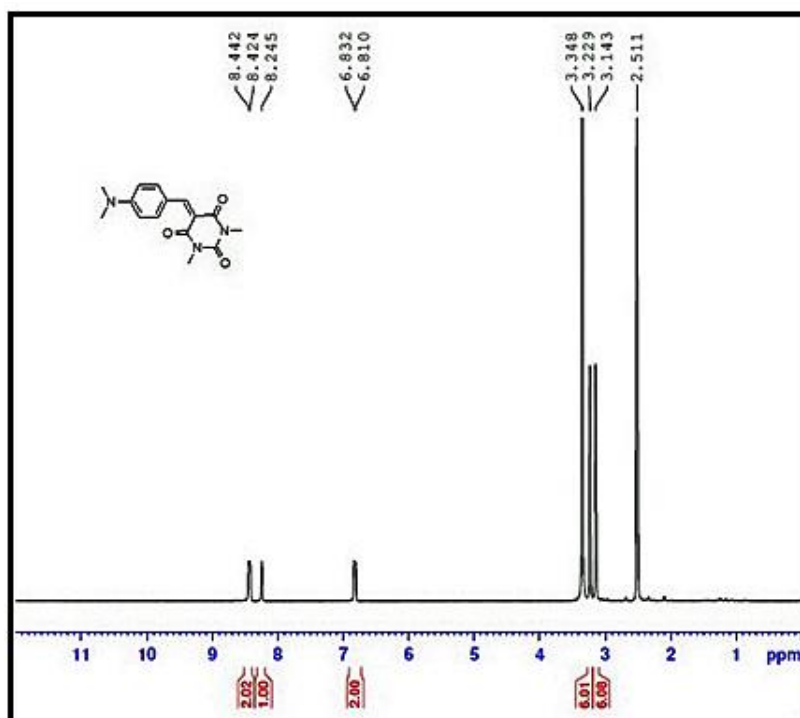
Fig 3.1: ^{1}H NMR spectrum of *n*-**C₂**
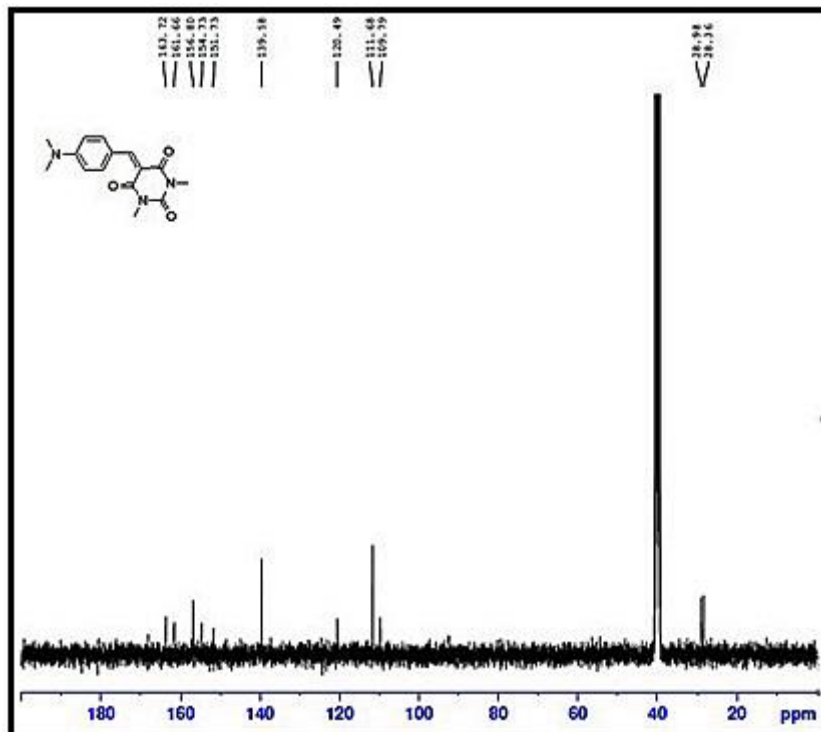
Fig 3.2: ^{13}C NMR spectrum of *n*-**C₂**
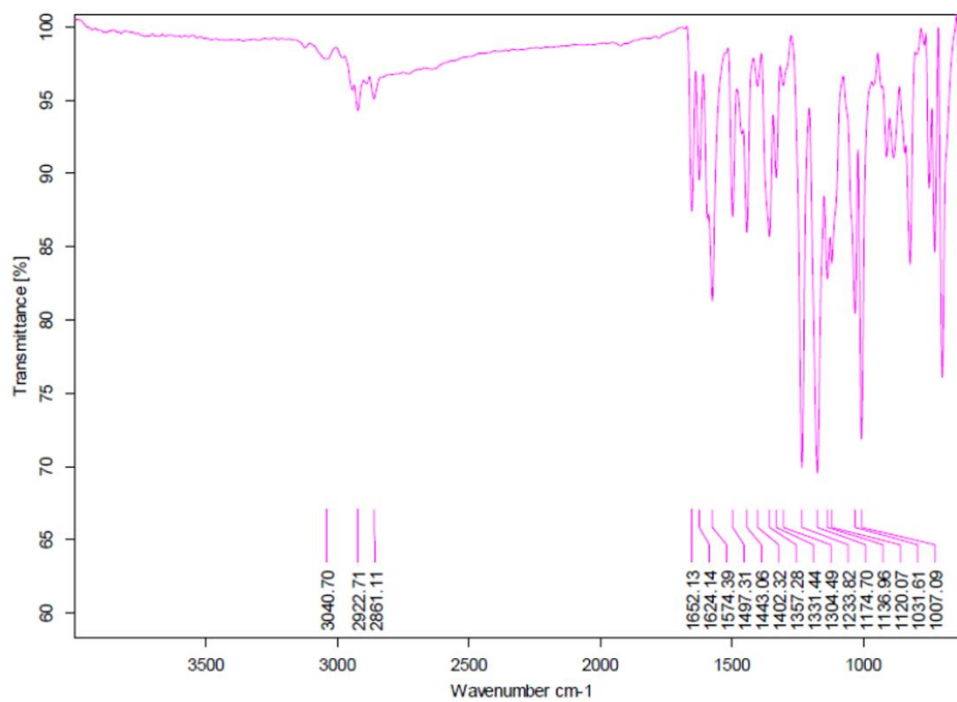
Fig 3.3: FTIR spectrum of *n*-**C₂**
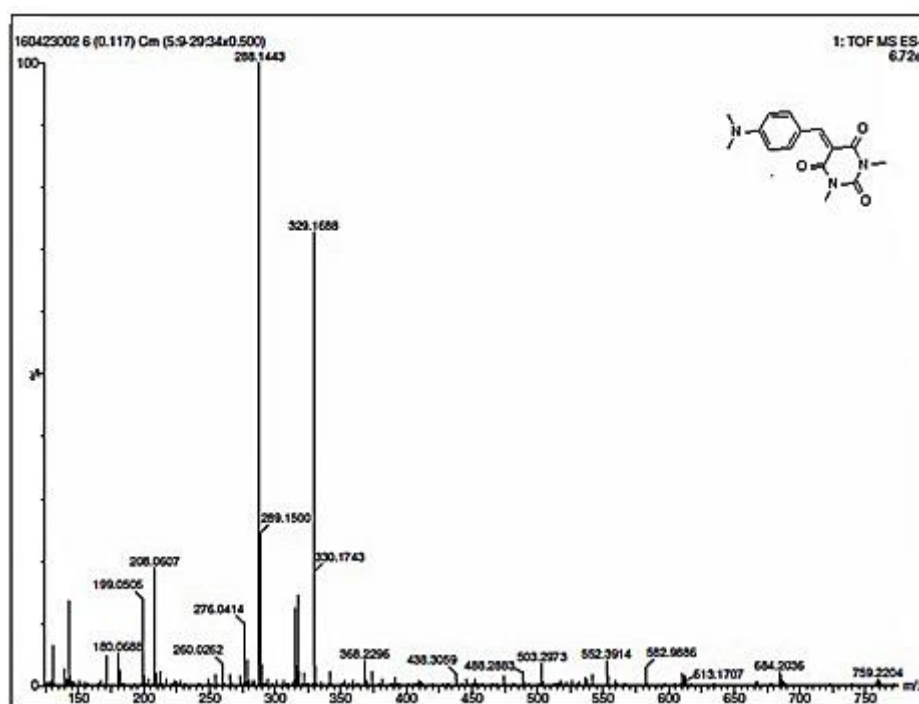
Fig 3.4: TOF-HRMS of *n*-**C₂**

Table 3.1: Crystal and structure refinement data for *n*-C₂ and *n*-C₄

Compound	*n*-**C₂**	*n*-**C₄**
Formula	$C_{15}H_{17}N_3O_3$	$C_{17}H_{21}N_3O_2S$
Formula weight	287.32	331.43
CCDC number	1456338	1490875
Temperature (K)	296(2)	296(2)
Crystal form	Block	Block
Color	Orange	Red
Crystal system	Triclinic	Triclinic
Space group	P-1	P-1
a (Å)	8.7515(3)	7.9072(2)
c (Å)	9.0880(3)	10.3716(3)
a (0)	81.822(2)	88.3470(10)
b (0)	81.299(2)	79.4360(10)
g (0)	83.835(2)	86.0360(10)
Volume ($Å^3$)	696.81(4)	823.95(4)
Z	2	2
Density (g cm⁻³)	1.369	1.336
μ (mm⁻¹)	0.097	0.210
F (000)+	304	352
$h_{min, \ max}$	-10, 10	-9, 9
$k_{min, \ max}$	-11, 10	-12, 12
$l_{min, \ max}$	-11, 11	-12, 12
Reflections collected	2736	3239
R_{all}, R_{obs}	0.0541, 0.0441	0.0440, 0.0393
wR2_all, wR2_obs	0.1350, 0.1207	0.1281, 0.1197
GOOF	0.674	0.835
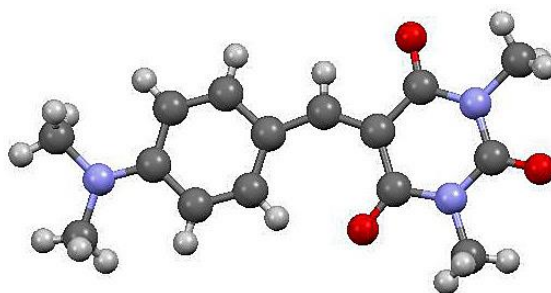
Fig 3.5a: ORTEP diagram of *n*-C$_2$
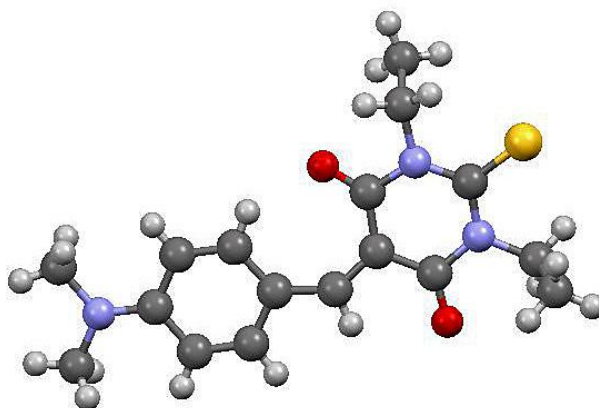
Fig 3.5b: ORTEP diagram of *n*-C$_4$

3.2.3.2 *n*-C$_{6-8}$ (Series-1B)

The chemical structures of all the intermediates and final compounds in this series were well characterized by ^{1}H NMR, ^{13}C NMR, Mass spectroscopy and elemental analysis. The compound *n*-C$_8$, in its ^{1}H NMR spectrum (**Fig 3.6**), showed two unique resonance peaks for aromatic amines of barbituric acid, *i.e.* one at δ 11.30 and the other at 11.19 ppm. Appearance of a sharp singlet at δ 9.31 ppm can be ascribed to the protons of vinylene group linked to aromatic carbazole ring at the 3rd position. All the other aromatic protons of carbazole ring resonated in between δ 8.30 to 7.31 ppm as multiplet. Further, appearance of a triplet in between δ 4.48 to 4.45 ppm can be assigned to two protons of methylene attached to the nitrogen N-CH$_2$. Also, the peaks in the region of 1.82 to 0.79 ppm correspond to primary and secondary protons of hexyl chain. The ^{13}C NMR spectrum of *n*-C$_8$ dye showed the characteristic signals at downfield region (**Fig 3.7**). The three carbonyl carbon atoms of barbituric acid resonated at δ164.71, 162.90 and 157.35 ppm. The signal appeared at δ150.77 ppm is

due to vinylene carbon of the structure. The signals in the region of δ 143.60 to 109.73 ppm are due to other aromatic carbons, whereas the aliphatic carbons appeared between 43.09 to 14.29 ppm. Further, its mass spectrum (**Fig 3.8)** exhibited the [M+H]$^+$ peak at 390.1840, which is in good agreement with the calculated molecular weight, which confirms the chemical structure of the synthesized dye **n-C₈**.
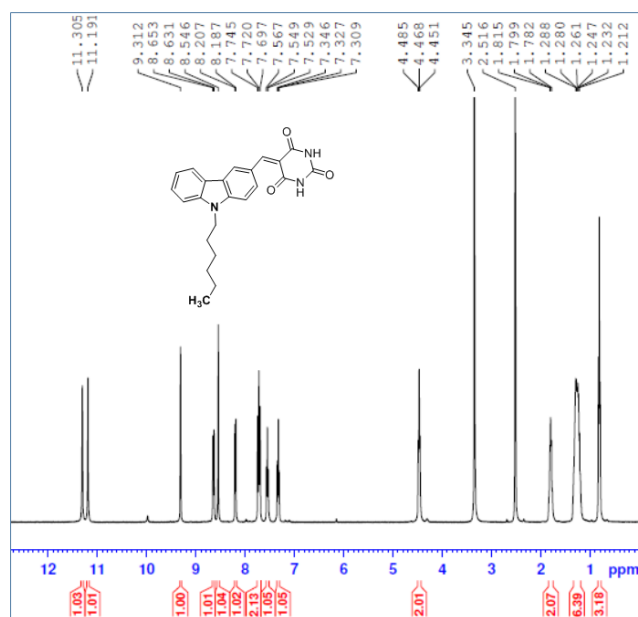
Fig 3.6: ^{1}H NMR spectrum of **n-C₈**
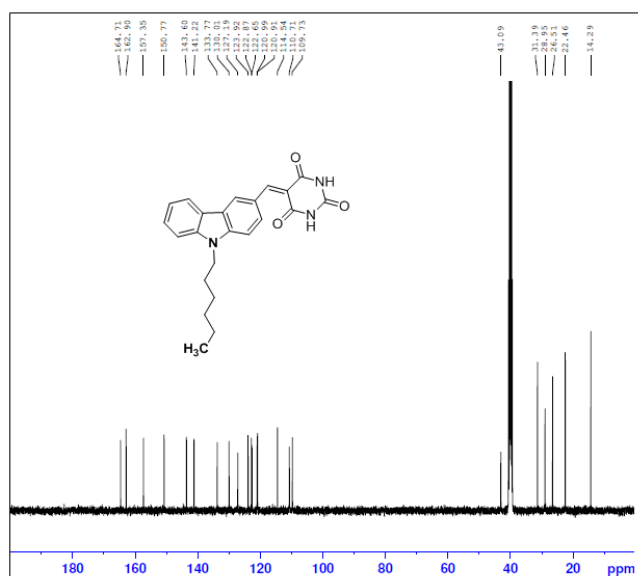
Fig 3.7: ^{13}C NMR spectrum of **n-C₈**
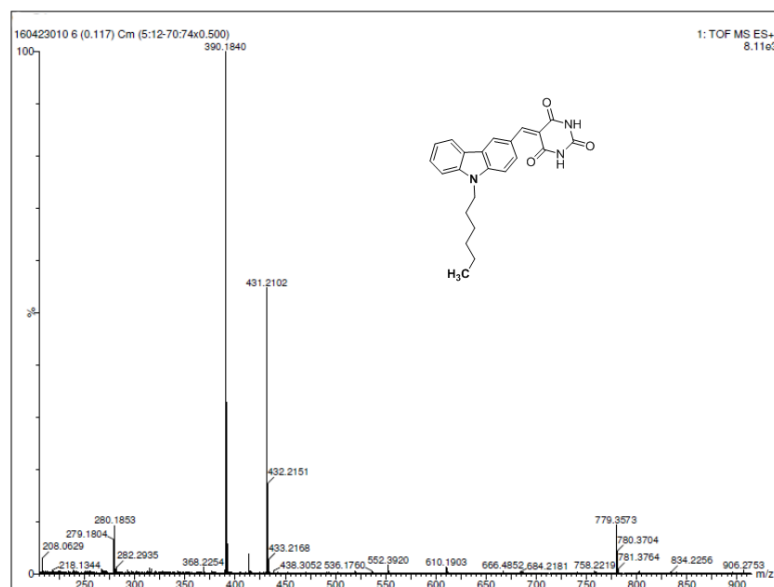
Fig 3.8: TOF-HRMS of *n*-C₈

3.2.3.3 *n*-C₉₋₁₂ (Series-2)

The molecular structures of the intermediates as well as final compounds in this series are well elucidated by ^{1}H NMR, ^{13}C NMR, Mass spectroscopy and elemental analysis. The ^{1}H NMR, ^{13}C NMR and mass spectra of the selected dye **n-C₁₀** are depicted in **Figs 3.9, 3.10** and **3.11**, respectively. In its ^{1}H NMR spectrum, all the aromatic protons of carbazole and phenylene ring appeared in between δ 8.64 to 7.22 ppm as medium multiplet. Further, appearance of a singlet peak at δ 4.75 ppm accounts for two protons of methylene (N-CH₂) in rhodanine-3-acetic acid scaffold, while appearance of a triplet in between δ 4.45 to 4.41 ppm is due to presence of two protons of methylene (N-CH₂) of hexyl chain in the assigned structure. Also, the peaks in the region of δ 1.81 to 0.82 ppm correspond to primary and secondary protons of hexyl chain. The ^{13}C NMR spectrum of **n-C₁₀** dye displayed the characteristic signals which appeared at higher frequency region. The carbonyl carbon atom of acid group resonated at δ 166.91 ppm, while thione and carbonyl carbon atoms of the rhodanine unit were observed at 193.56 and 167.79, respectively. The signals in the region of δ 144.17 to 110.04 ppm are due to other aromatic carbons. The aliphatic carbons have appeared between δ 45.62 to 14.33 ppm. Further, its mass spectrum exhibited the [M+H]⁺ peak at 529.49, which is in good agreement with the calculated molecular weight, which confirms the chemical structure of the synthesized dye **n-C₁₀**.
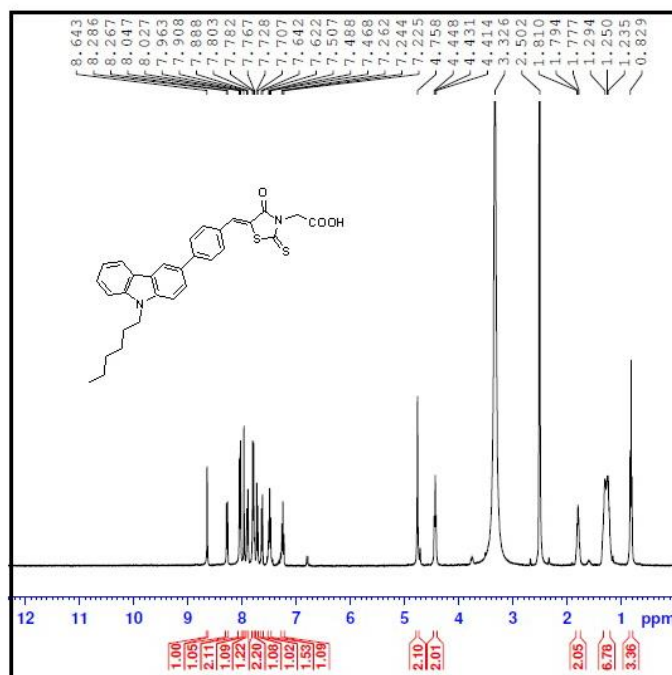
Fig 3.9: ^{1}H NMR spectrum of *n*-**C₁₀**
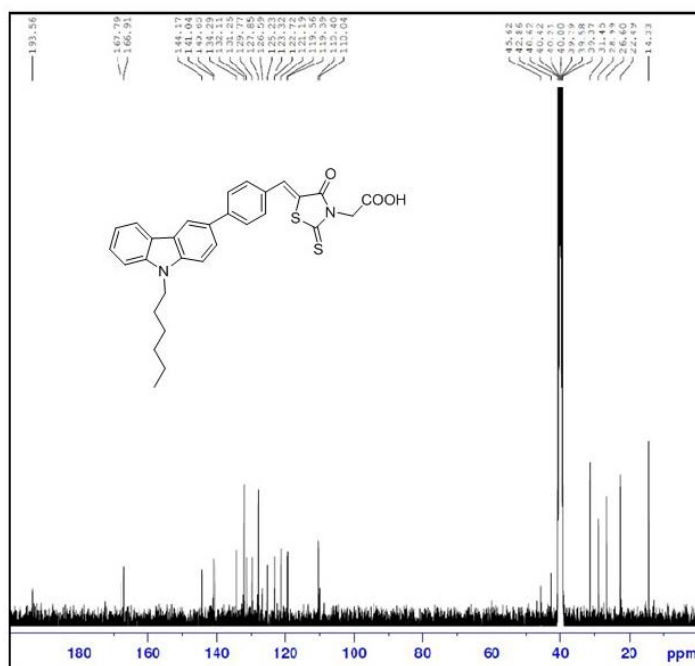
Fig 3.10: ^{13}C NMR spectrum of *n*-**C₁₀**
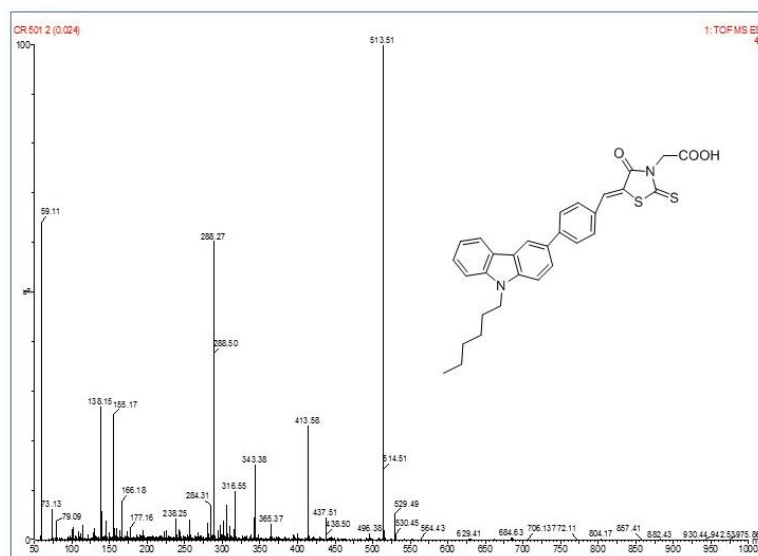
Fig 3.11: ESI Mass spectrum of *n*-C10

3.2.3.4 *n*-C13-15 (Series-3)

In this series, the structures of the synthesized target molecules and their intermediates were determined using spectral techniques. In ^{1}H NMR spectrum (**Fig 3.12**) of *n*-C13, all the aromatic protons of carbazole core and thiophene ring resonated in between δ 8.80 to 7.29 ppm. Further, an appearance of the triplet in between δ 4.48 to 4.44 ppm can be assigned to two protons of methylene (N-CH2) of hexyl chain in the assigned structure. Also, the peaks in the region of δ 1.81 to 0.82 ppm are due to the primary and secondary protons of hexyl chain. The ^{13}C NMR spectrum of *n*-C13 dye displayed the characteristic signals which appeared at the downfield region. The carbonyl carbon atom in acid group resonated at δ 167.03 ppm. The signals in the region of δ 154.21 to 102.05 ppm are due to other aromatic carbons, whereas the aliphatic carbons appeared between δ 58.42 to 19.21 ppm. Further, its mass spectrum exhibited the [m/z] peak at 479.10, which is in good agreement with the calculated molecular weight, which confirms the chemical structure of the synthesized dye *n*-C13.
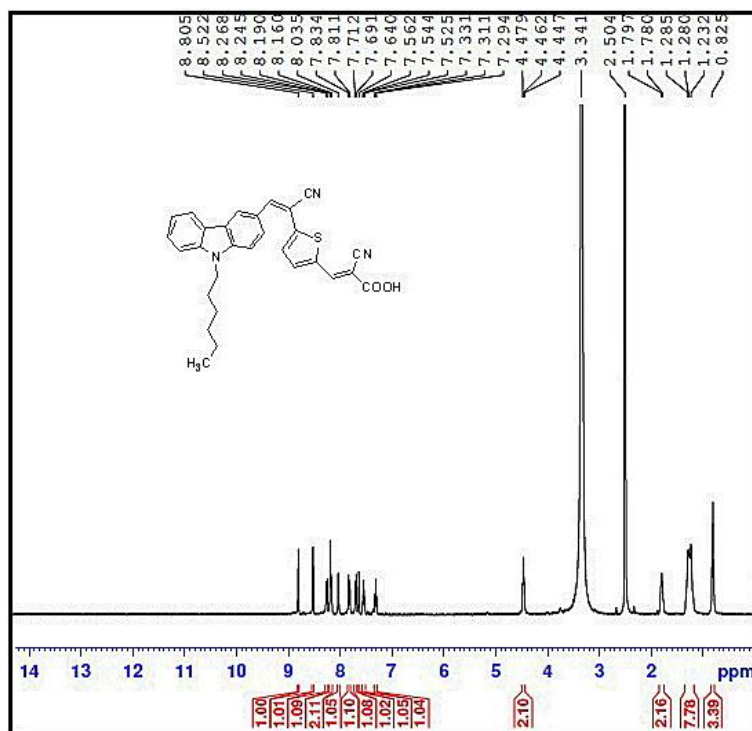
Fig 3.12: ^{1}H NMR spectrum of *n*-**C₁₃**
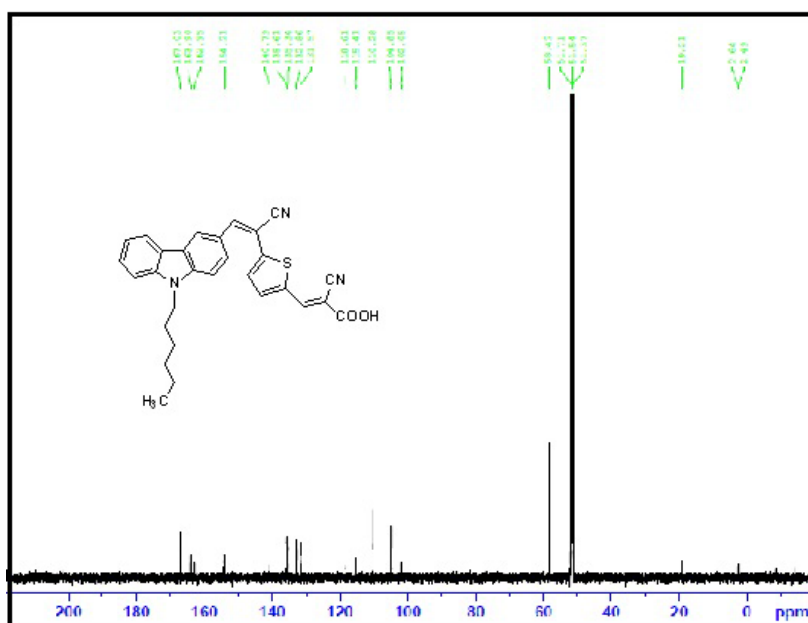
Fig 3.13: ^{13}C NMR spectrum of *n*-**C₁₃**
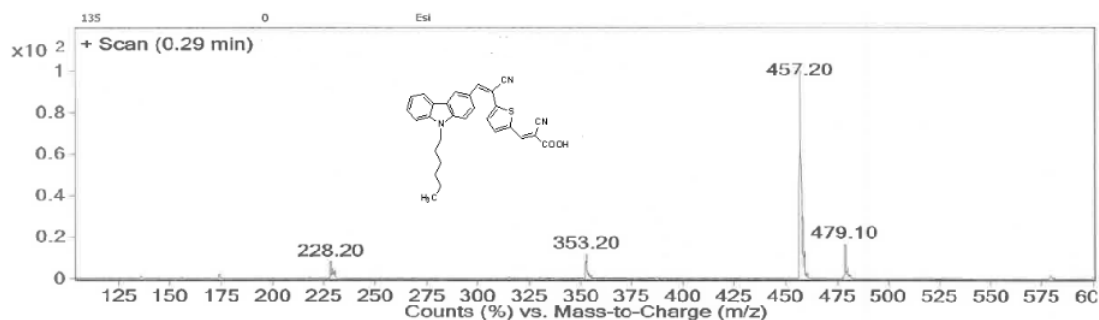
Fig 3.14: ESI Mass spectrum of *n*-**C₁₃**

3.2.3.5 *n*-C₁₆₋₁₈ (Series-4)

The structural interpretation of all the synthesized dyes and their intermediates were carried out using various spectral techniques. For example, *n*-**C₁₆** was well characterized using ^{1}H NMR, ^{13}C NMR and Mass spectral techniques. In its ^{1}H NMR spectrum, a unique resonance peak for carboxylic acid proton was observed at δ 13.69 ppm. A singlet at 8.91 ppm can be ascribed to vinylene proton, whereas all the other aromatic protons of carbazole core and anisole unit were observed in between δ 8.44 to 7.07 ppm. Further, the appearance of triplet signal in between δ 4.48 to 4.45 ppm can be attributed to two protons of N-CH₂. Also, three protons of methoxy group of anisole resonated as singlet peak at 3.82 ppm. In addition, the primary and secondary protons of hexyl group appeared as multiplet in the region of δ 1.79 to 0.79 ppm. The ^{13}C NMR spectrum of *n*-**C₁₆** dye exhibited the characteristic signals which appeared at the high frequency (downfield) region. The carbonyl carbon atom in acid group resonated at δ 164.63 ppm, while the vinylene carbon signal appeared at δ 158.97 ppm. The signals in the region of δ 143.60 to 109.73 ppm are due to other aromatic carbons. Likewise, the aliphatic carbons of the methoxy group and hexyl chain in the assigned structure appeared in between δ 43.09 to 14.31 ppm. Finally, the observed molecular ion peak at 453.60 in its mass spectrum is consistent with the calculated molecular weight for *n*-**C₁₆** with chemical formula $C_{29}H_{25}N_3O_2S$. **Figs 3.15- 3.17** show the ^{1}H NMR, ^{13}C NMR and mass spectra of the dye *n*-**C₁₆**, respectively.
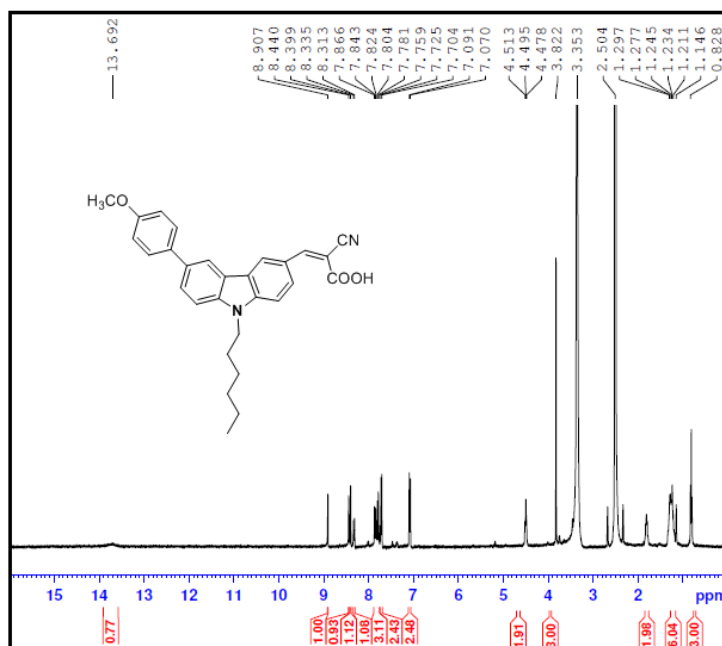
Fig 3.15: ^{1}H NMR spectrum of *n*-C$_{16}$
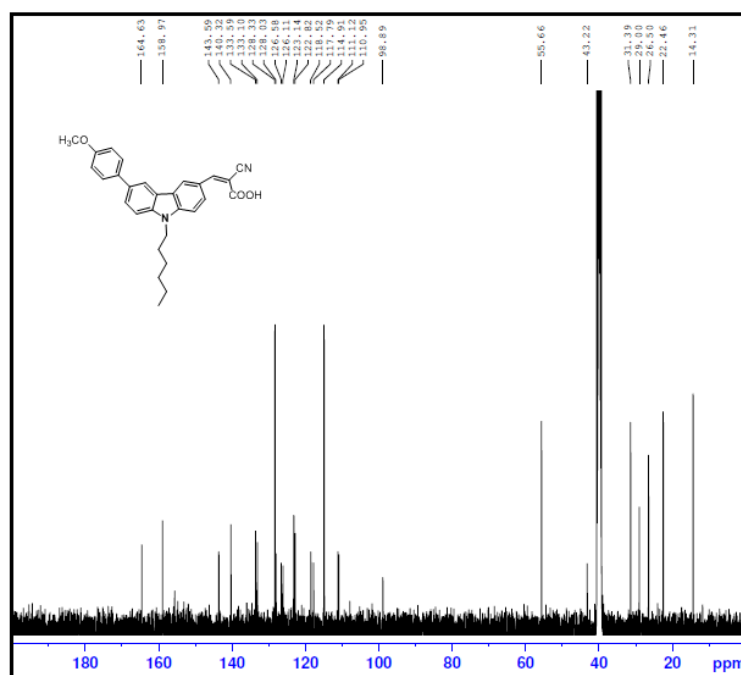
Fig 3.16: ^{13}C NMR spectrum of *n*-C$_{16}$
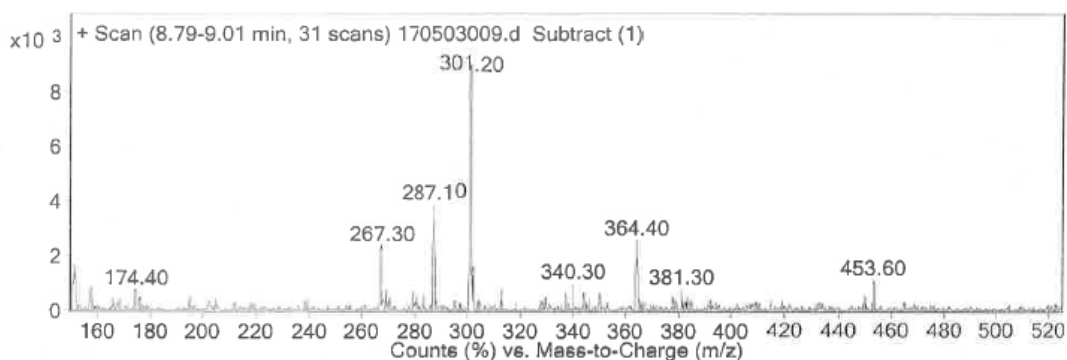
Fig 3.17: ESI-MS spectrum of *n*-**C₁₆**

3.2.3.6 *n*-**C₁₈₋₂₁** (Series-5)

The molecular structures belonging to the above mentioned series were confirmed using different spectral techniques and elemental analysis. ^{1}H NMR, ^{13}C NMR and mass spectra of the dye *n*-**C₂₁** are depicted in **Figs 3.18-3.20**, respectively. ^{1}H NMR spectrum of *n*-**C₂₁** accounts for all the protons present in the assigned structure. Appearance of unique resonance peaks between δ 11.40 to 11.20 ppm accounts for the four protons of aromatic amine present in two barbituric acid segments. Two singlet peaks of vinylene protons resonated at 9.36 and 9.32 ppm respectively, and all the other aromatic protons of carbazole core and phenyl ring were observed in the region of δ 8.75 to 7.74 ppm as multiplet. Also, the peaks in the region of δ 1.81 to 0.80 ppm correspond to primary and secondary protons of hexyl chain. The ^{13}C NMR spectrum of *n*-**C₂₁** dye showed the characteristic signals at the downfield region. The keto carbon atoms of two barbituric acid segments resonated in the region of δ164.65 to157.19 ppm. The sharp signals in the region of δ 154.94 to 110.03 ppm are due to other aromatic carbons, whereas the aliphatic carbons have appeared between δ 43.28 to 14.31 ppm. Furthermore, its mass spectrum exhibited the [M+H]$^+$ peak at 604.50, which is in good agreement with the calculated molecular weight confirming the chemical structure of the synthesized dye *n*-**C₂₁**.
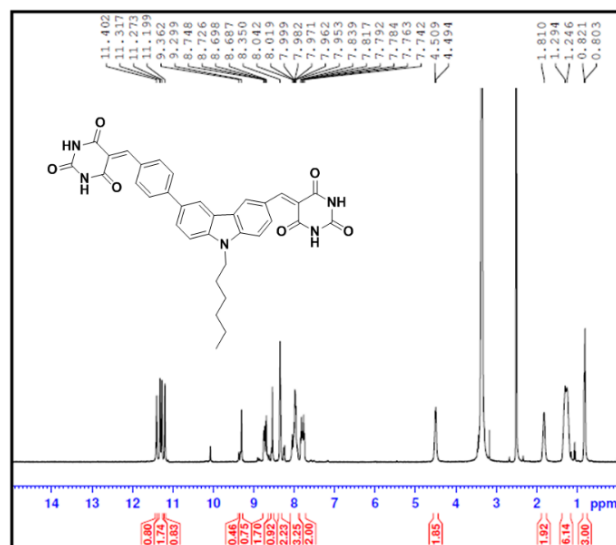
Fig 3.18: ^{1}H NMR spectrum of *n*-C$_{21}$
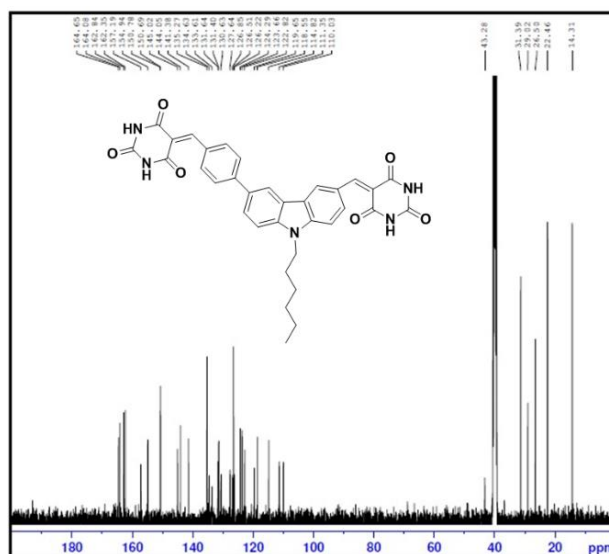
Fig 3.19: ^{13}C NMR spectrum of *n*-C$_{21}$
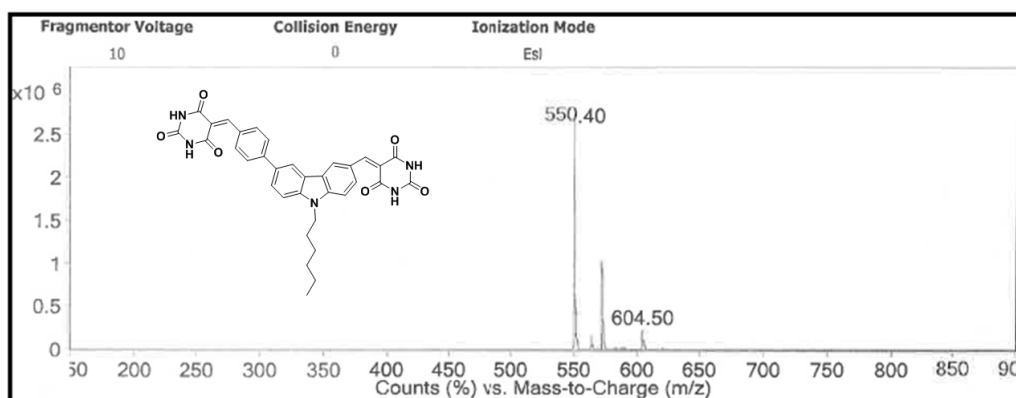
Fig 3.20: ESI-MS of *n*-C$_{21}$

3.2.3.7 *p*-C₁₋₃ (Series-6)

The chemical structures of *p*-**C₁₋₃** (**Series-6**) were confirmed by different spectral methods including elemental analysis. The ^{1}H NMR spectrum of *p*-**C₁**, displayed a single peak at δ 12.85 ppm corresponding to the proton present in the carboxylic acid group. A singlet peak resonated at δ 9.41 can be assigned to vinylene proton present in the structure, while all the other aromatic protons of carbazole ring were observed in the region of δ 8.82 to 7.80 ppm. Also, the peaks in the region of δ 1.82 to 0.83 ppm correspond to primary and secondary protons of hexyl chain. The ^{13}C NMR spectrum of *n*-**C₁₀** dye showed the characteristic signals which appeared at higher frequency region. The carbonyl carbon atom in acid group resonated at δ 166.91 ppm, wherein keto carbon units of the barbituric acid segment were observed at δ 163.21, 161.41 and 157.76 ppm. The carbon signals in the region of δ 151.62 to 110.15 ppm are due to other aromatic carbons of carbazole ring, whereas the aliphatic carbons of hexyl chain appeared in between δ 43.37 to 22.45 ppm. Furthermore, its mass spectrum exhibited the [M+H]$^+$ peak at 462.20, which is in good agreement with the calculated molecular weight. This confirms the chemical structure of the synthesized dye *p*-**C₁**. **Figs 3.21-3.23** show the ^{1}H NMR, ^{13}C NMR and mass spectra of the dye *p*-**C₁**, respectively.
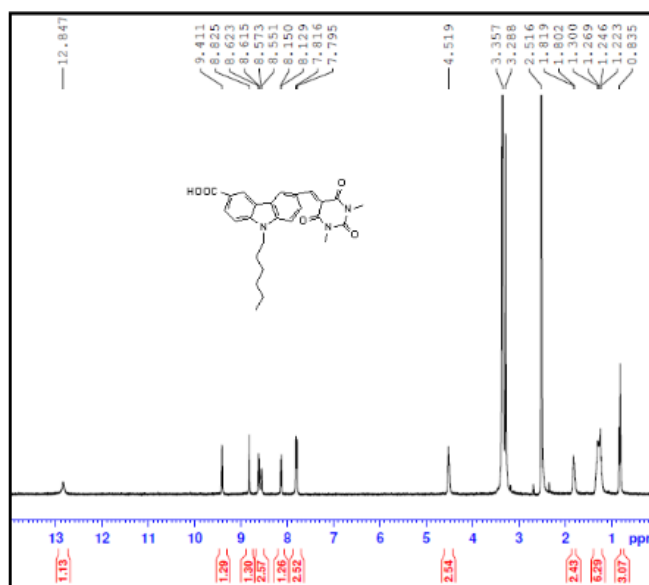
Fig 3.21: ^{1}H NMR spectrum of dye *p*-**C₁**
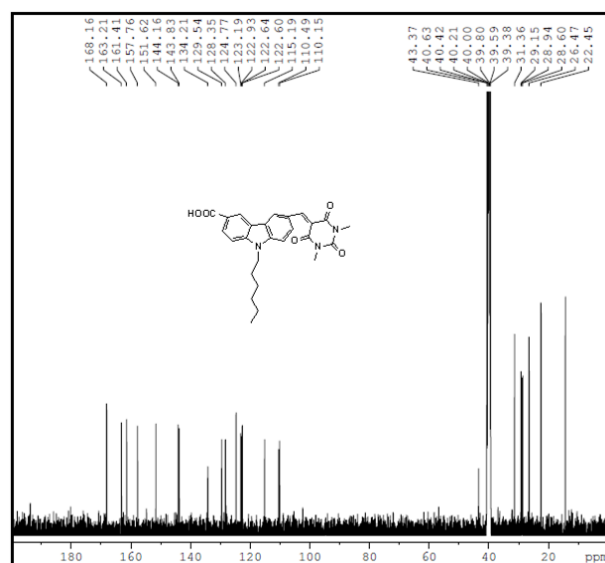
Fig 3.22: 13C NMR spectrum of dye *p*-**C₁**
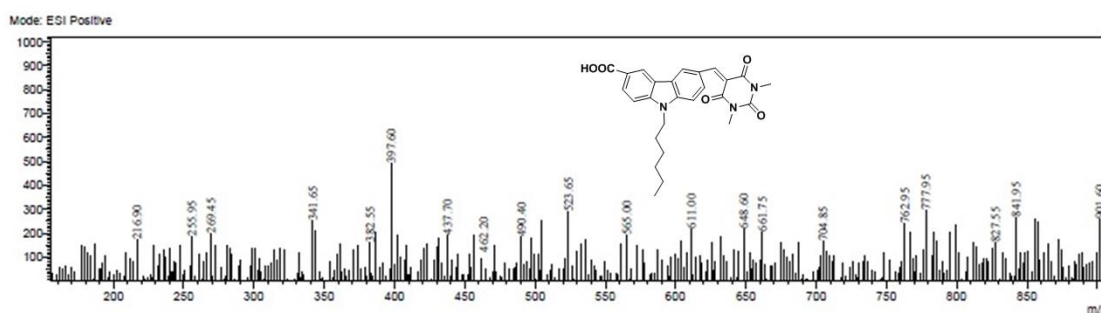
Fig 3.23: ESI-MS spectrum of dye *p*-**C₁**

3.4 CONCLUSIONS

In conclusion, seven new series containing twenty one *n*-type (***n*-C₁-₂₁**) and three *p*-type (***p*-C₁-₃**) dyes were successfully synthesized, following appropriate synthetic protocols, as per the **Schemes 3.1-3.7**. The synthetic routes were established with respect to yield, solvent and other reaction conditions. Also, their purification techniques have been developed. The chemical structures of all the final molecules and their intermediates were confirmed by different spectral techniques like FTIR, ^{1}H NMR, ^{13}C NMR, Mass spectroscopy and elemental analysis. Further, high-quality single crystals of the dyes ***n*-C₂** and ***n*-C₄** were grown and SCXRD study was carried out to confirm their 3D structures. In the next chapter, a detailed photophysical, electrochemical, molecular modeling studies of newly synthesized dyes have been discussed.

PHOTOPHYSICAL, ELECTROCHEMICAL AND THEORETICAL INVESTIGATIONS

Abstract:

This chapter comprises the photophysical (absorption and emission spectral) and electrochemical studies of the newly synthesized twenty one n-type ($n\text{-}C_{1\text{-}21}$) and three p-type ($p\text{-}C_{1\text{-}3}$) organic chromophores. Also, it involves the theoretical investigation of new dyes and their spectral behavior using DFT and TD-DFT simulations.

4.1 PHOTOPHYSICAL INVESTIGATION

Photophysical investigation of new organic dyes includes mainly their absorption and emission spectral studies. The obtained photophysical data are quite useful for selection of dyes as sensitizers/co-sensitizers in DSSCs.

4.1.1 Introduction to photophysical properties

The optical methods are widely used for the investigation of photophysical behavior of materials. These techniques involve study of interaction of electromagnetic radiations with the material. Amongst various techniques, UV-Vis absorption and molecular fluorescence spectroscopy are important, as they provide valuable information regarding material properties. It is well-established that, study of interaction between organic chromophores and light is essential for their optical characterization. Basically, absorption spectroscopy involves the electronic transitions from ground state to the excited state, while fluorescence spectroscopy deals with the electronic transitions from the excited state to the ground state. The results of optical studies are useful in evaluating the important parameters like optical band gap, molar extinction coefficient (ε) and Stokes shifts of organic dyes. These are valuable parameters for selecting such materials as sensitizers/co-sensitizers in photovoltaic applications. Therefore, all the synthesized organic dyes are subjected to UV-Vis and fluorescence spectral studies in order to evaluate their suitability for their applications in DSSCs as sensitizers/co-sensitizers.

4.1.2   Materials and methods

The UV-Vis absorption spectra of the dyes were recorded at room temperature using Analytik Jena SPECORD S 600 spectrophotometer. Further, the fluorescence emission spectra were obtained using Jasco FP 6200 spectrophotometer.

4.1.3   Experimental

The UV-Vis absorption spectra of synthesized dyes, ***n*-C$_{1-21}$** and ***p*-C$_{1-3}$** were measured at the concentration of 10^{-5} M in chloroform/DMF solutions. Further, their emission spectra were obtained by irradiative excitation at the wavelength of their λ_{abc}, using the above said concentration. Their optical band gap, molar extinction coefficient (ε) and Stokes shift values were calculated using the spectral data.

4.1.4   Results and discussion

Results of photochemical studies of new dyes have been discussed series-wise in the following section.

4.1.4.1 *n*-C$_{1-5}$ (Series-1A)

Figs 4.1 and **4.2** show the UV-Vis absorption and photoluminescence emission spectra of ***n*-C$_{1-5}$**, respectively. The relevant spectral results are presented in **Table 4.1.** From the absorption spectra, it is clear that the dyes ***n*-C$_{1-2}$** exhibit single distinct absorption band, while dyes ***n*-C$_{3-5}$** displayed two major absorption bands. In the case of ***n*-C$_{1-2}$**, the single peak at around 470 nm is attributed to the intramolecular charge transfer (ICT) from a donor, *i.e.* 4-(*N*,*N*-dimethylamino)phenylene group to the corresponding acceptor unit, *i.e.* barbituric acid, or *N*,*N*-dimethyl barbituric acid. While the dyes ***n*-C$_{3-5}$** shows absorption bands in the shorter wavelength (250 and 350 nm) corresponding to π-π* electronic excitations localized within the 4-(*N*,*N*-dimethylamino)phenylene group, whereas the intense band in the longer wavelength region (496, 500 and 376 nm) can be attributed to an intermolecular charge transfer (ICT) from the donor to the acceptor segment.
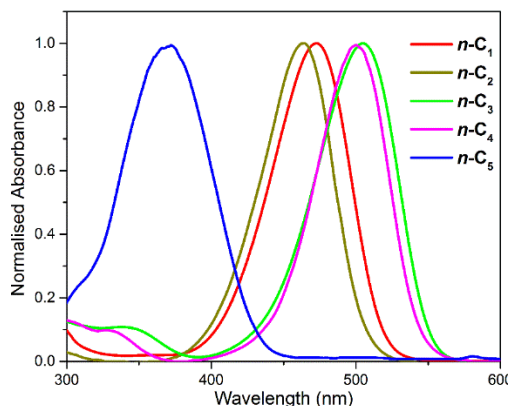
Fig 4.1: Absorption spectra of *n***-C₁₋₅**
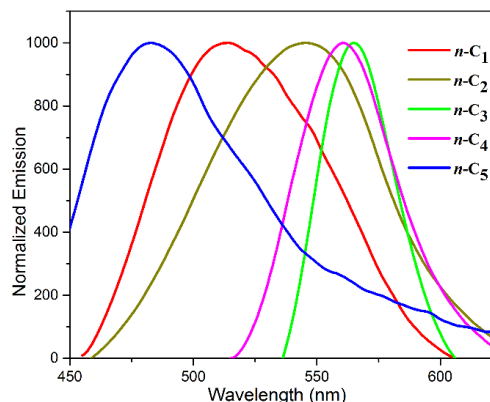
Fig 4.2: Emission spectra of *n***-C₁₋₅**

The fluorescence emission spectral data of the dyes *n***-C₁₋₅** recorded at its excitation wavelength are summarized in **Table 4.1.** All the dyes have exhibited a single band in the range of 488 to 561nm. The dye *n***-C₄** showed maximum redshift as compared with other dyes in the series. From the **Fig 4.2**, it is observed that the dye *n***-C₅** showed maximum Stokes shift compared to the other four dyes. This is may be due to strong electron withdrawing ability of the 4-aminobenzoic acid.

4.1.4.2 *n***-C₆₋₈** (Series-1B)

The UV-visible absorption spectra of the new organic sensitizers/co-sensitizers, *n***-C₆₋₈,** recorded in 10^{-5} M DMF solution are depicted in **Fig 4.3** and their corresponding characteristic spectral data are summarized in **Table 4.1**. From the **Fig 4.3**, it is worth to note that, all the synthesized dyes possess two distinctive absorption bands. The absorption band in the region of 291-316 nm can be assigned to the π-π* electronic excitations localized within the carbazole donor, whereas the peak corresponding to the longer wavelength, *i.e.* 343-427 nm can be attributed to the ICT from the carbazole donor to the electron acceptor. Moreover, the ε of *n***-C₆₋₈** were found to be 43,370, 34,870, and 41,280 $M^{-1}cm^{-1}$ respectively, which are higher than that of reported value of **NCSU-10** dye (20,650 $M^{-1}cm^{-1}$) demonstrating their good light-harvesting ability. In the present study, co-sensitization property of above said dyes was investigated using **NCSU-10** based DSSCs.

Further, the fluorescence emission spectra of sensitizers/co-sensitizers *n*-C$_{6-8}$ were recorded upon their excitation wavelengths in 10^{-5} M DMF solutions. **Fig 4.4** depicts the normalized emission spectra of the *n*-C$_{6-8}$ and their pertaining spectral data are tabulated in **Table 4.1**. The fluorescence spectra of dyes display a single emission band in the range of 449 to 545 nm. However, a broad red shifted peak has been observed for *n*-C$_8$, which is mainly due to heavy aggregation of dye in solution *via* strong hydrogen bonding between the solvent and NH groups of barbituric acid causing reorganization of the molecule (Shen et al. 2011; Yen et al. 2013). Further, Stokes shift values of sensitizers/co-sensitizers *n*-C$_{6-8}$ were calculated from their normalized UV-Vis absorption and fluorescence emission spectral data (**Table 4.1**). As well, optical band gaps of *n*-C$_{6-8}$ were determined from the intersection point of normalized absorption and emission spectra and their calculated values are tabulated in **Table 4.1**.
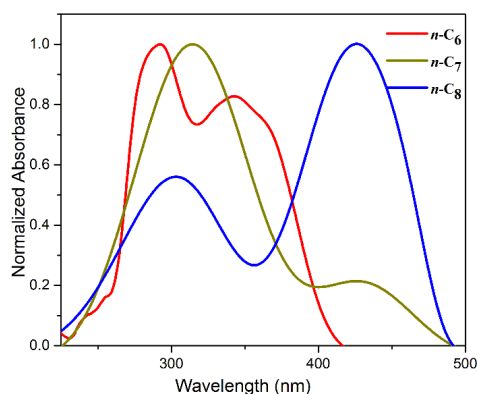
Fig 4.3: Absorption spectra of *n*-C$_{6-8}$
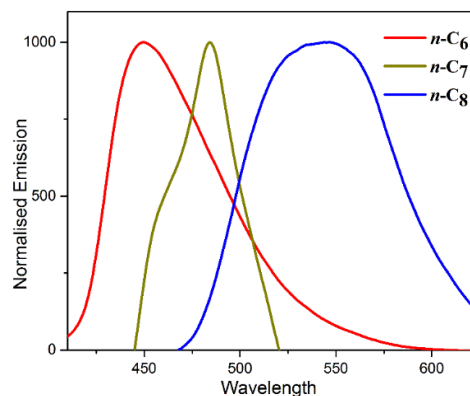
Fig 4.4: Emission spectra of *n*-C$_{6-8}$

4.1.4.3 *n*-C$_{9-12}$ (Series-2)

The UV-Vis absorption and fluorescence emission spectra of the synthesized sensitizers/co-sensitizers *n*-C$_{9-12}$, recorded in CHCl$_3$ (10^{-5} M) solutions are depicted in **Figs 4.5** and **4.6**, respectively and their corresponding results are summarized in **Table 4.1**. From the UV-Vis absorption spectra, it is clear that all dyes show two distinctive absorption bands. The band in the region of 278-360 nm is assigned to the π-π* electronic excitations localized within the carbazole donor and phenyl π-conjugated system, while the peak corresponding to the longer wavelength, *i.e.* 412-488 nm can be attributed to the ICT from

carbazole donor to the electron withdrawing/anchoring moiety. The ε of ***n*-C₉₋₁₂** were found to be 21,370, 23,000, 16,230 and 16,280 $M^{-1}cm^{-1}$ respectively, indicating their good light harvesting capability. Further, the fluorescence emission spectra of ***n*-C₉₋₁₂** were recorded in $CHCl_3$ at 10^{-5} M concentration upon their excitation at this absorption wavelength (λ_{abs}). Furthermore, their Stokes shift values were calculated from these normalized UV-Vis absorption and fluorescence emission spectral data (**Table 4.1**). It was observed that ***n*-C₉** showed a maximum shift of 134 nm when compared to other three dyes. The observed large value of Stokes shift indicates the effective ICT property of the dye ***n*-C₉**. Further, the optical band gaps of ***n*-C₉₋₁₂** were determined from the intersection between the UV-Vis absorption and fluorescence emission curves and the corresponding data are summarized in **Table 4.1**.
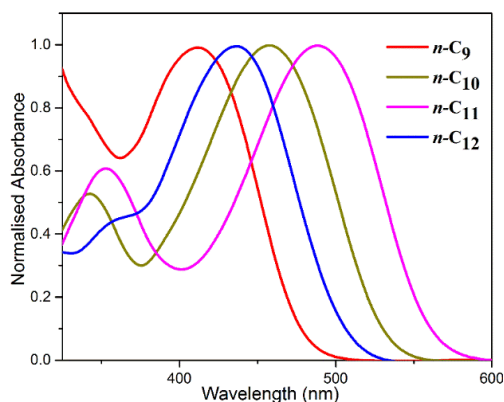
Fig 4.5: Absorption spectra of ***n*-C₉₋₁₂**   **Fig 4.6:** Emission spectra of ***n*-C₉₋₁₂**.
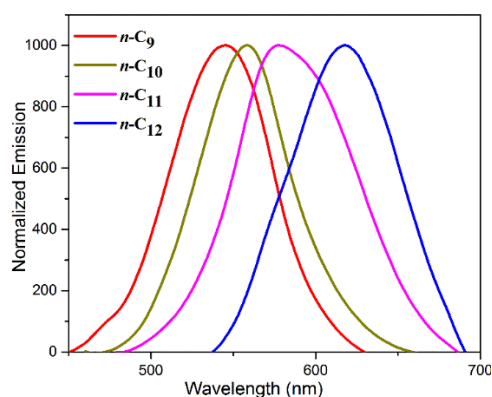
4.1.4.4 *n*-C₁₃₋₁₅ (Series-3)

The UV-Vis absorption and fluorescence emission spectra of sensitizers/co-sensitizers ***n*-C₁₃₋₁₅** were recorded over the range of wavelength (λ) using chloroform as solvent at the concentration of 10^{-5}M. **Fig 4.7** depicts the UV-Vis absorption spectra of dyes ***n*-C₁₃₋₁₅**. Their UV-Vis absorption spectra show the two distinctive absorption maxima in the region of 350-380 and 484-524 nm. The former region peaks (350-380 nm) are corresponding to π-π* electronic excitations localized within the carbazole and thiophene moieties. Wherein later region peaks (484-524 nm) are attributed to intermolecular charge transfer (ICT) from carbazole donor to the acceptor/anchoring

moiety. It is interesting to note that the ICT peak endorsed for the ***n*-C13** dye is red shifted when compared to other two dyes.
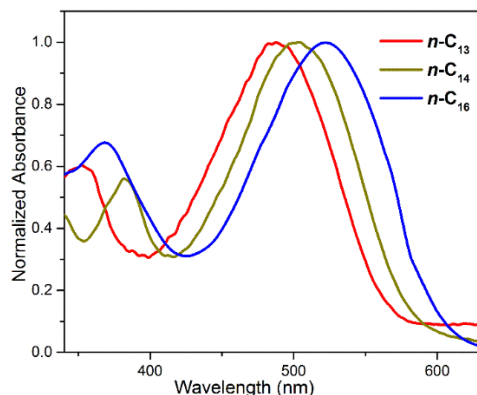
Fig 4.7: Absorption spectra of ***n*-C13-15**   **Fig 4.8:** Emission spectra of ***n*-C13-15**
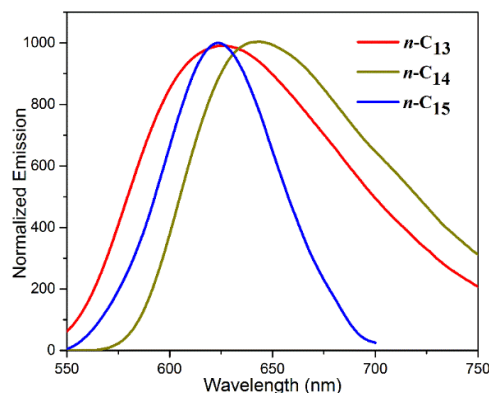
From their emission spectra (**Fig 4.8**), it is clear that they show strong luminescence maxima in the region of 624-640 nm. The optical band-gap was also calculated from the intersection between normalized absorption and emission spectra. Further, from the normalized absorption and emission spectral data Stokes shift values were estimated to be in the range of 100-142 nm. It is worthy to note that, the ***n*-C13** showed maximum Stokes shift of 142 nm and highest ε of 42,250 $M^{-1}cm^{-1}$ when compared to other two dyes, thus suggesting significant charge transfer from carbazole donor moiety to the respective acceptor/anchoring groups.

4.1.4.5 *n*-C16-18 (Series-4)

The UV-Vis absorption and emission spectra of sensitizers/co-sensitizers ***n*-C16-18** were recorded in 10^{-5} M CHCl$_3$ solution (**Figs 4.9** and **4.10,** respectively) and their pertaining results are summarized in **Table 4.1.** Their spectra display two distinct peaks corresponding to π-π^* electronic excitations localized within the carbazole donor and ICT from the carbazole donor to the electron acceptor. The dye carrying barbituric acid, as an acceptor/anchoring unit ***n*-C18** brings about red shift while other two dyes show blue shift. The ε of ***n*-C16-18** were determined to be 58,370, 26,800 and 47,500 $M^{-1}cm^{-1}$, respectively demonstrating their good light-harvesting ability.
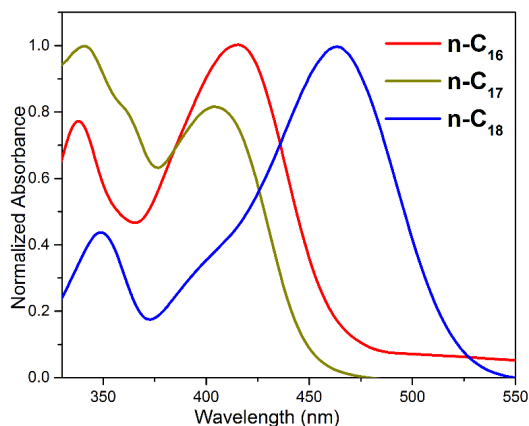
Fig 4.9: Absorption spectra of *n*-C$_{16-18}$ **Fig 4.10:** Emission spectra of *n*-C$_{16-18}$
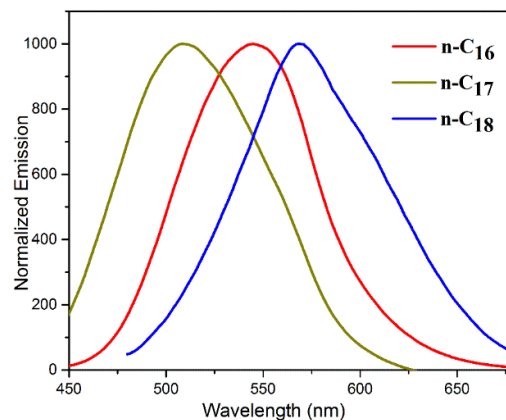
From their fluorescence emission spectra (**Fig 4.10**), it is clear that they show strong emission in the region of 509-569 nm. Their optical band-gaps were also calculated from the intersection between normalized absorption and emission spectra. Further, from the normalized absorption and emission spectral data Stokes shift values were estimated to be in the range of 91-138 nm. It is worthy to note that, the *n*-C$_{13}$ shows the maximum Stokes shift of 138 nm and ε of 58370 M^{-1}cm^{-1} while other two dyes exhibit lower values, thus suggesting significant charge transfer from carbazole donor moiety to the respective acceptor/anchoring group.

4.1.4.6 *n*-C$_{19-21}$ (Series-5)

The UV-Vis absorption spectra of the sensitizers/co-sensitizers *n*-C$_{19-21}$ were obtained over the range of wavelength (λ) using chloroform as solvent at 10^{-5} M concentration. The absorption spectra of *n*-C$_{16-18}$ are depicted in **Fig 4.11** and their related spectral data are summarized in **Table 4.1**. From the **Fig 4.11**, it is worth to note that, all the newly synthesized dyes show two distinctive absorption bands. The absorption band in the region of 333-338 nm can be assigned to the π-π* electronic excitations localized within the carbazole donor, whereas the peak corresponding to the longer wavelength, *i.e.* 385-457 nm can be attributed to the ICT from the carbazole donor to the electron acceptor. Moreover, the ε of the *n*-C$_{19-21}$ were found to be 45,340, 24,850, and 39,790 M^{-1}cm^{-1}, respectively, indicative of their good light-harvesting ability.

Further, the fluorescence emission spectra of sensitizers/co-sensitizers *n*-C$_{19\text{-}21}$ were recorded upon their excitation wavelengths in 10^{-5} M CHCl$_3$ solution. **Fig 4.12** depicts the normalized emission spectra of the *n*-C$_{19\text{-}21}$ and their characteristic spectral data are tabulated in **Table 4.1**. The spectra of *n*-C$_{19\text{-}21}$ display a single emission band in the range of 482-559 nm. Further, Stokes shift values of *n*-C$_{19\text{-}21}$ were calculated from their normalized UV-Vis absorption and fluorescence emission spectral data (**Table 4.1**). It was observed that, *n*-C$_{19}$ showed maximum Stokes shift of 127 nm when compared to other two dyes. The observed large value of Stokes shift indicates the effective ICT property of the dye *n*-C$_{19}$. As well, optical band gaps of *n*-C$_{19\text{-}21}$ were determined from the intersection point of normalized absorption and emission spectra and their calculated values are tabulated in **Table 4.1**.
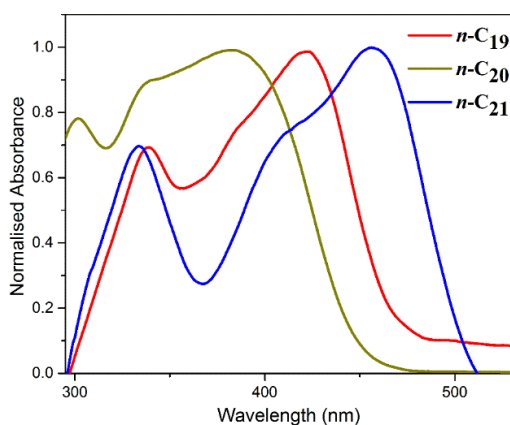
Fig 4.11: Absorption spectra of *n*-C$_{19\text{-}21}$ **Fig 4.12:** Emission spectra of *n*-C$_{19\text{-}21}$
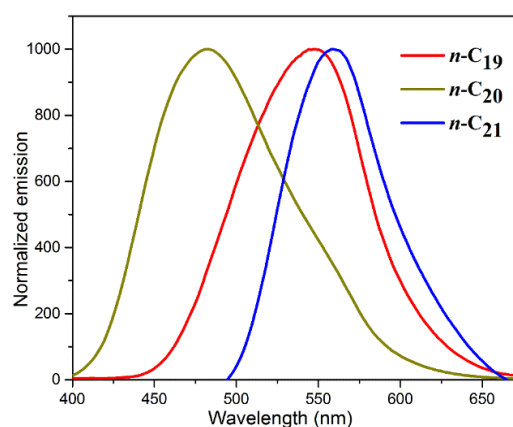
4.1.4.7 *p*-C$_{1\text{-}3}$ (Series-6)

The UV-Vis absorption spectra of the new sensitizers *p*-C$_{1\text{-}3}$ obtained in 10^{-5} M CHCl$_3$ solutions are depicted in **Fig 4.13** and their consequential spectral data are summarized in **Table 4.2**. From the absorption spectra of *p*-C$_{1\text{-}3}$, it is worth to note that, all the three synthesized dyes display two distinctive absorption bands. The absorption band in the region of 315-330 nm can be assigned to the π-π* electronic excitations localized within the carbazole donor, whereas the peak corresponding to the longer wavelength, *i.e.* 435-446 nm can be attributed to the ICT from the carbazole donor to the electron acceptor unit. Moreover, the molar extinction coefficient of the sensitizers *p*-C$_2$ (ε = 42,370 M^{-1}cm$^-$

[1]) is comparable with the reported value of a benchmark dye, **P1** (57,900 M^{-1}cm^{-1}) (Qin et al., 2010), used in *p*-type DSSC. This clearly demonstrates valuable light-harvesting ability of *p*-**C$_2$**. Further, the fluorescence emission spectra of dyes *p*-**C$_{1-3}$** were recorded upon their excitation wavelengths in 10^{-5} M chloroform solution. The normalized emission spectra of the sensitizers **C$_{1-3}$** are portrayed in **Fig 4.14** and their pertaining spectral data are tabulated in **Table 1**. The fluorescence emission spectra of sensitizers (*p*-**C$_{1-3}$**) display a single emission band in the range of 486 to 518 nm. In addition, Stokes shift values of sensitizers were calculated from their normalized absorption and emission spectral data (**Table 4.2**). As well, their optical band gaps were determined from the intersection of normalized absorption and emission spectra and their calculated values are summarized in **Table 4.2.**
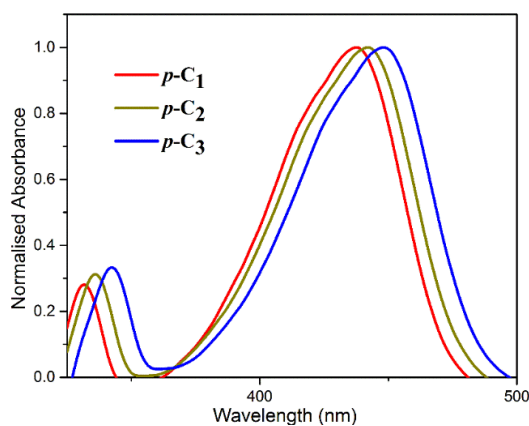

Fig 4.13: Absorption spectra of *p*-**C$_{1-3}$**   **Fig 4.14:** Emission spectra of *p*-**C$_{1-3}$**
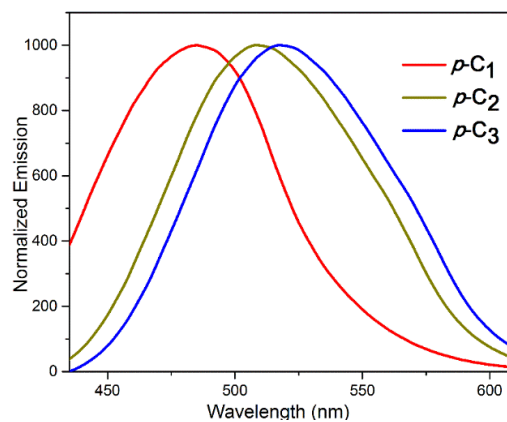
Conclusively, the photophysical studies revealed that, the presence of different electron donor and electron acceptor/anchoring units in the conjugated electron-bridge structure have led to varied absorption maxima (λ_{abs}) as well as emission maxima (λ_{em}) of dyes. The results showcased that, all the synthesized dyes displayed good emission as well as absorption of photons with higher ε values, which is desirable for better harvesting of sunlight. It has been well-documented that, for better photovoltaic performance, the metal-free organic dyes should possess tunable photophysical properties. On the basis of the photophysical data, all the synthesized dyes were selected as sensitizers/co-sensitizers for DSSC device fabrication.

4.2 ELECTROCHEMICAL STUDIES

Electrochemical study of organic dyes plays an important role in understanding their basic electronic structures. It describes their oxidation and reduction potentials, which are highly useful in determining their HOMO-LUMO energy levels and charge carrying properties. Generally, cyclic voltammetry (CV) is employed for electrochemical studies. It is a controlled potential technique, in which the potential (E) of the working electrode is swept between two values and the resulting current (i) is measured. Sweeping from a positive to a negative potential reduces the electro-active species at the working electrode surface. The current measured during a negative sweep is the cathodic current. The transfer of electrons from the electrode surface to the reactive species results in an increase in the cathodic current. The decrease in current that gives the peak shape, occurs when the rate of diffusion of reactants to the working electrode surface begins to limit the rate of reaction. Sweeping from a negative to a positive potential oxidizes the reduced electroactive species at the working electrode surface back to its oxidized form, resulting in a peak in the anodic current. The data plotted as a graph of E against i are referred to as voltammograms.

In the present work, CV studies were performed for both *n*-type and *p*-type sensitizers (**n-C$_{1\text{-}21}$** and **p-C$_{1\text{-}3}$**) in order to evaluate their excited state oxidation potential / lowest unoccupied molecular orbital (ESOP/LUMO) and ground state oxidation potential / highest occupied molecular orbital (GSOP/HOMO) energy levels. The ESOP and GSOP of the sensitizers were measured to gauge the prospects of effective charge injection as well as regeneration of dyes.

Generally, for better functioning of the dyes as sensitizers in *n*-type DSSCs, it necessitates that, the ESOP/LUMO level of the dye should be more electronegative than the CB edge of TiO$_2$ to ensure effective charge injection, while the GSOP/HOMO level of the co-sensitizer should be more positive than the redox potential of the electrolyte to ensure effective dye regeneration. However, the sensitizers for NiO based *p*-type DSSCs must fulfil the criteria that, the LUMO level must be sufficiently higher in energy than the redox potential of the I$_3^-$/I$_2^{-\bullet}$ couple (E(I$_3^-$/I$_2^{-\bullet}$)), while the HOMO level must be sufficiently

below the VB edge of the NiO in order to exhibit thermodynamically allowed charge transfer processes. So, all the dyes must satisfy the above mentioned conditions for employing them as *n*-/*p*-type sensitizers in DSSCs.

4.2.1 Materials and methods

The electrolytes tetrabutylammonium tetrafluoroborate and tetrabutylammoinium hexafluorophosphate were procured from Sigma Aldrich Company. All the CV measurements were performed on an Ivium Vertex Electrochemical Workstation.

4.2.2 Experimental

The CV measurements were performed for *n*-**C₁-₂₁** and *p*-**C₁-₃** in acetonitrile by using 0.1 M of (tetrabutylammonium tetrafluoroborate / tetrabutylammoinium hexafluorophosphate as supporting electrolyte. The system was initially calibrated with ferrocene/ferrocenium (Fe/Fe⁺). The CV experiments were conducted by using the three electrode system, consisting of glassy carbon as the working electrode, platinum as counter and Ag/AgCl as a reference electrode and data were recorded at a scan rate of 50-100 mV/s. The obtained oxidation and reduction potentials of all the dyes were summarized in **Tables 4.1** and **4.2**.

4.2.3 Results and discussion

4.2.3.1 *n*-Type sensitizers (*n*-**C₁-₂₁**)

The obtained onset oxidation potential of oxidation peak of cyclic voltammogram was used to compute the GSOP/HOMO energy level using the equation (**Eq 4.1**).

$$GSOP = - \left[E_{onset}^{oxd} + 4.7eV \right] \tag{4.1}$$

In the equation, E_{onset}^{oxd} is the onset oxidation potential of oxidation peak of CV curve. The optical band-gap $E_{0\text{-}0}$ and GSOP values were employed to calculate their excited state oxidation potentials (ESOP); the values in volts (V) against NHE were converted to electron volt (eV) according to the equation (**Eq 4.2**).

$$\text{ESOP} = \left[\text{GSOP} - \text{E}_{0-0}\right] \text{ eV} \qquad\qquad (4.2)$$

The estimated GSOP/HOMO and ESOP/LUMO energy levels are tabulated in **Table 4.1**. The CV traces of selected dyes, *i.e.* ***n*-C13-15** are depicted in **Fig 4.15**. It is apparent that, the calculated GSOP/HOMO levels of dyes ***n*-C1-21** were found to possess more negative values than the Nernst potential of I_3^-/I^- electrolyte system (Qu and Meyer 2001), showing that the oxidized dye can be effectively reduced and regenerated by the electrolyte species. Further, the estimated ESOP/LUMO levels of ***n*-C1-21** were found to be higher than the potential of CB of TiO_2 (Oskam et al. 2001).

Conclusively, all the dyes fulfilled the prerequisites for an effective electron injection and dye regeneration process in the fabricated devices (Koops et al. 2009). However, because of the presence of different conjugated electron-bridge structures, all the dyes demonstrated distinct HOMO and LUMO energy levels. **Fig 4.16** depicts the energy level diagram, showing the GSOP and ESOP values of dyes ***n*-C1-21**. The experimental results indicated the presence of ample driving force for effective dye regeneration and an efficient electron injection in the fabricated cell.
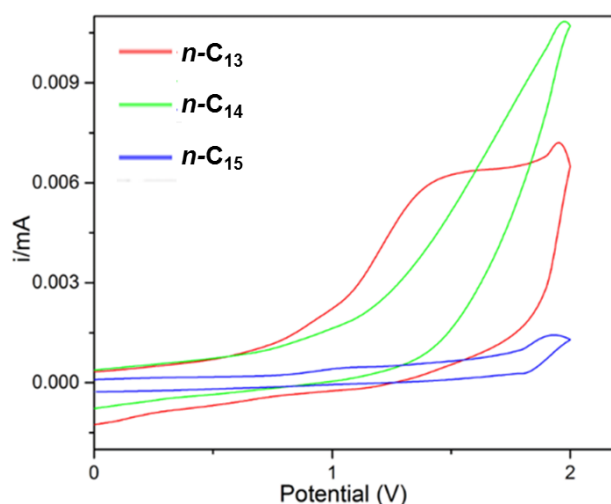
Fig 4.15: Cyclic voltammetry traces of ***n*-C13-15**

Table 4.1: Photophysical and electrochemical properties of dyes *n*-C$_{1-21}$

Series	Dyes	λ_{abs} (nm)	λ_{em} (nm)	Stokes shift (nm)	ε (M^{-1}cm^{-1})	E$_{0-0}$, (eV)	GSOP (eV)	ESOP (eV)
Series-1A	*n*-C$_1$	473	514	41	32,000	2.54	-5.65	-3.11
	n-C$_2$	467	546	79	45,500	2.57	-5.18	-2.67
	n-C$_3$	500	561	61	59,000	2.35	-5.52	-3.17
	n-C$_4$	498	566	68	83,000	2.36	-5.29	-2.93
	n-C$_5$	371	488	117	32,000	2.94	-5.43	-2.49
Series-1B	*n*-C$_6$	343	449	106	43,370	3.03	-5.62	-2.59
	n-C$_7$	425	484	59	34,870	2.66	-5.62	-2.96
	n-C$_8$	427	545	118	41,280	2.57	-5.31	-2.74
Series-2	*n*-C$_9$	412	546	134	21,370	2.61	-5.48	-2.87
	n-C$_{10}$	438	550	112	23,000	2.47	-5.54	-3.07
	n-C$_{11}$	458	578	120	16,230	2.39	-5.43	-3.04
	n-C$_{12}$	489	618	129	16,280	2.17	-5.56	-3.39
Series-3	*n*-C$_{13}$	488	630	142	42,250	2.21	-5.46	-3.25
	n-C$_{14}$	504	640	136	41,825	2.12	-5.43	-3.31
	n-C$_{15}$	524	624	100	41,500	2.12	-5.52	-3.40
Series-4	*n*-C$_{16}$	408	546	138	58,370	2.64	-5.61	-2.97
	n-C$_{17}$	418	509	91	26,800	2.81	-5.79	-2.98
	n-C$_{18}$	463	569	106	47,500	2.44	-5.62	-3.18
Series-5	*n*-C$_{19}$	421	548	127	45,340	2.63	-6.06	-3.43
	n-C$_{20}$	385	482	97	24,850	2.86	-6.11	-3.25
	n-C$_{21}$	457	559	102	39,790	2.46	-6.10	-3.64
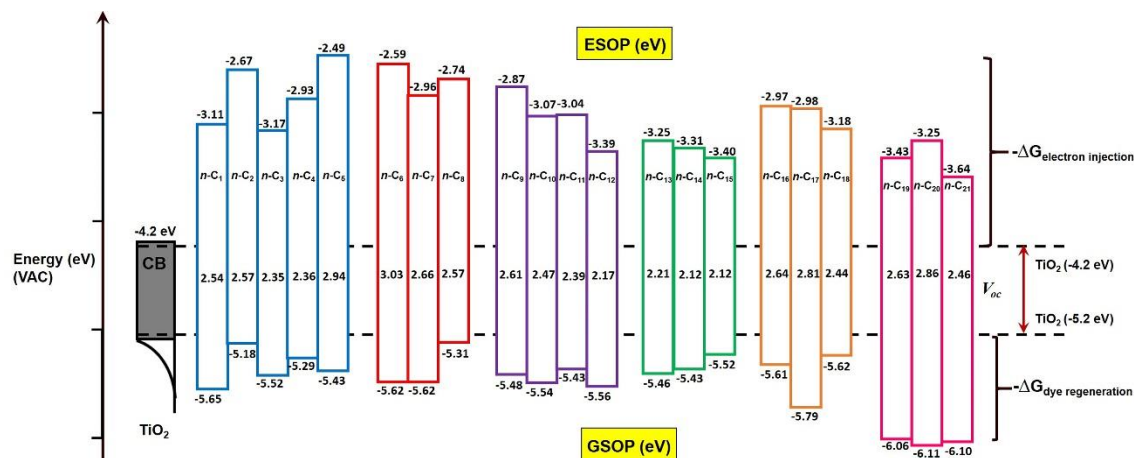
Fig 4.16: Energy level diagram of *n*-C$_{1-21}$

4.2.3.2 *p*-Type sensitizers (*p*-C$_{1-3}$)

The CV study of *p*-C$_{1-3}$ was performed in acetonitrile solution in order to evaluate their electrochemical processes as well as charge carrying behavior of the dyes *p*-C$_{1-3}$. In the CV experiments, the cyclic voltamagrams were recorded at the applied voltage of 0 to -2 V and resultant plots are presented in **Fig 4.16**. The Gibbs free energy to inject charge from the HOMO level of the dye to the VB edge of the NiO was estimated from the equation 4.3.

$$\Delta G°_{inj} = E_{VB}\,(NiO) - E_{Red}\,(dye*/dye^-) \qquad \ldots\ldots\ldots (4.3)$$

In the above equation, $\Delta G°_{inj}$ is the Gibbs free energy for injection, E_{Red} (dye*/dye) is the reduction potential of the dye and E_{VB} (NiO) is Nernst potential of the VB of NiO, *i.e.* 0.30 V vs SCE.

Further, Gibbs free energy for dye regeneration from electrolyte (ΔG_{reg}) was estimated from the difference between reduction potential of the dye and Nernst potential of I_3^-/I^- electrolyte system (-0.32 V) and it can be expressed as equation 4.4.

$$\Delta G_{reg} = E_{Red}\,(dye/dye^-) - E\,(I_3^-/I_2^{-\bullet}) \ldots\ldots\ldots\ldots \qquad (4.4)$$

Conclusively, the CV data reveal that all the dyes fulfilled the prerequisites for effective electron injection and dye regeneration processes in the fabricated devices.
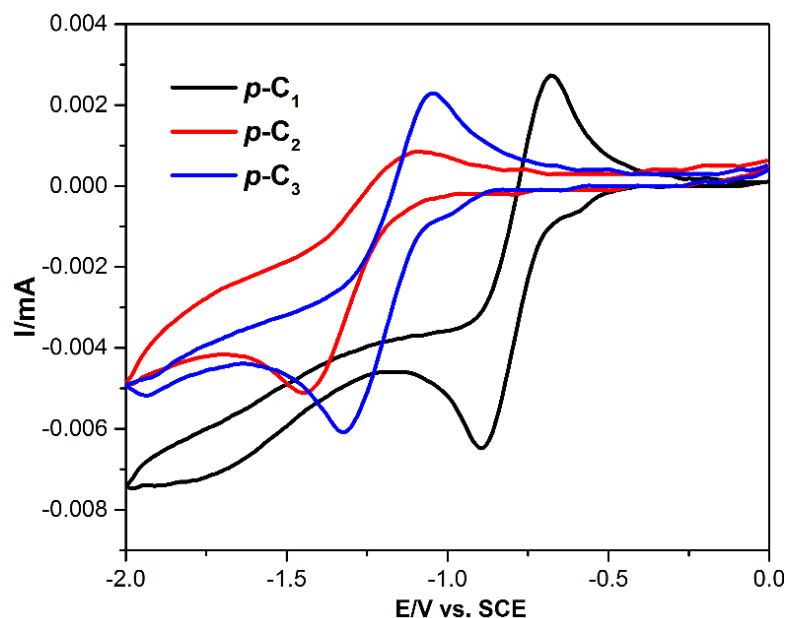
Fig 4.17: Cyclic voltammetry traces of *p*-C$_{1-3}$

Table 4.2: Photophysical and electrochemical properties of sensitizers (*p*-C$_{1-3}$)

Dyes	*p*-C$_1$	*p*-C$_2$	*p*-C$_3$
λ_{abs} (nm)	435	440	446
λ_{em} (nm)	486	508	518
Stoke Shift (cm^{-1})	2412	3042	3116
ε (M^{-1}cm^{-1}) at λ_{abs} (nm)	33,970, (435 nm)	40,370, (440 nm)	20,480 (446 nm)
E_{red} (V)	- 0.70	- 1.04	- 0.96
E_{0-0}, Optical (eV)	2.56	2.55	2.62
ΔG°_{inj} (eV)	- 1.56	- 1.21	- 1.36
ΔG_{reg} (eV)	- 0.38	- 0.72	- 0.64

$\Delta G^{\circ}_{inj}= E_{VB}$ (NiO) - E_{Red} (dye*/dye$^-$) with E_{VB} (NiO) = 0.30 V vs SCE.

$\Delta G_{reg} = E_{Red}$ (dye/dye$^-$) - $E(I_3^-/I_2^{-\bullet})$ with $E(I_3^-/I_2^{-\bullet}) = - 0.32$ V vs SCE (Boschloo et al., 2011; Farré et al., 2016; Black et al., 2017).

4.3   THEORETICAL INVESTIGATION

The development of DSSCs has been accompanied by computational studies that helps to rationalize the relationship between the molecular structure and device performance (Martsinovich and Troisi 2011). In particular, electronic and optical absorption properties of dye molecules, both isolated and adsorbed on the semiconductor (TiO$_2$) surfaces, have been extensively studied using density-functional theory (DFT) and time-dependent DFT. The spectral data of unknown compounds can be generated using the data. Moreover, theoretical investigation of the physical properties of sensitizers is very important to disclose the relationship among the molecular geometry and the photovoltaic performance, it is also helpful in designing new dyes as photosensitizers for achieving enhanced photovoltaic performance.

The adiabatic quantum calculations with hybrid functional are considered to be one of the reliable computational methodologies in the field of organic photovoltaics, especially DSSCs to estimate the frontier molecular orbital (FMO) levels of potential *n*- and *p*-type sensitizers.

4.3.1   Simulations

In the present study, the DFT simulations were carried out for isolated organic dyes in order to evaluate their ground state properties in gas phase. While, the vertical excitation and their response in the excited dye molecules were computed using TD-DFT simulations. All the aforementioned calculations were performed for dyes using Turbomole V7.1 software package. To begin with, dye's molecular geometry was first optimized using semi-empirical Austin Model 1 (AM1) in 3D molecular builder of T-Mole 4.2. The DFT simulations were carried out for all twenty one *n*-type (n-**C$_{1-21}$**) sensitizers/co-sensitizers and three *p*-type sensitizers (*p*-**C$_{1-3}$**) at B3LYP (Becke's three-parameter hybrid functional and Lee-Yang-Parr's gradient-corrected correlation functional) using def TZVPP level (Becke, 1988; Peach et al., 2008). Also TD-DFT calculations were performed for all the dyes at B3LYP using def TZVP level to generate optical absorption spectra.

4.3.2 Results and discussion

4.3.2.1 Molecular modeling of *n*-C₁-₅ (Series-1A)

The optimized geometries and electron density distributions in the HOMOs and LUMOs of the five dyes, *n*-C₁-₅ are summarized in **Fig 4.18**.

Dye	Optimized Geometry	HOMO	LUMO
n-C₁			
n-C₂			
n-C₃			
n-C₄			
n-C₅			
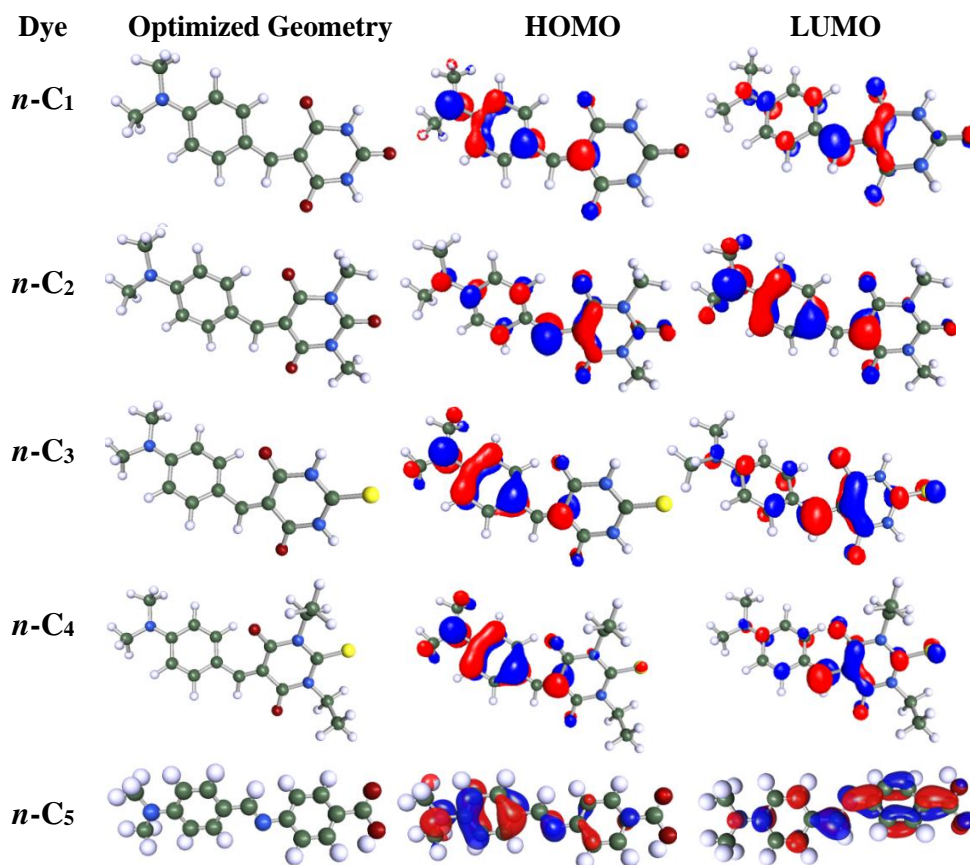
Fig 4.18: Optimized geometry and FMO energy levels of *n*-C₁-₅

As evidenced from the **Fig 4.18**, in the HOMO level, the electron density is mainly located on the *N,N*-dimethylaniline segment of all the dyes, whereas in the corresponding LUMOs, a clear shift of electron density towards acceptor group, *i.e.* barbituric acid, *N,N*-dimethyl barbituric acid, thio barbituric acid, *N,N* diethyl thiobarbituric acid and 4-aminobenzoic acid was observed. It has been noticed that, the LUMO electron density of *n*-C₅ is fully localized on anchoring –COOH group of 4-aminobenzoic acid facilitating the electronic coupling between the electron density at its LUMO level and the *d* orbitals of the TiO₂. Thus, a close proximity of the LUMO levels to the anchoring group would facilitate

considerable orbital overlap between the LUMO levels and 3*d* orbitals of titanium, which leads to better injection of excited electrons into the CB edge of TiO$_2$.

4.3.2.2 Molecular modeling of *n*-C$_{6\text{-}8}$ (Series-1B)

The optimized molecular geometries of *n*-C$_{6\text{-}8}$ and their corresponding electron density distributions in their HOMO and LUMO energy levels as obtained from T-mole visualizer are displayed in **Fig 4.19**. The 3-D optimized structures of the dyes indicate the effective charge separation in HOMO-LUMO energy levels. As expected, in their HOMO energy levels, the electron cloud is predominantly localized on carbazole donor in case of all the dyes. Conversely, at their LUMO energy levels, the electron cloud is shifted evidently from the electron donor (carbazole) to the electron acceptor (4-aminobenzoic acid, sulfanilic acid and barbituric acid) in different extent due to their varied electron accepting nature. It was worth to note that, the LUMO electron density of *n*-C$_6$ is fully localized on anchoring –COOH group of 4-aminobenzoic acid facilitating the electronic coupling between the electron density at its LUMO level and the *d* orbitals of the TiO$_2$.

Dye	Optimized Geometry	HOMO	LUMO
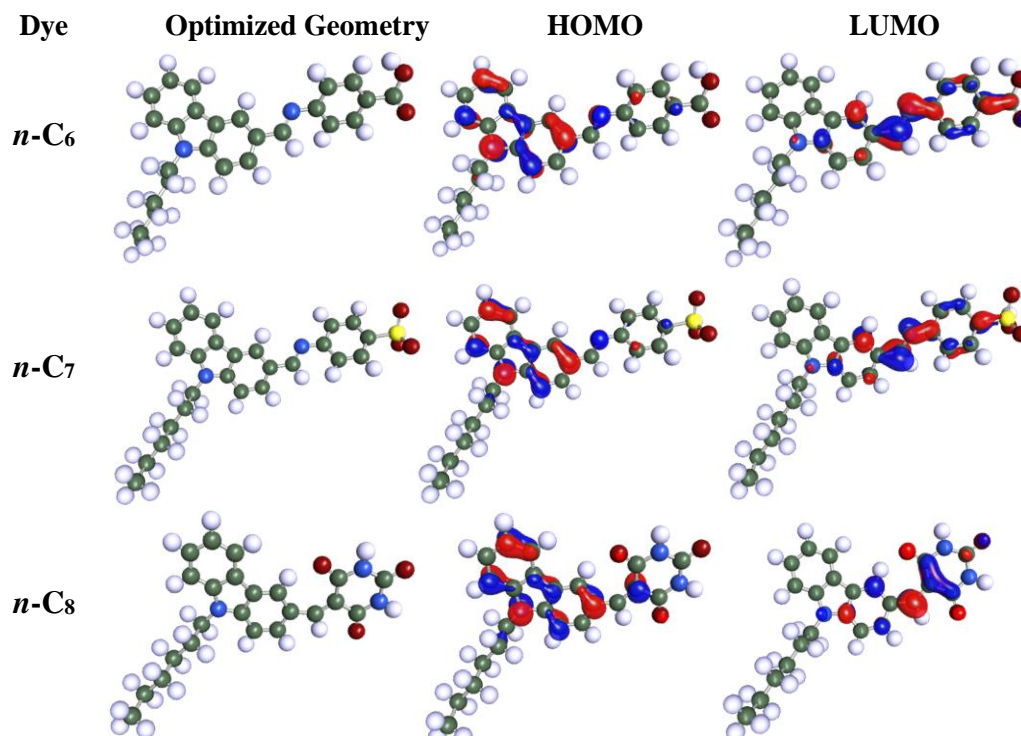
Fig 4.19: Optimized geometry and FMO energy levels of *n*-C$_{6\text{-}8}$

4.3.2.3 Molecular modeling of *n*-C$_{9-12}$ (Series-2)

The optimized molecular geometries of *n*-C$_{9-12}$ and their corresponding electron density distributions in their FMO energy levels as obtained from T-mole visualizer are shown in **Fig 4.20**.

Dye	Optimized Geometry	HOMO	LUMO
n-C$_9$			
n-C$_{10}$			
n-C$_{11}$			
n-C$_{12}$			
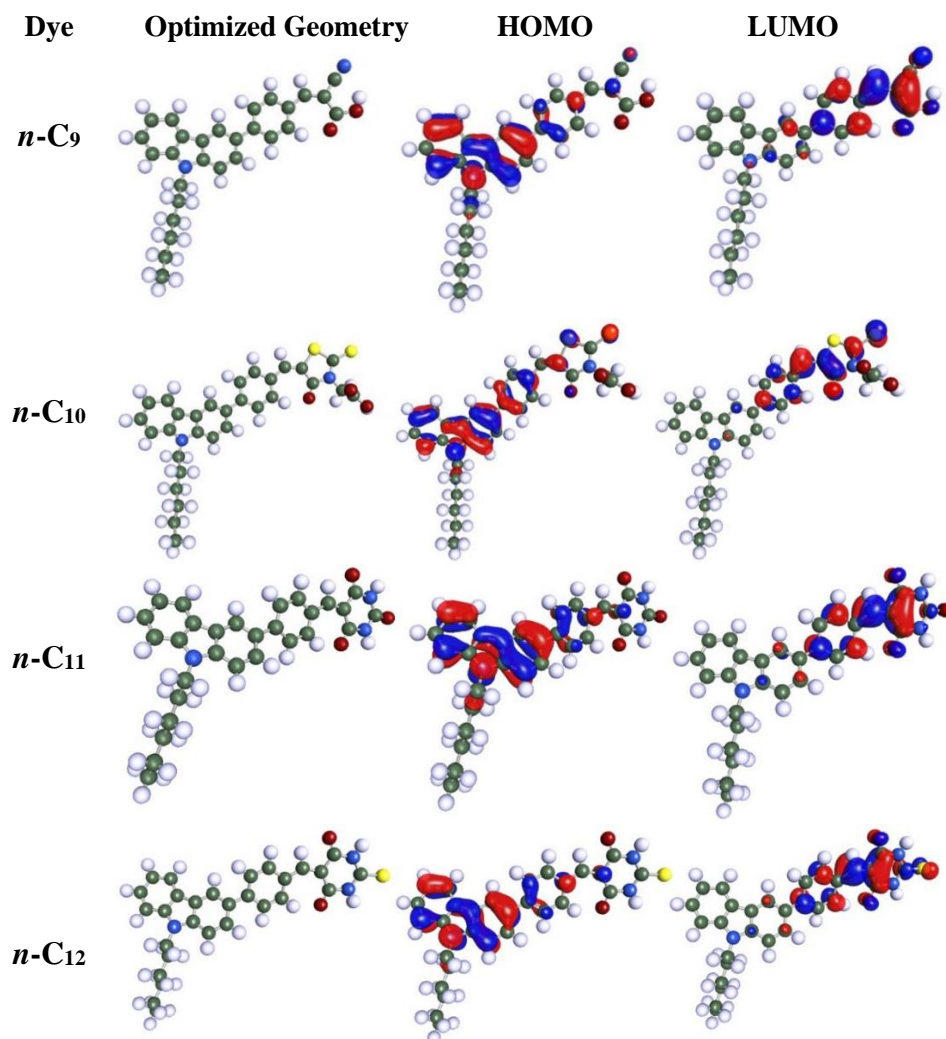
Fig 4.20: Optimized geometry and FMO energy levels of *n*-C$_{9-12}$

The 3-D structures indicate the effective charge separation in ground and excited states of the molecules. As evidenced from their HOMO energy levels, the electron cloud is predominantly localized on carbazole and phenyl ring in case of all the dyes. However, at their LUMO levels, the electron cloud is shifted clearly from the electron donor

(carbazole) to the electron acceptor (cyanoacetic acid, rhodanine-3-acetic acid, barbituric acid and thiobarbituric acid) in different extent due to their varied electron accepting nature. Interestingly, the LUMO electron density of *n*-C$_9$ is fully localized on anchoring cyano acetic acid moiety, facilitating the electronic coupling between the electron density at its LUMO level and the *d* orbitals of the TiO$_2$ and hence the overlapped HOMO and LUMO levels on carbazole core guarantees a fast photo-induced electron transfer from donor to acceptor group.

4.3.2.4 Molecular modeling of *n*-C$_{13-15}$ (Series-3)

The optimized molecular geometries of the dyes and their corresponding electronic cloud delocalization in FMO levels are portrayed in **Fig 4.21**. The 3-D vision of the molecules indicates the effectiveness of intramolecular charge separation *i.e.,* effective charge separation in the ground and excited states of the molecules. As evidenced from their HOMO energy levels, the electron cloud is predominantly delocalized on carbazole ring (donor) as well as vinyl thiophene system (π-spacer) in the dyes. However, at their LUMO levels, the electron cloud is clearly shifted from the electron donor (carbazole) to the electron acceptor (cyanoacetic acid, rhodanine-3-acetic acid and barbituric acid) to different extent due to the varied electron withdrawing nature. Interestingly, results for *n*-C$_{13-}$ dye, clearly indicated that its LUMO electron density is fully localized on cyanoacetic acid (anchoring group). Thus, a close proximity of the LUMO levels to the anchoring group would facilitate the electronic coupling between the electron density at the LUMO level of the dye and *d* orbitals of TiO$_2$. Hence, the well-overlapped HOMO and LUMO on carbazole core guarantees a fast photo induced electron transfer from donor to acceptor units. While in case of *n*-C$_{14}$, the electron density distribution in LUMO level is predominantly concentrated on rhodanine scaffold, typically on the carbonyl as well as thiocarbonyl group and thus resulting in the isolation of LUMO from the anchoring -COOH group and hence preventing proper injection of electron in CB of TiO$_2$ (Tian et al. 2008, 2007). In case of *n*-C$_{15}$ the LUMO level is largely localized on the carbonyl groups of barbituric acid (Beni et al. 2015).
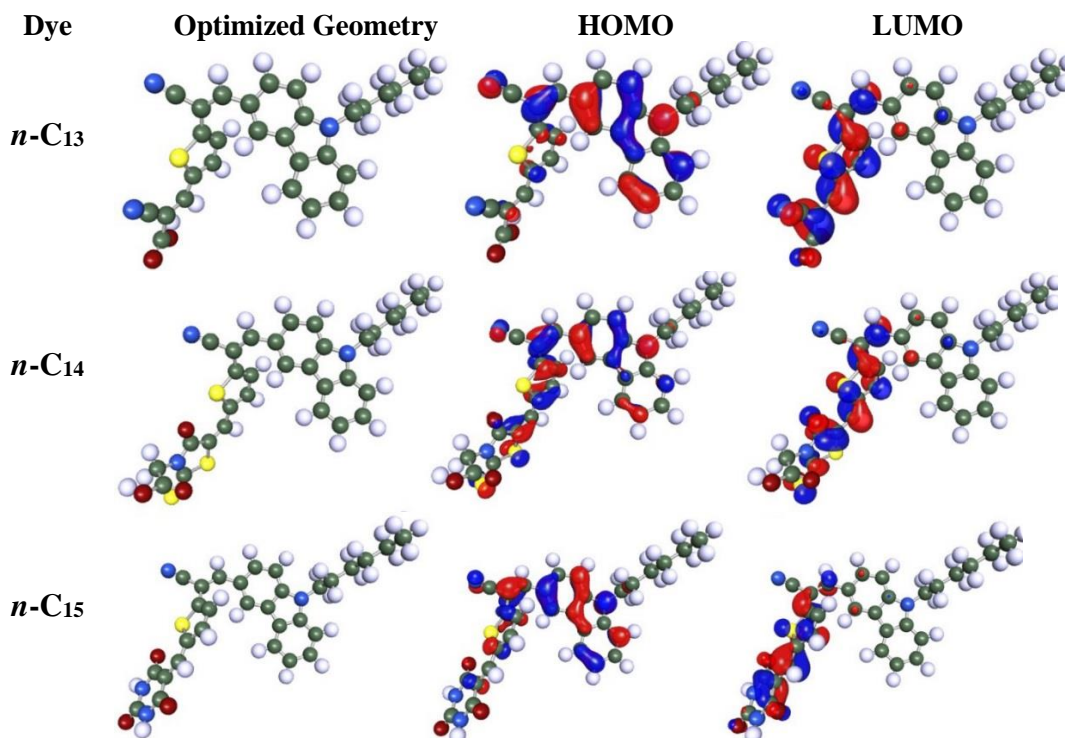
Fig 4.21: Optimized geometry and FMO energy levels of *n*-C$_{13-15}$

4.3.2.5 Molecular modeling of *n*-C$_{16-18}$ (Series-4)

The DFT calculations were done for the dyes *n*-C$_{16-18}$ at B3LYP/TZVPP level and their corresponding electron density distributions in their HOMO and LUMO energy levels as obtained from T-mole visualizer are shown in **Fig 4.22**. The 3-D optimized structures of the dyes indicate the effective charge separation in HOMO-LUMO energy levels. As expected, in their HOMO levels, the electron cloud is predominantly localized on anisole and carbazole units for all the dyes. Contrariwise, at their LUMO levels, the electron cloud is shifted evidently from the electron donor to the electron acceptor in different extent due to their varied electron accepting nature. Interestingly, the LUMO electron density of *n*-C$_{16}$ is fully localized on anchoring –COOH group facilitating the electronic coupling between the electron density at its LUMO level and the *d* orbitals of the TiO$_2$. Hence, the well-overlapped HOMO and LUMO on carbazole core guarantees a fast photo induced electron transfer from donor to acceptor units. While in case of *n*-C$_{17-18}$, the electron

density distribution in LUMO level is predominantly concentrated on the carbonyl groups of 2, 4-thiazolidinedione and barbituric acid scaffold (Beni et al. 2015).
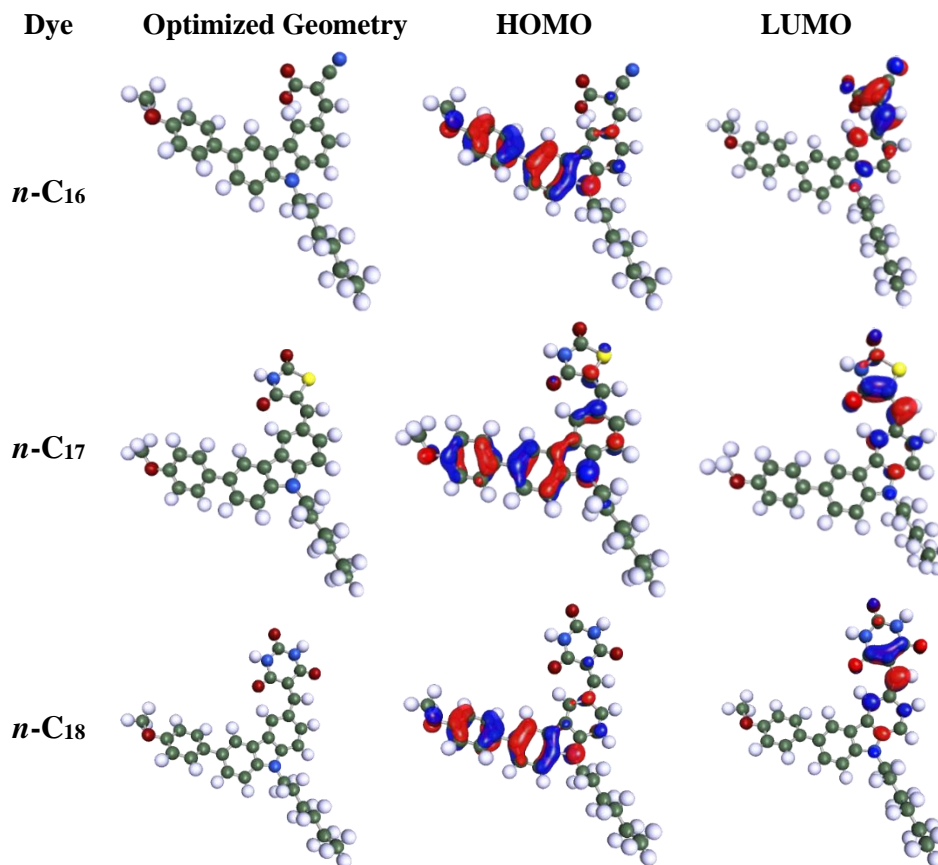
Fig 4.22: Optimized geometry and FMO energy levels of *n*-C$_{16-18}$

4.3.2.6 Molecular modeling of *n*-C$_{19-21}$ (Series-5)

The optimized molecular geometries of *n*-C$_{19-21}$ and their corresponding electron cloud delocalization between their HOMO- LUMO energy levels as achieved from T-mole 3D visualizer are given in **Fig 4.23**. The 3-D optimized structures of the organic dyes *n*-C$_{19-21}$ stipulates the effective charge separation in their FMOs energy level. As expected, all the dyes showcase the similar HOMO energy levels due to similar electron donating carbazole unit in the design. Contrariwise, at their LUMO energy levels, the electron cloud is shifted clearly from the electron donor (carbazole) to the electron acceptor (cyanoacetic acid, 2, 4 thiazolidinedione and barbituric acid) units in different extent due to varied electron accepting nature.

| Dye | Optimized Geometry | HOMO | LUMO |
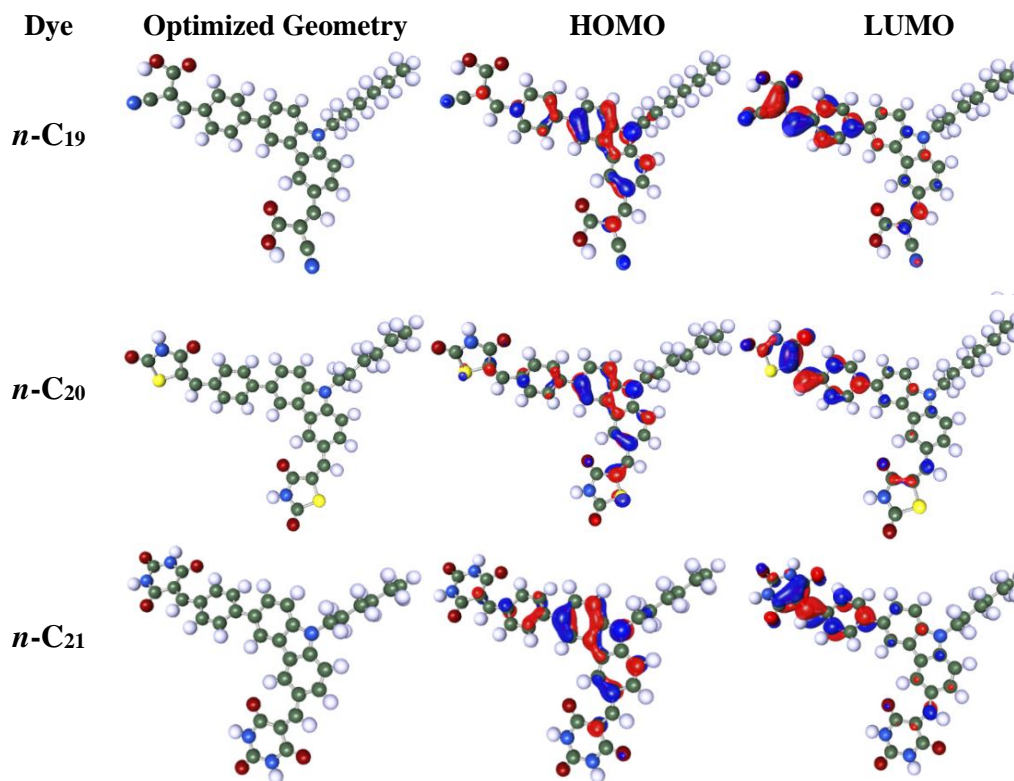
Fig 4.23: Optimized geometry and FMO energy levels of *n*-C$_{19\text{-}21}$

From the **Fig 4.23**, it is interesting to note that the electron cloud of LUMO energy levels of all the dyes have been shifted only towards acceptor/anchoring unit linked to phenylene π-spacer instead of anchoring group linked to vinylene unit. In case of *n*-C$_{19}$, the LUMO electron density has been localized significantly on cyanoacetic acid unit connected to phenylene ring, facilitating the electronic coupling between the electron density at its LUMO level and the *d* orbitals of the TiO$_2$. Thus, the effectively overlapped HOMO and LUMO levels guarantees a fast photo-induced electron transfer from donor carbazole to cyanoacetic acid unit. This phenomenon leads to favorable charge separation and hence impending the electron-hole recombination.

4.3.2.7 Molecular modeling of *p*-C$_{1\text{-}3}$ (Series-6)

The optimized structures of *p*-C$_{1\text{-}3}$ and their corresponding electron density delocalization in FMO energy levels as acquired from T-mole visualizer are displayed in **Fig 4.24**.

Dye	Optimized Geometry	HOMO	LUMO
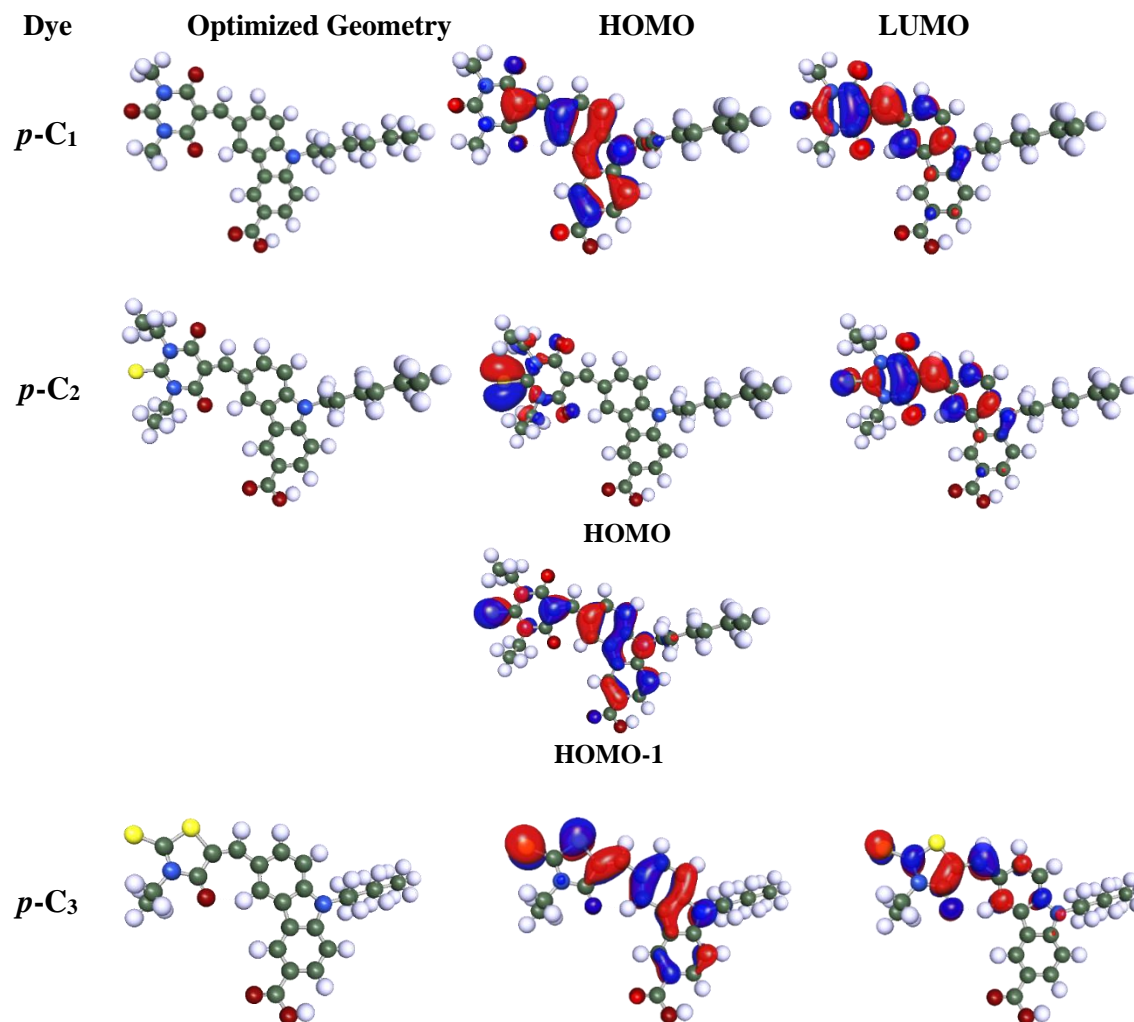
Fig 4.24: Optimized geometry and FMO energy levels of *p*-C$_{1\text{-}3}$

The obtained 3-D structures of the dyes indicate the effective charge separation in their ground and excited states. As shown in **Fig 4.24**, the HOMO levels of *p*-C$_1$ and *p*-C$_3$ are delocalized throughout the molecule, and the LUMO energy level of these two molecules mainly localized on the electron withdrawing groups, *i.e. N,N*-dimethyl barbituric acid and *N*-ethyl rhodanine. In contrast, the electron density of *p*-C$_2$ in HOMO level is mainly

localized on the thiocarbonyl carbon of the *N,N*-diethyl thiobarbituric acid group of the dye (Hosseinzadeh et al. 2015; Salimi Beni et al. 2015). However, the presence of terminal sulphur atom in the thiobarbituric acid has a prominent influence on the HOMO orbitals (Shu et al. 2014). In fact, the terminal >C=S bond is comprised of σ- and π- type molecular orbitals. As the bond length of >C=S is longer than that of >C=C< bond, there is greater contribution of σ-type molecular orbitals, that results in two HOMO energy levels, *i.e.* HOMO and HOMO-1, as shown in **Fig 4.24**. The obtained results clearly reveal that, the LUMO electron density of *p*-**C₂** is fully localized on electron withdrawing thiobarbituric acid moiety, consequently the holes generated in the carbazole have been injected into the VB of the NiO through anchoring carboxylic acid group of *p*-**C₂**.

4.3.2.8 TD-DFT simulations

In order to predict the spectral behavior of synthesized dyes, the calculations of the electronic excitation energies were performed for all the dyes, *(n-C₁₋₂₁ and p-C₁₋₃)* at the TD-DFT level using the long-range corrected B3LYP XC-functional in combination with def-TZVP basis set. The TD-DFT simulations greatly depend on the linear adiabatic approximation and it states that at any point of time the XC functional depends only on the instantaneous density. Accordingly, the XC functional applied for the optimized geometry of dyes derived from ground-state DFT simulations, *i.e.* B3LYP basis set can be employed in the TD-DFT simulations. Typically, the accurateness of the result acquired using TD-DFT extremely depends on the functional and basis set employed for the calculations. However, results of four selected dyes, *n*-**C₁**, *n*-**C₆**, *n*-**C₁₃** and *p*-**C₂** have been discussed as below.

Fig 4.25(a) displays the simulated absorption spectrum of *n*-**C₁** obtained at the B3LYP functional. It shows only one peak, corresponding to its charge transfer process. The simulated absorption spectra of *n*-**C₆**, *n*-**C₁₃** and *p*-**C₂** are given in **Figs 4.25(b)-(d)**, respectively, from which it is evident that the molecules exhibit two distinct bands in the UV-Visible region, corresponding to π-π* and charge transfer phenomenon as obtained from the experiment. The simulated data are well in accordance with the experimentally obtained spectra of all the dyes. Further, simulated vibration spectrum was estimated using

TD-DFT calculations with same conditions as above. The simulated IR spectra of *n*-C$_1$, *n*-C$_6$, *n*-C$_{13}$ and *p*-C$_2$ are shown in **Fig 4.26(a)-(d)**. It matches with experimentally obtained FTIR spectrum. These precise and reliable predictions made by TD-DFT studies indicate that the functional and basis set chosen for TD-DFT calculations are quite appropriate.
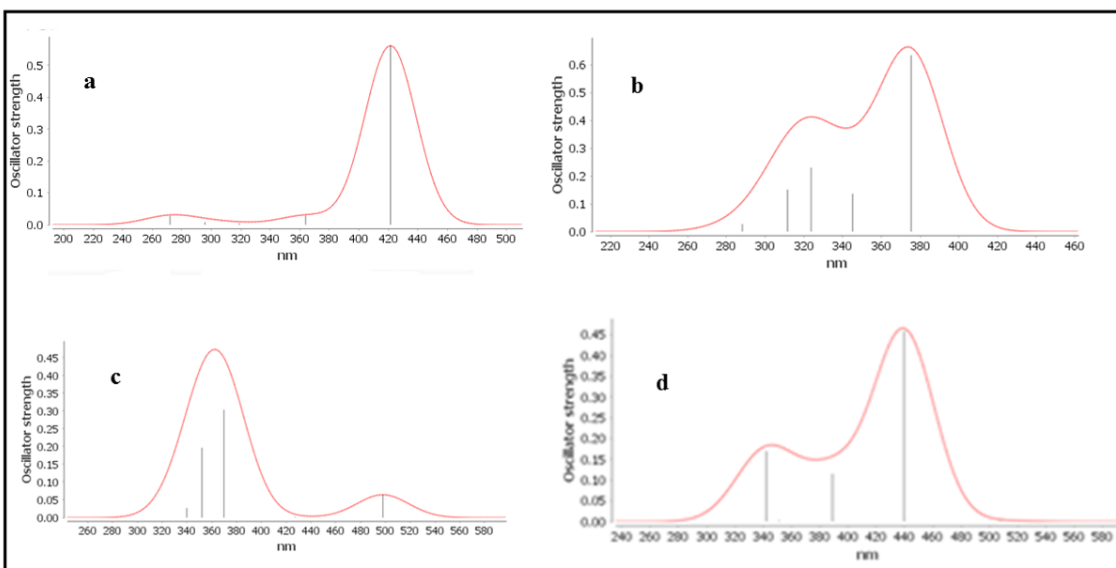
Fig 4.25: Simulated absorption spectra of **(a)** *n*-C$_1$, **(b)** *n*-C$_6$, **(c)** *n*-C$_{13}$ and **(d)** *p*-C$_2$
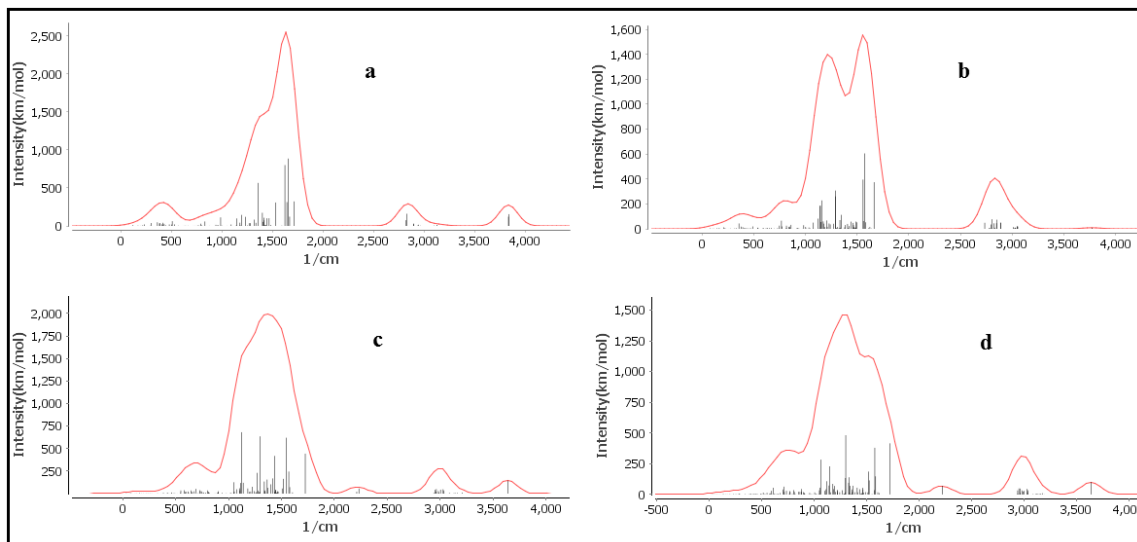
Fig 4.26: Simulated vibration spectra of **(a)** *n*-C$_1$, **(b)** *n*-C$_6$, **(c)** *n*-C$_{13}$ and **(d)** *p*-C$_2$

4.4   CONCLUSIONS

In summary, all the synthesized dyes *(n-C₁₋₂₁ and p-C₁₋₃)* were subjected to photophysical, electrochemical and molecular modeling studies. Their photophysical characterization reveals that all the dyes display good absorption in the range of 343-524 nm and emission in the range of 449-630 nm; Further, their CV study indicates that, all the dyes possess stringent requirements for electron injection and dye regeneration processes in the device. Furthermore, DFT calculations confirm a better charge separation between the HOMO and LUMO energy levels of the new dyes. Finally, the TD-DFT simulated absorption spectra of dyes are in accordance with experimental data indicating the basis set and XC functional chosen are quite appropriate for the calculations.

Based on the above results, the synthesized dyes (***n*-C₁₋₂₁** and ***p*-C₁₋₃**) were used in the fabrication of DSSCs, as sensitizers. Also, carbazole based dyes (***n*-C₆₋₂₁**) were employed as co-sensitizers in Ru (II) based DSSCs. In the next chapter, a detailed device fabrication studies and EIS studies are discussed.

PHOTOVOLTAIC AND ELECTROCHEMICAL IMPEDANCE STUDIES

Abstract:

*This chapter deals with the DSSC fabrication studies of newly synthesized n-type (**n-C$_{1-21}$**) and p-type (**p-C$_{1-3}$**) dyes as sensitizers. Also, it covers the investigation of sixteen carbazole based dyes **n-C$_{6-21}$** as co-sensitizers in Ru (II) sensitized DSSCs. Further, it includes the EIS studies of the fabricated devices as well as a detailed discussion on structure-device performance relationship of the dyes.*

5.1 PHOTOVOLTAIC INVESTIGATION

The photovoltaic investigation of DSSCs includes fabrication of *n-/p*-type photovoltaic devices using newly synthesized sensitizers/co-sensitizers and determination of photovoltaic parameters of the new dyes.

5.1.1 Introduction

A photovoltaic cell is a device, which converts incident photon to electrical energy. Generation of electrical power under illumination is achieved by the capability of the photovoltaic device to produce voltage over an external load and current through the load at the same time. This is characterized by the current-voltage (*J-V*) curve of the cell at certain illumination and temperature. When the cell is short circuited under illumination, the maximum current, the short circuit current (J_{SC}), is generated, while under open circuit conditions no current can flow and the voltage is at its maximum, called the open circuit voltage (V_{OC}). Another important characteristic of the solar cell performance is the fill factor (*FF*).

In the present work, all the synthesized dyes (*n*-**C$_{1-21}$** and *p*-**C$_{1-3}$**) were employed as sensitizers in DSSCs, while carbazole based dyes *n*-**C$_{6-21}$** were used as co-sensitizers in standard Ru-II complex based DSSCs. A detailed procedures for DSSC fabrication as well as discussion on obtained results are described in the following sections.

5.1.2 Material and methods

The *J-V* (Current-Voltage) characteristics of fabricated *n*-type devices were measured using Oriel SOL3A solar simulator connected to Keithley 2400 source meter. Further, *IPCE* (Incident photon conversion efficiency) spectra of all the fabricated DSSCs were recorded using QEX10 PV measurement system. Calibration of incident light was performed before measurements using a silicon photodiode (IF035, PV Measurements). All the measurements were carried out without the use of anti-reflecting film.

For *p*-type device fabrication studies, conductive glass substrates (F-doped SnO_2) were purchased from Solaronix (TEC15, sheet resistance 15 Ω/square). A set-up comprising Oriel solar simulator (AM 1.5G, 100 mW/cm²) calibrated with a silicon cell covered with a KG5 filter and attached to Keithley 2400 digital source meter was used for measuring photovoltaic parameters. *IPCE* experiments were carried out for the fabricated devices using ZAHNER's CIMPS-QE/IPCE system.

5.1.3 Experimental

As per the procedure described in the reported literature (El-Shafei et al. 2012 Cheema et al. 2014), DSSCs were fabricated using synthesized *n*-type dyes ***n*-C₁-₂₁** as sensitizers. Further, the carbazole based dyes (***n*-C₆-₂₁**) were exploited as co-sensitizers in the devices sensitized with Ru (II) complex (**NCSU-10/N3**). Finally, the *p*-type DSSCs were fabricated using sensitizers ***p*-C₁-₃** following the standard procedure reported by Fabrice group (Ameline et al. 2015; Warnan et al. 2014).

5.1.3.1 TiO₂ electrode preparation and fabrication of DSSCs sensitized with *n*-C₁-₂₁

The procedure followed for fabrication of *n*-type DSSCs is as follows: Fluorine-doped tin oxide (FTO) coated glasses (2.2 mm thickness, sheet resistance of 8 Ω/cm^2, TEC, Pilkington) were washed with detergent, water, acetone and ethanol, sequentially. After this FTO glass plates were immersed into a 40 mM aqueous TiCl₄ solution at 70 °C for 30 min and washed with water and ethanol. A thin layer (8-12 μm thick) of TiO₂ (Solaronix, Ti-Nanoxide D/SP) was deposited (active area, 0.18 cm^2) on transparent conducting glass by squeegee printing followed by drying at 350 °C for 10

min and curing at 500 °C for 30 min. Next, after drying the electrodes, scattering layer (5 μm thick) TiO_2 particles (Solaronix, Ti-Nanoxide R/SP) were printed onto the already deposited TiO_2 layer. The TiO_2 electrodes were heated under an air flow at 350 °C for 10 min, followed by heating at 500 °C for 30 min. After cooling to room temperature, the TiO_2 electrodes were treated with 40 mM aqueous solution of $TiCl_4$ at 70 °C for 30 min and then washed with water and ethanol. The electrodes were heated again at 500 °C for 30 min and left to cool to 80 °C before dipping them into the dye solution. The dye solutions (0.3 mM) were prepared in 10 mL 1:1:1 acetonitrile, *tert*-butanol and dimethyl sulfoxide. Chenodeoxycholic acid (CDCA) was added at a concentration of 10 mM. The electrodes were immersed in the dye solutions and then kept at 25 °C for 20 hours to adsorb the dye onto the TiO_2 surface.

For preparing the counter electrode, pre-cut TCO glasses were washed with water followed by 0.1M HCl in EtOH, and sonication in an acetone bath for 10 min. These washed TCO were then dried at 400 °C for 15 min. A thin layer of Pt-paste (Solaronix, Platisol T/SP) on TCO was printed and the printed electrodes were then cured at 450 °C for 10 min. The dye sensitized TiO_2 electrodes were sandwiched with Pt counter electrodes and the electrolyte (Solaronix, Iodolyte HI-30) was then injected into the cell, while the two electrodes were held together with the clips.

5.1.3.2 TiO_2 electrode preparation and fabrication of DSSCs co-sensitized with *n*-C$_{6-21}$

The procedure for fabrication of DSSCs co-sensitized with *n*-C$_{6-21}$ is as follows: FTO coated glasses (2.2 mm thickness, sheet resistance of 8 Ω/cm^2, TEC, Pilkington) were washed with detergent, water, acetone and ethanol, sequentially. After this FTO glass plates were immersed into a 40 mM aqueous $TiCl_4$ solution at 70 °C for 30 min and washed with water and ethanol. A thin layer (8-12 μm thick) of TiO_2 (Solaronix, Ti-Nanoxide D/SP) was deposited (active area, 0.18 cm^2) on transparent conducting glass by squeegee printing followed by drying at 350 °C for 10 min and curing at 500 °C for 30 min. Next, after drying the electrodes, scattering layer (5 μm thick) TiO_2 particles (Solaronix, Ti-Nanoxide R/SP) were printed onto the already deposited TiO_2 layer. The TiO_2 electrodes were heated under an air flow at 350 °C for 10 min, followed

by heating at 500 °C for 30 min. After cooling to room temperature, the TiO_2 electrodes were treated with 40 mM aqueous solution of $TiCl_4$ at 70 °C for 30 min and then washed with water and ethanol. The electrodes were heated again at 500 °C for 30 min and left to cool to 80 °C before dipping them into the dye solution. The dye solutions were prepared in 10 mL 1:1:1 acetonitrile, *tert*-butanol and dimethyl sulfoxide, and Ru (II) dye (**NCSU-10/N3**) and organic dyes (***n*-C_{6-21}**) were then dissolved based on the required concentration. The CDCA was added at a concentration of 10 mM. The electrodes were immersed in the dye solutions and then kept at 25 °C for 20 hours to adsorb the dye onto the TiO_2 surface.

In the preparation of the counter electrode, pre-cut TCO glasses were washed with water followed by 0.1M HCl in ethanol, and sonication in an acetone bath for 10 min. These washed TCO were then dried at 400 °C for 15 min. A thin layer of Pt-paste (Solaronix, Platisol T/SP) on TCO was printed and the printed electrodes were then cured at 450 °C for 10 min. The dye sensitized TiO_2 electrodes were sandwiched with Pt counter electrodes and the electrolyte (Solaronix, Iodolyte HI-30) was then injected into the cell, while the two electrodes were held together with the clips.

5.1.3.3 NiO electrode preparation and fabrication of DSSCs sensitized with *p*-C_{1-3}

The procedure used for fabrication of NiO based *p*-type DSSCs is as follows: Conductive glass substrates were successively cleaned by sonication in soapy water, then acidified ethanol for 10 min before being fired at 450 °C for 30 min. NiO dense layer was prepared by spin-coating onto the clean substrates of a 0.5 M nickel acetate solution containing 0.5 M ethanolamine in methoxyethanol at 3000 rpm for 30 s followed by thermal treatment at 500 °C for 0.5 hr. Then the FTO substrates with NiO dense layer (30±5 nm) were screen printed four times with a home-made NiO paste. The NiO screen-printing paste was produced by preparing a slurry of 3 g of NiO nanopowder (Inframat) suspended in 10 mL of distilled ethanol and ball-milled (500 rpm) for 24 h. The resulting slurry was mixed in a round-bottom flask with 10 mL of 10 wt % ethanolic ethyl cellulose (Sigma Aldrich) solution and 20 mL terpineol, followed by slow ethanol removal by rotary evaporation. The NiO films were subsequently sintered at 450°C for 30 min. The thickness of the resulting NiO layer

was 3.5 µm±50 nm. The NiO electrodes were soaked in a solution of nickel acetate in ethanol (20 mM) with 1% ethanolamine for 30 min at 60 °C followed by ethanol rinsing and drying in air. The electrodes NiO were finally annealed at 120 °C for 60 min, then were dipped in a solution of the dye (0.3 mmol.L^{-1} in CH$_3$CN) and stored at room temperature overnight.

Platinum counter electrodes were prepared by depositing a few drops of an isopropanol solution of hexachloroplatinic acid in distilled isopropanol (2 mg per mL) on FTO plates (TEC7, Solaronix). Substrates were then fired at 375 °C for 30 min. The photocathode and the counter electrode were placed on top of each other and sealed using a thin transparent film of Surlyn polymer (DuPont, 25 µm) as a spacer. A drop of the electrolyte was introduced through a predrilled hole in the counter electrode by vacuum backfilling, the hole was then sealed by a glass stopper with Surlyn. The cell had an active area of 0.25 cm^2. The electrolyte used is composed of 0.1 M I$_2$ and 1 M lithium iodide in acetonitrile.

5.1.4 Results and discussion

The series-wise results of DSSC device fabrication studies are summarized in **Tables 5.1-5.10** and pertaining discussion are elaborated in the following section.

5.1.4.1 Photovoltaic performance of Series-1A sensitizers (*n*-C$_{1-5}$)

Fig 5.1 shows *J-V* characteristic curves of sensitizers, *n*-C$_{1-5}$ based DSSCs. The observed photovoltaic parameters, *viz.* V_{OC}, J_{SC}, *FF* and *PCE* are summarized in **Table 5.1.** Amongst the tested dyes, the dye *n*-C$_5$ shows the better photovoltaic performance than other four dyes. The J_{SC} value of *n*-C$_5$ can be attributed to higher Gibbs negative free energy values compared to other dyes (**Fig 4.16,** energy level diagram). From the results, it is clear that, the dyes carrying barbituric acid derivatives (*n*-C$_{1-4}$) display much lower photovoltaic performance than *n*-C$_5$, which is mainly due to their heavy aggregation of dye molecules on the surface of TiO$_2$.

Among the barbituric acid derivatives (*n*-C$_{1-4}$), the dye *n*-C$_1$ shows a maximum efficiency of 0.244% due to the strong binding of barbituric acid on TiO$_2$. While the dye *n*-C$_2$ exhibits the lowest efficiency of 0.065% due to the non-availability of free

NH group to bind on the surface of mesoporous TiO_2 effectively. The dye ***n*-C$_3$** displays an efficiency 0.223%, which is comparable to that of ***n*-C$_1$**, owing to binding of sulfonyl as well as NH group on mesoporous TiO_2, whereas the dye ***n*-C$_4$** shows an efficiency of 0.108%, which is attributed to non-availability of free NH functionality for binding. Compared to ***n*-C$_1$** and ***n*-C$_3$**, the binding strength of ***n*-C$_2$** and ***n*-C$_4$** on TiO_2 surface is weak. The possible binding approach for ***n*-C$_2$** and ***n*-C$_4$** is mono-dentate coordinating mode through a C=O or C=S group with Ti on the surface of TiO_2; while in ***n*-C$_1$** and ***n*-C$_3$**, the binding mode is bi-dentate bridging due to their tautomeric forms (Zhang et al. 2015). Here, the weak binding strength has caused insufficient electron injection from the sensitizer to the TiO_2, leading to the decrease of J_{SC} and thereby the overall efficiency. However, the observed photovolatic performance for ***n*-C$_{1-5}$** dyes is not satisfactory.
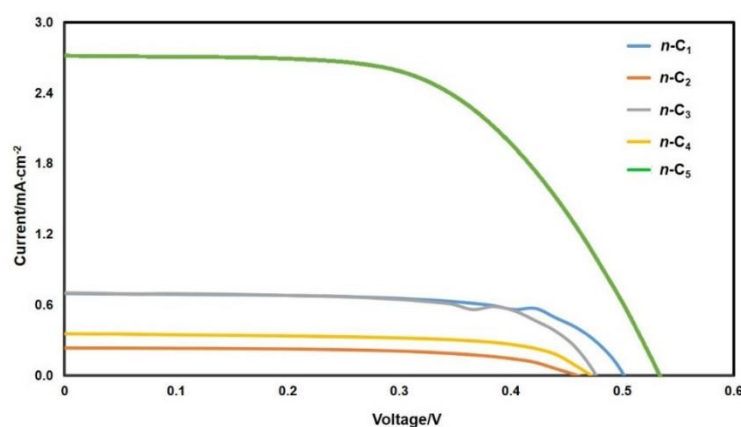
Fig 5.1: *J-V* characteristics of DSSCs sensitized with ***n*-C$_{1-5}$**

Table 5.1: Photovoltaic measurement data of **Series-1A**, ***n*-C$_{1-5}$**

Dye	V_{OC} (V)	J_{SC} (mA.cm^{-2})	FF%	η%
***n*-C$_1$**	0.501	0.69	69.97	0.244
***n*-C$_2$**	0.460	0.23	60.38	0.065
***n*-C$_3$**	0.476	0.69	67.11	0.223
***n*-C$_4$**	0.471	0.35	64.53	0.108
***n*-C$_5$**	0.537	2.72	76.8	1.0

5.1.4.2 Photovoltaic performance of Series-1B sensitizers/Co-sensitizers (n-C$_{6-8}$)

DSSCs sensitized with n-C$_{6-8}$

Figs 5.2 and 5.3 show the *J-V* and *IPCE* characteristic curves for DSSCs sensitized with dyes n-C$_{6-8}$ in the presence of CDCA and their detailed photovoltaic data are tabulated in **Table 5.2**. Here, photovoltaic performance of the fabricated devices was found to be in the order of n-C$_6$ > n-C$_8$ > n-C$_7$. The better efficiency of n-C$_6$ can be ascribed to the efficient electron withdrawing from electron rich carbazole donor followed by injection of electrons into the CB edge of TiO$_2$ by carboxylic acid anchoring group. Further, the estimated negative free energy values for electron injection were shown (**Fig 4.16**) to be in the order of n-C$_6$ (1.61 eV) > n-C$_8$ (1.46 eV) > n-C$_7$ (1.24 eV). From the results, it is clear that, the dye n-C$_6$ carrying 4-aminobenzoic acid would be more efficient for electron injection into the CB of TiO$_2$ than the other two dyes. In fact, the results of photovoltaic performance based on n-C$_{6-8}$ dyes follow the same order of their negative free energy values.
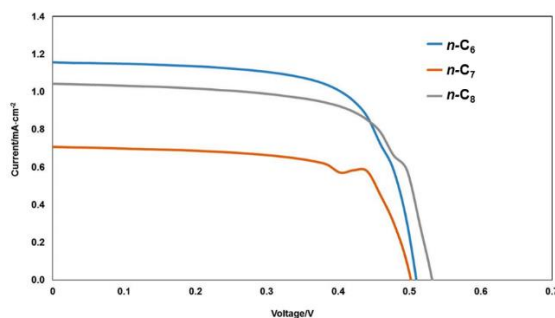
| **Fig 5.2:** *J-V* characteristics of DSSCs sensitized with n-C$_{6-8}$ | **Fig 5.3:** *IPCE* characteristics of DSSCs sensitized with n-C$_{6-8}$ |
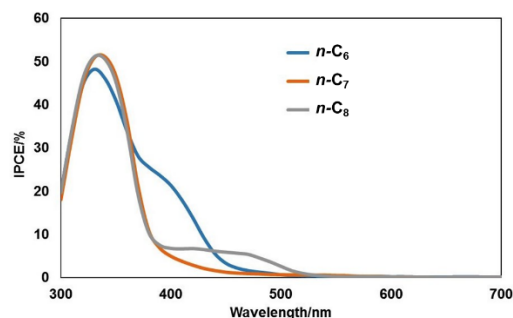
DSSCs co-sensitized using n-C$_{6-8}$ along with NCSU-10

Fig 5.4 displays *J-V* characteristic curves of the photovoltaic devices sensitized with **NCSU-10** alone and co-sensitized with dyes n-C$_{6-8}$. Their corresponding photovoltaic results are tabulated in **Table 5.2**. It is worth to note that, the DSSC co-sensitized with n-C$_6$ dye showcases enhanced *PCE* than the device sensitized with **NCSU-10** alone. From the results, it is clear that, the V_{OC} values are decreasing in the order of n-C$_6$ (0.672 V) > n-C$_6$ (0.670 V) > n-C$_6$ (0.641 V), upon co-sensitization with **NCSU-10** (0.667 V). This is mainly attributed to the fact that, the bulky **NCSU-10** dye molecules inadequately adsorb on the surface of TiO$_2$ leaving behind larger gaps

between the adsorbed molecules. The voids present between the adsorbed dye molecules of **NCSU-10** will be now covered by molecules of co-sensitizers **n-C$_{6-8}$** and thus providing an enhanced surface coverage, simultaneously reducing the dye aggregation of main dye as well the back reaction of I_3^-/I^- on TiO$_2$ surface in the cell. Further, according to reported literature, the co-sensitizers employed in the cells may reduce the dye loading up to 60%, which may considerably diminish the photocurrent density. The aforementioned reduction in dye loading has been witnessed in the **n-C$_6$** co-sensitized devices resulting in reduced light harvesting ability (J_{SC}). The J_{SC} values of the co-sensitized devices were found to be 22.85, 19.46 and 22.27 mA.cm^{-2} for **n-C$_{6-8}$**, respectively, while **NSCU-10** alone sensitized device showed 20.41 mA.cm^{-2}.
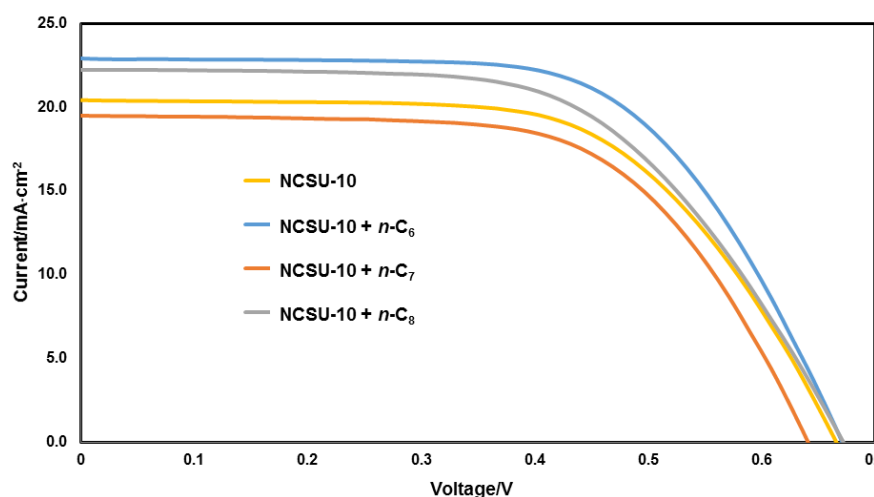
Fig 5.4: *J-V* curves of DSSC based on **NCSU-10** alone and co-sensitized with **n-C$_{6-8}$**

The *IPCE* traces of fabricated devices using co-sensitizers **n-C$_{6-8}$** and **NCSU-10** sensitizer alone at 0.2 mM concentration are displayed in **Fig 5.5**. It depicts the % *IPCE* as a function of the excited wavelength of the dyes coated on the mesoporous TiO$_2$. Under the same conditions, the *PCE* of the device co-sensitized with **n-C$_6$** and **n-C$_8$** were found to be higher than the device with **NCSU-10** dye alone, as shown in **Fig 5.4**. The superior photovoltaic performance of the devices co-sensitized with **n-C$_6$** and **n-C$_8$** can be attributed to the improved light harvesting efficiency of the devices. The presence of co-sensitizer has resulted in the improvement of J_{SC} as well as V_{OC} values, supporting the role of co-sensitizer in diminishing undesirable charge recombination within the fabricated cell.
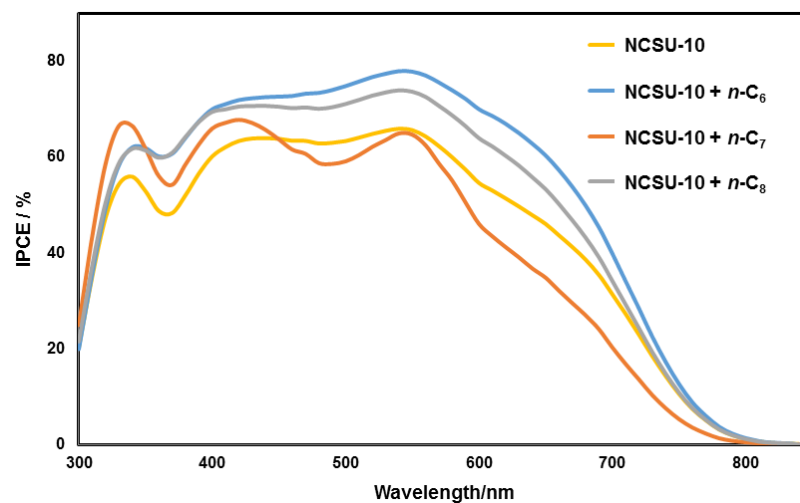
Fig 5.5: *IPCE* of DSSC sensitized with **NCSU-10** alone and co-sensitized with ***n*-C₆₋₈**

Table 5.2: Photovoltaic measurement data of fabricated DSSCs

Sensitizer/ co-sensitizer		CDCA (mM)	J_{SC} (mA.cm^{-2})	V_{OC} (V)	*FF* (%)	η (%)
NCSU-10 (mM)	Dye					
0.2	--	20	20.41 ± 0.03	0.667 ± 0.002	60.6 ± 0.4	8.25 ± 0.4
0.2	***n*-C₆** (0.2 mM)	20	22.85 ± 0.06	0.672 ± 0.002	62.2 ± 0.2	9.55 ± 0.03
0.2	***n*-C₇** (0.2 mM)	20	19.46 ± 0.09	0.641 ± 0.004	62.0 ± 0.1	7.74 ± 0.01
0.2	***n*-C₈** (0.2 mM)	20	22.27 ± 0.09	0.670 ± 0.004	58.6 ± 0.2	8.75 ± 0.01
--	***n*-C₆**	10	1.157 ± 0.002	0.508 ± 0.001	68.6 ± 0.1	0.403 ± 0.001
--	***n*-C₇**	10	0.707 ± 0.005	0.502 ± 0.002	72.6 ± 0.6	0.257 ± 0.001
--	***n*-C₇**	10	1.042 ± 0.001	0.530 ± 0.003	67.6 ± 0.5	0.373 ± 0.005

5.1.4.3 Photovoltaic performance of Series-2 sensitizer/Co-sensitizers (*n*-C$_{9-12}$)

DSSCs sensitized with n-C$_{9-12}$

The *J-V* characteristic curves of the photovoltaic devices sensitized with **n-C$_{9-12}$** are given in **Fig 5.6** and their detailed photovoltaic results are summarized in **Table 5.3**. The results indicate that the DSSC fabricated with **n-C$_9$** shows maximum *PCE* of 1.94 % (*J$_{SC}$*=4.68 mA.cm^{-2}, *V$_{OC}$*=0.588 V, and *FF*=70.3) when compared to DSSCs based on other dyes. From the results, it is clear that the device fabricated with the sensitizer **n-C$_9$** shows improved performance and the observed *PCE* values of the dyes are in decreasing order of **n-C$_9$** > **n-C$_{10}$** > **n-C$_{11}$** > **n-C$_{12}$**. Further, the better photovoltaic performance of **n-C$_9$** can be assigned to its thermodynamically favorable HOMO-LUMO levels (**Fig 4.16**) as well as their higher ε values than that of other dyes in the series (**Table 4.1**).
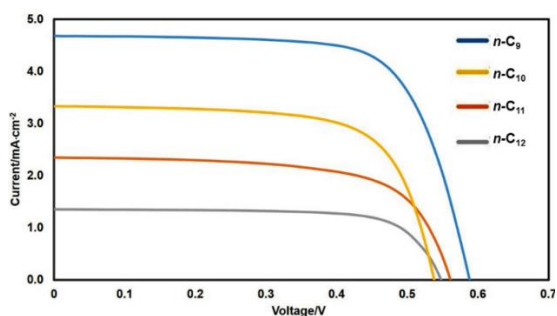
| Fig 5.6: *J-V* characteristics of DSSCs sensitized with dyes **n-C$_{9-12}$** | Fig 5.7: *IPCE* characteristics of DSSCs sensitized with **n-C$_{9-12}$** |
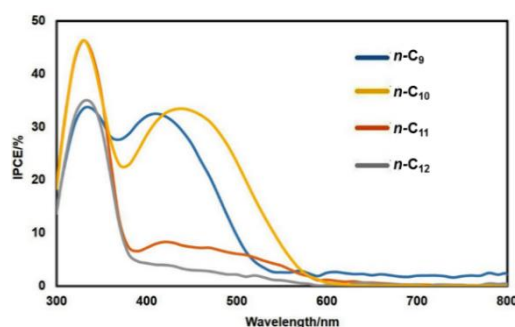
Fig 5.7 shows the *IPCE* spectra of DSSCs fabricated with **n-C$_{9-12}$**. The cell with **n-C$_{10}$** displayed the *IPCE* above 30% in the broad range of 380-570 nm, showing the highest value at 440 nm. However, it's *PCE* value was found to be 1.23% which is comparatively lower than that of **n-C$_9$**. The observed lower *PCE* of **n-C$_{10}$** may be attributed to the breakage in the π-conjugation owed to the presence of methylene group, leading to the LUMO level separation from the anchoring group of the dye. This is in agreement with the results of phenothiazine-based dyes as reported by (Tian et al. 2008, 2007). Further, the lower efficiency of **n-C$_{11}$** and **n-C$_{12}$** may be due to their lower *IPCE* values in comparison with other two dyes. The lowest *J$_{SC}$* and *PCE* values of **n-C$_{12}$** may be ascribed to the presence of sulphur (S) atom in the ring as observed by (Beni et al. 2014).

Table 5.3: Photovoltaic measurement data of ***n*-C$_{9\text{-}12}$**

Sensitizer	CDCA (mM)	J_{SC} (mA.cm^{-2})	V_{OC} (V)	FF (%)	η (%)
***n*-C$_9$**	10	4.68	0.588	70.3	1.94
***n*-C$_{10}$**	10	3.33	0.538	68.8	1.23
***n*-C$_{11}$**	10	2.55	0.568	66.5	0.96
***n*-C$_{12}$**	10	1.35	0.547	72.8	0.54

*DSSCs co-sensitized using **n*-C$_{9\text{-}12}$** along with N3 alone*

Performance parameters pertaining to fabricated DSSCs using **N3** along with the synthesized co-sensitizers ***n*-C$_{9\text{-}12}$** are tabulated in **Table 5.4.** The *J-V* and *IPCE* traces are presented in **Figs 5.8** and **5.9**, respectively. All the co-sensitized devices display lower photovoltaic performances than the cell sensitized by **N3** dye alone. The drop in V_{OC} values suggests that the electron recombination rate has amplified as a result of co-sensitization, thereby leading to the inferior performance of co-sensitized devices. The J_{SC} values of all the dyes were found to be lesser than that of **N3** dye alone. Here, the lowering of J_{SC} value can be attributed to the competitive adsorption of the co-sensitizer and **N3** molecules and thereby, resulting in a decrease in the adsorption of **N3** sensitizer on TiO$_2$ surface. This has resulted in reduced light harvesting proficiency.
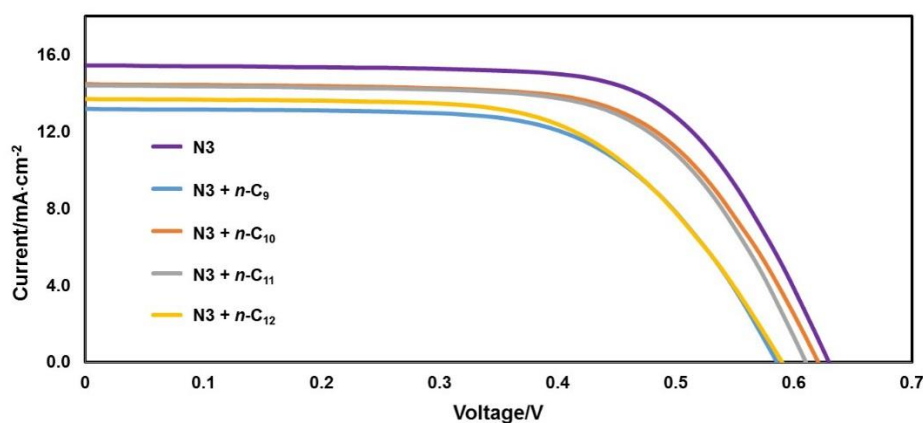
Fig 5.8: *J-V* curves of DSSC sensitized with **N3** and co-sensitized with ***n*-C$_{9\text{-}12}$**
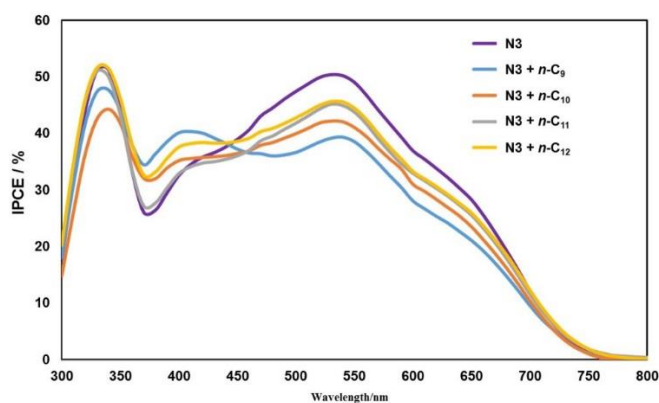
Fig 5.9: *IPCE* curves of DSSC sensitized with **N3** and co-sensitized with *n*-**C9-12**

Table 5.4: Photovoltaic measurement data of dyes *n*-**C9-12**

Sensitizer		CDCA (mM)	J_{SC} (mA·cm^{-2})	V_{OC} (V)	FF (%)	η (%)
N3 (mM)	Co-sensitizer					
0.2	--	20	15.44	0.629	67.6	6.56
0.2	*n*-**C9**	20	13.18	0.585	63.1	4.87
0.2	*n*-**C10**	20	13.69	0.590	61.6	4.97
0.2	*n*-**C11**	20	14.46	0.620	65.9	5.91
0.2	*n*-**C12**	20	14.40	0.610	66.2	5.81

5.1.4.4 Photovoltaic performance of Series-3 sensitizers/Co-sensitizers (*n*-C13-15)

DSSCs sensitized with n-C13-15

Fig 5.10 shows *J-V* curves for DSSCs sensitized with dyes *n*-**C13-15** under AM 1.5G simulated sunlight with a light intensity of 100 mW/cm^2. The observed photovoltaic parameters are summarized in **Table 5.5**. From the energy level diagram (**Fig 4.16)**, it is clear that, the dye *n*-**C13** shows an excellent thermodynamic feasibility for electron injection as well as dye regeneration. The DSSC device fabricated with the sensitizer *n*-**C13** shows maximum *PCE* and the highest *JSC* values compared to the dyes *n*-**C14** and *n*-**C15.** The observed low *PCE* as well as *JSC* values of dye *n*-**C14** can be attributed to the breakage in the π-conjugation leading to the LUMO level separation

from the anchoring group of the dye, as consequence of methylene group in the structure (Tian et al. 2008, 2007). While in case of n-C_{15}, the LUMO levels are largely localized on the carbonyl groups of barbituric acid causing much lower *PCE*, J_{SC} and *IPCE* values (Beni et al. 2015). Thus, the presence of three carbonyl groups has rendered the barbituric acid a poor anchoring unit, resulting in lower *PCE*. In spite, they display good photophysical and electrochemical properties, their conversion efficiency was poor, probably due to the unwanted dye aggregation influencing their electron injection behavior.
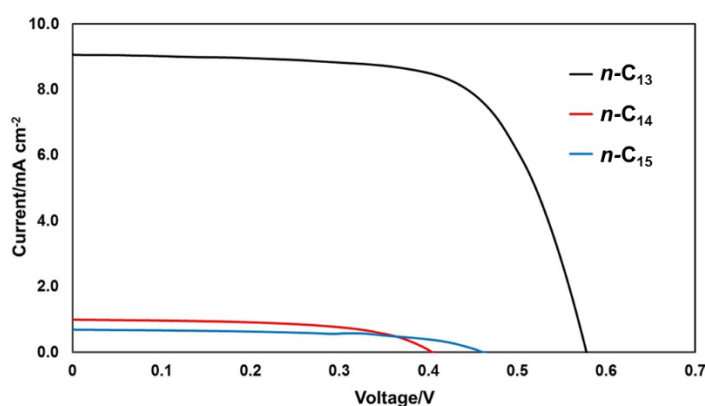
Fig 5.10: *J-V* characteristics of DSSCs sensitized with n-$C_{13\text{-}15}$

Fig 5.11 shows the % *IPCE* as a function of the excited wavelength of the dyes coated on the mesoporous TiO_2. From the results, it is clear that the *IPCE* of n-C_{13}, exhibits a broad band in the region of 340 to 650 nm with value 48%, while *IPCE* of n-C_{14} and n-C_{15} show bands in the region of 400 to 700 nm with values mostly less than 10% of absorbance. Better *IPCE* response of dye n-C_{13} is interpreted in terms of higher J_{SC} value of 9.06 mA.cm^{-2}, compared to that of n-C_{14} (1.00 mA.cm^{-2}) and n-C_{15} (0.69 mA.cm^{-2}) measured in presence of 10 mM CDCA co-adsorbent, which implies the structural optimization with D-π-A-π-A architecture is effective for DSSC application as sensitizer. The much lower dye loading capacity due to steric hindrance may be the main reason for much lower *IPCE* in n-C_{14} and n-C_{15} dyes. Thus, in n-C_{13} the effective increase in π-conjugation has caused the broadening of the visible absorption spectrum, thereby leading to significant enhancement of DSSC performance. This result is in good agreement with the results of dyes investigated by Sun group (Tian et al. 2008, 2007).
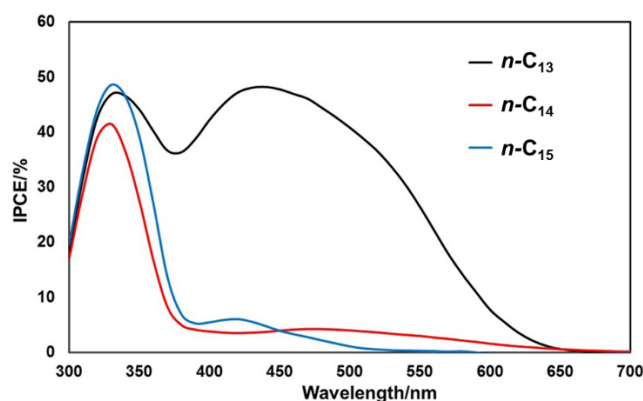
Fig 5.11: *IPCE* spectra of DSSCs based on *n*-C$_{13\text{-}15}$

Table 5.5: Photovoltaic measurement data of dyes *n*-C$_{13\text{-}15}$

Sensitizer	CDCA (mM)	J_{SC} (mA·cm^{-2})	V_{OC} (V)	*FF* (%)	η (%)
n-C$_{13}$	10	9.06	0.577	67.9	3.55
n-C$_{14}$	10	1.00	0.432	62.1	0.24
n-C$_{15}$	10	0.69	0.461	59.0	0.19

*DSSCs co-sensitized using **n**-C$_{13\text{-}15}$ along with **NCSU-10***

Figs 5.12 and **5.13** display *J-V* and *IPCE* characteristic curves of the photovoltaic devices sensitized with **NCSU-10** alone and co-sensitized with dyes ***n*-C$_{13\text{-}15}$**. Their corresponding photovoltaic results are tabulated in **Table 5.6**. It is interesting to note that, the two co-sensitizers ***n*-C$_{13}$** and ***n*-C$_{15}$** exhibit better *PCE* than that of **NCSU-10** alone. The DSSCs employing organic co-sensitizers ***n*-C$_{13\text{-}15}$** yield *PCE* of 8.29, 3.82 and 8.73%, respectively when compared to 8.25% of **NCSU-10** sensitized device. This difference in the photovoltaic performance of the devices can be attributed to the presence of varied acceptor/anchoring units like cyanoacetic acid, rhodanine-3-acetic acid and barbituric acid in the co-sensitizer's molecular structure. From the results, it is clear that, the V_{OC} values are decreasing in the order of ***n*-C$_{13}$** (0.671 V) > ***n*-C$_{14}$** (0.655V) > ***n*-C$_{15}$** (0.556 V), upon co-sensitization with **NCSU-10** (0.667 V). Their J_{SC} values were found to be 19.75, 10.52 and 19.87 mA.cm^{-2} for dyes ***n*-C$_{13\text{-}15}$**, respectively, while **NSCU-10** showed 20.41 mA.cm^{-2}.
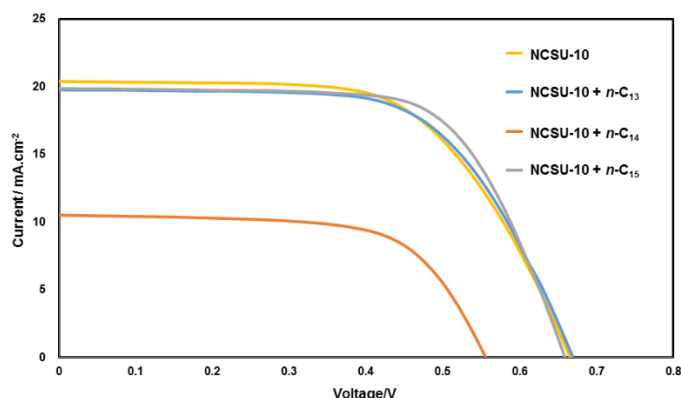
Fig 5.12: *J-V* curves of DSSCs sensitized with **NCSU-10** alone and co-sensitized with

n-**C₁₃₋₁₅**

From the results of *IPCE* experiments of the tested dyes, it is evident that the superior photovoltaic performance is shown by the co-sensitizers *n*-**C₁₃** and *n*-**C₁₅**. This can be largely attributed to their improved light harvesting efficiency. However, the J_{SC} values of *n*-**C₁₃** and *n*-**C₁₅** were found to be lesser than that of **NCSU-10** dye alone. Here, lowering of J_{SC} value can be ascribed to the competitive adsorption of the co-sensitizer and **NCSU-10** molecules and thereby, resulting in a decrease in the adsorption of **NCSU-10** sensitizer on TiO_2 surface. The presence of co-sensitizer in the device has resulted in the improvement of V_{OC} and *FF* values, supporting the role of co-sensitizer in diminishing undesirable charge recombination within the fabricated cell.

Fig 5.13: *IPCE* curves of DSSCs sensitized with **NCSU-10** and co-sensitized with *n*-**C₁₃₋₁₅**

Table 5.6: Photovoltaic measurement data of DSSCs sensitized with NCSU-10 alone and co-sensitized with **n-C$_{16-18}$**

Sensitizer (0.2 mM)	co-sensitizer (0.2 mM)	CDCA (mM)	J_{SC} (mA.cm^{-2})	V_{OC} (V)	FF (%)	η (%)
NCSU-10	--	20	20.41±0.03	0.667±0.002	60.6±0.4	8.25±0.4
	n-C$_{13}$	20	19.75±0.05	0.671±0.002	62.6±0.1	8.29±0.01
	n-C$_{14}$	20	10.52±0.04	0.556±0.002	65.3±0.1	3.82±0.01
	n-C$_{15}$	20	19.87±0.02	0.655±0.004	67.0±0.1	8.73±0.03

5.1.4.5 Photovoltaic performance of Series-4 sensitizers/Co-sensitizers (n-C$_{16-18}$)

*DSSCs sensitized with **n-C$_{16-18}$***

The photovoltaic performance characteristics of the DSSCs fabricated using sensitizers, **n-C$_{16-18}$** on the TiO$_2$ in presence of co-adsorbent CDCA are depicted in **Fig 5.14** and the corresponding data are summarized in **Table 5.7.** The results indicate that device fabricated with **n-C$_{16}$** shows maximum *PCE* of 2.204 % (J_{SC}= 5.220 mA.cm^{-2}, V_{OC}=0.623 V, and *FF*=67.7). The observed *PCE* values of dyes are in the order of **n-C$_{16}$** > **n-C$_{18}$** > **n-C$_{17}$**. The better photovoltaic performance of **n-C$_{16}$** can be attributed to its broad absorption with better ε values. Also, the LUMO/ESOP energy levels of the dyes were found to be more positive than CB edge of TiO$_2$ than other dyes, which leads to better charge injection (**Fig 4.16**).
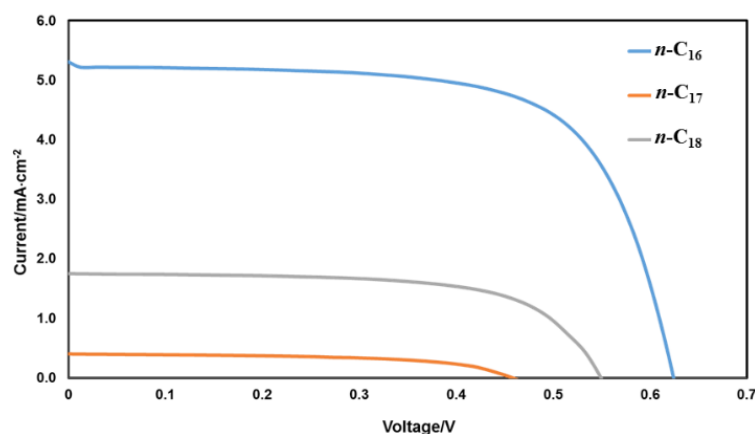
Fig 5.14: *J-V* curves of device sensitized with **n-C$_{16-18}$**

Fig 5.15 shows the *IPCE* curves of ***n*-C₁₆₋₁₈**. From the results, it is clear that the *IPCE* of ***n*-C₁₆** exhibits a broad band in the region of 375-550 nm with a maximum value of 58% at 420 nm, while ***n*-C₁₇** and ***n*-C₁₈** show less intense bands in the region of 400-700 nm with values showing below 10% of absorbance. In this series, the presence of auxiliary anisole unit linked to carbazole donor core with efficient electron acceptor/anchoring cyanoacetic acid has contributed to wider absorption region resulting in a higher J_{SC} value of 5.22 mA.cm^{-2}, compared to those of ***n*-C₁₇** (0.40 mA.cm^{-2}) and ***n*-C₁₈** (1.75 mA.cm^{-2}) measured in presence of 10 mM CDCA co-adsorbent, which implies the structural optimization with D-D-π-A architecture is effective in getting improved efficiency.
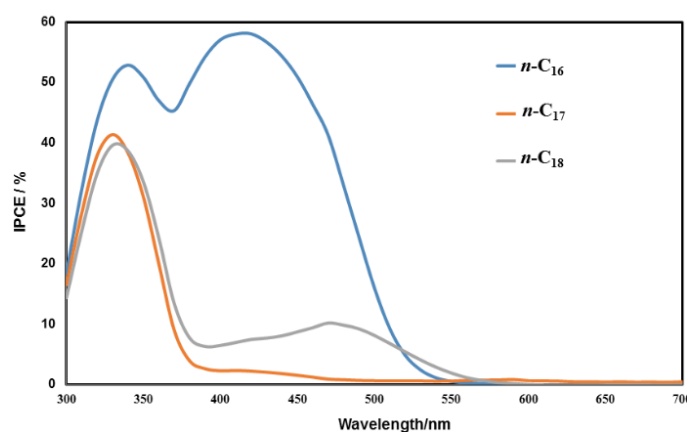
Fig 5.15: IPCE curves of device sensitized with ***n*-C₁₆₋₁₈**

*DSSCs co-sensitized using **n**-C₁₆₋₁₈ along with NCSU-10*

Fig 5.16 displays *J-V* curves of the **NCSU-10** sensitized device and ***n*-C₁₆₋₁₈** co-sensitized devices. **Table 5.7** shows their results. Interestingly, the device co-sensitized with ***n*-C₁₈** exhibits better *PCE* (8.32%) than the **NCSU-10** alone (8.25%). The results indicate that, the V_{OC} values are increasing as ***n*-C₁₆** (0.689 V) > ***n*-C₁₈** (0.680 V) > ***n*-C₁₇** (0.676 V), upon co-sensitization with **NCSU-10** (0.667 V). Also, the reduction in dye loading has been witnessed in all the three co-sensitized devices, resulting in reduced light harvesting ability (J_{SC}). The J_{SC} values of ***n*-C₁₆₋₁₈** are 18.82, 20.31 and 19.25 mA.cm^{-2}, respectively, while **NSCU-10** alone shows 20.41 mA.cm^{-2}.
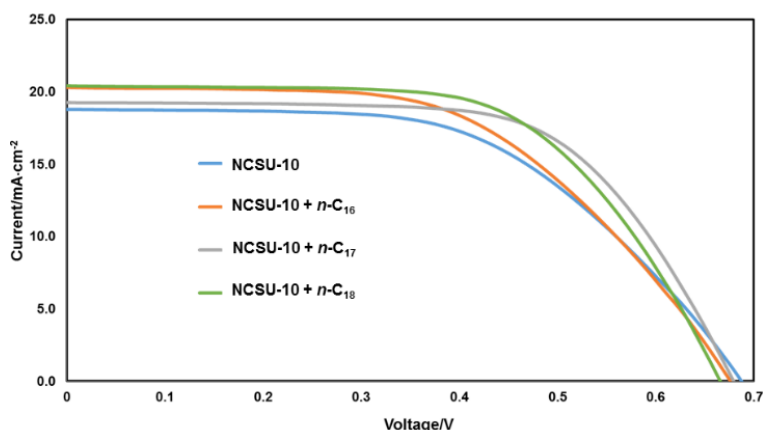
Fig 5.16: *J-V* curves of DSSCs sensitized with **NCSU-10** alone and co-sensitized with *n*-C$_{16\text{-}18}$

Fig 5.17 depicts the *IPCE* traces of devices using co-sensitizers *n*-C$_{16\text{-}18}$ and **NCSU-10** alone at 0.2 mM concentration. Here, *PCE* of DSSCs co-sensitized with *n*-C$_{18}$ was found to be higher than that of **NCSU-10** dye alone as shown in **Fig 5.16**. But the J_{SC} value of *n*-C$_{18}$ was found to be lesser than that of **NCSU-10** dye alone. The lowering of J_{SC} value can be attributed to the competitive adsorption of the co-sensitizer and **NCSU-10** molecules and thereby, resulting in a decrease in the adsorption of **NCSU-10** sensitizer on TiO$_2$ surface. This results in reduced light harvesting proficiency. Further, the presence of co-sensitizers has resulted in the improvement of V_{OC} value, supporting the role of co-sensitizer in diminishing undesirable charge recombination within the fabricated cell.
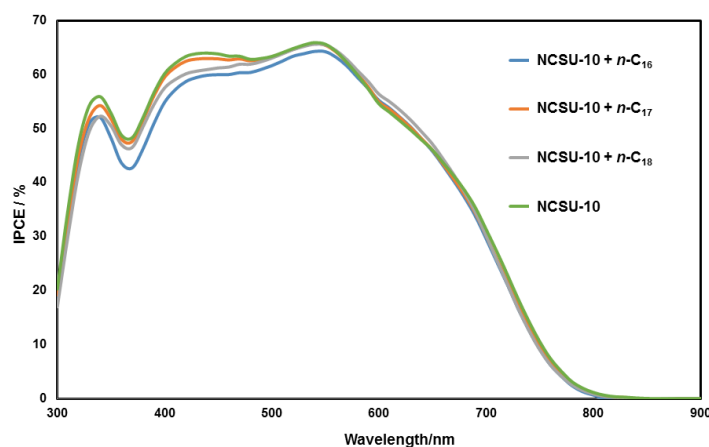
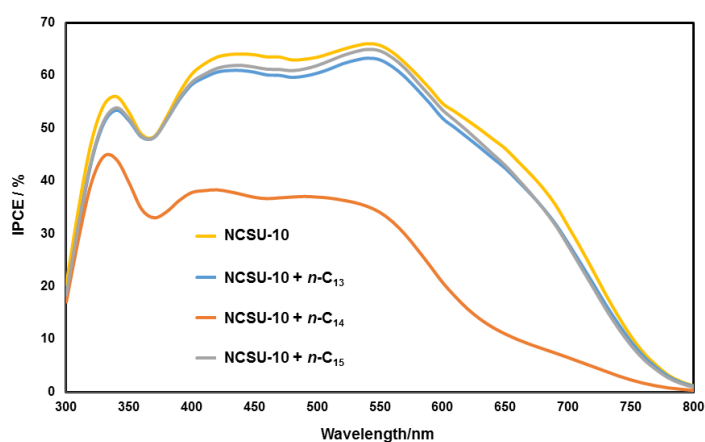**Fig 5.17:** *IPCE* of DSSCs based on **NCSU-10** alone and co-sensitized with *n*-C$_{16\text{-}18}$

Table 5.7: Photovoltaic measurement data of dyes *n*-C$_{16\text{-}18}$

Sensitizer/co-sensitizer		CDCA (mM)	J_{SC} (mA.cm^{-2})	V_{OC} (V)	FF (%)	η (%)
NCSU-10 (mM)	Dye					
0.2	--	20	20.41±0.03	0.667±0.002	60.6±0.4	8.25±0.4
0.2	*n*-C$_{16}$ 0.2 mM	20	18.82±0.05	0.689±0.003	54.1±0.9	7.02±0.5
0.2	*n*-C$_{17}$ 0.2 mM	20	20.31±0.03	0.676±0.001	54.0±0.6	7.41±0.4
0.2	*n*-C$_{18}$ 0.2 mM	20	19.25±0.01	0.680 ± 0.001	63.7±0.1	8.32±0.1
--	*n*-C$_{16}$	10	5.220±0.023	0.623±0.001	67.7±0.2	2.20±0.010
--	*n*-C$_{17}$	10	0.397±0.006	0.457±0.005	57.0±0.5	0.103±0.002
--	*n*-C$_{18}$	10	1.748±0.005	0.548±0.001	65.0±0.2	0.622±0.003

5.1.4.6 Photovoltaic performance of Series-5 sensitizers/Co-sensitizers (*n*-C$_{19\text{-}21}$)

*DSSCs sensitized with **n**-C$_{19\text{-}21}$*

Figs **5.18** and **5.19,** depict the *J-V* and IPCE characteristics curves, respectively of the DSSCs fabricated using *n*-C$_{19\text{-}21}$ and their corresponding data are summarized in **Table 5.8**. Here, photovoltaic performance of the fabricated devices was found to be in the order of *n*-C$_{19}$ > *n*-C$_{21}$ > *n*-C$_{20}$. It is worth to note that, among the sensitizers *n*-C$_{19\text{-}21}$, the highly conjugated *n*-C$_{19}$ carrying strong cyanoacetic acid moiety showcases higher *PCE* (2.38%), superior *J$_{SC}$* (6.36 mA.cm^{-2}) and better *V$_{OC}$* (0.599 V). The higher photovoltaic performance of *n*-C$_{16}$ can be ascribed to its better ICT and ε values (**Table 4.1**). From the **Fig 5.19**, it is clear that the *IPCE* of *n*-C$_{19}$ exhibits a broad band in the region of 375-550 nm with a maximum value of 57% at 420 nm, while *n*-C$_{20}$ and *n*-C$_{21}$ show less intense bands in the region of 400-700 nm with values showing below 10% of absorbance. Better *IPCE* response of *n*-C$_{19}$ is interpreted in terms of higher *J$_{SC}$* value of 6.36 mA.cm^{-2}, compared to those of *n*-C$_{20}$ (1.37 mA.cm^{-2}) and *n*-C$_{21}$ (1.45

mA.cm^{-2}) measured in presence of 10 mM CDCA co-adsorbent, which implies the structural optimization with asymmetric A-π-D-π-A architecture is effective in getting improved efficiency.
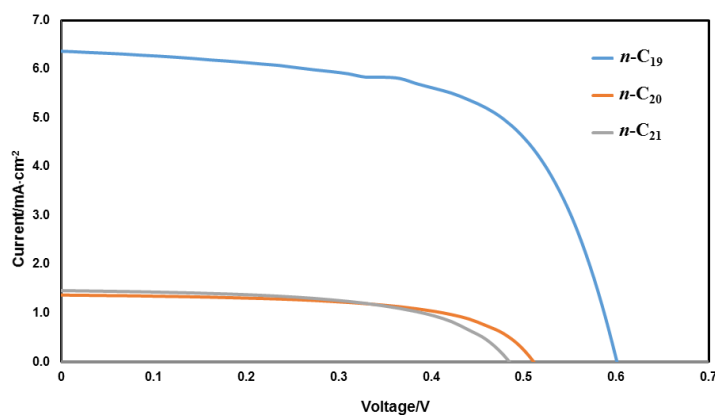

Fig 5.18: *J-V* characteristics of DSSCs sensitized with ***n*-C₁₉₋₂₁**
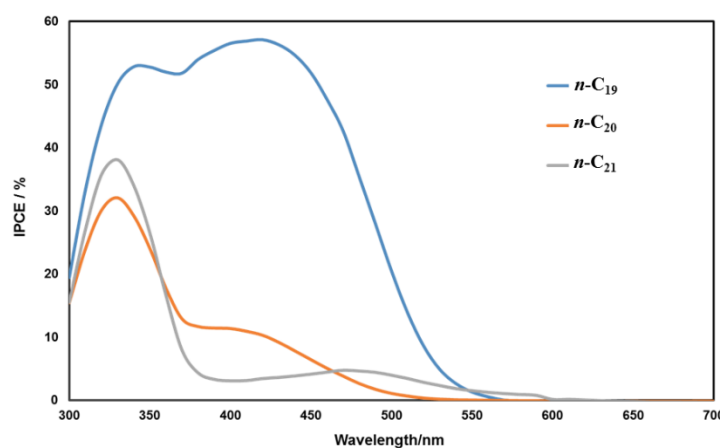
Fig 5.19: *IPCE* spectra of DSSCs based on sensitizers ***n*-C₁₉₋₂₁**

Table 5.8: *J-V* parameters of DSSCs sensitized with ***n*-C₁₉₋₂₁**

Sensitizer	CDCA (mM)	J_{SC} (mA·cm^{-2})	V_{OC} (V)	FF (%)	η (%)
***n*-C₁₉**	10	6.359 ± 0.012	0.599 ± 0.001	62.5 ± 0.2	2.383 ± 0.008
***n*-C₂₀**	10	1.369 ± 0.003	0.510 ± 0.003	59.8 ± 0.4	0.417 ± 0.002
***n*-C₂₁**	10	1.450 ± 0.015	0.484 ± 0.001	56.8 ± 0.1	0.399 ± 0.003

*DSSCs co-sensitized using **n-C$_{19-21}$** along with **NCSU-10***

In order to study the effect of co-sensitization of **n-C$_{19-21}$** in a device fabricated with an efficient Ru(II) complex based **NCSU-10** sensitizer, co-sensitized devices were fabricated using **n-C$_{19-21}$** and 0.2 mM of **NCSU-10** dye. Their *J-V* and *IPCE* plots are presented in **Fig 5.20** and **5.21**, respectively and corresponding performance parameters are tabulated in **Table 5.9.** The DSSCs employing **n-C$_{19-21}$** as co-sensitizers yielded *PCE* of 7.82, 6.42 and 5.09 %, respectively when compared to the 8.25 % of **NCSU-10** sensitized device. Even though the *PCE* values of the co-sensitized devices are found to be inferior to the **NCSU-10** alone, but the *V$_{OC}$* values of the co-sensitized devices are superior. The results indicate that, the *V$_{OC}$* values are increasing as **n-C$_{21}$** (0.689 V) > **n-C$_{20}$** (0.687 V) > **n-C$_{19}$** (0.680 V), upon co-sensitization with **NCSU-10** (0.667 V). The *J$_{SC}$* values of the co-sensitized devices were found to be 19.29, 20.51 and 18.20 mA.cm^{-2} for **n-C$_{19-21}$**, respectively, while **NSCU-10** alone sensitized device showed 20.41 mA.cm^{-2}. Moreover, co-sensitized **n-C$_{20}$**, displayed both improved *J$_{SC}$* and *V$_{OC}$* values than **NCSU-10** alone but *PCE* was found to be inferior due to lower *FF*.
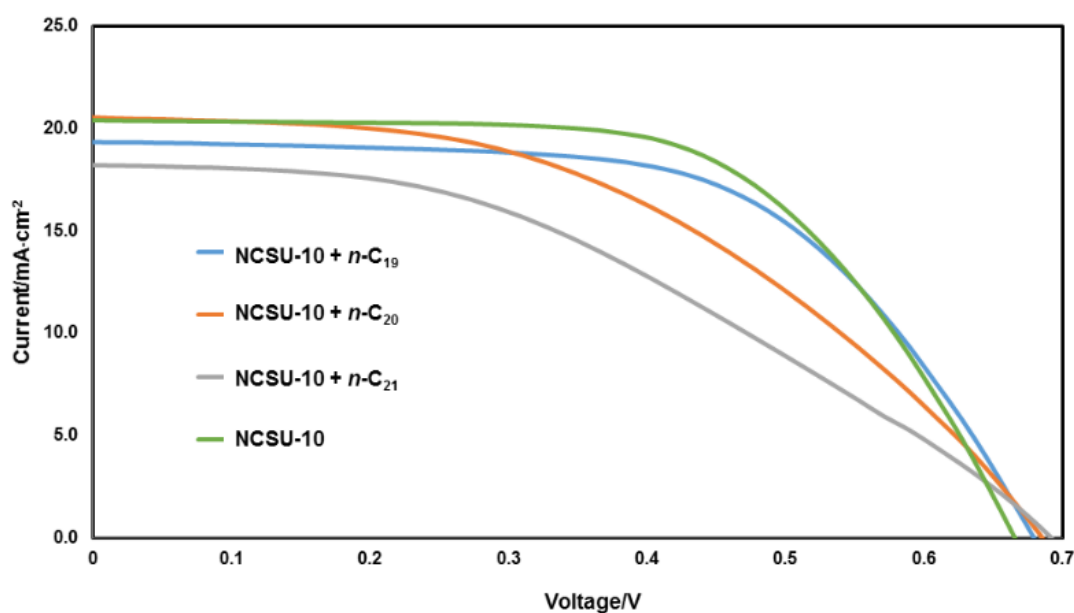
Fig 5.20: *J-V* curves of DSSCs sensitized with **NCSU-10** alone and co-sensitized using **n-C$_{19-21}$**
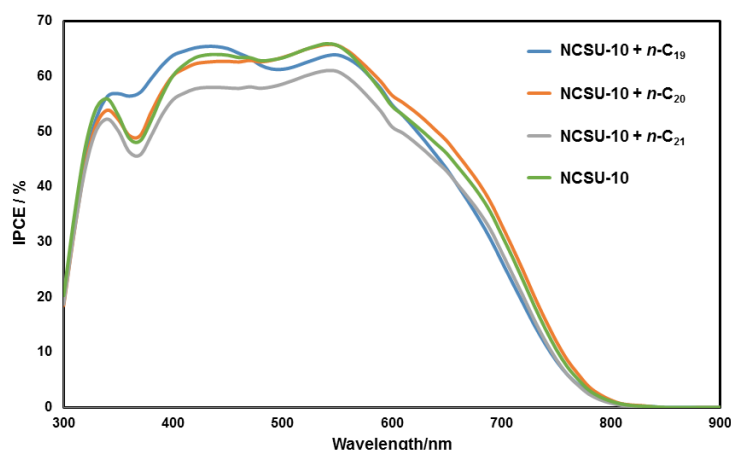
Fig 5.21: *IPCE* curves of DSSCs sensitized with **NCSU-10** alone and co-sensitized using ***n*-C19-21**

Table 5.9: *J-V* parameters of DSSCs sensitized with **NCSU-10** alone and co-sensitized using ***n*-C19-21**

Sensitizer		CDCA (mM)	J_{SC} (mA·cm^{-2})	V_{OC} (V)	FF (%)	η (%)
NCSU-10 (mM)	Dye					
0.2	***n*-C19** 0.2 mM	20	19.29 ± 0.09	0.680 ± 0.002	59.6 ± 0.1	7.82 ± 0.1
0.2	***n*-C20** 0.2 mM	20	20.51 ± 0.01	0.687 ± 0.003	45.6 ± 0.9	6.42 ± 1.1
0.2	***n*-C21** 0.2 mM	20	18.20 ± 0.03	0.689 ± 0.001	40.6 ± 0.5	5.09 ± 0.5
0.2	--	20	20.41 ± 0.03	0.667 ± 0.002	60.6 ± 0.4	8.25 ± 0.4

5.1.4.7 Photovoltaic performance of Series-6 sensitizers (*p*-C1-3)

Experimentally obtained photovoltaic parameters, *viz.* V_{OC}, J_{SC}, *FF* and *PCE* for the cells fabricated with ***p*-C1-3** and **P1** are summarized in **Table 5.10** and the corresponding *J-V* characteristic curves are depicted in **Fig 5.22**. Amongst the tested dyes, the photovoltaic performance was found to be in the decreasing order of **P1** > *p*-**C2** > *p*-**C1** > *p*- **C3**. It is interesting to note that the device fabricated with *p*-**C2** shows maximum *PCE* of 0.040 ± 0.005 % , J_{SC} of 2.41 ± 0.11 mA/cm^2, V_{OC} of 59 ± 4 mV, and *FF* of 29 ± 1 %), when compared to *p*-**C1** and *p*-**C3** and display better V_{OC} and *FF* values than that of **P1**.
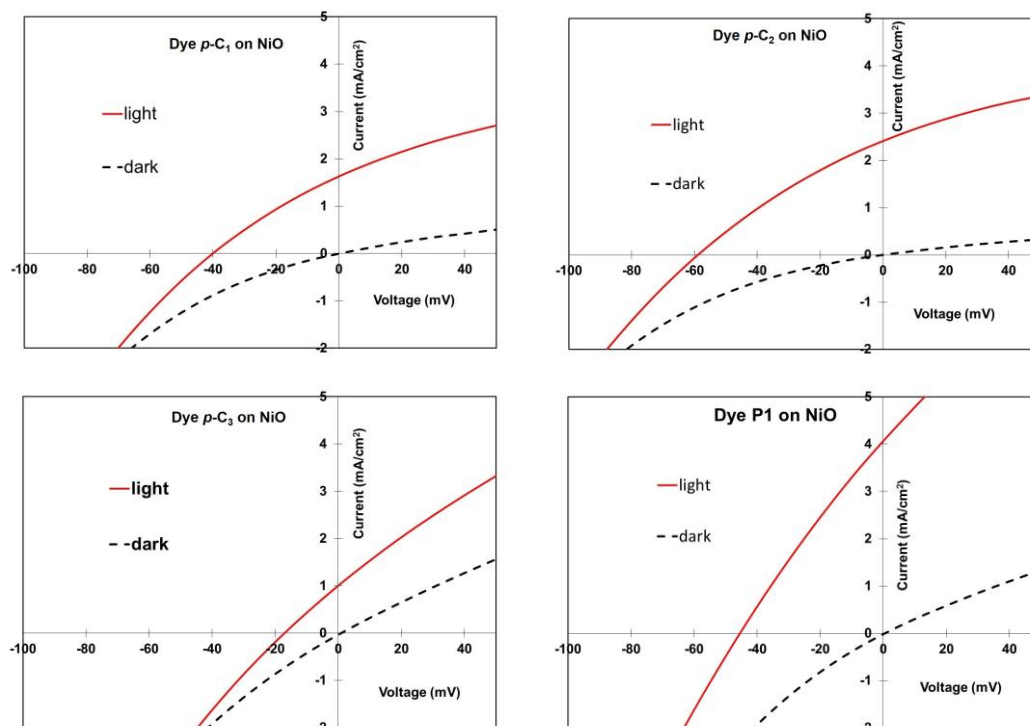
Fig 5.22: *J-V* curves of DSSCs sensitized with **(a)** *p*-**C₁**, **(b)** *p*-**C₂**, **(c)** *p*-**C₃** and **(d) P1**

Table 5.10: Photovoltaic performance data of dyes *p*-**C₁₋₃** and reference **P1** dye.

Dye	J_{SC} (mA.cm^{-2})	V_{OC} (mV)	*FF* (%)	*PCE* (%)
p-**C₁**	1.63 ± 0.15	40 ± 4	27 ± 1	0.016 ± 0.003
p-**C₂**	2.41 ± 0.11	59 ± 4	29 ± 1	0.040 ± 0.005
p-**C₃**	1.00 ± 0.10	17 ± 3	17 ± 1	0.001 ± 0.001
P1	4.06 ± 0.15	45 ± 4	26 ± 1	0.047 ± 0.006

Fig 5.23 shows the *IPCE* spectra of DSSCs fabricated with *p*-**C₁₋₃** and benchmark reference **P1**. Among the tested dyes, *p*-**C₂** displayed the maximum IPCE in the broad range of 440-640 nm. In general, the broadening of the *IPCE* spectra is desired for a larger photocurrent which describes the differences in *PCE* of fabricated dyes. The best dye is *p*-**C₂** owed to its higher short circuit photocurrent density. The improved *IPCE* can be attributed to its higher light harvesting efficiency. Indeed this dye has the most red shifted absorption band in the visible and the highest extinction coefficient among this series (**Table 4.2**). This is the natural consequence of the

strongest electron-withdrawing ability of the thiobarbituric acid moiety among the three electron-withdrawing groups explored herein. The comparison of the IPCE values of *p-C$_2$* with those recorded with **P1** dye, however, indicates that injection efficiency might be lower and can be rationalized by a lower electronic coupling stemming from a little spin density of the HOMO on the carboxylic acid for *p-C$_2$*.
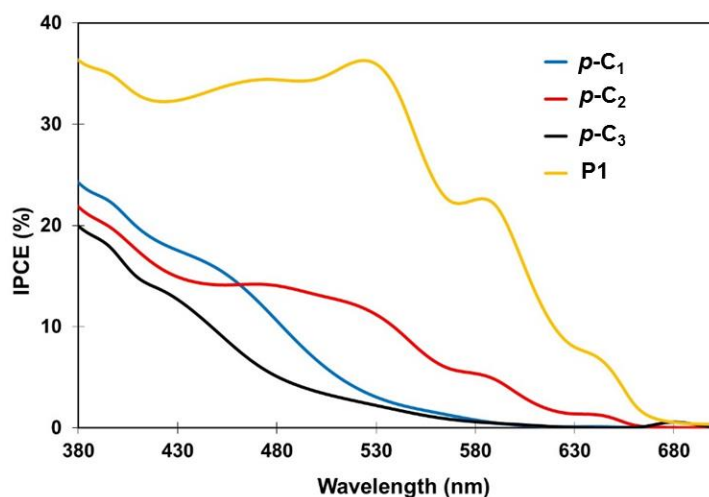
Fig 5.23: *IPCE* spectra of DSSCs fabricated with *p-C$_{1-3}$* and standard **P1** dye

The difference in the photovoltaic performance of *p-C$_{1-3}$* is mainly due to the electron accepting nature of the three acceptor units used in the dyes as it controls the strength of the charge transfer band in the excited state. Based on the electrochemical and photovoltaic results, the acceptors can be ranked as depicted in **Fig 5.24**.
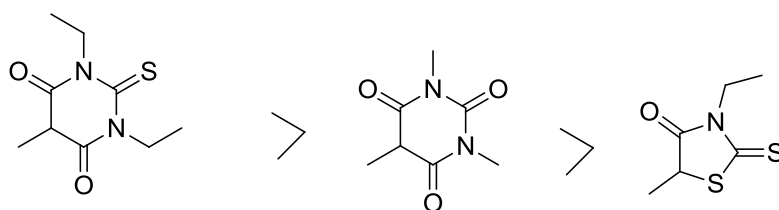
Fig 5.24: Ranking of the acceptors based on photovoltaic performance in *p*-type DSSCs

Interestingly, the solar cell sensitized with dye *p-C$_2$* also displays the highest *V$_{OC}$*, which is even significantly higher than that delivered by **P1**. Looking at the current/voltage characteristics, it has been noticed that, the dark current is lower with *p-C$_2$* than others; meaning that, the interfacial charge recombination with the electrolyte is diminished. The decrease in interfacial charge recombination points to a better

shielding of the NiO surface by this dye, which is most probably due to a denser packing on the surface.

5.2 ELECTROCHEMICAL IMPEDANCE SPECTROSCOPY STUDIES

Electrochemical impedance spectroscopy (EIS) is a powerful technique for characterizing a wide electrochemical systems and for determining the contribution of electrode or electrolytic processes in these systems. The obtained Nyquist plot from the EIS study depicts the imaginary impedance, which is indicative of the capacitive and inductive character of the cell, versus the real impedance of the cell. In fact, these Nyquist plots possess the advantage that activation-controlled processes with distinct time-constants show up as unique impedance curves and the shape of these curves provides insight into possible mechanism or governing phenomena. Whereas, the observed Bode plot from EIS study deals with the frequency response of a cell simultaneously in terms of phase and magnitude. More precisely, the log-magnitude *vs* phase frequency response curves are known as Bode plots. Such plots are useful for determining stability and system identification from the frequency response.

In the present work, the carbazole based sensitizers/co-sensitizers (***n*-C₆-₂₁**) were subjected to EIS studies in order to evaluate the charge dynamics of an operating DSSC. Further, the study helps in evaluating the interfacial charge recombination dynamics and redox processes taking place at photoactive anode/electrolyte interface. A detailed account the study has been discussed below.

5.2.1 Material and methods

The electrochemical impedance spectra, *i.e.* Nyquist and Bode plots for the fabricated devices were obtained from Biologic SP-150 potentiostat using solar simulator under the illumination of standard 1.5 G light source.

5.2.2 Experimental

The EIS studies were performed to analyze the interfacial charge recombination and carrier transport processes in fabricated DSSCs based on ***n*-C₆-₂₁** sensitizers/co-sensitizers (Fabregat-Santiago et al. 2005; Bisquert, 2003), using an impedance

analyzer potentiostat under solar illumination using a solar stimulator. The applied voltage was set at the V_{OC} of the DSSCs with AC amplitude fixed at 10 mV. The plots were fitted *via* Z-Fit software (Bio-Logic).

5.2.3 Results and discussion

Results of EIS studies of fabricated DSSCs with ***n*-C₆₋₂₁** and **NCSU-10/N3** as sensitizers/co-sensitizers were discussed in the following section.

5.2.3.1 EIS of Series-1B sensitizers/co-sensitizers (***n*-C₆₋₈**)

*DSSCs sensitized with **n*-C₆₋₈**

Figs 5.25 and **5.26** depict the Nyquist and Bode plots of fabricated DSSCs using the synthesized sensitizers, ***n*-C₆₋₈**, respectively. In Nyquist plot, all the devices have displayed two distinct semicircles, the first semicircle corresponds to the recombination resistance at the Pt/electrolyte interface, while the intermediate semicircle is related to TiO$_2$/dye/electrolyte interface (Wu et al. 2014). Generally, bigger the radius of the second semicircle, higher will be the charge recombination resistance (R_{ct}) from TiO$_2$ to the electrolyte that corresponds to Nernst impedance. Also, it is well-known that, radius of the same semicircle indicates resistance to charge diffusion (R_d) under Gerischer impedance (Wang et al. 2005). In the Nyquist plots, the semicircles obtained for ***n*-C₆₋₈** sensitized cells are due to the Gerischer impedance. The radius of semi circle intermediate-frequency regime were found to be in the order of ***n*-C₇** > ***n*-C₆** > ***n*-C₈**. The results indicates that, the electron recombination resistance decreases in the order of ***n*-C₈** > ***n*-C₆** > ***n*-C₇**. The aforementioned trend is in agreement with obtained V_{OC} values (**Table 5.2**).
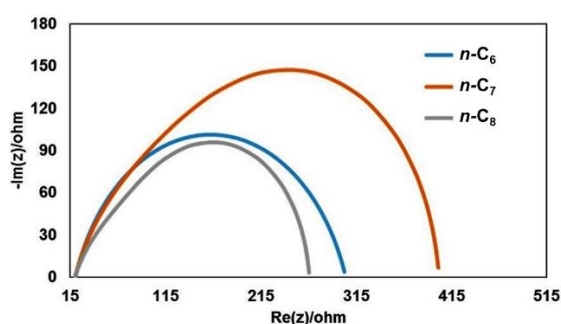
Fig 5.25: Nyquist plots of DSSC based on ***n*-C₆₋₈**
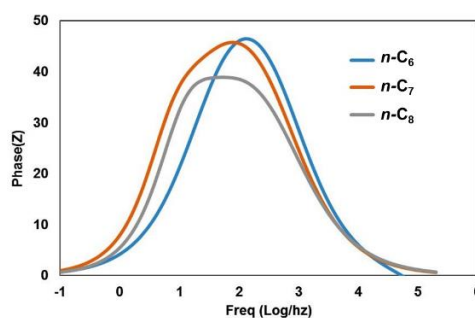
Fig 5.26: Bode plots of DSSC based on ***n*-C₆₋₈**

Normally, the Bode frequency plots are used to estimate the effective lifetime (τ_{eff}) of electrons injected into the CB of TiO_2. As reported in the literature, the τ_{eff} values were calculated using **Eq. 5.1**.

$$\tau_{eff} = \frac{1}{2\pi f} \tag{5.1}$$

Where f is the frequency of the Bode plot. The electron lifetime values resulting from Bode curve fitting for **n-C$_{6-8}$** sensitized devices were calculated to be **n-C$_8$** (3.33 ms) > **n-C$_7$** (1.96 ms) > **n-C$_6$** (1.84 ms), respectively. The longer electron lifetime was observed for **n-C$_6$** when compared to **n-C$_7$** and **n-C$_8$**. In general, longer electron lifetime in the CB of TiO_2 indicates improved suppression of back reaction between the electrons injected into TiO_2 and the electrolyte, leading to improvement of V_{OC} values. In the present study, the V_{OC} values (**Table 5.2**) of the DSSCs increase in accordance with their electron lifetimes (Luo et al. 2016; Mao et al. 2015; He et al. 2011).

*DSSCs co-sensitized using **n-C$_{6-8}$** along with **NCSU-10***

Nyquist and Bode plots of fabricated devices using **n-C$_{6-8}$** as co-sensitizers as well as **NCSU-10** as a sensitizer are depicted in **Fig 5.27** and **5.28**, respectively. In Nyquist plot, the radius of the second semicircle of the fabricated DSSCs was found to be in the order of **n-C$_6$** > **n-C$_8$** > **NCSU-10** > **n-C$_7$**. The obtained results indicate that the co-sensitizers play an important role in suppression of dark current/back reaction in co-sensitized DSSCs. The aforementioned trend is in consistent with the observed V_{OC} values for the fabricated cells as tabulated in **Table 5.2**.
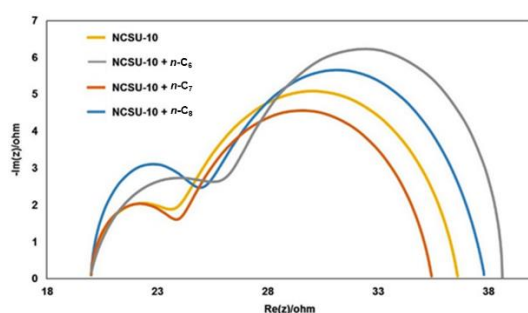
Fig 5.27: Nyquist plots for DSSC sensitized with **NCSU-10** alone and co-sensitized with **n-C$_{6-8}$**	**Fig 5.28:** Bode plots for DSSCs sensitized with **NCSU-10** alone and co-sensitized with **n-C$_{6-8}$**
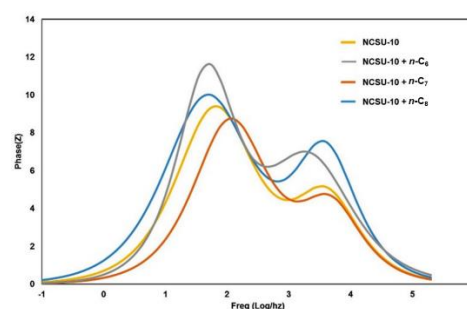
The electron lifetimes (τ_{eff}) in CB edge of TiO_2 of the fabricated devices were found to be in the decreasing order of ***n*-C$_6$** (3.19 ms) > ***n*-C$_8$** (3.08 ms) > **NCSU-10** (2.60 ms) > ***n*-C$_7$** (2.32 ms). The highest V_{OC} was observed in the case of co-sensitizer ***n*-C$_6$** which may be attributed to its higher lifetime in the CB edge of TiO_2. Further, the calculated lifetimes for all the dyes are in good agreement with the observed V_{OC} values of the devices (**Table 5.2**). Furthermore, it was well-documented that, the addition of CDCA as a co-adsorbent in the cell effectively reduces the electron recombination and hence extends the electron lifetime, which ultimately leads to enhanced V_{OC} values as well as *PCE* of fabricated devices. From the results, it is quite clear that, the co-sensitizer ***n*-C$_6$** carrying 4-aminobenzoic acid as an acceptor/anchoring moiety is reasonably efficient in suppressing the unwanted charge recombination process on the TiO_2 surface.

5.2.3.2 EIS of Series-2 sensitizers/co-sensitizers (*n*-C$_{9-12}$)

*DSSCs sensitized with **n*-C$_{9-12}$*

Fig 5.29 shows the Nyquist traces obtained from EIS measurements for ***n*-C$_{9-12}$** as sensitizers. In Nyquist plot, radius of intermediate semicircle increases in the order of ***n*-C$_9$** < ***n*-C$_{10}$** < ***n*-C$_{11}$** < ***n*-C$_{12}$**, indicating the electron recombination resistance decreases in the order of ***n*-C$_9$** > ***n*-C$_{10}$** > ***n*-C$_{11}$** > ***n*-C$_{12}$**. The V_{oc} values of the DSSCs were found to be decreasing in the order of ***n*-C$_9$** (0.588 V) > ***n*-C$_{11}$** (0.568 V) > ***n*-C$_{12}$** (0.547 V) > ***n*-C$_{10}$** (0.538 V). According to Nernst and Gerischer impedance principles, the V_{OC} of ***n*-C$_9$** is greater than ***n*-C$_{10}$** while that of ***n*-C$_{11}$** is higher than ***n*-C$_{12}$** and these values are well in accordance with experimentally obtained values. Further, the large difference in the impedance behavior of ***n*-C$_{11-12}$** and that of ***n*-C$_{9-10}$** is due to the nature of impedance involved. Here, the impedance of ***n*-C$_{11-12}$** may be attributed to the Nernst impedance, whereas impedance of ***n*-C$_{9-10}$** corresponds to Gerischer impedance.
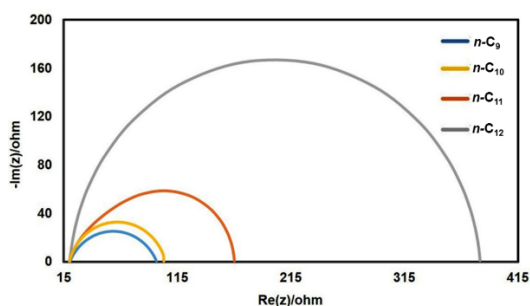
Fig 5.29: Nyquist plots of DSSCs based on *n*-C₉₋₁₂
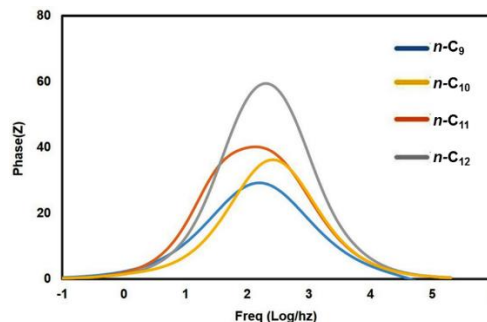
Fig 5.30: Bode plots of DSSC based on *n*-C₉₋₁₂

Fig 5.30 depicts the Bode curve plots obtained for fabricated DSSCs using *n*-C₉₋₁₂ as sensitizers**.** The electron lifetimes (τ_{eff}) of the fabricated devices were found to be in the decreasing order of *n*-C₁₁ (1.08 ms) > *n*-C₉ (0.97 ms) > *n*-C₁₂ (0.85 ms) > *n*-C₁₀ (0.61 ms). In the case of *n*-C₁₀, the lowest V_{OC} was observed, which may be attributed to the least electron lifetime of it (Wu et al. 2014; Wang et al. 2015). It is interesting to note that, dyes bearing carboxylic acid (*n*-C₉₋₁₀) exhibit comparatively better photovoltaic performance than dyes carrying barbituric acid and thiobarbituric acid (*n*-C₁₁₋₁₂) as anchoring groups, even though *n*-C₉₋₁₀ show low lifetime.

DSSCs co-sensitized using n-C₉₋₁₂ along with N3

Nyquist and Bode plots of fabricated devices using *n*-C₉₋₁₂ as co-sensitizers as well as **N3** as a sensitizer are depicted in **Figs 5.31** and **5.32**, respectively. In Nyquist plot, all the devices have displayed two distinct semicircles. The second semicircle indicates the electron transport through mesoporous TiO₂ and back electron transfer from TiO₂ to electrolyte, which is directly related to the V_{OC} of the fabricated cells. In Nyquist plot, the radii of the intermediate semicircle of the fabricated DSSCs were found to be in the order of **N3** > *n*-C₉ > *n*-C₁₀ > *n*-C₁₁ > *n*-C₁₂. The results indicate that, the co-sensitizer *n*-C₉₋₁₂ are inefficient in suppression of dark current/back reaction in co-sensitized DSSCs. The aforementioned is consistent with the observed lower V_{OC} values for the fabricated cells as tabulated in **Table 5.4.**

Fig 5.31: Nyquist plots for DSSC based on **N3** alone and co-sensitized with *n*-C₉₋₁₂
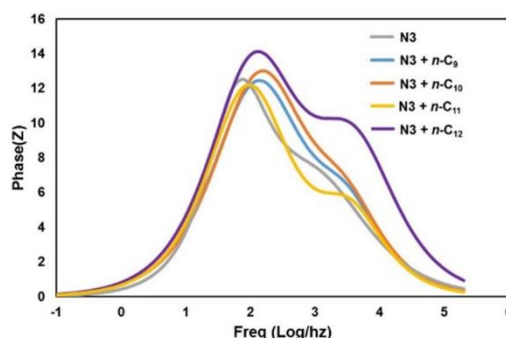
Fig 5.32: Bode plots for DSSCs based on **N3** alone and co-sensitized with *n*-C₉₋₁₂

Further, using the Bode plot, the electron lifetimes (τ_{eff}) in CB edge of TiO_2 in fabricated devices were calculated. The lifetime in CB edge of TiO_2 of the fabricated devices was found to be in the decreasing order of **N3** (3.19 ms) > ***n*-C₁₁** (3.08 ms) > ***n*-C₁₂** (3.04 ms) > ***n*-C₁₀** (2.32 ms) > ***n*-C₉** (2.30 ms). In the present study, the V_{OC} values (**Table 5.4**) of the DSSCs increase in accordance with their electron lifetimes. Further, these results showcase the co-sensitizers were inefficient in suppressing the unwanted back reaction between with TiO_2.and electrolyte in the fabricated devices. Further adequate matching between the Ru-II complex and co-sensitizers, better photovoltaic performance can be achieved.

5.2.3.3 EIS of Series -3 sensitizers/co-sensitizers (*n*-C₁₃₋₁₅)

*DSSCs sensitized with **n**-C₁₃₋₁₅*

Fig 5.33 and **5.34** depict the Nyquist and Bode plots of fabricated DSSCs using the sensitizers ***n*-C₁₃₋₁₅**, respectively. In the Nyquist plot, the radius of semi-circle intermediate-frequency regime obtained for ***n*-C₁₃₋₁₅** sensitized cells were found to be in the order of ***n*-C₁₅** > ***n*-C₁₄** > ***n*-C₁₃** dye based devices. The trend indicates that the charge transfer is in the order of ***n*-C₁₃** > ***n*-C₁₄** > ***n*-C₁₅**. The observed results coincide with achieved *PCE* values of ***n*-C₁₃₋₁₅** based DSSCs (Beni et al. 2015).
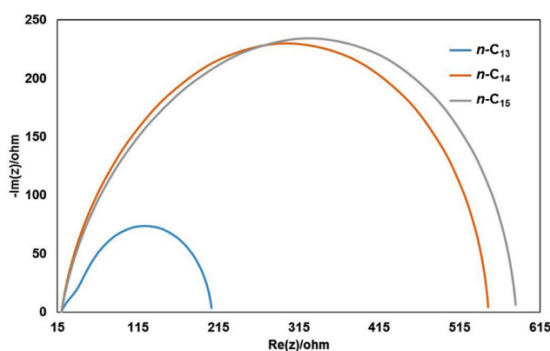
Fig 5.33: Nyquist plots of DSSCs based on *n-*C$_{13-15}$
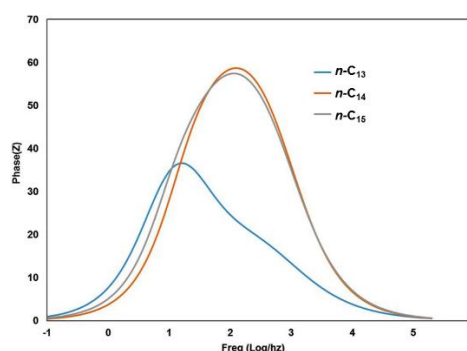
Fig 5.34: Bode plots of DSSCs based on *n-*C$_{13-15}$

The electron lifetime values resulting from Bode curve fitting for *n-*C$_{13-15}$ sensitized devices were calculated to be *n-*C$_{13}$ (9.82 ms) > *n-*C$_{14}$ (1.42 ms) > *n-*C$_{15}$ (1.27 ms) respectively. The longer electron lifetime was observed for *n-*C$_{13}$ when compared to *n-*C$_{14}$ and *n-*C$_{15}$. Normally, the longer lifetime for a sensitizer in the fabricated device is beneficial for charge accumulation in the CB of TiO$_2$ under open circuit voltage. In the present study, the V_{OC} values (**Table 5.5**) of the DSSCs have increased in accordance with their electron lifetimes (Luo et al. 2016; Mao et al. 2015; He et al. 2011). Further, these results showcase the profound influence of acceptor groups on the electron recombination processes between the electrolyte species and electrons injected into the TiO$_2$ semiconductor film.

*DSSCs co-sensitized using **n-**C$_{13-15}$ along with NCSU-10 alone*

Nyquist and Bode plots of fabricated devices using *n-*C$_{13-15}$ as co-sensitizers as well as **NCSU-10** as a sensitizer are depicted in **Figs 5.35** and **5.36** respectively. Results of EIS measurements of *n-*C$_{13-15}$ dyes showed separate semi-circles in case of Nyquist plots and clear frequency peaks in Bode plots. In Nyquist plot, the radius of the intermediate semicircle of the fabricated DSSCs were found to be in the order of *n-*C$_{13}$ > **NCSU-10** > *n-*C$_{15}$ > *n-*C$_{14}$. The obtained results indicate that the co-sensitizer *n-*C$_{13}$ plays an important role in suppression of dark current/back reaction in co-sensitized DSSCs. The aforementioned observation is in consistent with the observed V_{OC} values for the fabricated cells tabulated in **Table 5.6**.
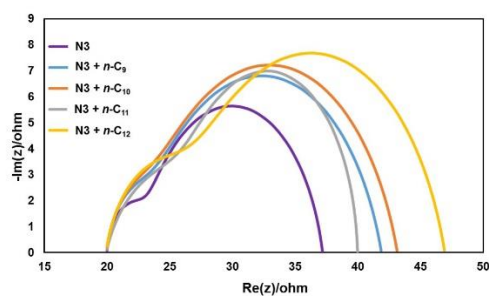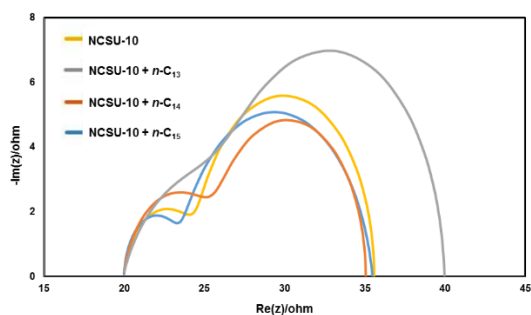
**Fig 5.35:** Nyquist plots of DSSCs based on **NCSU-10** alone and co-sensitized with *n*-C$_{13\text{-}15}$
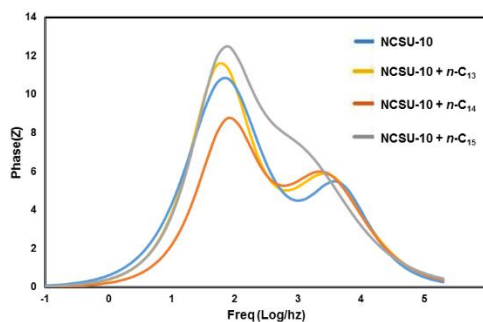
Fig 5.36: Bode plots for DSSCs sensitized with **NCSU-10** alone and co-sensitized with *n*-C$_{13\text{-}15}$

Further, using the Bode plot, the electron lifetimes (τ_{eff}) in CB edge of TiO$_2$ in fabricated devices were calculated. In general, longer electron lifetime in the CB of TiO$_2$ (eTiO$_2$) indicates improved suppression of back reaction between the electrons injected into TiO$_2$ and the electrolyte and thus leads to improvement of V_{OC} values. The lifetimes in CB edge of TiO$_2$ of the fabricated devices were found to be in the decreasing order of *n*-C$_{13}$ (3.19 ms) > **NCSU-10** (3.08 ms) > *n*-C$_{15}$ (3.04 ms) > *n*-C$_{14}$ (2.32 ms). The highest V_{OC} was observed in the case of *n*-C$_{13}$ which may be attributed to its higher lifetime in the CB edge of TiO$_2$. Further, the calculated electron lifetimes for all the dyes are in good agreement with the observed V_{OC} values (**Table 5.6**). From the results, it is quite clear that the co-sensitizers *n*-C$_{13}$ and *n*-C$_{15}$ are reasonably efficient in suppressing the unwanted charge recombination process on the TiO$_2$ surface.

5.2.3.4 EIS of Series-4 sensitizers/co-sensitizers (*n*-C$_{16\text{-}18}$)

DSSCs sensitized with ***n*-C$_{16\text{-}18}$**

In the Nyquist plot (**Fig 5.37**), the radius of second frequency semi-circle obtained for *n*-C$_{16\text{-}18}$ sensitized cells were found to be in the order of *n*-C$_{17}$ > *n*-C$_{18}$ > *n*-C$_{16}$ based devices. The trend indicates that the charge transfer is in the order of *n*-C$_{16}$ > *n*-C$_{18}$ > *n*-C$_{17}$. The observed results coincide with achieved *PCE* values of *n*-C$_{16\text{-}18}$ based DSSCs.

The Bode frequency plots (**Fig 5.38**) were used to estimate the effective lifetime (τ_{eff}) of electrons injected into the CB of TiO$_2$. The electron lifetime values resulting from Bode curve fitting for *n*-C$_{16\text{-}18}$ sensitized devices were calculated to be *n*-C$_{16}$ (4.00

ms) $> n\text{-}C_{18}$ (2.03 ms) $> n\text{-}C_{17}$ (0.71 ms), respectively. The longer electron lifetime was observed for $n\text{-}C_{16}$ when compared to $n\text{-}C_{17}$ and $n\text{-}C_{18}$. Normally, the longer lifetime for a sensitizer in the fabricated device is beneficial for charge accumulation in the CB of TiO$_2$ under open circuit voltage. In the present study, the V_{OC} values (**Table 5.7**) of the DSSCs increase in accordance with their electron lifetimes. Further, these results showcase the profound influence of acceptor groups on the electron recombination processes between the electrolyte species and electrons injected onto the TiO$_2$ semiconductor film.

Fig 5.37: Nyquist plots of DSSC based on $n\text{-}C_{16\text{-}18}$

Fig 5.38: Bode plots of DSSC based on $n\text{-}C_{16\text{-}18}$

DSSCs co-sensitized using $n\text{-}C_{16\text{-}18}$ along with NCSU-10 alone

Nyquist and Bode plots of fabricated devices using $n\text{-}C_{16\text{-}18}$ as co-sensitizers as well as **NCSU-10** as a sensitizer are depicted in **Fig 5.39** and **5.40** respectively. In Nyquist plot, the radii of the second semicircle of the fabricated DSSCs were found to be in the order of $n\text{-}C_{16} > n\text{-}C_{18} > n\text{-}C_{17} > $ **NCSU-10**. The obtained results indicate that, the co-sensitizers was efficient in suppressing dark current/back reaction in co-sensitized DSSCs which led to improved V_{OC}. The aforementioned trend is consistent of the observed V_{OC} values for the fabricated cells tabulated in **Table 5.7**. Further, τ_{eff} values of the fabricated devices were estimated from the EIS Bode plot and it was found to be in the decreasing order of $n\text{-}C_{16}$ (3.82 ms) $> n\text{-}C_{17}$ (2.52 ms) $> $ **NCSU-10** (2.45 ms) $> n\text{-}C_{18}$ (2.42 ms). The highest V_{OC} was observed in the case of co-sensitizer $n\text{-}C_{16}$ which may be attributed to its higher lifetime in the CB edge of TiO$_2$. Further, the calculated lifetimes for all the dyes are in good agreement with the observed V_{OC} values of the devices (**Table 5.7**).

Fig 5.39: Nyquist plots of DSSC based on **NCSU-10** alone and co-sensitized with *n*-**C₁₆₋₁₈**
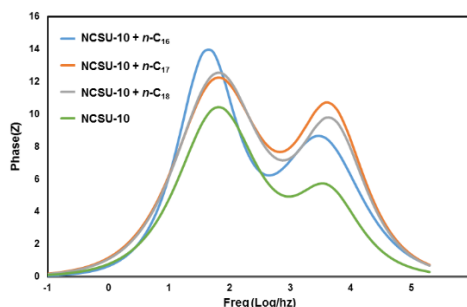
Fig 5.40: EIS Bode plots for DSSC sensitized with **NCSU-10** alone and devices co-sensitized with *n*-**C₁₆₋₁₈**

5.2.3.5 EIS of Series -5 sensitizers/co-sensitizers (*n*-**C₁₉₋₂₁**)

*DSSCs sensitized with **n-C₁₉₋₂₁***

Figs 5.41 and **5.42** depict the Nyquist and bode plots of fabricated DSSCs using the synthesized dyes *n*-**C₁₉₋₂₁**, respectively. In the Nyquist plot, the radius of intermediate frequency semi-circle obtained for *n*-**C₁₉₋₂₁** sensitized cells was found to be in the order of *n*-**C₂₁**> *n*-**C₂₀**> *n*-**C₁₉** dye based devices. The trend indicates that the charge transfer is in the order of *n*-**C₁₉**> *n*-**C₂₀**> *n*-**C₂₁**. Further, the effective lifetime (τ_{eff}) of electrons injected into the CB of TiO_2 were estimated from Bode plot. The electron lifetime values resulting from curve fitting of *n*-**C₁₉₋₂₁** sensitized devices were calculated to be *n*-**C₁₉** (3.35 ms) > *n*-**C₂₁** (1.41 ms) > *n*-**C₂₀** (1.39 ms), respectively. The longer electron lifetime was observed for *n*-**C₁₉** when compared to *n*-**C₂₀** and *n*-**C₂₁**, indicating its lower rate of charge recombination in the cell. Here, the V_{OC} values (**Table 5.8**) of the DSSCs increase in accordance with their electron lifetime. Further, these results showcase the profound influence of acceptor groups on the electron recombination processes between the electrolyte species and electrons injected into the TiO_2 semiconductor film.
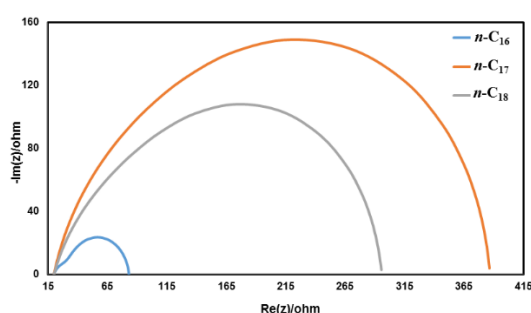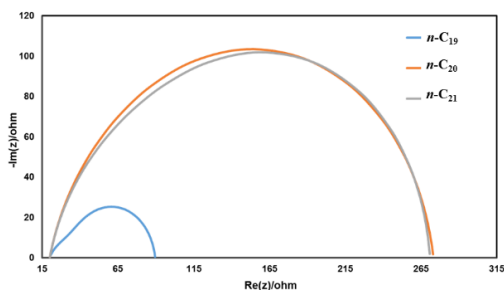
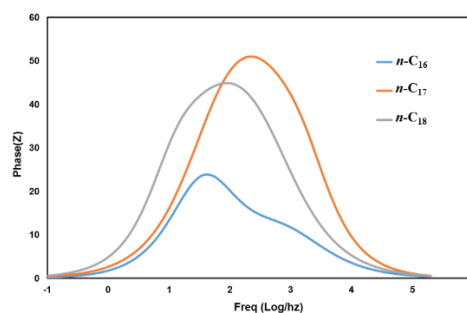**Fig 5.41:** Nyquist plots of DSSCs based on *n*-**C₁₉₋₂₁**
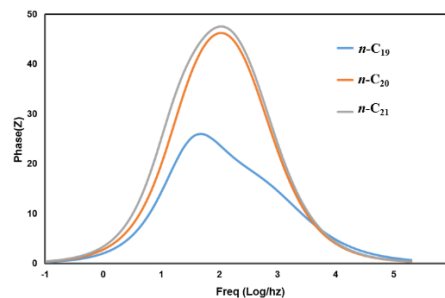
Fig 5.42: Bode plot of DSSCs based on *n*-**C₁₉₋₂₁**

*DSSCs co-sensitized using **n-C₁₉₋₂₁** along with NCSU-10 alone*

      Figs 5.43 and **5.44** depict the Nyquist plot and Bode plots of DSSCs fabricated using co-sensitizers **n-C₁₉₋₂₁** and **NCSU-10** alone. As discussed for Nyquist plots of sensitized devices, here two distinct semi-circles were observed and it was interesting to note that, the radius of the second semicircle of the fabricated DSSCs were found to be in the order of **n-C₁₉** > **n-C₂₁** > **n-C₂₀** > **NCSU-10**. The acquired results indicate that, the co-sensitizer **n-C₁₉** plays a significant role in suppression of dark current/back reaction in the cell. The aforementioned trend is in accordance with the observed V_{OC} values for the fabricated cells tabulated in **Table 5.9**. The estimated lifetimes in CB edge of TiO₂ of the fabricated devices were estimated from the Bode plots and it was found to be in the decreasing order of **n-C₂₁** (4.38 ms) > **n-C₂₀** (3.35 ms) > **n-C₁₉** (3.03 ms) > **NCSU-10** (2.64 ms). The highest V_{OC} was observed in the case of **E₃** which may be attributed to its higher lifetime in the CB edge of TiO₂. Further, the calculated lifetimes for all the dyes are in agreement with the observed V_{OC} values (**Table 5.9**).

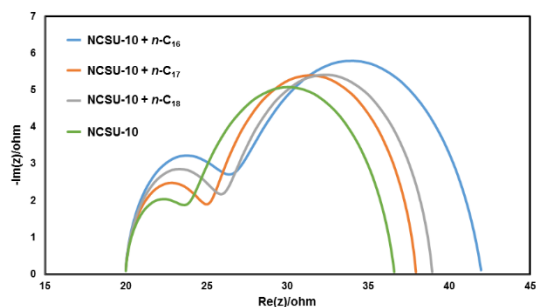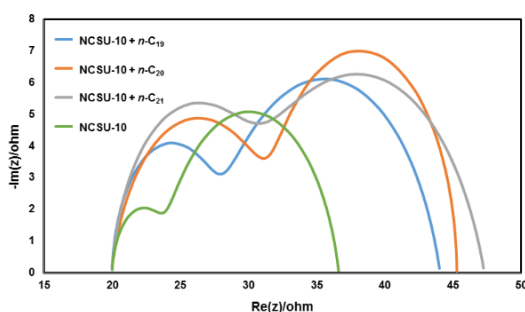**Fig 5.43**: Nyquist plots for DSSCs sensitized with **NCSU-10** alone and co-sensitized using *n*-**C₁₉₋₂₁**
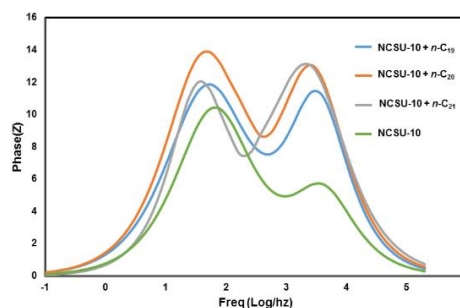
Fig 5.44: Bode plots for DSSCs sensitized with **NCSU-10** alone and co-sensitized using *n*-**C₁₉₋₂₁**

5.3 CONCLUSIONS

The newly synthesized *n*-type organic dyes (***n*-C1-21**) were subjected to DSSC fabrication studies as sensitizers. The study reveals that, the device sensitized with ***n*-C9**, ***n*-C13**, ***n*-C16** and ***n*-C18** dyes showcase good photovoltaic performance due to presence of strong cyanoacetic acid as acceptor/anchoring unit. Further, sixteen new *n*-type organic dyes (***n*-C6-21**) based on carbazole were successfully employed as co-sensitizers in DSSCs sensitized with standard Ru (II) sensitizers (**NCSU-10/N3**). The co-sensitization studies indicate that the device co-sensitized using D-A configured ***n*-C6** dye with 0.2 mM of **NCSU-10** sensitizer showcases an improved *PCE* of 9.55%, V_{OC} of 0.672 V and *FF* of 62.2%, whereas the DSSC fabricated with dye **NCSU-10** alone displayed *PCE* of 8.25%, V_{OC} of 0.667 V and *FF* of 60.6 %. Finally, three newly synthesized *p*-type organic dyes ***p*-C1-3** were employed in the fabrication of *p*-type DSSCs as sensitizers and the results obtained were compared with that of standard **P1** dye. From the results it is clear that, ***p*-C2** sensitized DSSC showed *PCE* = 0.040%, J_{SC} = 2.41 mA.cm^{-2}, V_{OC} = 59 mV and *FF* = 29%, which are comparable with that of bench mark reference **P1** (*PCE* = 0.047%, J_{SC} = 4.06 mA.cm^{-2}, V_{OC} = 45 mV and *FF* = 26%).

SUMMARY AND CONCLUSIONS

Abstract:

This chapter contains summary and important conclusions drawn from present research work. It also includes a brief account on the scope for further work.

6.1 SUMMARY

Solar energy has the potential to fulfill ever increasing energy demand in the world. From past three decades, the quest for clean and cost-effective energy generation has led to enhanced attention towards research on organic photovoltaics. In the field of organic photovoltaics, the DSSCs have emerged as attractive and promising low-cost energy generation solar device after the inventive research work reported by Gratzel group. Among the various components, the dye which acts as a photosensitizer plays a crucial role in exerting light harvesting and initiating the electrochemical processes for electricity generation. Several dyes have been investigated as sensitizers as well as co-sensitizers in order to uphold the photovoltaic performance of the DSSCs.

In this context, the present research work has mainly focused on molecular design and synthesis of new push-pull configured both *n*-and *p*-type chromophores with favorable photophysical properties and thermodynamic feasibility. It has been also aimed at studying their photovoltaic behavior and their structure-performance relationship.

Further, based on the detailed literature survey, six new series of *n*-type organic dyes containing *N,N* dimethyl-4-vinyl aniline as well as carbazole core as a donor with various electron accepting/anchoring units, were designed. The new design includes D-A (**Series-1A** and **1B**), D-π-A (**Series-2**), D-π-A- π-A (**Series-3**), D-D-π-A (**Series-4**), and A-π-D-π-A (**Series-5**) architectures. Also, a new series of D-A configured *p*-type carbazole based sensitizers (**Series-6**), carrying different accepting/anchoring groups, has been designed. The newly designed organic dyes were synthesized following standard synthetic protocols starting from simple organic molecules. The chemical structures of newly synthesized dyes and their intermediates were confirmed by various spectral techniques including elemental analysis. Further, their photophysical, electrochemical and theoretical studies were carried out in order to evaluate their suitability for their applications in DSSCs as sensitizers/co-sensitizers.

Furthermore, DSSSs were fabricated using *n*-type organic dyes (***n*-C₁₋₂₁**) as sensitizers and their photovoltaic parameters were evaluated. Also, the carbazole based dyes (***n*-C₆₋₂₁**) were employed as co-sensitizers in order to study their effect on the performance of the device sensitized with standard Ru II complex (**NCSU-10/N3** dye). In addition, *p*-type DSSCs were fabricated using ***p*-C₁₋₃** as sensitizers and obtained results were compared with that of standard benchmark dye **P₁**. Finally, the structure-photovoltaic performance relationship of ***n*-C₁₋₂₁** and ***p*-C₁₋₃** was established on the basis of their photophysical, electrochemical, theoretical and EIS studies.

6.2 CONCLUSIONS

On the basis of experimental results, following significant conclusions have been drawn from present research work.

1. Based on detailed literature survey, six new series of *n*-type organic dyes with various design strategies such as D-A (**Series-1A** and **-1B**), D-π-A (**Series-2**), D-π-A-π-A (**Series-3**), D-D-π-A (**Series-4**), and A-π-D-π-A (**Series-5**) architecture as well as a new series of *p*-type sensitizers (**Series-6**) with D-A architecture, have been successfully designed.

2. Twenty one metal-free organic dyes (***n*-C₁₋₂₁**) as *n*-type sensitizers/co-sensitizers and three new organic dyes (***p*-C₁₋₃**) as *p*-type sensitizers have been successfully synthesized, their synthetic protocols and chemical structures have been established by spectral techniques.

3. From their photophysical studies, it is clear that all the dyes possess good absorption in the region of UV-visible range and display λ_{abs} in the range of 371 to 524 nm. Further, they exhibit single emission band (λ_{em}) in the visible region ranging from 449 to 640 nm.

4. From their electrochemical studies, it is evident that, almost all the dyes possess prerequisites to act as good sensitizers.

5. From their theoretical studies, it is concluded that, all the dyes possess good charge separation in their FMO levels.

6. From the results of sensitization studies in devices, it is clear that, among the tested *n*-type dyes, the ***n*-C₁₃** exhibits the optimum *PCE* of **3.55** %. The dyes ***n*-**

C$_9$ (1.94%), **n-C$_{16}$** (2.20%) and **n-C$_{19}$** (2.38%) as sensitizers, display comparatively moderate photovoltaic performance.

7. From the co-sensitization studies of dyes (**n-C$_{6-21}$**) in DSSC, it can be concluded that, co-sensitizer **n-C$_6$** with 0.2 mM of **NCSU-10** sensitizer showcases an improved *PCE* of 9.55 %, V_{OC} of 0.672 V and *FF* of 62.2 %, whereas sensitizer **NCSU-10** alone displays *PCE* of 8.25 %, V_{OC} of 0.667 V and *FF* of 60.6 %. Also, the co-sensitizers **n-C$_8$** (8.75%), **n-C$_{13}$** (8.29%), **n-C$_{15}$** (8.73%) and **n-C$_{18}$** (8.32%) exhibit improved photovoltaic performance when compared to that of **NCSU-10** alone.

8. From the results of tested *p*-type organic chromophores in DSSC, it can be concluded that, sensitizer **p-C$_2$** shows *PCE* = 0.40 %, J_{SC} = 2.41 mA.cm^{-2}, V_{OC} = 59 mV and *FF* = 29%, which are comparable with that of benchmark reference **P1** (*PCE* = 0.47 %, J_{SC} = 4.06 mA.cm^{-2}, V_{OC} = 45 mV and *FF* = 26%).

Conclusively, in the present work twenty four new *n/p*-type organic sensitizers/co-sensitizers with various design strategies, have been synthesized and characterized. Based on their photophysical, electrochemical, theoretical and photovoltaic studies, the role of acceptor/anchoring moieties on the device performance has been evaluated. It has been observed that, the chemical structure and position of acceptor/anchoring groups play a vital role in determining the overall *PCE* of the DSSCs.

6.3 SCOPE FOR FUTURE WORK

As concluded, the sensitizer **n-C$_{13}$** with D-π-A-π-A architecture displays the highest photovoltaic performance. Evidently, the photovoltaic efficiency of the **n-C$_{13}$** based device can be further improved by modifying the structure of the sensitizer as well as optimizing the other components such as semiconductor, electrolyte and counter electrolyte of the device.

In the present work, for the first time, carbazole based dyes with push-pull architecture have been explored as potential *p*-type sensitizers. Their photovoltaic performances are quite encouraging. So, adequate structural modification of **p-C$_2$** may lead to improvement in photovoltaic performance. The combination of the aforesaid *n*-type and *p*-type dyes with suitable semiconductor can be explored as effective photoactive anode and cathode, for the best performing tandem cells.

Ambrosio, F., Martsinovich, N. and Troisi, A. (2012). "Effect of the Anchoring Group on Electron Injection: Theoretical Study of Phosphonated Dyes for Dye-Sensitized Solar Cells." *J. Phys. Chem. C.*, 116, 2622-2629.

Ameline, D., Diring, S., Farre, Y., Pellegrin, Y., Naponiello, G., Blart, E., Charrier, B., Dini, D., Jacquemin, D., and Odobel, F. (2015). "Isoindigo derivatives for application in p-type dye sensitized solar cells." *RSC Adv.*, 5(104), 85530-85539.

Babu, D. D., Elsherbiny, D., Cheema, H., El-shafei, A., and Vasudeva, A. (2016). "Dyes and Pigments Highly efficient panchromatic dye-sensitized solar cells: Synergistic interaction of ruthenium sensitizer with novel co-sensitizers carrying different acceptor units." *Dye. Pigment.*, 132, 316-328.

Babu, D.D., Su, R., El-Shafei, A. and Adhikari, A.V. (2016). "From Molecular Design to Co-sensitization; High performance indole based photosensitizers for dye-sensitized solar cells." *Electrochimica Acta*, 198, 10-21.

Bae, S. H., Seo, K. D., Choi, W. S., Hong, J. Y., and Kim, H. K. (2015). "Near-IR organic sensitizers containing squaraine and phenothiazine units for dye-sensitized solar cells." *Dye. Pigment.*, 113, 18-26.

Barpuzary, D., Patra, A. S., Vaghasiya, J. V, Solanki, B. G., Soni, S. S., and Qureshi, M. (2014). "Highly Efficient One-Dimensional ZnO Nanowire-Based Dye-Sensitized Solar Cell Using a Metal-Free, D-π-A-Type, Carbazole Derivative with More than 5% Power Conversion." *ACS Appl. Mater. Interfaces*, 6(15), 12629-39.

Becke, A.D. (1988). "Density-functional exchange-energy approximation with correct asymptotic behavior." *Phys. Rev. A*, 38 (6), 3098-3100.

Becke, A.D. (1993). "A new mixing of Hartree-Fock and local density-functional theories." *The Journal of Chemical Physics*, 98 (2), 1372-1377.

Bisquert, J. (2003). "Chemical capacitance of nanostructured semiconductors: its origin and significance for nanocomposite solar cells." *Phys. Chem. Chem. Phys.*, 5 (24), 5360-5364.

Black, F.A., Clark, C.A., Summers, G.H., Clark, I.P., Towrie, M., Penfold, T., George, M.W. and Gibson, E.A. (2017). "Investigating interfacial electron transfer in dye-sensitized NiO using vibrational spectroscopy." *Phys. Chem. Chem. Phys.*, 19 (11), 7877-7885.

Borgström, M., Blart, E., Boschloo, G., Mukhtar, E., Hagfeldt, A., Hammarström, L. and Odobel, F. (2005). "Sensitized Hole Injection of Phosphorus Porphyrin into NiO: Toward New Photovoltaic Devices." *J. Phys. Chem. B*, 109 (48), 22928-22934

Cheema, H., Islam, A., Han, L., and El-Shafei, A. (2014a). "Influence of number of benzodioxan-stilbazole-based ancillary ligands on dye packing, photovoltage and photocurrent in dye-sensitized solar cells." *ACS Appl. Mater. Interfaces*, 6(14), 11617-24.

Cheema, H., Islam, A., Younts, R., Gautam, B., Bedja, I., Gupta, R.K., Han, L., Gundogdu, K. and El-Shafei, A. (2014b). "More stable and more efficient alternatives of Z-907: carbazole-based amphiphilic Ru(II) sensitizers for dye-sensitized solar cells." *Phys. Chem. Chem. Phys.*, 16 (48), 27078-27087.

Chiba Y., Islam A., Watanabe Y., Komiya R., Koide N. and Han L. Y. (2006). Jpn. J. Appl. Phys., Part 2, 45, L638-L640.

Click, K.A., Beauchamp, D.R., Garrett, B.R., Huang, Z., Hadad, C.M. and Wu, Y. (2014). "A double-acceptor as a superior organic dye design for p-type DSSCs: high photocurrents and the observed light soaking effect." *Phys. Chem. Chem. Phys.*, 16 (47), 26103-26111.

Cui, J., Lu, J., Xu, X., Cao, K., Wang, Z., Alemu, G., Yuang, H., Shen, Y., Xu, J., Cheng, Y. and Wang, M. (2014). "Organic Sensitizers with Pyridine Ring Anchoring Group for p-Type Dye-Sensitized Solar Cells." *J. Phys. Chem. C*, 118 (30), 16433-16440.

El-Shafei, A., Hussain, M., Atiq, A., Islam, A., and Han, L. (2012). "A novel carbazole-based dye outperformed the benchmark dye N719 for high efficiency dye-sensitized solar cells (DSSCs)." *J. Mater. Chem.*, 22(45), 24048.

Fabregat-Santiago, F., Bisquert, J., Garcia-Belmonte, G., Boschloo, G. and Hagfeldt, A. (2005). "Influence of electrolyte in transport and recombination in dye-sensitized solar cells studied by impedance spectroscopy." *Solar Energy Materials and Solar Cells*, 87 (1-4), 117-131.

Farré, Y., Raissi, M., Fihey, A., Pellegrin, Y., Blart, E., Jacquemin, D. and Odobel, F. (2017). "A Blue Diketopyrrolopyrrole Sensitizer with High Efficiency in Nickel-Oxide-based Dye-Sensitized Solar Cells." *ChemSusChem*, 10 (12), 2618-2625.

Farré, Y., Zhang, L., Pellegrin, Y., Planchat, A., Blart, E., Boujtita, M., Hammarström, L., Jacquemin, D. and Odobel, F. (2016). "Second Generation of Diketopyrrolopyrrole Dyes for NiO-Based Dye-Sensitized Solar Cells." *J. Phys. Chem. C*, 120 (15),

7923-7940.

Furche, F., Ahlrichs, R., Hättig, C., Klopper, W., Sierka, M., and Weigend, F. (2014). "Turbomole." *Wiley Interdiscip. Rev. Comput. Mol. Sci.*, 4(2), 91-100.

Gibson, E.A., Smeigh, A.L., Le Pleux, L., Fortage, J., Boschloo, G., Blart, E., Pellegrin, Y., Odobel, F., Hagfeldt, A. and Hammarström, L. (2009). "A p-Type NiO-Based Dye-Sensitized Solar Cell with an Open-Circuit Voltage of 0.35 V." *Angewandte Chemie International Edition*, 48 (24), 4402-4405.

Gong, J., Liang, J. and Sumathy, K. (2012). "Review on dye-sensitized solar cells (DSSCs): Fundamental concepts and novel materials." *Renewable and Sustainable Energy Reviews*, 16 (8), 5848-5860.

Grätzel, M. (2001). "Photoelectrochemical cells." *Nature*, 414 (6861), 338-344.

Grätzel, M. (2005). "Solar Energy Conversion by Dye-Sensitized Photovoltaic Cells." *Inorg. Chem.*, 44 (20), 6841-6851.

Gupta, K. S. V, Suresh, T., Singh, S. P., Islam, A., Han, L., and Chandrasekharam, M. (2014). "Carbazole based A-π-D-π-A dyes with double electron acceptor for dye-sensitized solar cell." *Org. Electron. physics, Mater. Appl.*, 15(1), 266-275.

Hagfeldt, A., Boschloo, G., Sun, L., Kloo, L. and Pettersson, H. (2010). "Dye-Sensitized Solar Cells." Chem. Rev., 110, 6595-6663.

Haldar, M. K., Scott, M. D., Sule, N., Srivastava, D. K., and Mallik, S. (2008). "Synthesis of barbiturate-based methionine aminopeptidase-1 inhibitors." *Bioorganic Med. Chem. Lett.*, 18(7), 2373-2376.

Han, L., Kang, R., Zu, X., Cui, Y., and Gao, J. (2015). "Novel coumarin sensitizers based on 2-(thiophen-2-yl)thiazole π-bridge for dye-sensitized solar cells." *Photochem. Photobiol. Sci.*, 14(11), 2046-2053.

Hara, K., Kurashige, M., Ito, S., Shinpo, A., Suga, S., Sayama, K., and Arakawa, H. (2003). "Novel polyene dyes for highly efficient dye-sensitized solar cells." *Chem. Commun. (Camb).*, (2), 252-253.

Hara, K., Sato, T., Katoh, R., Furube, A., Yoshihara, T., Murai, M., Kurashige, M., Ito, S., Shinpo, A., Suga, S., and Arakawa, H. (2005). "Novel conjugated organic dyes for efficient dye-sensitized solar cells." *Adv. Funct. Mater.*, 15(2), 246-252.

Hasan, M. A., and Sumathy, K. (2010). "Photovoltaic thermal module concepts and their performance analysis: A review." *Renew. Sustain. Energy Rev.*, 14(7), 1845-1859.

He, J., Lindström, H., Hagfeldt, A. and Lindquist, S.-E. (2000). "Dye-sensitized nanostructured tandem cell-first demonstrated cell with a dye-sensitized photocathode." *Solar Energy Materials and Solar Cells*, 62, 265-273.

He, J., Lindström, H., Hagfeldt, A. and Lindquist, S.-E. (1999). "Dye-Sensitized Nanostructured p-Type Nickel Oxide Film as a Photocathode for a Solar Cell." *J. Phys. Chem. B.,* 103, 8940-8943.

Hosseinzadeh, B., Salimi Beni, A., Najafi Chermahini, A., Ghahary, R., and Teimouri, A. (2015). "Novel organic dyes with anchoring group of barbituric/thiobarbituric acid and their application in dye-sensitized solar cells." *Synth. Met.*, 209, 1-10.

Hu, Y., Chen, Z., Le, Z., and Zheng, Q. (2004). "Organic Reactions in Ionic Liquids: Ionic Liquid Promoted Knoevenagel Condensation of Aromatic Aldehydes with (2-Thio)Barbituric Acid." *Synth. Commun.*, 34(24), 4521-4529.

Ito, S., Zakeeruddin, S.M., Humphry-Baker, R., Liska, P., Charvet, R., Comte, P., Nazeeruddin, M.K., Péchy, P., Takata, M., Miura, H., Uchida, S. and Grätzel, M. (2006). "High-Efficiency Organic-Dye- Sensitized Solar Cells Controlled by Nanocrystalline-TiO2 Electrode Thickness." *Adv. Mater.*, 18 (9), 1202-1205.

Ji, Z., Natu, G., Huang, Z., and Wu, Y. (2011). "Linker effect in organic donor-acceptor dyes for p-type NiO dye sensitized solar cells." *Energy Environ. Sci.*, 4(8), 2818.

Jose, R., Kumar, A., Thavasi, V. and Ramakrishna, S. (2008). "Conversion efficiency versus sensitizer for electrospun TiO2 nanorod electrodes in dye-sensitized solar cells." *Nanotechnology*, 19 (42), 424004.

Khanasa, T., Prachumrak, N., Kochapradist, P., Namuangruk, S., Keawin, T., Jungsuttiwong, S., Sudyoadsuk, T., and Promarak, V. (2014). "The design, synthesis, and characterization of D-π-A-π-A type organic dyes as sensitizers for dye-sensitized solar cells (DSSCs)." *Tetrahedron Lett.*, 55(21), 3244-3248.

Komatsu, M., Nakazaki, J., Uchida, S., Kubo, T., and Segawa, H. (2013). "A donor-acceptor type organic dye connected with a quinoidal thiophene for dye-sensitized solar cells." *Phys. Chem. Chem. Phys.*, 15(9), 3227-32.

Koops, S.E., O'Regan, B.C., Barnes, P.R.F. and Durrant, J.R. (2009). "Parameters Influencing the Efficiency of Electron Injection in Dye-Sensitized Solar Cells." *J. Am. Chem. Soc.*, 131 (13), 4808-4818.

Lewis, N. S. (2007). "Toward Cost-Effective Solar Energy Use." *Science.*, 315(5813), 798-801.

Li, L., Gibson, E.A., Qin, P., Boschloo, G., Gorlov, M., Hagfeldt, A. and Sun, L. (2010). "Double-Layered NiO Photocathodes for p-Type DSSCs with Record IPCE." *Adv. Mater.*, *22* (15), 1759–1762.

Li, S.-L., Jiang, K.-J., Shao, K.-F. and Yang, L.-M. (2006). "Novel organic dyes for efficient dye-sensitized solar cells." *Chem. Commun.*, (26), 2792-2794.

Li, Q., Lu, L., Zhong, C., Shi, J., Huang, Q., Jin, X., Peng, T., and Qin, J. (2009). "New Indole-Based Metal-Free Organic Dyes for Dye-Sensitized Solar Cells." *J. Phys. Chem. B.*, 113, 14588-14595.

Lin, R. Y.-Y., Wu, F.-L., Chang, C.-H., Chou, H.-H., Chuang, T.-M., Chu, T.-C., Hsu, C.-Y., Chen, P.-W., Ho, K.-C., Lo, Y.-H., and Lin, J. T. (2014). "Y-shaped metal-free D-π-(A)2 sensitizers for high-performance dye-sensitized solar cells." *J. Mater. Chem. A*, 2(9), 3092-3101.

Liu, F., Yang, Y., Wang, H., Liu, J., Hu, C., Huo, F., Bo, S., Zhen, Z., Liu, X., and Qiu, L. (2015). "Comparative studies on structure-nonlinearity relationships in a series of novel second-order nonlinear optical chromophores with different aromatic amine donors." *Dye. Pigment.*, 120, 347-356.

Liu, X., Cao, Z., Huang, H., Liu, X., Tan, Y., Chen, H., Pei, Y., and Tan, S. (2014). "Novel D-D-π-A organic dyes based on triphenylamine and indole-derivatives for high performance dye-sensitized solar cells." *J. Power Sources*, 248, 400-406.

Luo, J., Wan, Z., Jia, C., Wang, Y., and Wu, X. (2016a). "A co-sensitized approach to efficiently fill the absorption valley, avoid dye aggregation and reduce the charge recombination." *Electrochim. Acta*, 215, 506-514.

Luo, J., Wan, Z., Jia, C., Wang, Y., Wu, X., and Yao, X. (2016b). "Co-sensitization of Dithiafulvenyl-Phenothiazine Based Organic Dyes with N719 for Efficient Dye-Sensitized Solar Cells." *Electrochim. Acta*, 211, 364-374.

Manoharan, S., Asiri, A. M., and Anandan, S. (2016). "Impact of anchoring groups for improving the binding nature of organic dyes toward high efficient dye sensitized solar cells." *Sol. Energy*, 126, 22-3.

Martsinovich, N., and Troisi, A. (2011). "Theoretical studies of dye-sensitised solar cells : from electronic structure to elementary processes." *Energy Environ. Sci.*, 4,

4473-4495.

Mao, J., Zhang, X., Liu, S.-H., Shen, Z., Li, X., Wu, W., Chou, P.-T. and Hua, J. (2015). "Molecular engineering of D-A-π-A dyes with 2-(1,1-dicyanomethylene)rhodanine as an electron-accepting and anchoring group for dye-sensitized solar cells." *Electrochimica Acta*, 179, 179-186.

Matsui, M., Ito, A., Kotani, M., Kubota, Y., Funabiki, K., Jin, J., Yoshida, T., Minoura, H., and Miura, H. (2009). "The use of indoline dyes in a zinc oxide dye-sensitized solar cell." *Dye. Pigment.*, 80(2), 233-238.

Matsui, M., Shiota, T., Kubota, Y., Funabiki, K., Jin, J., Yoshida, T., Higashijima, S., and Miura, H. (2012). "N-(2-Alkoxyphenyl)-substituted double rhodanine indoline dyes for zinc oxide dye-sensitized solar cell." *Tetrahedron*, 68(22), 4286-4291.

Mathew, S., Yella, A., Gao, P., Humphry-Baker, R., Curchod, B.F.E., Ashari-Astani, N., Tavernelli, I., Rothlisberger, U., Nazeeruddin, M.K. and Grätzel, M. (2014). "Dye-sensitized solar cells with 13% efficiency achieved through the molecular engineering of porphyrin sensitizers." *Nature Chemistry*, 6 (3), 242-247.

Meng, F.S., Yao, Q.H., Shen, J.G., Li, F.L., Huang, C.H., Chen, K.C. and Tian, H. (2003). "Novel Cyanine Dyes with Multi-carboxyl Groups and their Sensitization on Nanocrystalline TiO2 Electrode." *Synthetic Metals*, *137* (1-3), 1543-1544.

Michinobu, T., Satoh, N., Cai, J., Li, Y., and Han, L. (2014). "Novel design of organic donor-acceptor dyes without carboxylic acid anchoring groups for dye-sensitized solar cells." *J. Mater. Chem. C*, 2(17), 3367.

Murali, M. G., Wang, X., Wang, Q., and Valiyaveettil, S. (2016). "New banana shaped A-D-π-D-A type organic dyes containing two anchoring groups for high performance dye-sensitized solar cells." *Dye. Pigment.*, 134, 375-381.

Morandeira, A., Fortage, J., Edvinsson, T., Le Pleux, L., Blart, E., Boschloo, G., Hagfeldt, A., Hammarström, L. and Odobel, F. (2008). "Improved Photon-to-Current Conversion Efficiency with a Nanoporous p-Type NiO Electrode by the Use of a Sensitizer-Acceptor Dyad." *J. Phys. Chem. C*, 112 (5), 1721-1728.

Mori, S., Fukuda, S., Sumikura, S., Takeda, Y., Tamaki, Y., Suzuki, E. and Abe, T. (2008). "Charge-Transfer Processes in Dye-Sensitized NiO Solar Cells." *J. Phys. Chem. C*, 112 (41), 16134-16139.

Nakasa, A., Usami, H., Sumikura, S., Hasegawa, S., Koyama, T. and Suzuki, E. (2005).

"A High Voltage Dye-sensitized Solar Cell using a Nanoporous NiO Photocathode." *Chemistry Letters*, 34 (4), 500-501.

Nattestad, A., Mozer, A.J., Fischer, M.K.R., Cheng, Y.-B., Mishra, A., Bäuerle, P. and Bach, U. (2010). "Highly efficient photocathodes for dye-sensitized tandem solar cells." *Nat Mater*, 9 (1), 31-35.

Nazeeruddin, M.K., Kay, A., Rodicio, I., Humphry-Baker, R., Mueller, E., Liska, P., Vlachopoulos, N. and Graetzel, M. (1993). "Conversion of light to electricity by cis-X2bis(2,2'-bipyridyl-4,4'-dicarboxylate)ruthenium(II) charge-transfer sensitizers (X = Cl-, Br-, I-, CN-, and SCN-) on nanocrystalline titanium dioxide electrodes." *J. Am. Chem. Soc.*, *115* (14), 6382-6390.

Ning, Z., Fu, Y. and Tian, H. (2010). "Improvement of dye-sensitized solar cells: what we know and what we need to know." *Energy Environ. Sci.*, 3 (9), 1170-1181.

Odobel, F., Le Pleux, L., Pellegrin, Y. and Blart, E. (2010). "New Photovoltaic Devices Based on the Sensitization of p-type Semiconductors: Challenges and Opportunities." *Acc. Chem. Res.*, 43 (8), 1063-1071.

Odobel, F., Pellegrin, Y., Gibson, E.A., Hagfeldt, A., Smeigh, A.L. and Hammarström, L. (2012). "Recent advances and future directions to optimize the performances of p-type dye-sensitized solar cells." *Coordination Chemistry Reviews*, *256* (21), 2414-2423.

Oskam, G., Bergeron, B. V, Meyer, G. J., and Searson, P. C. (2001). "Pseudohalogens for dye-sensitized TiO2 photoelectrochemical cells." *J. Phys. Chem. B*, 105(29), 6867-6873.

Ooyama, Y. and Harima, Y. (2009). "Molecular Designs and Syntheses of Organic Dyes for Dye-Sensitized Solar Cells." *Eur. J. Org. Chem.*, 18, 2903-2934.

Park, J. H., Cho, N. S., Jung, Y. K., Cho, H. J., Shim, H. K., Kim, H., and Lee, Y. S. (2007). "Polymeric light emitting properties and structural relationships of fluorene-based conjugated copolymers containing various hole transporting derivatives." *Org. Electron. physics, Mater. Appl.*, 8(2-3), 272-285.

Peach, M.J.G., Benfield, P., Helgaker, T. and Tozer, D.J. (2008). "Excitation energies in density functional theory: An evaluation and a diagnostic test." *The Journal of Chemical Physics*, 128, 044118.

Qin, P., Linder, M., Brinck, T., Boschloo, G., Hagfeldt, A. and Sun, L. (2009). "High Incident Photon-to-Current Conversion Efficiency of p-Type Dye-Sensitized Solar Cells

Based on NiO and Organic Chromophores." *Adv. Mater.*, 21 (29), 2993-2996.

Qin, P., Wiberg, J., Gibson, E.A., Linder, M., Li, L., Brinck, T., Hagfeldt, A., Albinsson, B. and Sun, L. (2010). "Synthesis and Mechanistic Studies of Organic Chromophores with Different Energy Levels for p-Type Dye-Sensitized Solar Cells." *J. Phys. Chem. C*, 114 (10), 4738-4748.

Qin, P., Zhu, H., Edvinsson, T., Boschloo, G., Hagfeldt, A. and Sun, L. (2008). "Design of an Organic Chromophore for P-Type Dye-Sensitized Solar Cells." *J. Am. Chem. Soc.*, 130 (27), 8570-8571.

Qu, P. and Meyer, G.J. (2001). "Proton-Controlled Electron Injection from Molecular Excited States to the Empty States in Nanocrystalline TiO2." *Langmuir*, 17 (21), 6720-6728.

Park, J.-H., Cho, N.S., Jung, Y.K., Cho, H.-J., Shim, H.-K., Kim, H. and Lee, Y.S. (2007). "Polymeric light emitting properties and structural relationships of fluorene-based conjugated copolymers containing various hole transporting derivatives." Org. Electron. 8, 272–285.

Pleux, L.L., Smeigh, A.L., Gibson, E., Pellegrin, Y., Blart, E., Boschloo, G., Hagfeldt, A., Hammarström, L. and Odobel, F. (2011). "Synthesis, photophysical and photovoltaic investigations of acceptor-functionalized perylenemonoimide dyes for nickel oxide p-type dye-sensitized solar cells." *Energy Environ. Sci.*, 4 (6), 2075-2084.

Powar, S., Wu, Q., Weidelener, M., Nattestad, A., Hu, Z., Mishra, A., Bäuerle, P., Spiccia, L., Cheng, Y.-B. and Bach, U. (2012). "Improved photocurrents for p-type dye-sensitized solar cells using nano-structured nickel (II) oxide microballs." *Energy Environ. Sci.*, 5 (10), 8896-8900.

Ramkumar, S., and Anandan, S. (2013). "Synthesis of bianchored metal free organic dyes for dye sensitized solar cells." *Dye. Pigment.*, 97(3), 397-404.

Ramkumar, S., Manoharan, S., and Anandan, S. (2012). "Synthesis of D-(π-A)2 organic chromophores for dye-sensitized solar cells." *Dye. Pigment.*, 94(3), 503-511.

Rezende, M. C., Campodonico, P., Abuin, E., and Kossanyi, J. (2001). "Merocyanine-type dyes from barbituric acid derivatives." *Spectrochim. Acta Part A Mol. Biomol. Spectrosc.*, 57(6), 1183-1190.

Salimi Beni, A., Zarandi, M., Madram, A.R., Bayat, Y., Najafi Chermahini, A. and

Ghahary, R. (2015). "Synthesis and characterization of organic dyes bearing new electron-withdrawing group for dye-sensitized solar cells." *Electrochimica Acta*, *186,* 504-511.

Saritha, G., Mangalaraja, R.V. and Anandan, S. (2017). "High-efficiency dye-sensitized solar cells fabricated using D-D-π-A (donor-donor/π-spacer-acceptor) architecture." *Solar Energy*, 146, 150-160.

Singh, S.P., Chandrasekharam, M., Gupta, K.S.V., Islam, A., Han, L. and Sharma, G.D. (2013). "Co-sensitization of amphiphilic ruthenium (II) sensitizer with a metal free organic dye: Improved photovoltaic performance of dye sensitized solar cells." *Organic Electronics*, 14 (5), 1237-1241.

Sivanadanam, J., Ganesan, P., Madhumitha, R., Nazeeruddin, M. K., and Rajalingam, R. (2015). "Effect of π-spacers on the photovoltaic properties of D-π-A based organic dyes." *J. Photochem. Photobiol. A Chem.*, 299, 194-202.

Seo, K. D., Song, H. M., Lee, M. J., Pastore, M., Anselmi, C., Angelis, F. De, Nazeeruddin, M. K., Gräetzel, M., and Kim, H. K. (2011). "Coumarin dyes containing low-band-gap chromophores for dye-sensitised solar cells." *Dye. Pigment.*, 90(3), 304-310.

Shen, P., Liu, X., Jiang, S., Huang, Y., Yi, L., Zhao, B., and Tan, S. (2011). "Effects of aromatic π-conjugated bridges on optical and photovoltaic properties of N,N-diphenylhydrazone-based metal-free organic dyes." *Org. Electron.*, 12(12), 1992-2002.

Soni, S.S., Fadadu, K.B., Vaghasiya, J.V., Solanki, B.G., Sonigara, K.K., Singh, A., Das, D. and Iyer, P.K. (2015). "Improved molecular architecture of D-π-A carbazole dyes: 9% PCE with a cobalt redox shuttle in dye sensitized solar cells." *J. Mater. Chem. A*, 3 (43), 21664-21671.

Subbaiah, M., Sekar, R., Palani, E. and Sambandam, A. (2013). "One-pot synthesis of metal free organic dyes containing different acceptor moieties for fabrication of dye-sensitized solar cells." *Tetrahedron Letters*, 54 (24), 3132-3136.

Sumikura, S., Mori, S., Shimizu, S., Usami, H., and Suzuki, E. (2008). "Syntheses of NiO nanoporous films using nonionic triblock co-polymer templates and their application to photo-cathodes of p-type dye-sensitized solar cells." *J. Photochem. Photobiol. A Chem.*, 199(1), 1-7.

Tang, J., Hua, J., Wu, W., Li, J., Jin, Z., Long, Y., and Tian, H. (2010). "New starburst sensitizer with carbazole antennas for efficient and stable dye-sensitized solar cells." *Energy Environ. Sci.*, 3(11), 1736.

Tarsang, R., Promarak, V., Sudyoadsuk, T., Namuangruk, S., and Jungsuttiwong, S. (2014). "Tuning the electron donating ability in the triphenylamine-based D-??-A architecture for highly efficient dye-sensitized solar cells." *J. Photochem. Photobiol. A Chem.*, 273, 8-16.

Thomas, K. R. J., Venkateswararao, A., Lee, C., and Ho, K. (2015). "Dyes and Pigments Organic dyes containing fl uoreneamine donor and carbazole p -linker for dye-sensitized solar cells." *Dye. Pigment.*, 123, 154-165.

Thomas, S., Deepak, T. G., Anjusree, G. S., Arun, T. A., Nair, S. V., and Nair, A. S. (2014). "A review on counter electrode materials in dye-sensitized solar cells." *J. Mater. Chem. A*, 2(13), 4474-4490.

Tian, H., Yang, X., Chen, R., Pan, Y., Li, L., Hagfeldt, A. and Sun, L. (2007). "Phenothiazine derivatives for efficient organic dye-sensitized solar cells." *Chem. Commun.*, (36), 3741-3743.

Tian, H., Yang, X., Chen, R., Zhang, R., Hagfeldt, A. and Sun, L. (2008). "Effect of Different Dye Baths and Dye-Structures on the Performance of Dye-Sensitized Solar Cells Based on Triphenylamine Dyes." *J. Phys. Chem. C*, 112 (29), 11023-11033.

Ullrich, C.A. (2006). "Time-dependent density-functional theory beyond the adiabatic approximation: Insights from a two-electron model system." *The Journal of Chemical Physics*, 125 (23), 234108.

Venkateswararao, A., Thomas, K. R. J., Lee, C. P., Li, C. T., and Ho, K. C. (2014). "Organic dyes containing carbazole as donor and ??-linker: Optical, electrochemical, and photovoltaic properties." *ACS Appl. Mater. Interfaces*, 6(4), 2528-2539.

Venkateswararao, a., Justin Thomas, K. R., Li, C.-T., and Ho, K.-C. (2015). "Functional tuning of organic dyes containing 2,7-carbazole and other electron-rich segments in the conjugation pathway." *RSC Adv.*, 5(23), 17953-17966.

Venkateswararao, a, Thomas, K. R. J., Lee, C.-P., and Ho, K.-C. (2013). "Synthesis and characterization of organic dyes containing 2,7-disubstituted carbazole π-linker." *Tetrahedron Lett.*, 54(30), 3985-3989.

Wan, Z., Jia, C., Duan, Y., Zhou, L., Lin, Y., and Shi, Y. (2012).

"Phenothiazine-triphenylamine based organic dyes containing various conjugated linkers for efficient dye-sensitized solar cells." *J. Mater. Chem.*

Wang, C., Fang, Y., Cao, Z., Huang, H., Zhao, B., Li, H., Liu, Y., and Tan, S. (2013). "Synthesis and photovoltaic properties of new branchlike organic dyes containing benzothiadiazole or triphenylamine-linked consecutive vinylenes units." *Dye. Pigment.*, 97(3), 405-411.

Wang, G., Wu, Y., Ding, W., Yu, G., Hu, Z., Wang, H., Liu, S., Zou, Y., and Pan, C. (2015). "Photovoltaic performance of long-chain poly(triphenylamine-phenothiazine) dyes with a tunable π-bridge for dye-sensitized solar cells." *J. Mater. Chem. A*, 3(27), 14217-14227.

Wang, P., Zakeeruddin, S. M., Moser, J. E., Nazeeruddin, M. K., Sekiguchi, T., and Grätzel, M. (2003). "A stable quasi-solid-state dye-sensitized solar cell with an amphiphilic ruthenium sensitizer and polymer gel electrolyte." *Nat. Mater.*, 2(6), 402-407.

Wang, Y., Wan, Z., Jia, C., and Yao, X. (2016). "Indole-based organic dyes with different electron donors for dye-sensitized solar cells." *Synth. Met.*, 211, 40-48.

Warnan, J., Pellegrin, Y., Blart, E., Zhang, L., Brown, A., Hammarström, L., Jacquemin, D., and Odobel, F. (2014). "Acetylacetone anchoring group for NiO-based dye-sensitized solar cell." *Dye. Pigment.*, 105, 174-179.

Wu, Y. and Zhu, W. (2013). "Organic sensitizers from D-π-A to D-A-π-A: effect of the internal electron-withdrawing units on molecular absorption, energy levels and photovoltaic performances." *Chem. Soc. Rev.*, *42* (5), 2039-2058.

Wu, Z., Ma, W., Meng, S., Li, X., Li, J., Zou, Q., Hua, J., and Tian, H. (2016). "New sensitizers containing amide moieties as electron-accepting and anchoring groups for dye-sensitized solar cells." *RSC Adv.*, 6(78), 74039-74045.

Yen, Y.-S., Chou, H.-H., Chen, Y.-C., Hsu, C.-Y. and Lin, J.T. (2012). "Recent developments in molecule-based organic materials for dye-sensitized solar cells." *J. Mater. Chem.*, *22* (18), 8734-8747.

Yen, Y. S., Lee, C. T., Hsu, C. Y., Chou, H. H., Chen, Y. C., and Lin, J. T. (2013). "Benzotriazole-containing D-π-A conjugated organic dyes for dye-sensitized solar cells." *Chem. - An Asian J.*, 8(4), 809-816.

Zhang, L., and Cole, J. M. (2015). "Anchoring Groups for Dye-Sensitized Solar Cells." *ACS Appl. Mater. Interfaces*, 7, 3427-3455.

Zhang, L.-P., Jiang, K.-J., Li, G., Zhang, Q.-Q. and Yang, L.-M. (2014). "Pyrazino[2,3-g]quinoxaline dyes for solar cell applications." *J. Mater. Chem. A*, *2* (36), 14852-14857.

Zhang, Q.-Q., Jiang, K.-J., Huang, J.-H., Zhao, C.-W., Zhang, L.-P., Cui, X.-P., Su, M.-J., Yang, L.-M., Song, Y.-L., and Zhou, X.-Q. (2015). "A push-pull thienoquinoidal chromophore for highly efficient p-type dye-sensitized solar cells." *J. Mater. Chem. A*, 3(i), 7695-7698.

Zhang, S., Islam, A., Yang, X., Qin, C., Zhang, K., Numata, Y., Chen, H., and Han, L. (2013). "Improvement of spectral response by co-sensitizers for high efficiency dye-sensitized solar cells." *J. Mater. Chem. A*, 1(15), 4812.

Zheng, Q., Yao, Z., Cheng, J., Shen, Y., and Lu, Z. (2000). "Synthesis and Nonlinear Optical Properties of p- (Dimethylamino) benzylidene Dyes Containing Different Acceptors." Chemistry Letters., 29 (12), 1426-1427.

Zhu, L., Yang, H.B., Zhong, C. and Li, C.M. (2014). "Rational design of triphenylamine dyes for highly efficient p-type dye sensitized solar cells." *Dye. Pigment.*, 105, 97-104.

LIST OF PUBLICATIONS

Papers published in international journals

Praveen Naik, Rui Su, Mohamed R. Elmorsy, Dickson D Babu, Ahmed El-Shafei, Airody Vasudeva Adhikari, "Molecular design and theoretical investigation of new metal-free heteroaromatic dyes with D-π-A architecture as photosensitizers for DSSC application". *Journal of Photochemistry and Photobiology A: Chemsitry*, **2017**, 345, 63-73.

Praveen Naik, Mohamed R. Elmorsy, Rui Su, Ahmed El-Shafei, Dickson D Babu, Airody Vasudeva Adhikari, "New carbazole based metal-free organic dyes with D-π-A-π-A architecture for DSSCs: synthesis, theoretical and cell performance studies". *Solar Energy*, **2017,** 153, 600-610**.**

Praveen Naik, Rui Su, Dickson D Babu, Ahmed El-Shafei, A. Vasudeva Adhikari, "Structurally simple D-A type organic sensitizers for dye-sensitized solar cells: Synthesis, characterization, and performance studies". *Journal of Iranian Chemical Society*, **2017**, 14, 2457-2466.

Praveen Naik, Aurélien Planchat, Yann Pellegrin, Fabrice Odobel, A. Vasudeva Adhikari "Exploring the application of new carbazole based dyes as effective *p*-type photosensitizers in dye-sensitized solar cells". *Solar Energy*, **2017**, 157, 1064-1073.

Praveen Naik, Rui Su, Ahmed El-Shafei, Airody Vasudeva Adhikari, "Improved photovoltaic performances of Ru (II) complex sensitized DSSCs by co-sensitization of carbazole based chromophores". *Inorganic Chemistry Communications,* **2017**, 86, 241-245.

Praveen Naik, Rui Su, Mohamed R. Elmorsy, Ahmed El-Shafei, Airody Vasudeva Adhikari, "Investigation of new carbazole based metal-free dyes as active photosensitizers/co-sensitizers for DSSCs". *Dyes and Pigments*, **2018**, 149, 117-187.

Praveen Naik, Rui Su, Mohamed R. Elmorsy, Ahmed El-Shafei, Airody Vasudeva Adhikari, "New carbazole based dyes as effective co-sensitizers for DSSCs sensitized with

Ruthenum(II) complex (NCSU-10)". *Journal of Energy Chemistry*, Accepted manuscript, DOI: 10.1016/j.jechem.2017.12.013.

Praveen Naik, Rui Su, Mohamed R. Elmorsy, Ahmed El-Shafei, Airody Vasudeva Adhikari, "New di-anchoring A-π-D-π-A configured organic chromophores for DSSC application: Sensitization and co-sensitization studies". *RSC Photochemical and Photobiological Sciences*, Accepted manuscript, DOI: 10.1039/C7PP00351J.

Papers communicated to international journals

Praveen Naik, Rui Su, Ahmed El-Shafei, Airody Vasudeva Adhikari, "Enhancing photovoltaic performance of DSSCs sensitized with Ru-II complexes by D-π-A configured carbazole based co-sensitizers". *RSC-New Journal of Chemistry*, Communicated on January 30, 2018, under review.

Praveen Naik, Rui Su, Ahmed El-Shafei, Airody Vasudeva Adhikari, "An comparative study of new carbazole based dyes carrying barbituric acid for effective co-sensitization in DSSCs sensitized using NCSU-10 dye". *Solar Energy*, Communicated on February 10, 2018, under review.

Papers in proceedings

Praveen Naik, Rui Su, Ahmed El-Shafei, A. Vasudeva Adhikari, "Synthesis, Characterization and Performance studies of a New Metal-Free Organic Sensitizer for DSSC application". *Materials Today; Proceedings*, communicated on June 10, 2016.

Praveen Naik, A. Vasudeva Adhikari, "Molecular Engineering of a New Organic Chromophore with D-π-A Architecture for Dye-Sensitized Solar Cells". *Materials Today; Proceedings*, communicated on October 20, 2016.

Papers presented

Praveen Naik, Dickson D. Babu, A. Vasudeva Adhikari, "Design and synthesis of a new metal-free organic chromophore for dye sensitized solar cell application", 10th Mid-Year CRSI Symposium in Chemistry, NIT, Trichy, Tamil Nadu, July 23-25, 2015.

Praveen Naik, Dickson D. Babu, A. Vasudeva Adhikari, "Design, Synthesis and Characterization of a New D-A type Metal-free Organic Chromophore for Dye Sensitized Solar Cell Application", International Conference on Advances in Chemical Engineering (ICACE-2015), NITK Surathkal, Karnataka, Dec. 20-22, 2015.

Praveen Naik, Dickson D. Babu, A Vasudeva Adhikari "Design, Synthesis and Computational Modeling of a New Metal-free Organic Chromophore for Dye Sensitized Solar Cell Application", National Conference on Recent Trends in Chemical Sciences (NCRTCS), MIT, Manipal, Karnataka, Jan. 11-12, 2016.

Praveen Naik, Dickson D. Babu, A. Vasudeva Adhikari "Design and Synthesis of a new carbazole based organic chromophore for Dye Sensitized Solar Cell Application", International Conference on Materials Science and Technology (ICMST-2016), St. Thomas College, Palai, Kerala, Jun. 05-08, 2016.

Praveen Naik, Su Rui, Dickson D. Babu, Ahmed El-Shafei, A. Vasudeva Adhikari, "Synthesis, Characterization and Performance Studies of a New Metal-Free organic Sensitizer for DSSC application", International Conference on Advanced Materials and Applications (ICAMA-2016), BMS college of Engineering, Bangalore, Karnataka, Jun. 15-17, 2016.

Praveen Naik, A. Vasudeva Adhikari, "Molecular Engineering of a New Organic Chromophore with D-π-A Architecture for Dye-Sensitized Solar Cells", International Conference on Smart Emerging Materials (ICSEM-2016), RV College, Bangalore, Karnataka, Oct. 20-22, 2016.

* * * * *

BIO-DATA

Name	: **Praveen Naik**
Permanent Address	No. 4-9/1, Nemmadi House,
	Kunjal Jeddu, Neelavara Post & village,
	Udupi Taluk & District
	Karnataka - 576 213, India
Contact Details:	
	Email: praveennaik018@gmail.com
	Mobile: +919538729415
Age	: 28
Date of Birth	: 06-08-1989
Name of Father	: A. Annappa Naik

EDUCATION:

COURSE	UNIVERSITY	DURATION	POSITION SECURED
Ph. D. in Chemistry	National Institute of Technology Karnataka, Surathkal, India	2013-	-
Post-Graduation- M.Sc. Chemistry	Manipal University, Manipal, Karnataka, India	2013	First Class
Graduation - B.Sc. Chemistry	Mangalore University	2011	First Class

RESEARCH PUBLICATIONS

Papers published in international journals	: 10
Papers Presented in National/International Conferences	: 10

Praveen Naik